University of Alberta

Directional and Spatio-temporal Tuning of Neurons in the Accessory Optic System and Pretectum of the Pigeon

by

Nathan Allan Crowder 

A thesis submitted to the Faculty of Graduate Studies and Research in partial fulfillment of the requirements for the degree of Doctor of Philosophy

Centre for Neuroscience

Edmonton, Alberta

Fall 2003

Your file Votre référence
ISBN: 0-612-87956-9
Our file Notre référence
ISBN: 0-612-87956-9

University of Alberta

Library Release Form

Name of Author: Nathan Allan Crowder

Title of Thesis: Directional and Spatio-temporal Tuning of Neurons in the Accessory Optic System and Pretectum of the Pigeon

Degree: Doctor of Philosophy

Year this Degree Granted: 2003

August 27, 2003

University of Alberta

Faculty of Graduate Studies and Research

The undersigned certify that they have read, and recommend to the Faculty of Graduate Studies and Research for acceptance, a thesis entitled Directional and Spatio-temporal Tuning of Neurons in the Accessory Optic System and Pretectum of the Pigeon submitted by Nathan Allan Crowder in partial fulfillment of the requirements for the degree of Doctor of Philosophy.

Dr. Douglas Wong-Wylie

Dr. Keir Pearson

Dr. Dallas Treit

Dr. Kathryn Todd

Dr. Clayton Dickson

Dr. Laurence Harris

Aug 25/03

Abstract

The nucleus of the basal optic root (nBOR) of the accessory optic system (AOS) and the pretectal nucleus lentiformis mesencephali (LM) are involved in the analysis of the whole-field visual motion, or optic flow, that results from self-motion. Neurons in the nBOR and LM have extremely large receptive fields, and exhibit direction-selectivity to large-field visual stimuli moving in the contralateral visual field. In this dissertation, the directional and spatio-temporal tuning of neurons in the pigeon's nBOR and LM was investigated using large-field sine wave gratings as visual stimuli. When neurons in the nBOR and LM were presented with large-field "plaids" in order to determine their ability to detect the global direction of pattern motion (pattern-selectivity), as opposed to the direction of motion of the components within the plaids (component-selectivity), most LM and nBOR neurons showed pattern-selectivity, and very few showed component-selectivity. In response to drifting sine wave gratings of varying spatial frequency (SF) and temporal frequency (TF) neurons in the LM and nBOR were tuned to either low SF/high TF or high SF/low TF stimuli. As velocity = TF/SF, these were referred to as "*fast*" and "*slow*" neurons, respectively. *Fast* neurons were tuned for TF, while the tuning of *slow* neurons was more closely related to velocity than to TF. Both *fast* and *slow* spatio-temporal tuning could be modeled by a correlation-type motion detector, which provides insight into the neural mechanisms involved in the detection of motion by this system. When the directional and spatio-temporal tuning of LM neurons was recorded before and after the nBOR was inactivated with tetrodotoxin, the spatio-temporal tuning of LM neurons was dramatically altered, but their directional tuning was not affected. When the projection from the Wulst to the LM was investigated, it was shown that even

though all LM neurons could be orthodromically stimulated from the Wulst, inactivating the Wulst with lidocaine did not affect the directional or spatio-temporal response properties of LM neurons. This dissertation demonstrates that the spatio-temporal response properties of neurons that detect visual motion are an important but often overlooked aspect of visual processing.

Acknowledgements

First, I would like to thank the Natural Sciences and Engineering Research Council of Canada (NSERC) for four years of financial support. I would like to thank my supervisor, Dr. Douglas Wong-Wylie, for showing me how to do electrophysiology. I would also like to thank a number of individuals that made these projects work much more smoothly: Dr. Connie Varnhagen, for reminding me how statistics work; Dr. Clayton Dickson and Dr. Dallas Treit, for being my surrogate supervisors; Dr. Michael Dawson, for enlightening explanations of computer simulations; Dr. J. Anthony Movshon for a very informative e-mail; and Isaac Lank, my favorite member of the psychology shop. Furthermore, I would like to thank my lab-mates Ian Winship, Angela Nguyen, Catherine Ogilvie, and Ryan Barkley for putting up with my shenanigans in the laboratory. Finally, Carolyn Leung, my parents, and my friends provided me with amazing support every single day.

Table of Contents

List of Tables

List of Figures

List of Abbreviations

AOS	accessory optic system
CCR	cervico-collic reflex
COR	cervico-ocular reflex
cpd	cycles per degree
DGC	displaced retinal ganglion cells
DTN	dorsal terminal nucleus
ER	excitatory response contour plot
IO	inferior olive
IOmc	medial column of the inferior olive
IR	inhibitory response contour plot
LM	lentiformis mesencephali
LMl	lentiformis mesencephali pars lateralis
LMm	lentiformis mesencephali pars medialis
LMmc	lentiformis mesencephali magnocellular
LMpc	lentiformis mesencephali parvocellular
LTN	lateral terminal nucleus
MST	middle superior temporal area
MT	medial temporal area
MTN	medial terminal nucleus
nBOR	nucleus of the basal optic root
nBORd	nBOR pars dorsalis
nBORl	nBOR pars lateralis
nBORp	nBOR proper
NOT	nucleus of the optic tract
OCR	opto-collic reflex
OKN	optokinetic nystagmus
OKR	optokinetic response
PSTH	peri-stimulus time histogram
SF	spatial frequency
SR	spontaneous firing rate
TF	temporal frequency
TTX	tetrodotoxin
V1	primary visual cortex
VbC	vestibulocerebellum
VCR	vestibulo-collic reflex
VIP	ventral intraparietal area
VOR	vestibulo-ocular reflex

Chapter 1

Introduction

Introduction to Optic Flow

The movement of animals through the environment creates two distinct demands on visual motion detection systems: the visual detection of object movement in the environment, and the detection of the visual consequences of ones' own motion. In the first case, the visual system functions as an exteroceptive sense for the detection of predators, prey, conspecifics, and other small moving visual stimuli from their motion relative to stationary objects in the environment. In the second case, visual motion detection functions as a proprioceptive sense by extracting information about the animal's own self-motion relative to stationary objects in the environment. As organisms move through an environment containing numerous visual stimuli, distinct and informative flow-fields, or optic flow, occurs across the entire retina (Gibson, 1954). Specific patterns of optic flow provide information to an organism about its current position, speed, and trajectory through the environment (Gibson, 1966; Harris and Rogers, 1999; Koenderink and van Doorn, 1987; Lappe et al., 1999; Lee, 1974, 1980; Owen, 1990; Warren et al., 2001).

Depicted as a sphere surrounding the observer (Gibson, 1966), Figure 1.1 shows two examples of optic flow created by self-motion. Figure 1.1a shows that head rotation to the left creates rightward optic flow across the "equator", and circular optic flow at the "poles". Figure 1.1b shows the pattern of optic flow created by forward translation. There is an expanding motion pattern directly in front of the observer with motion vectors that radiate outward from a *focus of expansion*. At the equator of the flow-field, the motion vectors are parallel to one another, and point backward relative to the observer. Directly behind the observer, the motion vectors converge at a *focus of contraction*. Optic flow

patterns generated by organisms are rarely as simple as the examples above. Most naturally occurring optic flow patterns contain both translational and rotational components because the retina is placed atop a series of mobile supports (e.g. eyeball, head, torso, and hips) (e.g. van den Berg, 2000).

This dissertation discusses neural mechanisms in the pigeon that are responsible for processing optic flow. Extracellular single unit recordings, and large-field computer generated visual stimuli, are used to explore the visual response properties of neurons in the pigeon's visual system that process optic flow.

Vision as a Proprioceptive Sense

Gibson (1966) suggested that optic flow could be used to determine the location, orientation, and movement of the body. The importance of vision in maintaining balance has been demonstrated using a special room in which the floor remained stationary, but the walls and ceiling could swing forward and backward (Lee and Aronson, 1974; Lee, 1980). The moving walls generated optic flow, which caused the subjects to sway approximately in phase with the walls' movement. Toddlers, and some adults who failed to brace themselves, could even be knocked over by their compensatory movements. In another study, subjects walking on a treadmill that was being towed around at different speeds reported changes in the perceived speed of walking (Rieser et al., 1995). These examples illustrate the interaction between visual, kinesthetic, and vestibular information in the control of posture and locomotion.

One of the uses of optic flow is to generate the optokinetic response (OKR) to assist retinal image stabilization. Visual acuity degrades when retinal image motion

exceeds 4°/s, so it is vital to maintain a stable retinal image to ensure optimal visual acuity and velocity discrimination (Westheimer and McKee, 1973, 1975; Carpenter, 1977; Murphy, 1978; Barnes and Smith, 1981; Nakayama, 1981). There are a number of reflexes that all work together to help maintain a stable retinal image (Wilson and Melvill Jones, 1979; Gioanni, 1988). The OKR is a general term encompassing several of these visually driven reflexes. The most commonly known, optokinetic nystagmus (OKN), is the eye movements that result when a subject is exposed to a continuously moving large-field pattern. The OKN consists of two phases: a slow phase where the eyes track the visual motion attempting to reduce the retinal slip velocity to zero, and a fast phase where eye position is reset by a saccade-like movement in the opposite direction. The Opto-collic reflex (OCR) consists of similar tracking and resetting phases, except it involves movement of the head rather than the eyes. The vestibulo-ocular reflex (VOR) and vestibulo-collic reflex (VCR) are driven by vestibular input, and act to stabilize the retinal image during head or body movement. The VOR causes the eyes to rotate in a direction opposite of head rotation, which acts to maintain gaze direction during head movements. The VCR causes the neck to turn in order to stabilize the position of the head during body movements. The cervico-collic reflex (CCR) and cervico-ocular reflex (COR) are driven by proprioceptive input from the neck muscles, and act to maintain a stable retinal image through neck and eye movements, respectively.

The Accessory Optic-Pretectal System

Anatomical, physiological, and lesion studies suggest that the Accessory Optic System (AOS) and pretectum are involved in the analysis of optic flow and the control of

the OKR (Simpson, 1984; Simpson et al., 1988; Grasse and Cynader, 1990). The AOS and pretectum are highly conserved in terms of evolution, and have homologous structures among all vertebrates (Fite, 1985; McKenna and Wallman, 1985a; Weber, 1985). Initially, this pathway had received relatively little attention compared to the tectofugal and thalamofugal pathways, and was originally thought to have no normal function (Marg, 1973). In the past 20 years, a tremendous amount has been discovered about the structure and function of the AOS and pretectum.

Anatomy of the Avian AOS and Pretectum

As pointed out by McKenna and Wallman (1985a), the Accessory Optic System is neither accessory nor a system. In birds, the AOS consists of the nucleus of the basal optic root (nBOR), which along with the pretectal nucleus lentiformis mesencephali (LM), form the major visual input to the optokinetic system (Simpson, 1984; McKenna and Wallman, 1985a; Simpson et al., 1988). The nBOR is located in the ventral mesencephalon, medial to the optic tectum and anterior to the third cranial nerve (Karten and Hodos, 1967). The nBOR is divided into three sub-nuclei based on cell morphology: nBOR proper (nBORp), nBOR pars dorsalis (nBORd), and nBOR pars lateralis (nBORl) (Brecha et al., 1980). The nBORp is the main body of the nucleus, and contains large basophilic stellate-shaped cells, medium ovoid-shaped cells, and small spindle-shaped cells. The nBORd contains small spindle-shaped cells and forms a thin cap on the medial, dorsal, and caudal borders of the nBORp. The nBORl is located rostro-lateral to the nBORp, and contains large sparsely distributed neurons (Brecha et al., 1980). The LM is located in the rostal-most pole of the optic tectum, lateral to the nucleus rotundus

(Gamlin and Cohen 1988a,b). Previous studies had divided the LM into magnocellular (LMmc) and parvocellular (LMpc) sub-nuclei, even though both divisions were cytoarchitecturally very similar, leading to confusion in the literature (Ehrlich and Mark, 1984; Gottlieb and McKenna, 1986). Gamlin and Cohen (1988a) proposed re-naming the two divisions lentiformis mesencephali pars medialis (LMm) and lentiformis mesencephali pars lateralis (LMl) since one division is located rostro-medial to the other. McKenna and Wallman (1985a) have argued that the nBORl should be considered part of the LM rather than a component of the AOS because 1) the nBORl and LM lie adjacent to each other with no definable border; 2) their neurons have similar cytoarchitecture; 3) they have similar visual response properties (see *Visual Response Properties of Neurons in the Avian AOS and Pretectum* below).

Figure 1.2 shows a wiring diagram illustrating the afferent and efferent connections of the nBOR and LM. The nBOR receives afferent projections from displaced retinal ganglion cells (DGCs) in the contralateral retina (Karten et al., 1977; Reiner et al., 1979; Fite et al., 1981). DGCs are morphologically distinct from other ganglion cells because they are located in the inner plexiform layer of the retina rather than in the ganglion cell layer, and are also larger and more sparsely distributed than other retinal ganglion cells (Karten et al., 1977; Reiner et al., 1979). DGCs project exclusively to the nBOR because injections of retrograde tracers into the nBOR, but not the tectum or thalamus, results in labeling of DGCs (Karten et al., 1977; Reiner et al., 1979; Fite et al., 1981). Other afferents to the nBOR include the ipsilateral LM (Azevedo at al., 1983), the contralateral nBOR (Brecha et al., 1980), the lateral cerebellar nucleus (Arends and Zeigler, 1991), and the ipsilateral Wulst (Miceli et al., 1979; Rio et al.,

1983), which is thought to be the avian homolog of primary visual cortex (Karten and Shimizu, 1989; Medina and Reiner, 2000). The LM also receives direct retinal input from the contralateral eye (Gamlin and Cohen, 1988a). Other afferents to the LM include the ipsilateral nBOR (Brecha et al., 1980; Wylie et al., 1997), the lateral cerebellar nucleus (Arends and Zeigler, 1991), and the ipsilateral Wulst (Miceli et al., 1979).

The efferent connections of the nBOR have been investigated using retrograde and anteriograde tracers (Brecha et al., 1980; Wylie et al., 1997). The nBOR sends bilateral projections to the vestibulocerebellum (VbC; as mossy fibers), the inferior olive (IO; mainly from nBORd), the oculomotor nuclear complex, the vestibular nuclei, and the interstitial nucleus of Cajal. The nBOR also sends projections to the contralateral nBORd, medial mesencephalic reticular formation, and the area ventralis of Tsai. Finally, the heaviest efferent projection of the nBOR is to the ipsilateral LM (Wylie et al., 1997).

The efferent projections of the LM have been investigated by Gamlin and Cohen (1988b). The LM sends predominantly ipsilateral projections to the lateral pontine nucleus, the nucleus papillioformis, the nucleus mesencephalicus profundus, the nucleus principalis precommissuralis, the red nucleus, the IO, the VbC (as mossy fibers), the nBORd and nBORl. Because the IO sends climbing fiber projections to the contralateral VbC (Lau et al., 1998; Wylie et al., 1999a,b; Crowder et al., 2000), the nBOR and LM send direct mossy fiber and indirect (via the IO) climbing fiber inputs to the VbC. The mossy fiber projection from the nBOR and LM innervates folia IXcd of the VbC (Gamlin and Cohen, 1988b).

Visual Response Properties of Neurons in the Avian AOS and Pretectum

The visual response properties of AOS and pretectal neurons have been examined in almost every vertebrate class. Across species, AOS and pretectal neurons have extremely large receptive fields, and exhibit direction-selectivity to large-field visual stimuli moving in the contralateral visual field (salamanders: Manteuffel, 1982, 1984; frogs: Cochran et al., 1984; Gruberg and Grasse, 1984; Katte and Hoffmann, 1980; turtles: Rosenberg and Ariel, 1990; rabbits: Collewijn 1975; Maekawa et al., 1984; Simpson et al., 1979; rats: Natal and Britto, 1987, 1988; cats: Hoffmann and Schoppmann, 1981; Grasse and Cynader, 1984, 1990; opossum: Volchan et al., 1989; monkey: Hoffmann et al., 1988; Mustari and Fuchs, 1989; Westheimer and Blair, 1974; chicken: Burns and Wallman, 1981; McKenna and Wallman, 1981, 1985b; pigeon: Britto et al., 1981; Morgan and Frost, 1981; Winterson and Brauth, 1985; Wylie and Frost, 1990a, 1990b, 1999; Wolf-Oberhollenzer and Kirschfeld, 1994; Wylie, 2000; wallaby: Ibboston et al., 1994; Ibbotson and Price, 2001). The response properties of AOS and pretectal neurons contrast with those of motion sensitive cells in the tectofugal and thalamofugal visual pathways (Frost et al., 1990). Neurons in the tectofugal and thalamofugal pathways prefer small moving stimuli, and have relatively small receptive fields with inhibitory surrounds. These neurons do not respond to the large-field visual stimulation generated by optic flow (Frost et al., 1990). Conversely, neurons in the AOS and pretectum have large receptive fields lacking an inhibitory surround, and prefer large-field visual stimuli.

Although broadly tuned, most nBOR and LM neurons are maximally excited in response to motion in the "preferred" direction, and strongly inhibited in response to motion in the (approximately) opposite "anti-preferred" direction (Winterson and Brauth, 1985; Wolf-Oberhollenzer and Kirschfeld, 1994; Wylie and Frost, 1996, 1999; Wylie, 2000; Wylie and Crowder, 2000). Most LM neurons prefer forward (temporal-to-nasal) motion, with fewer neurons preferring up, down, and backward (nasal-to-temporal) motion (Katte and Hoffmann, 1980; McKenna and Wallman, 1985b; Winterson and Brauth, 1985; Fite et al., 1989; Fan et al., 1995; Wylie and Frost, 1996; Wylie and Crowder, 2000). Most neurons in the nBOR prefer up, down or backward motion, while few prefer forward (Burns and Wallman 1981; Morgan and Frost 1981; Gioanni et al. 1984; Rosenberg and Ariel, 1990; Wylie and Frost 1990). The nBOR is topographically organized in terms of direction preference, with up cells in the dorsal portion of the nucleus, down cells ventral to up cells, back cells along the ventral and lateral surface of the nBOR, and forward cells in the posterior-dorsolateral margin of the nucleus (Burns and Wallman, 1981; Wylie and Frost, 1990a). However, this topographical organization does not follow the morphological subdivisions of the nBOR because the border between up and down cells is consistently ventral to the border between the nBORd and nBORp (McKenna and Wallman, 1985a,b). A consistent topographical organization for the LM has yet to be discovered.

Information from the nBOR and LM is integrated in the IO and VbC to form large panoramic receptive fields sensitive to specific types of optic flow resulting from self-translation and self-rotation. Visually responsive neurons in the VbC and the medial column of the IO (IOmc) are topographically organized in terms of optic flow preference

(Wylie et al., 1993; Wylie et al., 1998, 1999b; Wylie and Frost, 1999; Crowder et al., 2000). The VbC is divided into a medial zone that prefers translational optic flow called the ventral uvula and nodulus, and a lateral zone that prefers rotational optic flow called the flocculus. Unlike the gross anatomical distinction between the flocculus and uvula/nodulus in mammals, the distinction in pigeons is based solely on optic flow preference (Wylie et al., 1993). The direction preferences of nodulus cells are classified using a three-axis system where +X, +Y, and +Z represent rightward, upward and forward self-motion, respectively. There are four types of translation cells: +Y, -Y, -X-Z, and -X+Z (assuming recording from the left side of the head). These neurons are organized into three parasagittal zones in the nodulus based on optic flow preference: the –X-Z zone is most medial, followed by –X+Z, and then a –Y/+Y zone (Wylie et al., 1998, 2003; Wylie and Frost, 1999; Crowder et al., 2000). There are two types of rotational neurons in the flocculus: cells that prefer rotation about the vertical axis (rVA neurons), and cells that prefer rotation about a horizontal axis oriented at 135° ipsilateral azimuth (H-135 neurons) (Wylie and Frost, 1993; Wylie et al., 1999b). Using retrograde tracers, it was discovered that the neurons in the IOmc that send climbing fibre projections to translational and rotational cells in the VbC are also topographically organized. Neurons in the caudo-medial and rostro-medial IOmc send projections to rVA and H-135 neurons in the flocculus, respectively (Wylie et al., 1999b). Neurons in the lateral IOmc send projections to the nodulus. Moving caudal to rostral, one encounters IOmc neurons that project to –X-Z, +Y, -X+Z, and –Y zones in the nodulus, respectively (Crowder et al., 2000). Furthermore, it was shown that the nBOR sends projections mainly to the rostral IOmc, and the LM sends projections mainly to the caudal IOmc

(Wylie, 2001). This is not surprising because the rostral IOmc contains H-135, -Y, +Y, and –X+Z neurons whose optic flow preferences consist of up, down or backward motion in the contralateral hemifield, and the caudal IOmc contains rVA and -X-Z neurons whose optic flow preferences consist of forward motion in the contralateral hemifield. Note that small subpopulations of nBOR and LM neurons also have binocular receptive fields and respond best to particular patterns of optic flow resulting from either self-rotation or self-translation (Wylie and Frost, 1990b, 1999; Wylie et al., 1998; Wylie, 2000). Most binocular nBOR neurons were found in the nBORd, which receives heavy inputs from the contralateral nBORp (Brecha et al., 1980; Wylie et al., 1997). However, these binocular neurons show marked contralateral dominance compared to the complex spike activity of neurons in the VbC, suggesting that further binocular integration occurs in the IO and VbC (Wylie and Frost 1990a, 1999; Wylie, 2001).

Common Reference Frame for Processing Self-Motion

There is strong evidence that the sensory systems involved in the analysis of self-motion (visual and vestibular systems), and the output of these systems (extraocular eye muscles), share a common spatial reference frame (Simpson and Graf, 1985; Simpson et al., 1981; Ezure and Graf 1984; Leonard et al., 1988; Graf et al., 1988; Baldo, 1990; Wylie and Frost, 1993, 1996, 1999; van der Steen et al., 1994; Dickman, 1996; Wylie et al., 1998). In the pigeon, VbC neurons in the nodulus prefer translational optic flow along three orthogonal axes: a vertical axis (+Y and –Y neurons) and two horizontal axes oriented at 45° to the midline (-X-Z and –X+Z neurons) (Wylie et al., 1998; Wylie and Frost, 1999). Neurons in the flocculus prefer rotational optic flow about a vertical axis

(rVA neurons), or about a horizontal axis 45° to the midline (H-135 neurons) (Graf et al., 1988; Wylie and Frost, 1993). The semi-circular canals share a similar configuration, where the horizontal canals respond to rotation about the vertical axis, and each anterior canal (and the contralateral co-planar posterior canal) responds to rotation about a horizontal axis oriented 45° to the midline (Simpson et al., 1981; Baldo, 1990). Finally, the extraocular eye muscles also share this configuration: the horizontal recti rotate the eyeball about a vertical axis, the vertical recti rotate the eyeball about a horizontal axis oriented at 135° ipsilateral azimuth, and the obliques rotate the eyeball about a horizontal axis oriented at 45° ipsilateral azimuth (Graf and Simpson, 1981; Simpson and Graf, 1981; Wylie and Frost, 1996). Wylie and Frost (1999) suggest that there is a computational advantage to a common spatial reference frame, since it would simplify integration of information between the visual, vestibular, and motor systems.

Mammalian AOS and Pretectum

The mammalian AOS also consists of three divisions: the medial terminal nucleus (MTN), the dorsal terminal nucleus (DTN), and the lateral terminal nucleus (LTN) (Simpson, 1984; McKenna and Wallman, 1985a). Physiological, anatomical, and lesion studies suggest that the mammalian pretectal nucleus of the optic tract (NOT) is homologous to the avian LM, and the mammalian MTN and LTN are homologous to the avian nBOR (Simpson, 1984; McKenna and Wallman, 1985a; Fite, 1985; Weber, 1985; Simpson et al., 1988). Furthermore, the mammalian DTN is often considered continuous with the NOT (e.g. Ibbotson et al., 1994), which parallels the relationship between the

nBORl and LM, and suggests that the mammalian DTN is homologous to the avian nBORl (McKenna and Wallman, 1985a).

The Role of the AOS and Pretectum in Optokinetic Nystagmus

It is believed that the AOS and pretectum play a major role in the control of OKN because lesions to the AOS or pretectum severely impair OKN, while lesions to thalamofugal or tectofugal structures leave OKN relatively unaffected (pigeons: Gioanni et al., 1983a,b; for reviews see Simpson, 1984; McKenna and Wallman 1985a; Simpson et al., 1988). In birds, nBOR lesions abolished vertical OKN and monocular horizontal OKN in response to backward motion (Wallman et al., 1981; Gioanni et al., 1983b). LM lesions abolished monocular horizontal OKN in response to forward motion (Gioanni et al., 1983a). These lesion results match well with the visual response properties of neurons in the nBOR and LM. Recall that most neurons in the nBOR prefer up, down, or backwards optic flow, whereas most LM neurons prefer forward optic flow (nBOR: Burns and Wallman 1981; Morgan and Frost 1981; Gioanni et al. 1984; Wylie and Frost 1990; LM: McKenna and Wallman, 1985b; Winterson and Brauth, 1985; Fite et al., 1989; Fan et al., 1995; Wylie and Frost, 1996; Wylie and Crowder, 2000).

Spatio-temporal Tuning of Pretectal Neurons

Most of the studies investigating the visual response properties of AOS and pretectal neurons used large-field stimuli consisting of random dot patterns, square-wave gratings and/or checkerboards. However, when Ibbotson et al. (1994) presented wallaby pretectal neurons with drifting sine wave gratings of varying spatial frequency (SF) and

temporal frequency (TF), they found that pretectal neurons preferred certain SFs and TFs over others (i.e. they were tuned in the spatio-temporal domain). They described two types of cells: those that preferred high SFs (0.5-1.0 cycles per degree (cpd)) and low TFs (<1 Hz) vs. those that preferred low SFs (0.1-0.5 cpd) and high TFs (>10Hz). As velocity = TF/SF, these two groups were referred to as "slow" and "fast" neurons, respectively. Neurons that were similarly tuned in the spatio-temporal domain were found in the LM of pigeons (Wylie and Crowder, 2000). Wolf-Oberhollenzer and Kirchfeld (1994) examined the spatio-temporal tuning of pigeon nBOR neurons, but they used a limited range of SFs (<0.185 cpd) that did not include the SFs that maximally stimulate slow neurons in pigeon and wallaby pretectum (Ibbotson et al., 1994; Wylie and Crowder, 2000).

Two main types of motion-detector are discussed in the modeling literature: gradient models (e.g. Marr and Ullmann, 1981; Buchner, 1984, Srinivasan, 1990) and correlation models (e.g. Reichardt, 1957, 1961; Barlow and Levick, 1965; van Santen and Sperling, 1985). In gradient models, the velocity of a visual stimulus is calculated by dividing a spatial intensity gradient by a temporal intensity gradient. The spatial intensity gradient is obtained by measuring the intensity of the visual stimulus at two separate locations at the same time. The temporal intensity gradient is obtained by measuring the intensity of the visual stimulus at one location at two points in time. Gradient models provide a measure of image velocity irrespective of the texture or contrast of the visual stimulus. The correlation model of motion detection is also known as the delay-and-compare model or Reichardt model. The structure of the basic component of the correlation model, called a half-detector, is shown in Figure 1.3a. The half-detector has

two input channels, A and B, separated by a fixed distance. Detection of motion depends on the signals from A and B arriving at the comparator (X) at the same time (i.e. the timing of the two signals must be *correlated*). When the visual stimulus moves to the right, the delayed signal from A and the un-delayed signal from B arrive at the comparator simultaneously, and a movement signal is generated. When the visual stimulus moves to the left, the un-delayed signal from B arrives much sooner than the delayed signal from A, and a movement signal is not generated. However, the half-detector shown in Figure 1.3a provides an ambiguous motion signal because it will also respond to non-directional stimuli such as a stationary flickering light source. Summing the signals from two anti-symmetric half-detectors to form a fully balanced correlation motion detector, as in Figure 1.3b, can eliminate this ambiguity. Here, any non-directional changes in luminance will cause the signals from the two anti-symmetric half-detectors (S1 and S2) to cancel each other out when their signals are pooled (Σ). Unlike the gradient model of motion detection, the outputs of correlation motion detectors are strongly dependent on the texture and contrast of the visual stimulus. Furthermore, correlation motion detectors produce a signal that is tuned to a particular temporal frequency rather than velocity. Both Ibbotson et al. (1994) and Wolf-Oberhollenzer and Kirschfeld (1994) emphasized that pretectal and AOS neurons were tuned to TF rather than stimulus velocity, suggesting that motion sensitivity was calculated by the correlation model of elementary motion detectors (Reichardt, 1957, 1961; Barlow and Levick, 1965; van Santen and Sperling, 1985) as opposed to the gradient model, which predicts velocity tuning over a broad range of SFs and TFs (e.g. Marr and Ullmann, 1981; Buchner, 1984, Srinivasan, 1990).

Other Visual Structures Involved in Processing Optic Flow

Although not the subject of this dissertation, areas in the primate visual cortex have also been shown to process optic flow. In the geniculostriate pathway, visual information is relayed from the retina, through the lateral geniculate nucleus in the thalamus, to the visual cortex. Beyond the primary visual cortex (area V1), visual information processing is split into two streams: a dorsal stream for visuomotor control, and a ventral stream for perceptual representation (Goodale and Milner, 1992; Milner and Goodale, 1993, 1995; Ungerleider and Mishkin, 1982; Ungerleider and Haxby, 1994). For the dorsal stream, area V1 projects either directly to the middle temporal area (MT), or indirectly via area V2. Although there are neurons in areas V1, V2, and MT that respond to moving stimuli, their receptive field characteristics are not ideal for optic flow stimuli. Area MT projects to the medial superior temporal area (MST) and the ventral intraparietal area (VIP) (Maunsell and Van Essen, 1983). Neurons in MST and VIP have very large receptive fields and respond to large-field visual stimulation that results from self-rotation or self-translation (Bremmer et al., 1997; Duffy and Wurtz. 1991a,b; Lappe et al., 1996; Schaafsma and Duysens, 1996; Schaafsma et al., 1997; Tanaka et al., 1993). Furthermore, neurons in area 7A, which receives projections from both MST and VIP, also respond to optic flow stimuli (Read and Siegel, 1997). Not surprisingly, many of the cortical areas that process optic flow send projections to the AOS and pretectum (Boussaoud et al., 1992; Ilg and Hoffmann, 1993; Lui et al., 1995; Hoffmann et al., 2002).

Summary and Outline of Chapters

Self-motion of an organism through an environment containing numerous visual stimuli creates distinct and informative flow-fields, or optic flow, across its retina (Gibson, 1954). Optic flow can provide information about the animal's motion through space, and work with other proprioceptive senses to facilitate postural stability (Frost and Wylie, 2000). The AOS and pretectum are retinal recipient visual nuclei that are involved in the processing of optic flow and the generation of optokinetic responses like OKN and OCR (for reviews see Simpson 1984; McKenna and Wallman, 1985a; Simpson et al. 1988; Grasse and Cyander 1990).

In this dissertation, the visual response properties of neurons in the pigeon's AOS and pretectum are investigated using extracellular single unit recording. Sine wave gratings are used as visual stimuli to measure the directional and spatio-temporal tuning of neurons in the nBOR and LM. In Chapter 2, directional tuning curves are collected from neurons in the nBOR and LM with "plaid" stimuli composed of two non-parallel sine-wave gratings to investigate these neurons' ability to detect the global direction of pattern motion, as opposed to the direction of motion of the components within the plaids. In Chapter 3, the spatio-temporal tuning of nBOR neurons was investigated using a broad spectrum of SFs and TFs. It was shown that nBOR neurons clustered into two categories: "Fast" neurons preferred low SFs and high TFs, and "Slow" neurons preferred high SFs and low TFs. In Chapter 4, it was shown that fast nBOR neurons were tuned for TF, and slow nBOR neurons exhibited velocity-like tuning. The role of extra-retinal inputs to the LM were examined in Chapters 5 and 6 when the visual response properties

of LM neurons were measured before and following pharmacological inactivation of the nBOR and Wulst, respectively.

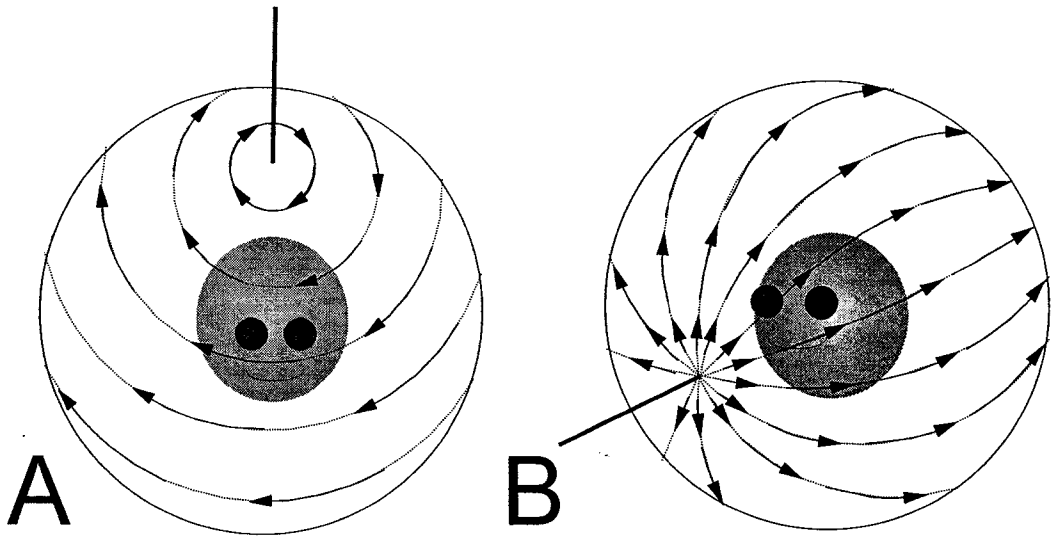

Figure 1.1

Schematics of the flow-fields produced by self-rotation (**A**) and self-translation (**B**). Arrows indicate the motion vectors in the optic flow-field.

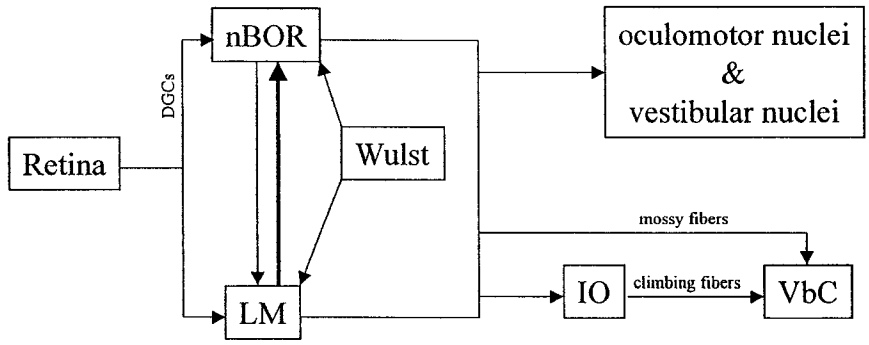

Figure 1.2

Simplified wiring diagram of the afferent and efferent connections of the Accessory Optic System and Pretectum. LM, nucleus lentiformis mesencephali; nBOR, nucleus of the basal optic root; IO, inferior olive; VbC, vestibulocerebellum; DGCs, displaced retinal ganglion cells.

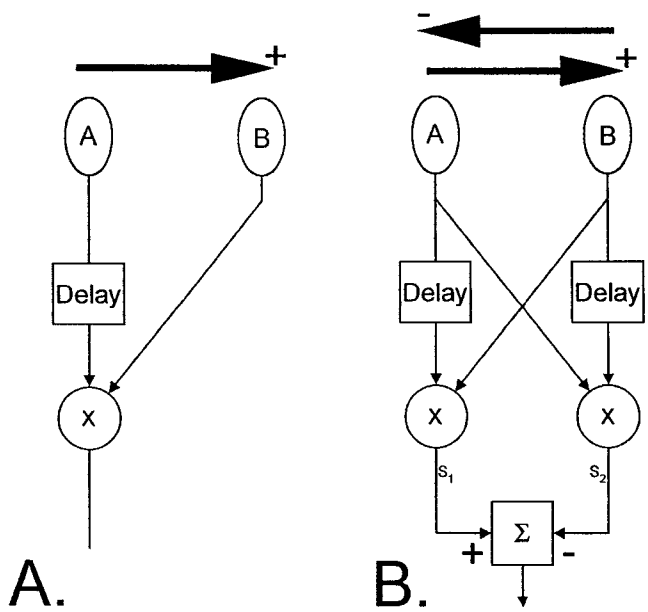

Figure 1.3

A shows a schematic representation of a correlation half-detector. **B** shows a fully balanced correlation detector, where the outputs of two anti-symmetric half-detectors (S1 and S2) are combined in a pooling stage (Σ). See text and Appendix 2 for details.

References

Arends JJ, Zeigler HP. Organization of the cerebellum in the pigeon (Columba livia): II. Projections of the cerebellar nuclei. *J Comp Neurol* 306:245-272, 1991.

Azevedo TA, Cukiert A, Britto LRG. A pretectal projection upon the accessory optic nucleus in the pigeon: an anatomical and electrophysiological study. *Neurosci Lett* 43: 13-18, 1983.

Baldo MV. The spatial arrangement of the semicircular canals of the pigeon. *Braz J Med Biol Res* 23: 914-917, 1990.

Barlow HB, Levick WR. The mechanism of directionally selective units in rabbit's retina. *J Physiol* 178: 477-504, 1965.

Barnes GR, Smith R. The effects of visual discrimination of image movement across the stationary retina. *Aviat Space Environ Med* 52: 466-472, 1981.

Boussaoud D, Desimone R, Ungerleider LG. Subcortical connections of visual areas MST and FST in macaques. *Vis Neurosci* 9: 291-302, 1992.

Brecha N, Karten HJ, Hunt SP. Projections of the nucleus of basal optic root in the pigeon: An autoradiographic and horseradish peroxidase study. *J Comp Neurol* 189: 615-670, 1980.

Bremmer F, Ilg UJ, Thiele A, Distler C, Hoffmann KP. Eye position effects in monkey cortex. I. Visual and pursuit-related activity in extrastriate areas MT and MST. *J Neurophysiol* 77: 944-961, 1997.

Britto LR, Natal CL, Marcondes AM. The accessory optic system in pigeons: receptive field properties of identified neurons. *Brain Res*. 206: 149-154, 1981.

Buchner E. Behavioral analysis of spatial vision in insects. In: *Photoreception and Vision in Invertebrates*, edited by Ali MA. New York: Plenum Press, 1984, p. 561-621.

Burns S, Wallman J. Relation of single unit properties to the occulomotor function of the nucleus of the basal optic root (AOS) in chickens. *Exp Brain Res* 42: 171-180, 1981.

Carpenter RHS. *Movement of the Eyes.* London: PION Ltd, 1977.

Cochran SL, Dieringer N, Precht W. Basic optokinetic-ocular reflex pathways in the frog. *J Neurosci* 4: 43-57, 1984.

Collewijn H. Direction-selective units in the rabbit's nucleus of the optic tract. *Brain Res* 100: 489-508, 1975.

Crowder NA, Winship IR, Wylie DR. Topographic organization of inferior olive cells projecting to translational zones in the vestibulocerebellum of pigeons. *J Comp Neurol* 419: 87-95, 2000.

Dickman JD. Related Vestibular afferent projections to the brain stem in pigeons. *Ann N Y Acad Sci* 781: 611-613, 1996.

Duffy CJ, Wurtz RH. Sensitivity of MST neurons to optic flow stimuli. I. A continuum of response selectivity to large-field stimuli. *J Neurophysiol* 65: 1329-1345, 1991a.

Duffy CJ, Wurtz RH. Sensitivity of MST neurons to optic flow stimuli. II. Mechanisms of response selectivity revealed by small-field stimuli. *J Neurophysiol* 65: 1346-1359, 1991b.

Ehrlich D, Mark R. The course of axons of retinal ganglion cells within the optic nerve and tract of the chick (Gallus gallus). *J Comp Neurol* 223: 583-591, 1984.

Ezure K, Graf W. A quantitative analysis of the spatial organization of the vestibulo-ocular reflexes in lateral- and frontal-eyed animals--I. Orientation of semicircular canals and extraocular muscles. *Neuroscience* 12: 85-93, 1984.

Fan TX, Weber AE, Pickard GE, Faber KM, Ariel M. Visual responses and connectivity in the turtle pretectum. *J Neurophysiol* 73: 2507-2521, 1995.

Fite KV, Brecha N, Karten HJ, Hunt SP. Displaced ganglion cells and the accessory optic system of pigeon. *J Comp Neurol* 195: 279-88, 1981.

Fite KV, Kwei-Levy C, Bengston L. Neurophysiological investigation of the pretectal nucleus lentiformis mesencephali in *Rana pipiens*. *Brain Behav Evol* 34: 164-170, 1989.

Fite KV. Pretectal and accessory-optic visual nuclei of fish, amphibia and reptiles: themes and variations. *Brain Behav Evol* 26: 71-90, 1985.

Frost BJ, Wylie DR. A common frame of reference for the analysis of optic flow and vestibular information. *Int Rev Neurobiol* 44: 121-140, 2000.

Frost BJ, Wylie DR, Wang Y-C. The processing of object and self-motion in the tectofugal and accessory optic pathways of birds. *Vision Res* 30: 1677-1688, 1990.

Gamlin PDR, Cohen DH. Retinal projections to the pretectum in the pigeon (*Columba livia*). *J Comp Neurol* 269:1-17, 1988a.

Gamlin PDR, Cohen DH. Projections of the retinorecipient pretectal nuclei in the pigeon (*Columba livia*). *J Comp Neurol* 269: 18-46, 1988b.

Gibson JJ. The visual perception of object motion and subjective movement. *Psychol Rev* 61: 304-314, 1954.

Gibson JJ. The problem of temporal order in stimulation and perception. *J Psychol* 62: 141-149, 1966.

Gioanni H, Rey J, Villalobos J, Richard D, Dalbera A. Optokinetic nystagmus in the pigeon (*Columba livia*). II. Role of the pretectal nucleus of the accessory optic system. *Exp Brain Res* 50: 237-247, 1983a.

Gioanni H, Villalobos J, Rey J, Dalbera A. Optokinetic nystagmus in the pigeon (*Columba livia*). III. Role of the nucleus ectomammilaris (nEM): interactions in the accessory optic system. *Exp Brain Res* 50: 248-258, 1983b.

Gioanni H, Rey J, Villalobos J, Dalbera A. Single unit activity in the nucleus of the basal optic root (nBOR) during optokinetic, vestibular and visuo-vestibular stimulations in the alert pigeon (*Columba livia*). *Exp Brain Res* 57: 49-60, 1984.

Gioanni H. Stabilizing gaze reflexes in the pigeon (*Columba livia*). I. Horizontal and vertical optokinetic eye (OKN) and head (OCR) reflexes. *Exp Brain Res* 69: 567-582, 1988.

Goodale MA, Milner AD. Separate visual pathways for perception and action. *Trends Neurosci* 15: 20-25, 1992.

Gottlieb MD, McKenna OC. Light and electron microscopic study of an avian pretectal nucleus, the lentiform nucleus of the mesencephalon, magnocellular division. *J Comp Neurol* 248: 133-145, 1986.

Graf W, Simpson JI, Leonard CS. Spatial organization of visual messages of the rabbit's cerebellar flocculus. II. Complex and simple spike responses of Purkinje cells. *J Neurophysiol* 60: 2091-2121, 1988.

Grasse KL, Cyander MS, Douglas RM. Alterations in response properties in the lateral and dorsal terminal nuclei of the cat accessory optic system following visual cortex lesions. *Exp Brain Res* 55: 69-80, 1984.

Grasse KL, Cyander MS. The accessory optic system in frontal-eyed animals. In: *Vision and Visual Dysfunction. The Neuronal Basis of Visual Function*, edited by Leventhal A. New York: McMillan, 1990, p. 111-139.

Gruberg ER, Grasse KL. Basal optic complex in the frog (*Rana pipiens*): a physiological and HRP study. **J Neurophysiol** 51: 998-1010, 1984.

Harris JM, Rogers BJ. Going against the flow. *Trends Cogn Sci* 3: 449-450, 1999.

Hoffmann KP Schoppmann A. A quantitative analysis of the direction-specific response of neurons in the cat's nucleus of the optic tract. *Exp Brain Res* 42: 146-157, 1981.

Hoffmann KP, Distler C, Erickson RG, Mader W. Physiological and anatomical identification of the nucleus of the optic tract and dorsal terminal nucleus of the accessory optic tract in monkeys. *Exp Brain Res* 69: 635-644, 1988.

Hoffmann KP, Bremmer F, Thiele A, Distler C. Directional asymmetry of neurons in cortical areas MT and MST projecting to the NOT-DTN in macaques. *J Neurophysiol* 87: 2113-2123, 2002.

Ibbotson MR, Price NS. Spatiotemporal tuning of directional neurons in mammalian and avian pretectum: a comparison of physiological properties. *J Neurophysiol* 86: 2621-2624, 2001.

Ibbotson MR, Mark RF, Maddess TL. Spatiotemporal response properties of direction-selective neurons in the nucleus of the optic tract and the dorsal terminal nucleus of the wallaby, Macropus eugenii. *J Neurophysiol* 72: 2927-2943, 1994.

Ilg UJ, Hoffmann KP. Functional grouping of the cortico-pretectal projection. *J Neurophysiol* 70: 867-869, 1993.

Karten HJ, Hodos W. *A stereotaxic Atlas of the Brain of the Pigeon (Columba livia)*. Baltimore: Johns Hopkins Press, 1967.

Karten HJ, Shimizu T. The origins of the neocortex: connections and lamination as distinct events in evolution. *J Cognitive Neurosci* 1: 291-301, 1989.

Karten HJ, Fite KV, Brecha N. Specific projection of displaced retinal ganglion cells upon the accessory optic system in the pigeon (*Columba livia*). *Proc Natl Acad Sci* 74: 1752-1756, 1977.

Katte O, Hoffmann KP. Direction specific neurons in the pretectum of the frog (*Rana esculenta*). *J Comp Physiol* 140: 53-57, 1980.

Koenderink JJ, van Doorn AJ. Facts on optic flow. *Biol Cybern* 56: 247-254, 1987.

Lappe M, Bremmer F, Pekel M, Thiele A, Hoffmann KP. Optic flow processing in monkey STS: a theoretical and experimental approach. *J Neurosci* 16: 6265-6285, 1996.

Lappe M, Bremmer F, van Ben Berg AV. Reply to Harris and Rogers. *Trends Cogn Sci* 3: 450, 1999.

Lau KL, Glover RG, Linkenhoker B, Wylie DR. Topographical organization of inferior olive cells projecting to translation and rotation zones in the vestibulocerebellum of pigeons. *Neuroscience* 85: 605-614, 1998.

Lee, DN, Aronson E. Visual proprioceptive control of standing in human infants. *Perception & Psychophysics*. 15: 529-532, 1974.

Lee DN. Visual information during locomotion. Perception: *Essays in honor of James J. Gibson*. edited by MacLeod RB, Pick HL. New York: Cornell University Press, 1974, p.250-267.

Lee, DN. The optic flow field: The foundation of vision. *Transactions of the Royal Society*. 290B: 169-179, 1980.

Leonard CS, Simpson JI, Graf W. Spatial organization of visual messages of the rabbit's cerebellar flocculus. I. Typology of inferior olive neurons of the dorsal cap of Kooy. *J Neurophysiol* 60: 2073-2090, 1988.

Lui F, Gregory KM, Blanks RH, Giolli RA. Projections from visual areas of the cerebral cortex to pretectal nuclear complex, terminal accessory optic nuclei, and superior colliculus in macaque monkey. *J Comp Neurol* 363: 439-460, 1995.

Maekawa K, Takeda T, Kimura M. Responses of the nucleus of the optic tract neurons projecting to the nucleus reticularis tegmenti pontis upon optokinetic stimulation in the rabbit. *Neurosci Res* 2: 1-25, 1984.

Manteuffel G. The accessory optic system in the newt, *Triturus cristatus*: unitary response properties from the basal optic neuropil. *Brain Behav Evol* 21: 175-184, 1982.

Manteuffel G. Electrophysiology and anatomy of direction-specific pretectal units in *Salamandra salamandra. Exp Brain Res* 54: 415-425, 1984.

Marg E. Neurophysiology of the accessory optic system. In *Handbook of sensory physiology*, Vol. VII, edited by Jung R. New York: Springer-Verlag.

Marr D, Ullman S. Directional selectivity and its use in early visual processing. *Proceedings of the Royal Society of London - Series B: Biological Sciences.* 211: 151-180, 1981.

Maunsell JH, van Essen DC. The connections of the middle temporal visual area (MT) and their relationship to a cortical hierarchy in the macaque monkey. *J Neurosci* 3: 2563-2586, 1983.

McKenna OC, Wallman J. Identification of avian brain regions responsive to retinal slip using 2-deoxyglucose. *Brain Res* 210: 455-460, 1981.

McKenna OC, Wallman J. Accessory optic system and pretectum of birds: comparisons with those of other vertebrates. *Brain Behav Evol* 26: 91-116, 1985a.

McKenna OC, Wallman J. Functional postnatal changes in avian brain regions responsive to retinal slip: a 2-deoxy-D-glucose study. *J Neurosci* 5: 330-342, 1985b.

Medina L, Reiner A. Do birds possess homologues of mammalian primary visual, somatosensory and motor cortices? *Trends Neurosci* 23: 1-12, 2000.

Miceli D, Gioanni H, Reperant J, Peyrichoux J. The avian visual wulst: I. An anatomical study of afferent and efferent pathways. II. An electrophysiological study of the functional properties of single neurons. In: *Neural Mechanisms of*

Behavior of the Pigeon, edited by Granda, AM, Maxwell JH. New York, NY: Plenum Press, 1979, p. 223-354.

Milner AD, Goodale MA. Visual pathways to perception and action. *Prog Brain Res* 95: 317-337, 1993.

Milner AD, Goodale MA. *The visual brain in action*. Oxford: Oxford Press.

Morgan B, Frost BJ. Visual response characteristics of neurons in nucleus of basal optic root of pigeons. *Exp Brain Res* 42:181-188, 1981.

Murphy BJ. Pattern thresholds for moving and stationary gratings during smooth eye movement. *Vision Res* 18: 521-530, 1978.

Mustari MJ, Fuchs AF. Response properties of single units in the lateral terminal nucleus of the accessory optic system in the behaving primate. *J Neurophysiol.* 61: 1207-1220, 1989.

Nakayama K. Differential motion hyperacuity under conditions of common image motion. *Vision Res* 21:1475-1482, 1981.

Natal CL, Britto LRG. The pretectal nucleus of the optic tract modulates the direction selectivity of the accessory optic neurons in rats. *Brain Res* 419: 320-323, 1987.

Natal CL, Britto LR. The rat accessory optic system: effects of cortical lesions on the directional selectivity of units within the medial terminal nucleus. *Neurosci Lett* 91: 154-159, 1988.

Owen DH. Perception and control of changes in self-motion: A functional approach to the study of information and skill. In: *Perception and Control of Self-Motion*, edited by Warren R, Fuchs AF. Hillsdale: Lawrence Erlbaum, 1990, p. 289-322.

Read HL, Siegel RM. Modulation of responses to optic flow in area 7a by retinotopic and oculomotor cues in monkey. *Cereb Cortex* 7: 647-661, 1997.

Reichardt W. Autokorrelationsauswertung als Funktionsprinzip des Zentralnervensystems. *Z Naturforsch* 12: 448-457, 1957.

Reichardt W. Autocorrelation, a principle for the evaluation of sensory information by the central nervous system. In: *Sensory Communication*, edited by Rosenblith WA. New York: Wiley, 1961, p. 303-317.

Reiner A, Brecha N, Karten HJ. A specific projection of retinal displaced ganglion cells to the nucleus of the basal optic root in the chicken. *Neurosci* 4: 1679-88, 1979.

Rieser JJ, Pick HL Jr, Ashmead DH, Garing AE. Calibration of human locomotion and models of perceptual-motor organization. *J Exp Psychol Hum Percept Perform*. 21: 480-497, 1995.

Rio JP, Villalobos J, Miceli D, Reperant J. Efferent projections of the visual wulst upon the nucleus of the basal optic root in the pigeon. *Brain Res* 271: 145-151, 1983.

Rosenberg AF, Ariel M. Visual-response properties of neurons in turtle basal optic nucleus in vitro. *J Neurophysiol* 63: 1033-1045, 1990.

Schaafsma SJ, Duysens J. Neurons in the ventral intraparietal area of awake macaque monkey closely resemble neurons in the dorsal part of the medial superior temporal area in their responses to optic flow patterns. *J Neurophysiol* 76: 4056-4068, 1996.

Schaafsma SJ, Duysens J, Gielen CC. Responses in ventral intraparietal area of awake macaque monkey to optic flow patterns corresponding to rotation of planes in depth can be explained by translation and expansion effects. *Vis Neurosci* 14: 633-646, 1997.

Simpson JI. The accessory optic system. *A Rev Neurosci* 7: 13-41, 1984.

Simpson JI, Graf W. Eye-muscle geometry and compensatory eye movements in lateral-eyed and frontal-eyed animals. *Ann N Y Acad Sci* 374:20-30, 1981.

Simpson JI, Graf W. The selection of reference frames by nature and its investigators. *Rev Oculomot Res* 1: 3-16, 1985.

Simpson JI, Soodak RE, Hess R. The accessory optic system and its relation to the vestibulocerebellum. *Prog Brain Res* 50: 715-724, 1979.

Simpson JI, Graf W, Leonard C. The coordinate system of visual climbing fibres to the flocculus. In: *Progress in oculomotor research*, edited by Fuchs AF Becker W. Amsterdam/New York/Oxford: Elsevier/North Holland, 1981.

Simpson JI, Leonard CS, Soodak RE. The accessory optic system: II. Spatial organization of direction selectivity. *J Neurophysiol* 60: 2055-2072, 1988.

Srinivasan MV. Generalized gradient schemes for the measurement of two-dimensional image motion. *Biol Cybern* 63: 421-431, 1990.

Tanaka K, Sugita Y, Moriya M, Saito H. Analysis of object motion in the ventral part of the medial superior temporal area of the macaque visual cortex. *J Neurophysiol* 69: 128-142, 1993.

Ungerleider LG, Haxby JV. 'What' and 'where' in the human brain. *Curr Opin Neurobiol* 4: 157-165, 1994.

Ungerleider LG, Mishkin M. Two cortical visual systems. In: *Analysis of Visual Behavior*. Edited by Ingle DJ, Goodale MA, Mansfield RJW. Cambridge: MIT press, 1982, p. 549-586.

van den Berg AV. Human ego-motion perception. *Int Rev Neurobiol* 44: 3-25, 2000.

van der Steen J, Simpson JI, Tan J. Functional and anatomic organization of three-dimensional eye movements in rabbit cerebellar flocculus. *J Neurophysiol* 72:31-46, 1994.

van Santen JP, Sperling G. Elaborated Reichardt detectors. *Journal of the Optical Society of America A-Optics & Image Science* 2: 300-321, 1985.

Volchan E, Rocha-Miranda CE, Picanco-Diniz CW, Zinsmeisser B, Bernardes RF, Franca JG. Visual response properties of pretectal units in the nucleus of the optic tract of the opossum. *Exp Brain Res* 78: 380-386, 1989.

Wallman J, McKenna OC, Burns S, Velez J, Weinstein B. Relation of the accessory optic system and pretectum to optokinetic responses in chickens. In *Progress in Oculomotor Research Developmental Neuroscience,* edited by Fuchs AF, Becker W. Amsterdam: Elsevier, 1981, p. 435-442.

Warren WH Jr, Kay BA, Zosh WD, Duchon AP, Sahuc S. Optic flow is used to control human walking. *Nat Neurosci* 4: 213-216, 2001.

Weber JT. Pretectal complex and accessory optic system in alert monkeys. *Brain Behav Evol* 26: 117-140, 1985.

Westheimer G, Blair SM. Unit activity in accessory optic system in alert monkeys. *Invest Ophthalmol* 13: 533-534, 1974.

Westheimer G, McKee SP. Failure of Donders' law during smooth pursuit eye movements. *Vision Res*. 13: 2145-253, 1973.

Westheimer G, McKee SP. Visual acuity in the presence of retinal-image motion. J Opt Soc Am 65: 847-850, 1975.

Wilson VJ, Melvill Jones G. *Mammalian Vestibular Physiology*. New York: Plenum Press.

Winterson BJ, Brauth SE. Direction-selective single units in the nucleus lentiformis mesencephali of the pigeon (*Columba livia*). *Exp Brain Res* 60: 215-226, 1985.

Wolf-Oberhollenzer F, Kirschfeld K. Motion sensitivity in the nucleus of the basal optic root of the pigeon. *J Neurophysiol* 71: 1559-1573, 1994.

Wylie DR. Binocular neurons in the nucleus lentiformis mesencephali in pigeons: responses to translational and rotational optic flowfields. *Neurosci Lett* 291: 9-12, 2000.

Wylie DR. Projections from the nucleus of the basal optic root and nucleus lentiformis mesencephali to the inferior olive in pigeons (*Columba livia*). *J Comp Neurol* 429: 502-513, 2001.

Wylie DR, Crowder NA. Spatiotemporal properties of fast and slow neurons in the pretectal nucleus lentiformis mesencephali in pigeons. *J Neurophysiol* 84: 2529-2540, 2000.

Wylie DR, Frost BJ. Visual response properties of neurons in the nucleus of the basal optic root of the pigeon: A quantitative analysis. *Exp Brain Res* 82: 327-336, 1990.

Wylie DR, Frost BJ. Binocular neurons in the nucleus of the basal optic root (nBOR) of the pigeon are selective for either translational or rotational visual flow. *Vis Neurosci* 5: 489-495, 1990b.

Wylie DR, Frost BJ. Responses of pigeon vestibulocerebellar neurons to optokinetic stimulation. II. The 3-dimensional reference frame of rotation neurons in the flocculus. *J Neurophysiol* 70: 2647-259, 1993.

Wylie DRW, Frost BJ. The pigeon optokinetic system: Visual input in extraocular muscle coordinates. *Vis Neurosci* 13: 945-953, 1996.

Wylie DR, Frost BJ. Responses of neurons in the nucleus of the basal optic root to translational and rotational flowfields. *J Neurophysiol* 81: 267-276, 1999.

Wylie DR, Kripalani T, Frost BJ. Responses of pigeon vestibulocerebellar neurons to optokinetic stimulation. I. Functional organization of neurons discriminating between translational and rotational visual flow. *J Neurophysiol* 70: 2632-2646, 1993.

Wylie DR, Linkenhoker B, Lau KL. Projections of the nucleus of the basal optic root in pigeons (*Columba livia*) revealed with biotinylated dextran amine. *J Comp Neurol* 384: 517-536, 1997.

Wylie DR, Bischof WF, Frost BJ. Common reference frame for neural coding of translational and rotational optic flow. *Nature* 392: 278-282, 1998.

Wylie DR, Lau KL, Lu X, Glover RG, Valsangkar-Smyth M. Projections of purkinje cells in the translation and rotation zones of the vestibulocerebellum in pigeon (*Columba livia*). *J Comp Neurol* 413: 480-493, 1999a.

Wylie DR, Winship IR, Glover RG. Projections from the medial column of the inferior olive to different classes of rotation-sensitive Purkinje cells in the flocculus of pigeons. *Neurosci Lett* 268: 97-100, 1999b.

Wylie DR, Brown MR, Barkley RR, Winship IR, Crowder NA, Todd KG. Zonal organization of the vestibulocerebellum in pigeons (*Columba livia*): II. Projections of the rotation zones of the flocculus. *J Comp Neurol* 456:140-153, 2003.

Chapter 2

Responses of Optokinetic Neurons in the Pretectum and Accessory Optic System of the Pigeon to Large-field Plaids

A version of this chapter has been published. Crowder NA, Wylie DRW. 2002. Journal of Comparative Physiology A. 188: 109-119.

Introduction

Neurons in the accessory optic system (AOS) and pretectum are important for the analysis of the optic flow that results from self-motion (Gibson 1954), and the generation of optokinetic nystagmus (OKN) to facilitate gaze stabilization. AOS and pretectal neurons exhibit direction-selectivity in response to moving large-field stimuli that are rich in visual texture (for reviews see Simpson 1984; Simpson et al. 1988; Grasse and Cyander 1990).

Previous psychophysical and neurophysiological studies of motion sensitive pathways within the geniculostriate system, which is more concerned with object-motion as opposed to self-motion (Frost 1982; 1985; Frost et al. 1990; 1994), have used "plaids" to illustrate the two-stage process of motion perception (motion integration) (Adelson and Movshon 1982; Albright 1984; Movshon et al. 1985; Rodman and Albright 1989; Welch 1989; Gizzi et al. 1990; Scannell et al. 1996; Merabet et al. 1998). The features of a sine-wave grating allow only one dimension of movement to be visible; therefore any motion detected is indistinguishable from motion perpendicular to the orientation of the grating. For plaids composed of symmetrically moving gratings (so-called "Type I" plaids; Ferrera and Wilson 1990) the perceived movement appears as a velocity vector that bisects the angle separating the orientation of its component gratings, even though no local motion components are moving in that direction (e.g. Adelson and Movshon 1982; Welch 1989; Stoner and Albright 1992). Most directionally selective neurons in the primary visual cortex (V1) respond to the individual components within a plaid ("component-selective neurons") indicating that the motion detectors in V1 are orientation-sensitive (Movshon et al. 1985; Gizzi et al. 1990). Neurons in extrastriate areas respond to the global

direction of motion, reflecting an integration of many orientation-sensitive motion direction signals into a global motion direction ("pattern-selective neurons"; Albright 1984; Rodman and Albright 1989; Gizzi et al. 1990; Stoner and Albright 1992; Scannell et al. 1996). Motion sensitive neurons that have orientation-insensitive inputs would also be expected to respond as pattern-selective neurons (see Smith and Harris 1991).

Smith and Harris (1991) recorded the OKN in cats in response to plaid stimuli. The eye movements were predominantly in the direction of the components of the plaid, (although always biased toward the direction of the overall pattern). Based on the implicit assumption that the retinal input calculates overall direction of motion "directly" (i.e. the retinal input is orientation-insensitive), Smith and Harris (1991) concluded that the OKN in cats is primarily driven by cortical component-selective neurons. In cats there is a rather robust projection from visual cortical areas to the AOS and pretectum (Schoppmann 1981; see also Grasse and Cynader 1990).

In the present study we recorded the responses of optokinetic neurons in the pigeon's visual system to large-field gratings and plaids. In birds, OKN is mediated by the pretectal nucleus lentiformis mesencephali (LM) and the nucleus of the basal optic root (nBOR) of the AOS (Fite et al. 1979; McKenna and Wallman 1985; Gioanni et al. 1983a,b). The LM and nBOR are retinal recipient (Karten et al. 1977; Reiner et al. 1979; Fite et al. 1981; Gamlin and Cohen 1988a) and also receive input from the visual Wulst (the homolog of mammalian visual cortex; Karten and Shimizu 1989) although this projection is sparse (Miceli et al. 1979; Azevedo et al. 1983; Rio et al. 1983). Given the sparse cortical projection, one might expect that the LM and nBOR neurons would show pattern-selective as opposed to component-selective responses.

Methods

Surgery and Extracellular recording

The methods reported herein conform to the guidelines established by the Canadian Council on Animal Care and were approved by the Biological Sciences Animal Services at the University of Alberta. Silver King and Racing Homer pigeons were anesthetized with an intramuscular injection of a ketamine (65mg/kg)/xylazine (8mg/kg) cocktail; supplemental doses were administered as necessary. Animals were placed in a stereotaxic device with pigeon ear bars and beak adapter such that the orientation of the skull conformed to the atlas of Karten and Hodos (1967). Based on the stereotaxic coordinates of Karten and Hodos (1967), sections of bone and dura were removed to expose the brain and allow access to either nBOR or LM.

Extracellular recordings were made with either tungsten microelectrodes (2 to 5 MΩ impedance; Frederick Haer Inc.) or glass micropipettes (4-5 μm tip diameter, containing 2M NaCl), which were lowered into nBOR or LM with an hydraulic microdrive (Frederick Haer). The signal was amplified, filtered, fed through a window discriminator, and displayed on an oscilloscope. The window discriminator produced TTL pulses, each representing single spikes, which were fed into a 1401*plus* (Cambridge Electronic Designs; CED). The stimuli (see below) were synchronized with the collection of TTL pulses, and peristimulus time histograms were constructed with *Spike2 for Windows* software (CED).

Stimulus Presentation

After neurons in either nBOR or LM were isolated, the optic flow preference and approximate receptive field location of the neuron was determined by moving a large (90° X 90°) hand-held stimulus in various directions in the contralateral visual field. Once the receptive field of a neuron was established, the responses to sine-wave gratings and plaids were obtained. These stimuli were generated by a VSG*Three* graphics computer (Cambridge Research Services), and were displayed in one of two ways: either a SONY multiscan 17se II computer monitor or a data projector (*InFocus* LP750) that back-projected the images onto a tangent screen. For the monitor, the diameter of the stimulus measured 35° visual angle, and for the back-projected stimulus the diameter was 75°.

Initially, the cell was presented with gratings of varying spatial frequencies (SF, 0.03-2 cycles per degree [cpd]), and temporal frequencies (TF, 0.03-16 Hz). Sine wave gratings are very effective stimuli for AOS and pretectal neruons (Ibbotson et al. 1994; Wolf-Oberhollenzer and Kirschfeld 1994; Wylie and Crowder 2000; Crowder and Wylie 2001). The stimulus was oscillated along the preferred axis to determine the optimal spatial and temporal frequencies (although nBOR and LM neurons are broadly tuned in this respect; see Wylie and Crowder 2000; Crowder and Wylie 2001). Direction-tuning curves (response as a function of the direction of motion) were then established. Each neuron was tested with gratings and 135° plaids (i.e. symmetrical plaids with component gratings separated by 135 °) in 16 directions, and/or gratings and 150° plaids in 24 directions. The gratings used for the directional tuning were of an optimal SF and TF. The SF for the plaids was of the same SF used for the gratings. The TF of the plaids was adjusted such that the overall pattern velocity matched that of the gratings. Each sweep consisted of 4 second motion in one direction, a 3 second pause, a 4 second motion in the

opposite direction, followed by a 3 second pause. For single gratings, the contrast was 0.95 (where the conventional definition of contrast was used; [$Luminance_{MAX}$ - $Luminance_{MIN}$] / [$Luminance_{MAX}$ + $Luminance_{MIN}$]). The plaids were generated by simultaneously displaying two non-parallel sine-wave gratings of half the contrast of the grating stimuli. Thus, the overall contrast of the plaids was also 0.95. During the pause the stimulus was a uniform gray of the standard mean luminance. Within a block of trials, the presentation of gratings, plaids, and directions was randomized to reduce the effect of response variability. The resultant directional tuning curves in response to plaids and gratings were averaged over 3-8 sweeps.

Data Analysis

The direction tuning curves in response to the gratings were then used to generate the predicted pattern and component responses to the plaids. The procedure for distinguishing between such component and pattern selective neurons is illustrated in Figure 2.1. Polar plots of the idealized directional tuning curves in response to single gratings and plaids are shown for pattern-selective and component-selective neurons. A pattern-selective neuron shows identical directional tuning to gratings and plaids (Fig. 2.1, left side), while the tuning curve for the predicted component response was calculated, from the tuning curve in response to gratings, by taking the sum of the two components of the plaid for each direction (Fig. 2.1, right side). Following Movshon et al. (1985) cells were classified as component or pattern selective by comparing the direction tuning curves for the plaids to the predicted component response and the predicted pattern response using the following formula:

$$R_P = (r_P - r_C * r_{PC}) / [(1 - r_C^2) * (1 - r_{PC}^2)]^{1/2}$$

where, R_P is the partial correlation coefficient for the pattern prediction, r_C is the correlation coefficient of the plaid response with the component prediction, r_P is the correlation coefficient of the plaid response with the pattern prediction, and r_{PC} is the correlation coefficient of the of the pattern and component predictions. To calculate the partial correlation coefficient for the component motion prediction (R_C), r_P is exchanged with r_C and visa versa.

The statistical significance of R_P and R_C was calculated by performing a Fisher Z-transform on the correlation coefficients ($Zf = ½ * \ln((1+R)/(1-R))$), and then calculating the difference between these z-scores (Papoulis 1990):

$$z = (Zf_P - Zf_C) / (1/(N_P-3) + 1/(N_C-3))^{1/2}$$

where: Zf_P is the Fisher Z-transform for R_P, Zf_C is the Fisher Z-transform for R_C, $N_P = N_C$ = number of directions (16 for 135° plaids, or 24 for 150° plaids).

These data were then plotted as in Figure 2.2 (adapted from Movshon et al. 1985; Gizzi et al. 1990, Scannell et al. 1996). The abscissa plots the component-prediction correlations (R_c) and the ordinate plots the pattern-prediction correlations (R_p). The scatter plot is divided into three regions, which are marked by solid lines for 150° plaids and dashed lines for 135° plaids. The region marked "Component Cells" contains those cells for which the component prediction significantly exceeds either zero or the value of the pattern prediction. Similarly, the region marked "Pattern Cells" contains those cells for which the pattern prediction significantly exceeds either zero or the value of the component prediction. The region marked "Unclassifiable Cells" contains cells where the two predictions do not significantly differ from each other or from zero. The conventional

criterion probability of 0.1 was used to define the three regions in the scatter plot (Crow et al. 1960). This criterion has been justified by the fact that this method is not a true test for statistical significance, but a convenient way to reduce data (Movshon et al. 1985; Gizzi et al. 1990; Scannell et al. 1996). Clearly, neurons whose firing properties are better described by the component prediction will fall in the "Component" region, and neurons whose firing properties are better described by the pattern prediction will fall in the "Pattern" region. Neurons may fall in the "Unclassifiable" region because their data is too variable to permit satisfactory analysis, or because the two predictions are too similar to be distinguished by the partial correlation computation.

There are other problems associated with using this statistical method for classification. For example, this partial correlation method effectively compares the shape of the tuning curves but does not take into account absolute depth of modulation. Thus, we also classified the neurons as pattern-selective, component-selective, or unclassifiable by visual inspection of the tuning curves.

Histology

In some cases, when the tungsten microelectrodes were used, electrolytic lesions (30 μamps, 10 sec, electrode +ve) were made at known locations relative to recording sites. At the end of the experiment, animals were given a lethal dose of sodium pentobarbitol (100 mg/kg i.p.) and immediately perfused with saline followed by 4% para-formaldehyde. The brains were extracted, post-fixed for several hours (4% para-formaldehyde with 20% sucrose) and then left in 30% sucrose for at least 24 hours. Using a microtome, frozen sections (45 μm thick in the coronal plane) through the

brainstem and pretectum were collected. The sections were mounted onto gelatin coated slides, dried, counterstained with neutral red, and coverslipped with Permount. Light microscopy was used to localize electrode tracts and the lesion sites.

Results

Quantitative data was obtained from 47 nBOR neurons and 49 LM neurons (from 38 birds). LM and nBOR neurons have large receptive fields (30 to 150° diameter) in the contralateral eye, and exhibit directional tuning in response to moving largefield stimuli. Most neurons are spontaneously active and motion in one direction (the "preferred" direction) results in excitation, whereas motion in the opposite direction results in inhibition (the "anti-preferred" direction). These properties have been examined extensively elsewhere and will not be discussed (Burns and Wallman 1981; Morgan and Frost 1981; Winterson and Brauth 1985; Wylie and Frost 1990; Wylie and Crowder 2000; for reviews see Simpson 1984; Simpson et al. 1988; Grasse and Cynader 1990).

As described in the Methods section, directional tuning curves in response to plaid stimuli were compared to pattern-selective and component-selective predictions, and partial correlations (R_p and R_c) were calculated.

Figure 2.2 shows the distribution of nBOR neurons as filled circles (150° plaids) or triangles (135° plaids), and the distribution of LM neurons as empty circles (150° plaids) or triangles (135° plaids); the predominance of pattern-selectivity is evident. Of the 47 direction selective units recorded from nBOR, 21 (45%) cells were classified as pattern cells, 6 (13%) cells were classified as component cells, and the remaining 20 (43%) cells fell in the unclassifiable region. Of the 49 direction-selective units recorded

from LM, 26 (53%) cells were classified as pattern cells, 2 (4%) were classified as component cells, and 21 (43%) cells fell in the unclassifiable region. Collapsing the LM and nBOR samples, of 96 cells, 47 (49%) were pattern-selective, 8 (8%) were component-selective, and 41 (43%) were unclassifiable.

In Figure 2.3, direction-tuning curves of representative LM (Fig 2.3A-D) and nBOR (Fig. 2.3E-H) neurons that were selective for pattern motion are shown. In this and subsequent figures, the firing rate relative to the spontaneous rate is plotted as a function of the direction of motion in polar coordinates (polar plots). Directional tuning curves of the predicted component-selective responses to plaids, and the neuronal responses to gratings and plaids are shown as dashed, dotted, and solid lines, respectively. Error bars, representing +/- 1 standard deviation, are shown for the cell in A. The values of R_P and R_C, as well as the type of plaid used, is also indicated for each neuron. The close correspondence between tuning curves in response to gratings and in response to plaids indicates that these neurons signal the global direction of motion irrespective of local motion signals. In some cases, for example the neuron in 3C, there is clearly a very tight correspondence between the response to plaids and the response to gratings. In Fig. 2.3G, note that the two small lobes on the plaid tuning curve in response to upward and downward motion are in the direction of the two maxima of the predicted component response. For the cells in Figures 2.3E and F, the response to the plaids was actually greater than the response to gratings, although this was uncommon.

Figure 2.4 shows polar plots of direction tuning curves representative of nBOR (Fig. 2.4A, B, D) and LM (Fig. 2.4C) neurons selective for component motion. For these neurons, the tuning curves in response to plaids closely correspond to the predicted tuning

curves for component-selective responses. The cell shown in Figure 2.4C was one of two LM cells that were classified as component-selective based on statistical criteria. This cell was somewhat odd: whereas all other LM cells we recorded from showed a unidirectional tuning curve in response to gratings, this had a bi-directional response to gratings. That is, gratings moving forward and backward resulted in an approximately equal amount of excitation. Such bi-directional LM cells have been reported previously (Wylie and Crowder 2000). In response to plaids, the neuron was excited by upward and downward motion, matching the component prediction.

Figure 2.5 shows tuning curves of other nBOR (Fig. 2.5B,F-H) and LM (Fig. 2.5A,C-E) neurons that could not be classified as pattern- or component-selective. A number of neurons were unclassifiable because they showed an attenuated response to plaids (Fig. 2.5A-C and F), and some neurons did not respond at all to the plaids (Fig. 2.5D). For the neurons shown in Figures 2.5C,G and H the pattern and component predictions are quite similar, which reduces the likelihood of finding a definitive difference between the two predictions (Stoner and Albright 1994). For the neurons in Figures 2.5E-H the directional tuning curve in response to plaids falls somewhere between those of the component-selective and pattern-selective predictions.

Classification by Visual Inspection

We also classified cells as pattern-selective, component-selective or unclassifiable based on a simple visual inspection of the tuning curves. Using this subjective method, of the 47 nBOR cells, 17 (36%) cells were classified as pattern cells, 9 (19%) cells were classified as component cells, and the remaining 21 (45%) cells fell in the unclassifiable

region. Of the 49 LM neurons, 22 (45%) cells were classified as pattern cells, 7 (14%) were classified as component cells, and 20 (41%) cells fell in the unclassifiable region. Collapsing the LM and nBOR samples, of 96 cells, 39 (41%) were pattern-selective, 16 (17%) were component-selective, and 41 (43%) were unclassifiable. Thus, compared with the partial correlation analysis, the inspection method results in slightly fewer pattern-selective neurons (41% vs. 48%) and doubles the proportion of neurons classified as component-selective (17% vs 8%). Comparing the two methods of classification for individual cells, there was a concordance rate of 81% (78/96). Of the discordances, there were 8 cells classified as pattern-selective with the statistical method that were unclassifiable by inspection. Two cells, unclassifiable by the statistical method were pattern-selective by inspection. Two cells were pattern-selective with the statistical method, but component-selective by inspection. Finally, there were 6 cells that were unclassifiable by the partial correlation method that were appeared to be component-selective by inspection. Four of these cells are shown in Figure 2.6, in addition to a cell that was pattern-selective based on the statistical criteria but component-selective by inspection. For all of these cells, it appeared that the tuning curve in response to plaids resembles the predicted component response as opposed to the predicted pattern response. This is particularly evident for Fig. 2.6B. For some of these cells, R_C was greater than R_P, although the difference was not significant (e.g. Figs. 2.6A,B).

Discussion

In the present study, following the methods of previous studies of direction selective neurons in mammalian visual cortex, we recorded the responses of optokinetic

neurons to large-field gratings and plaids. Most cells in the nBOR and LM were pattern-selective, about 50% according to the statistical classification proposed by Movshon et al. (1985). Fewer showed component motion selectivity, 13% of the nBOR neurons and 4% of the LM neurons, and many cells were unclassifiable (43%). Stoner and Albright (1994) suggested that this type of classification system should be used with caution. The ability to discriminate pattern- and component-cells depends on the similarity between the component and pattern conditions, which is affected by the breadth of directional tuning, and the angular distance between the component and pattern motions. In particular, Stoner and Albright (1994) emphasize that because a neuron is assigned to the unclassifiable group it does not preclude the neuron from being pattern- or component-sensitive. Indeed, with Figure 2.6, we assert that several unclassifiable neurons were component by visual inspection.

Previous studies in the mammalian geniculostriate system have found that most neurons in V1 are component-selective, while there are subpopulations of neurons in extrastiate cortex that that are component-selective (about 33%), and pattern selective (about 30%; Albright 1984; Movshon et al. 1985, Rodman and Albright 1989; Gizzi et al. 1990; Stoner and Albright 1992; Scannell et al. 1996). This functional separation forms the basis for models where component-selective neurons provide the input for pattern-selective neurons in an explicit two-stage process of motion integration in the cortex (e.g. Movshon et al. 1985; Stoner and Albright 1994), although Merabet et al. (1998) suggested that motion integration results from processing in a number of cortico-thalamic loops.

In the present study we have found that most pretectal and AOS neurons exhibit pattern-selectivity. Indeed the percentage of neurons showing pattern-selectivity in the nBOR and LM (~50%) is higher than that reported for studies of extrastriate cortex (~30%; Albright 1984; Movshon et al. 1985, Rodman and Albright 1989; Stoner and Albright 1992; Scannell et al. 1996). However, this is not to say that this represents motion integration of inputs that are orientation sensitive. It is possible that the pattern motion is detected directly with orientation-insensitive motion detectors (see Smith and Harris 1991).

Retinal and Telencephalic Contributions to Motion Processing in the Optokinetic System

In response to large-field plaid stimuli, Smith and Harris (1991) found that in cats, the optokinetic eye movements were predominantly in the direction of the components of the plaid, although always biased in the direction of the overall pattern. They proposed that the motion detectors within the optokinetc system are dominated by descending orientation-sensitive cortical inputs whereas orientation-insensitive retinal inputs play less of a role.

Given that we found that a majority of AOS and pretectal neurons showed pattern-selectivity, whereas relatively few showed component-selectivity, our findings are seemingly at odds with those of Smith and Harris (1991). However, to reiterate, Smith and Harris (1991) suggest that the component-sensitivity in the optokinetic system is due to descending orientation-selective cortical inputs. In pigeons, the descending telencephalic input to the LM and nBOR is considered sparse. Figure 2.7 shows a schematic of the visual inputs to the optokinetic nuclei in birds. There is a direct retinal

input to LM (Gamlin and Cohen 1998a) and nBOR (Karten et al. 1977; Reiner et al. 1979; Fite et al. 1981) in addition to a weaker input from the visual Wulst (Karten et al. 1977; Reiner et al. 1979; Fite et al. 1981). (The visual Wulst is thought to be the avian homolog of primary visual cortex (Karten and Shimizu 1989)). There is also a strong reciprocal connection between LM and nBOR (Clarke 1977; Brecha et al. 1980; Gamlin and Cohen 1988b; Wylie et al. 1997). This pattern of connectivity is essentially identical to that found in mammals (see Simpson 1984) except that the cortical input is quite variable between species. The cortical input to the mammalian nucleus of the optic tract (homologous to the avian LM) is quite heavy in cats and monkeys (Schoppmann 1981; Hoffmann et al. 1991; Ilg and Hoffmann 1993; Mustari et al. 1994) but is absent in other frontal-eyed species (opossum, Pereira et al 2000). A cortical input has also been found in rats (Shintani et al. 1999), guinea pigs (Lui et al. 1994) and rabbits (Hollander et al. 1979), but not in hamsters (Lent 1982) or tree shrews (Huerta et al. 1985). In animals with a sparse cortical input to the AOS and pretectum there is a strong naso-temporal asymmetry in the OKN (rabbits: Collewijn 1969; pigeons: Gioanni 1988; Zolotilina et al. 1995), which is not apparent in animals with a robust cortical input (e.g. Grasse and Cynader, 1990).

The predominance of pattern-selective neurons in LM and nBOR might reflect a large contribution from orientation-insensitive retinal inputs. However, the presence of component-selective cells in the LM and nBOR clearly indicates that orientation-sensitive information is entering the pigeon optokinetic system, perhaps from the visual Wulst. Orientation-sensitivity has been demonstrated in the avian Wulst (Wilson 1980). Moreover, some of the tuning curves of some pattern-selective (e.g. Fig. 2.3G) and

unclassifiable neurons (e.g. Fig. 2.6E-H) might represent integration of orientation-insensitive retinal inputs and component-sensitive telencephalic inputs.

As a cautionary note, the assumption that the retinal input is orientation-insensitive has yet to be directly evaluated. Although Smith and Harris (1991) cite the fact that retinal ganglion cells in mammals have circular receptive fields and are orientation insensitive, the AOS and pretectum receive input from a particular class of ganglion cells. In birds, the retinal input to the AOS is only from the displaced ganglion cells (Karten et al. 1977; Reiner et al. 1979; Fite et al. 1981), and we are unaware of any studies addressing their orientation sensitivity. Thus, it is possible that the pattern-selectivity arises from motion integration of retinal inputs, or integration of endogenous connections within and between LM and nBOR. It is also possible that there is integration of descending inputs from the Wulst.

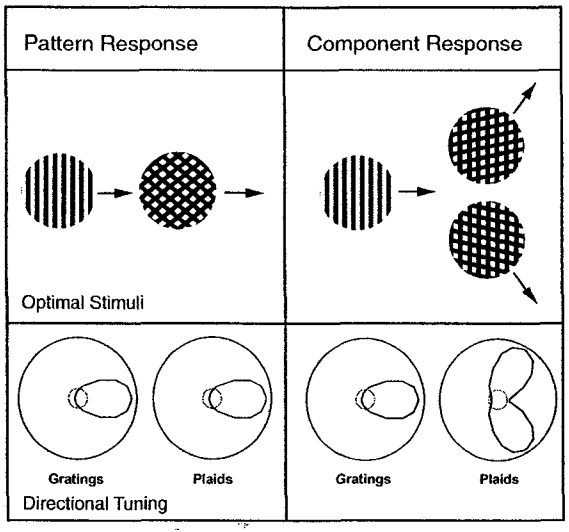

Figure 2.1

Idealized pattern (left) and component (right) responses for directionally selective neurons. For hypothetical neurons that prefer rightward motion, the responses to single gratings, and plaids composed of two overlapping gratings separated by 120° (120° plaids). On the left, the optimal stimuli (top) and directional tuning curves (bottom) for gratings and plaids are shown for a pattern-selective neuron. Direction tuning is plotted in polar coordinates where the radius represents neuronal response magnitude, and polar angle represents the direction of the stimulus motion. The plaid tuning curve is identical to that of the single grating, indicating sensitivity of the neuron to the direction of coherent pattern motion and not the individual components within the plaid. On the right, the optimal stimuli (top) and directional tuning curves (bottom) for gratings and plaids are shown for a component-selective neuron. The response to a plaid in a given direction is the sum of the response to the two components. Thus, the optimal plaid stimuli contain a component that is moving rightward and the overall tuning curve reflects the sensitivity to directions of both components within the plaid. Adapted from Rodman and Albright (1989).

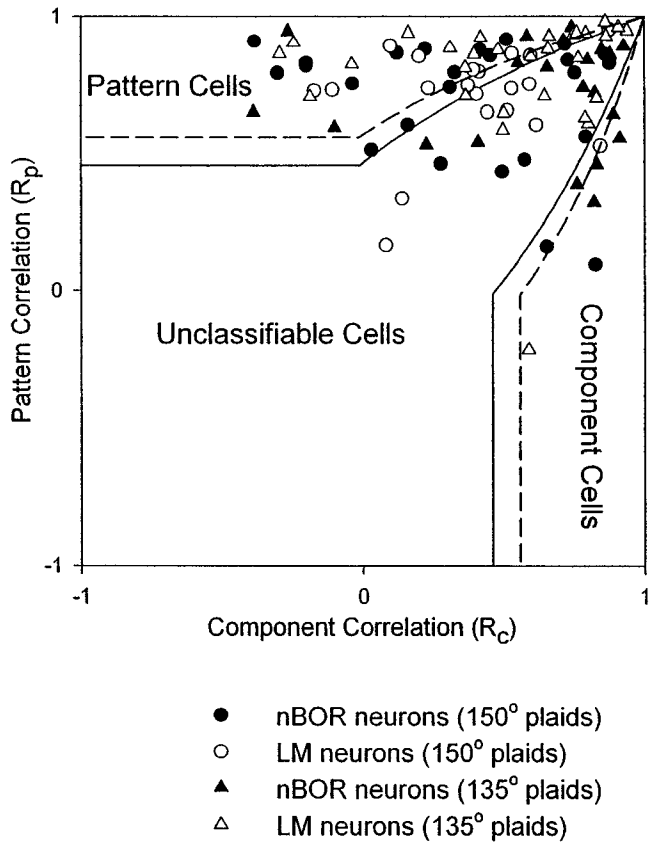

Figure 2.2

Scatter plots of partial correlations for pattern (R_P) and component (R_C) selectivity. Each data point indicates the degree to which the direction tuning for nBOR and LM neurons are correlated with pattern and component predictions. The data space is divided into three regions based on statistical criteria by a solid line for 150° plaids and a dashed line for 135° plaids (see Methods). Cells falling in the upper left, middle, or lower right areas are classified as pattern-selective, unclassifiable, or component-selective, respectively. The nBOR neurons are shown as filled circles (150° plaids) or triangles (135° plaids), and the LM neurons are shown as empty circles (150° plaids) or triangles (135° plaids). Note the predominance of pattern-selective neurons.

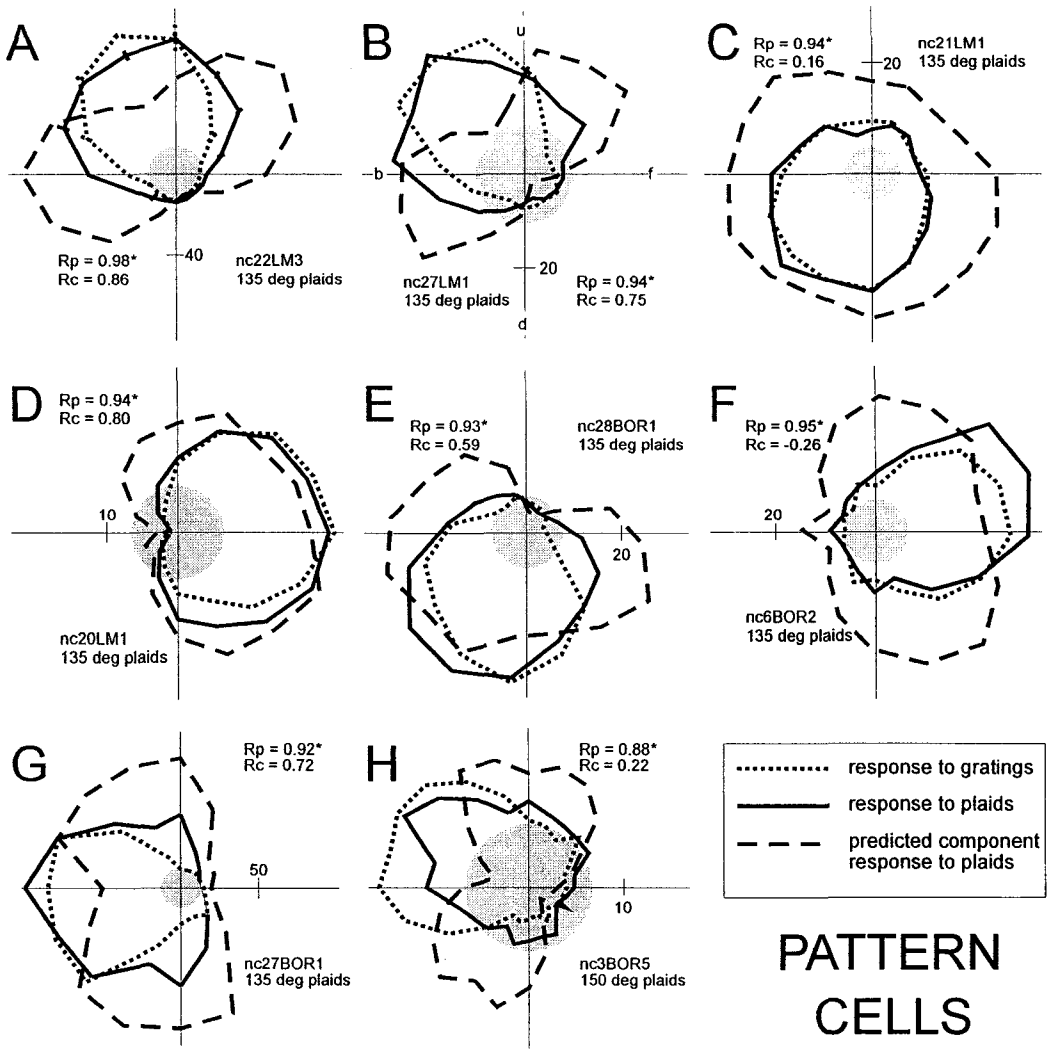

Figure 2.3

Polar plots illustrating the responses (spikes/sec) of pattern-selective LM (**A-D**) and nBOR (**E-H**) neurons to gratings and plaids. Firing rate relative to the spontaneous rate (SR; gray circle) is plotted as a function of the direction of motion in polar coordinates. (i.e. the SR has been set to zero; outside the gray circle= excitation, inside = inhibition). The responses to gratings and plaids are shown as dotted and solid lines, respectively. The predicted response to plaids for component-selective neurons is shown with a dashed line (see Fig. 2.1, and methods). Error bars representing +/- 1 standard deviation are shown for the neuron in **A**. u, b, d, and f represent up, back (nasal to temporal), down,

and forward (temporal to nasal) motion. Partial correlations (R_P and R_C) for each neuron are also shown; an asterisk (*) indicates statistical significance ($p<0.1$). The type of plaid (135^o or 150^o plaid) used is also indicated.

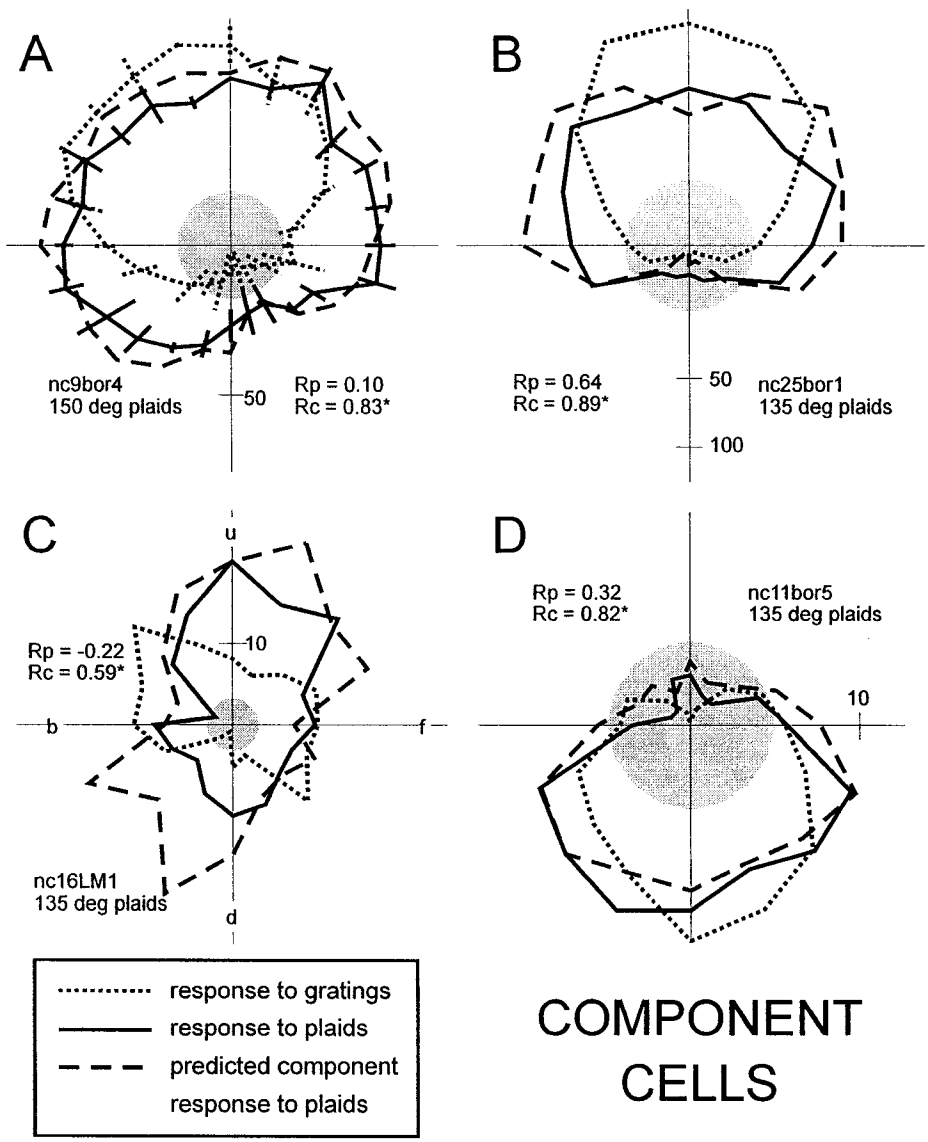

Figure 2.4

Polar plots illustrating the responses of component-selective nBOR (**A**, **B**, **D**) and LM (**C**) neurons to gratings and plaids. See legend to Figure 2.3 for details.

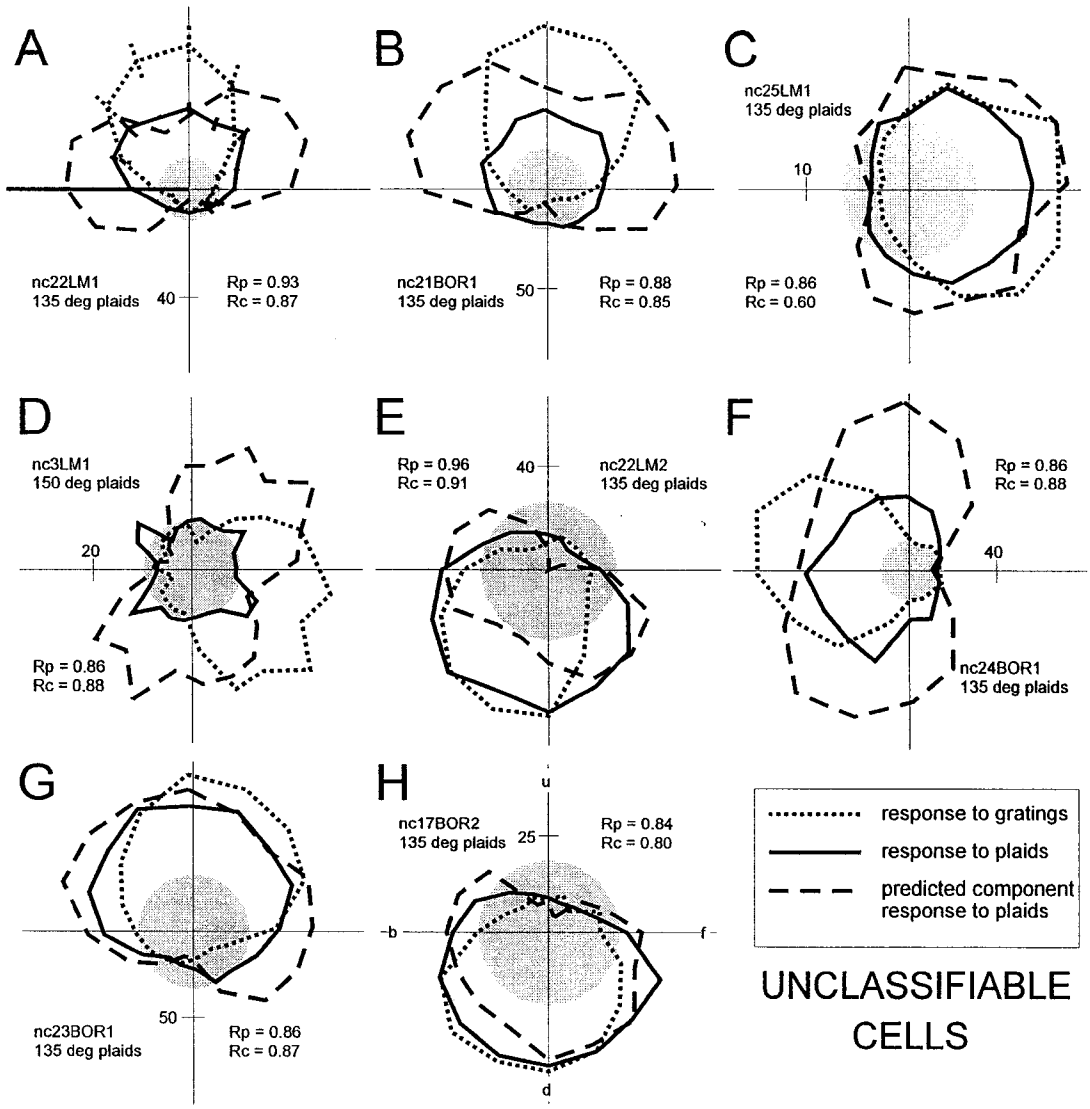

Figure 2.5

Polar plots illustrating the responses of unclassifiable neurons in LM (**A**, **C-E**) and nBOR (**B**, **F-H**) to gratings and plaids. See legend to Figure 2.3 for details. See text for detailed description.

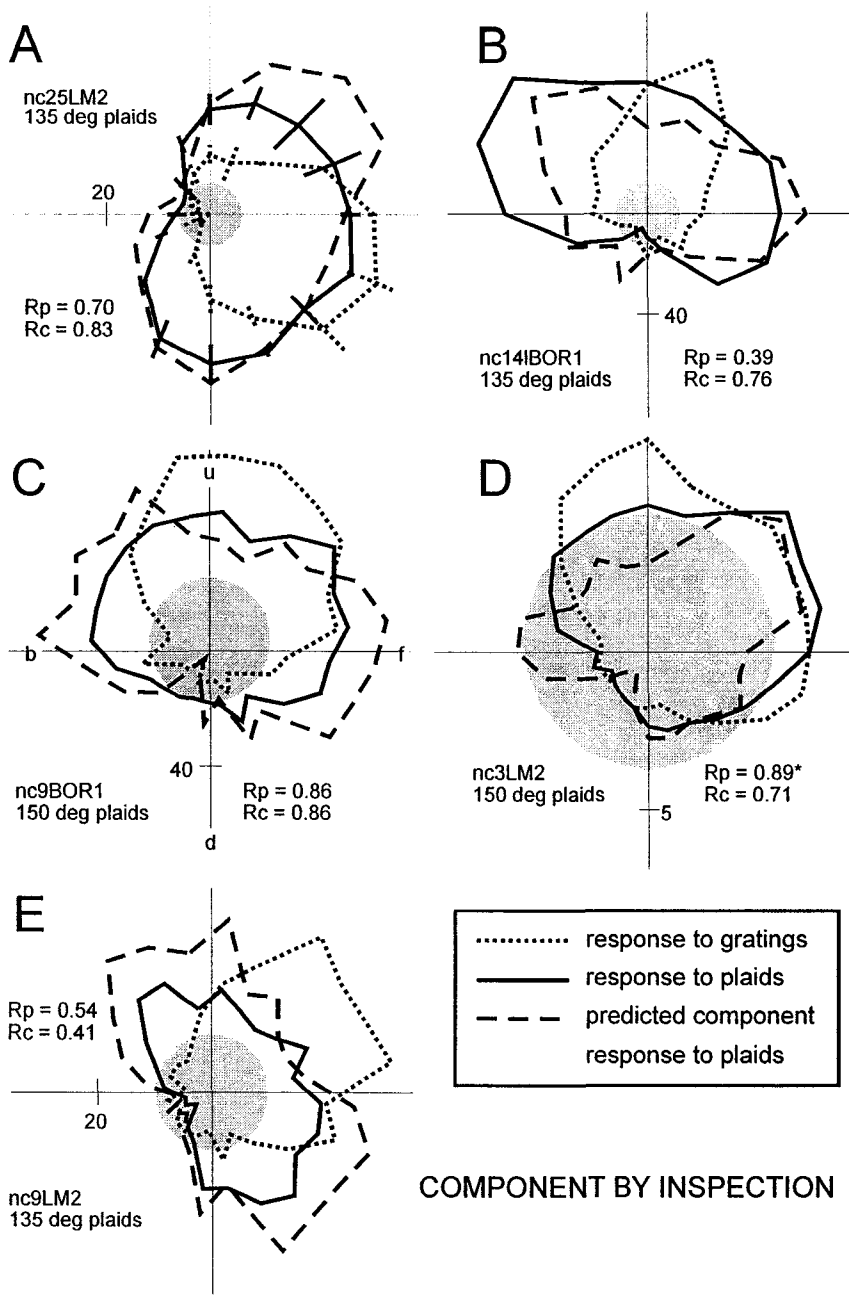

Figure 2.6

Polar plots illustrating the responses of neurons in nBOR (**B, C**) and LM (**A, D, E**) neurons to gratings and plaids. See legend to Figure 2.3 for details. For these neurons, although the response to plaids appears to match the predicted component response, these neurons were not classified as component-selective by the statistical criteria.

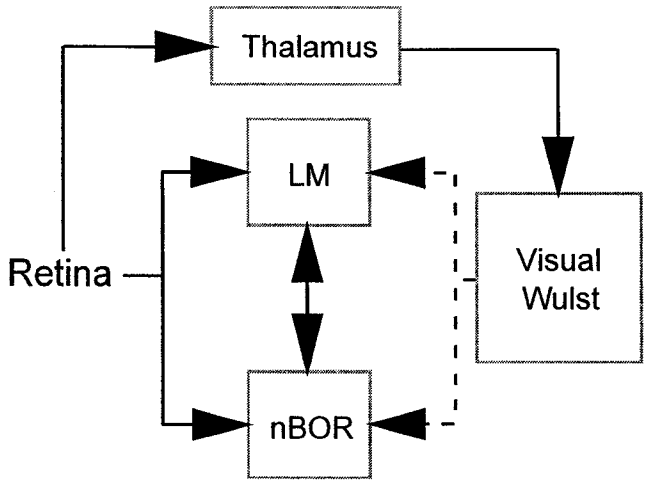

Figure 2.7

A simplified schematic of sources of visual information to the nucleus of the basal optic root (nBOR) of the accessory optic system, and pretectal nucleus lentiformis mesencephali (LM). The dashed lines represent weaker projections. See text for discussion.

References

Adelson EH, Movshon JA. Phenomenal coherence of moving visual patterns. *Nature* 300: 523-525, 1982.

Albright TD. Direction and orientation selectivity of neurons in visual area MT of the macaque. *J Neurophysiol* 52: 1106-1130, 1984.

Azevedo TA, Cukiert A, Britto LRG. A pretectal projection upon the accessory optic nucleus in the pigeon: an anatomical and electrophysiological study. *Neurosci Lett* 43: 13-18, 1983.

Burns S, Wallman J. Relation of single unit properties to the occulomotor function of the nucleus of the basal optic root (AOS) in chickens. *Exp Brain Res* 42: 171-180, 1981.

Brecha N, Karten HJ, Hunt SP. Projections of the nucleus of basal optic root in the pigeon: An autoradiographic and horseradish peroxidase study. *J Comp Neurol* 189: 615-670, 1980.

Clark PGH. Some visual and other connections to the cerebellum of the pigeon. *J Physiol* 243: 267-285, 1977.

Collewijn H. Optokinetic eye movements in the rabbit: input-output relations. *Vision Res* 9: 117-32, 1969.

Crow EL, Davis FA, Maxfield MW. *Statistics Manual, With Examples Taken from Ordinance Development*. New York: Dover, 1960.

Crowder NA, Wylie DRW. Fast and slow neurons in the nucleus of the basal optic root in pigeons. *Neurosci Let* 304: 133-136, 2001.

Ferrera VP, Wilson HR. Perceived direction of moving two-dimensional pattern. *Vision Res* 30: 273-287, 1990.

Fite KV, Reiner T, Hunt S. Optokinetic nystagmus and the accessory optic system of pigeon and turtle. *Brain Behav Evol* 16: 192-202, 1979.

Fite KV, Brecha N, Karten HJ, Hunt SP. Displaced ganglion cells and the accessory optic system of pigeon. *J Comp Neurol* 195: 279-88, 1981.

Frost BJ. Mechanisms for discriminating object motion from self-induced motion in the pigeon. In *Analysis of Visual Behavior* edited by Ingle DJ, Goodale MA, Mansfield JW. Cambridge: MIT Press, 1982, p. 177-196.

Frost BJ. Neural mechanisms for detecting object motion and figure-ground boundaries contrasted with self-motion detecting systems. In *Brain Mechanisms of Spatial Vision* edited by Ingle DJ, Jeannerod M, Lee D. Dordrecht: Matrinus Nijhoft, 1985, p. 415-449.

Frost BJ, Wylie DR, Wang Y-C. The processing of object and self-motion in the tectofugal and accessory optic pathways of birds. *Vision Res* 30: 1677-1688, 1990.

Frost BJ, Wylie DR, Wang Y-C. The analysis of motion in the visual systems of birds. In *Perception and Motor Control in Birds* edited by Green P, Davies M. Berlin: Springer-Verlag, 1994, p. 249-266.

Gamlin PDR, Cohen DH. The retinal projections to the pretectum in the pigeon (*Columba livia*). *J Comp Neurol* 269: 1-17, 1988a.

Gamlin PDR, Cohen DH. Projections of the retinorecipient pretectal nuclei in the pigeon (*Columba livia*). *J Comp Neurol* 269: 18-46, 1988b.

Gibson JJ. The visual perception of object motion and subjective movement. *Psychol Rev* 61: 304-314, 1954.

Gioanni H, Rey J, Villalobos J, Richard D, Dalbera A. Optokinetic nystagmus in the pigeon (*Columba livia*). II. Role of the pretectal nucleus of the accessory optic system. *Exp Brain Res* 50: 237-247, 1983a.

Gioanni H, Villalobos J, Rey J, Dalbera A. Optokinetic nystagmus in the pigeon (*Columba livia*). III. Role of the nucleus ectomammilaris (nEM): interactions in the accessory optic system. *Exp Brain Res* 50: 248-258, 1983b.

Gioanni H. Stabilizing gaze reflexes in the pigeon (Columba livia). I. Horizontal and vertical optokinetic eye (OKN) and head (OCR) reflexes. *Exp Brain Res* 69: 567-582, 1988.

Gizzi MS, Katz E, Schumer RA, Movshon JA. Selectivity for orientation and direction of motion of single neurons in cat striate and extrastriate visual cortex. *J Neurophysiol* 63: 1529-1543, 1990.

Grasse KL, Cyander MS. The accessory optic system in frontal-eyed animals. In *Vision and Visual Dysfunction. The Neuronal Basis of Visual Function* edited by Leventhal A. New York: McMillan, 1990, p. 111-139.

Hoffmann KP, Distler C, Erickson RG. Functional projections from striate cortex and superior temporal sulcus to the nucleus of the optic tract (NOT) and dorsal terminal nucleus of the accessory optic tract (DTN) of macaque monkeys. *J Comp Neurol* 313: 707-724, 1991.

Hollander H, Tietze J, Distel H. An autoradiographic study of the subcortical projections of the rabbit striate cortex in the adult and during postnatal development. *J Comp Neurol* 184: 783-794, 1979.

Huerta MF, Weber JT, Rothstein LR, Harting JK. Subcortical connections of area 17 in the tree shrew: an autoradiographic analysis. *Brain Res* 340: 163-170, 1985.

Ibbotson MR, Mark RF, Maddess TL. Spatiotemporal response properties of direction-selective neurons in the nucleus of the optic tract and the dorsal terminal nucleus of the wallaby, *Macropus eugenii*. *J Neurophysiol* 72: 2927-2943, 1994.

Ilg UJ, Hoffmann KP. Functional grouping of the cortico-pretectal projection. J Neurophysiol 70: 867-869, 1993.

Karten HJ, Hodos W. *A stereotaxic Atlas of the Brain of the Pigeon (Columba livia)*. Baltimore: Johns Hopkins Press, 1967.

Karten HJ, Fite KV, Brecha N. Specific projection of displaced retinal ganglion cells upon the accessory optic system in the pigeon (*Columba livia*). *Proc Natl Acad Sci* 74: 1752-1756, 1977.

Karten HJ, Shimizu T. The origins of the neocortex: connections and lamination as distinct events in evolution. *J Cognitive Neurosci* 1: 291-301, 1989.

Lent R. The organization of subcortical projections of the hamster's visual cortex. *J Comp Neurol* 206: 227-242, 1982.

Lui F, Giolli RA, Blanks RH, Tom EM. Pattern of striate cortical projections to the pretectal complex in the guinea pig. *J Comp Neurol* 344: 598-609, 1994.

McKenna OC, Wallman J. Functional postnatal changes in avian brain regions responsive to retinal slip: a 2-deoxy-D-glucose study. *J Neurosci* 5:330-342, 1985.

Merabet L, Desautels A, Minville K, Casanova C. Motion integration in a thalamic visual nucleus. *Nature* 396:265-268, 1998.

Miceli D, Gioanni H, Reperant J, Peyrichoux J. The avian visual wulst: I. An anatomical study of afferent and efferent pathways. II. An electrophysiological study of the functional properties of single neurons. In *Neural Mechanisms of Behavior of the Pigeon* edited by Granda, AM, Maxwell JH. New York: Plenum Press, 1979, p. 223-354.

Morgan B, Frost BJ. Visual response properties of neurons in the nucleus of the basal optic root of pigeons. *Exp Brain Res* 42: 184-188, 1981.

Movshon JA, Adelson EH, Gizzi MS, Newsome WT. The analysis of visual moving patterns. In *Study group on pattern recognition mechanisms* edited by Chagas C, Gattass R, Gross C. Vatican City: Pontificia Academia Scientiarum, 1985, p. 117-151.

Mustari MJ, Fuchs AF, Kaneko CR, Robinson FR. Anatomical connections of the primate pretectal nucleus of the optic tract. *J Comp Neurol* 349: 111-128, 1994.

Papoulis A. *Probability and Statistics*. New York: Prentence-Hall International Editions, 1990.

Pereira A, Volchan E, Vargas CD, Penetra L, Rocha-Miranda CE. Cortical and subcortical influences on the nucleus of the optic tract of the opossum. *Neurosci* 95: 953-963, 2000.

Reiner A, Brecha N, Karten HJ. A specific projection of retinal displaced ganglion cells to the nucleus of the basal optic root in the chicken. *Neurosci* 4: 1679-88, 1979.

Rio JP, Villalobos J, Miceli D, Reperant J. Efferent projections of the visual wulst upon the nucleus of the basal optic root in the pigeon. *Brain Res* 271: 145-151, 1983.

Rodman HR, Albright TD. Single-unit analysis of pattern-motion selective properties in the middle temporal visual area (MT). *Exp Brain Res* 75: 53-64, 1989.

Scannell JW, Sengpiel F, Tovee MJ, Benson PJ, Blakemore C, Young MP. Visual motion processing in the anterior ectosylvian sulcus of the cat. *J Neurophysiol* 76: 895-907, 1996.

Schoppmann A. Projections from areas 17 and 18 of the visual cortex to the nucleus of the optic tract. *Brain Res* 223: 1-17, 1981.

Shintani T, Hoshino K, Meguro R, Kaiya T, Norita M. A light and electron microscopic analysis of the convergent retinal and visual cortical projections to the nucleus of the optic tract (NOT) in the pigmented rat. *Neurobiology* 7: 445-460, 1999.

Stoner GR, Albright TD. Neural correlates of perceptual motion coherence. *Nature* 358: 412-414, 1992.

Stoner GR, Albright TD. Visual Motion Integration. In V*isual Detection of Motion* edited by Smith TA, Snowden RJ. London: Academic, 1994, p. 253-290.

Simpson JI. The accessory optic system. *A Rev Neurosci* 7: 13-41, 1984.

Simpson JI, Leonard CS, Soodak RE. The accessory optic system: II. Spatial organization of direction selectivity. *J Neurophysiol* 60: 2055-2072, 1988.

Smith AT, Harris LR. Use plaid patterns to distinguish the cortical and direct retinal inputs to the brainstem optokinetic nystagmus generator. *Exp Brain Res* 86: 324-332, 1991.

Welch L. The perception of moving plaids reveals two motion-processing stages. *Nature* 337: 734-736, 1989.

Wilson P. The organization of the visual hyperstriatum in the domestic chick. II. Receptive field properties of single units. *Brain Res* 188: 333-345, 1980.

Winterson BJ, Brauth SE. Direction selective single units in the nucleus lentifomis mesencephali of the pigeon (*Columba livia*). *Exp Brain Res* 60: 215-226, 1985.

Wolf-Oberhollenzer F, Kirschfeld K. Motion sensitivity in the nucleus of the basal optic root of the pigeon. *J Neurophysiol* 71: 1559-1573, 1994.

Wylie DR, Crowder NA. Spatiotemporal properties of fast and slow neurons in the pretectal nucleus lentiformis mesencephali in pigeons. *J Neurophysiol* 84: 2529-2540, 2000.

Wylie DR, Frost BJ. Visual response properties of neurons in the nucleus of the basal optic root of the pigeon: A quantitative analysis. *Exp Brain Res* 82: 327-336, 1990.

Wylie DR, Linkenhoker B, Lau KL. Projections of the nucleus of the basal optic root in pigeons (*Columba livia*) revealed with biotinylated dextran amine. *J Comp Neurol* 384: 517-536, 1997.

Zolotilina EG, Eremina SV, Orlov IV. Horizontal optokinetic nystagmus in the pigeon during static tilts in the frontal plane. *Neuroscience & Behavioral Physiology* 25: 300-306, 1995.

Chapter 3

Fast and Slow Neurons in the Nucleus of the Basal Optic Root in Pigeons

A version of this chapter has been published. Crowder NA, Wylie DRW. 2001. Neuroscience Letters. 304: 133-136.

Introduction

The pretectum and the Accessory Optic System (AOS) are involved in the analysis of optic flow and the generation of the optokinetic response (OKR; for reviews see Grasse and Cynader, 1990; Simpson, 1984; Simpson et al., 1988). Neurons in the nucleus of the basal optic root (nBOR) of the AOS and the pretectal nucleus lentiformis mesencephali (LM) exhibit direction-selectivity in response to largefield stimuli moving in the contralateral visual field (Burns and Wallman, 1981; Gioanni et al., 1984; Morgan and Frost, 1981; Winterson and Brauth, 1985; Wylie and Frost, 1990). Wylie and Crowder (2000) examined the responses of pigeon LM neurons to drifting sine-wave gratings varying in spatial and temporal frequency (SF, TF). Two groups of neurons were found: *fast* neurons preferred low SFs/high TFs (0.03-0.25 cycles per degree (cpd), 0.5-16 Hz) and *slow* neurons preferred high SFs/low TFs (0.35-2 cpd, 0.125-2 Hz). Fast and slow neurons have also been found in the nucleus of the optic tract (NOT), the mammalian homolog of the LM (Ibbotson et al., 1994). Wolf-Oberhollenzer and Kirschfeld (1994) examined the responses of pigeon nBOR neurons to drifting sine wave gratings but the SF range used (0.024 to 0.185 cpd) did not encompass that of the slow LM neurons. In the present study, we recorded from pigeon nBOR neurons in response to drifting sine wave gratings using a broad range of SFs and TFs. We found that, as is the case in LM, there are fast and slow cells in the nBOR.

Methods

The methods employed conformed to the Guidelines established by the Canadian Council on Animal Care and were approved by the University of Alberta Biosciences

Animal Welfare Committee. Details for anaesthesia, extracellular recording, stimulus presentation and data analysis have been described by Wylie and Crowder (2000; Appendix 1). Briefly, pigeons were anaesthetized with a ketamine (65 mg/kg) - xylazine (8 mg/kg) mixture (i.m.) and supplemental doses were administered as necessary. The animals were placed in a stereotaxic device and sufficient bone and dura were removed to expose the brain and allow access to the nBOR based on the pigeon stereotaxic atlas (Karten and Hodos, 1967). Recordings were made with either tungsten microelectrodes (10μm exposed tips; impedance 2-5MΩ) or glass micropipettes filled with 2M NaCl (tip diameter 4-5μm; impedance 2-5MΩ). The extracellular signal was amplified, filtered, displayed on an oscilloscope and fed to a window discriminator. TTL pulses representing single spikes were fed to a 1401*plus* (Cambridge Electronic Designs (CED)) and peri-stimulus time histograms were constructed with *Spike2* software (CED). The stimuli were high contrast (0.95) sine wave gratings produced using a visual stimulus generator (VSG*Three*, Cambridge Research Services). The stimuli were displayed on a SONY multiscan 17se II monitor that was placed 35cm from the bird (50° X 40° visual angle) or backprojected by an *InFocus* LP750 projector onto a tangent screen placed 50 cm from the bird (90° X 75°). Once a responsive cell was isolated, a directional tuning curve (15° or 22.5° increments) was obtained using gratings of an effective SF and TF. Each neuron's direction preference was calculated from the best-fit cosine. Subsequently, the spatio-temporal properties were determined by presenting gratings in the preferred and anti-preferred directions. Several different SFs (0.015-2 cpd) were presented at several different TFs (0.15-16 Hz). Each sweep consisted of 4-5s motion in the preferred direction, a 3-5s pause, 4-5s of motion in the anti-preferred direction, followed by a 3-5s

pause. Firing rates were averaged from at least 3 sweeps. Contour plots of the mean firing rate in the spatio-temporal domain were made using *Sigma Plot*. The maximum in the contour plot was used to assign the preferred SF/TF combination for each neuron. At the end of the experiments, the birds were given an overdose of sodium pentobarbitol (100 mg/kg i.p.) and immediately perfused with saline followed by 4% para-formaldehyde. The brains were extracted and sectioned such that the electrode tracts could be localized using light microscopy.

Results

We recorded from 32 nBOR neurons. The average spontaneous rate (SR) was 35 spikes/s (range = 11-70 spikes/s). Spatio-temporal contour plots for both the preferred and anti-preferred directions were obtained for all neurons. Because, for most neurons, largefield motion in the preferred direction elicits excitation and motion in the anti-preferred direction inhibits the spontaneous activity, we refer to these as excitatory response plots (ER plots) and inhibitory response plots (IR plots), respectively. Figure 3.1 shows ER and IR plots of three neurons. For the majority of contour plots, there was a single peak in the spatio-temporal domain (e.g. ER plots of Fig. 3.1A,C; IR plot of Fig. 3.1C). The ER plot in Figure 3.1B contains two clear peaks. Similarly, the IR plot in Figure 3.1A also contains two peaks of approximately equal size. In total, 13 ER plots and 10 IR plots showed multiple peaks. Wylie and Crowder (2000) reported similar properties for LM neurons (26% of the ER and IR plots had multiple peaks).

In some cases, for a given neuron, the ER plot was similar to the IR plot. That, is the SF/TF combination that elicited maximal excitation to motion in the preferred

direction also elicited maximal inhibition when moved in the anti-preferred direction (e.g. Fig 3.1C). However, this was not the norm. For example, in Fig. 3.1B, the peak in the ER plot was at mid-high SFs and low TFs, whereas the peak in the IR plot was at mid-high SFs and mid-TFs. Of the 28 neurons for which we obtained both ER and IR plots, 19 (68%) had markedly different spatio-temporal response profiles for the ER and IR. Wylie and Crowder (2000) found that the proportion of LM neurons showing an independence of IR and ER was even higher (81%).

In Figure 3.2 the locations of the response maxima are shown for the ER and IR plots of nBOR neurons. For those contour plots in which there were multiple peaks, the location of the primary peak was plotted. One IR and one ER plot that had multiple minima/maxima of equal size was excluded from this analysis, as was one IR plot that showed a broad plateau. On the upper left, the peaks from the nBOR ER plots are shown. A Ward's cluster analysis with squared-Euclidean distance measures revealed two distinct clusters. Ten neurons comprised a group that preferred low-mid SFs (0.031-0.125 cpd) and TFs in the range of 0.125-4 Hz. The second group consisted of 21 neurons that preferred mid-high SFs (0.3-1 cpd) and TFs in the range of 0.063-2 Hz. We refer to these groups as fast and slow ERs, respectively (velocity = TF/SF). The average SF, TF and velocity of the fast ERs were, 0.074 cpd, 0.76 Hz and 10.2 °/s, respectively. The average SF, TF and velocity of the slow neurons were, 0.56 cpd, 0.33 Hz and 0.59 °/s, respectively.

The upper right section of Figure 3.2 shows locations of the peaks from the nBOR IR plots. Like the ERs, the locations of the peak IRs fell into two groups, although the clustering is not as obvious (there are two peaks at high TFs that are outliers from both

groups). The average SF, TF and velocity of the 8 fast IRs were, 0.068 cpd, 0.68 Hz and 9.9 °/s, respectively. The average SF, TF and velocity of the 16 slow IRs were, 0.51 cpd, 0.48 Hz and 0.94 °/s, respectively. The average TFs of these two groups were not significantly different (t-test, p=0.36).

The lower half of Figure 3.2 shows the locations of the peak ERs and IRs for LM neurons (from Wylie and Crowder, 2000). The ERs of LM neurons clustered into fast and slow groups, however, the IRs of LM neurons do not. Note the higher proportion of LM neurons (61%) with fast ERs compared to the nBOR sample (32%). The ERs of the slow LM and nBOR neurons were not significantly different with respect to average SF, TF or velocity. The ERs of the fast LM and nBOR neurons were not significantly different with respect to average SF, however the average TF and velocity were significantly lower for the fast nBOR neurons (TF; nBOR, 0.76 Hz; LM, 2.88 Hz; $p < .01$: velocity; nBOR, 10.2 °/s; LM, 29.2 °/s; $p < .05$).

Discussion

Previous research has shown that the pigeon LM and nBOR are complementary with respect to direction preference of neurons. In the nBOR, neurons preferring upward, downward and backward (nasal to temporal) motion are equally abundant, but neurons that prefer forward (temporal to nasal) motion are rare (<10%) (Gioanni et al., 1984; Wylie and Frost, 1990). In contrast, most neurons (~50%) in LM prefer forward motion, fewer neurons prefer backward motion, and neurons that prefer upward or downward motion are the least common (Fu et al., 1998a,b; Winterson and Brauth, 1985; Wylie and Crowder, 2000). Figure 3.2 also shows the direction preference of each neuron. There is a

clear interaction between the spatio-temporal preference and the direction preference for both LM and nBOR neurons. With respect to direction preference, in both LM and nBOR, it is the most common cell types that prefer slow stimuli. As seen in the plots of the peak ERs, forward cells are slow cells in the LM. Upward, downward, and backward cells are slow cells in the nBOR. Fast cells code all directions in both nuclei.

The fact that the LM contains more neurons responsive to fast stimuli than does the nBOR, and the fact that the fast LM ERs prefer faster stimuli than their nBOR counterparts, is consistent with behavioral observations. In pigeons, the gain of the OKR in response to nasal to temporal (forward) motion does not decline until velocities of 20-40 °/s. In contrast, the gain declines at lower velocities for stimuli moving backward, upward and downward (Gioanni et al., 1981; Gioanni, 1988). Furthermore, and consistent with our physiological findings, lesion experiments by Gioanni et al. (1983a,b, 1984) showed that the LM is important for generating the OKR to stimuli drifting forward in the contralateral eye, whereas the nBOR is involved in driving the OKR to stimuli drifting upward, downward or backward.

Ibbotson et al. (1994) found fast and slow neurons in the NOT in the wallaby. The discovery of fast and slow neurons in the nBOR suggests that this functional division is not a specific feature of pretectal neurons but of all optokinetic nuclei. Thus, we predict that fast and slow cells would be found in the mammalian AOS as well.

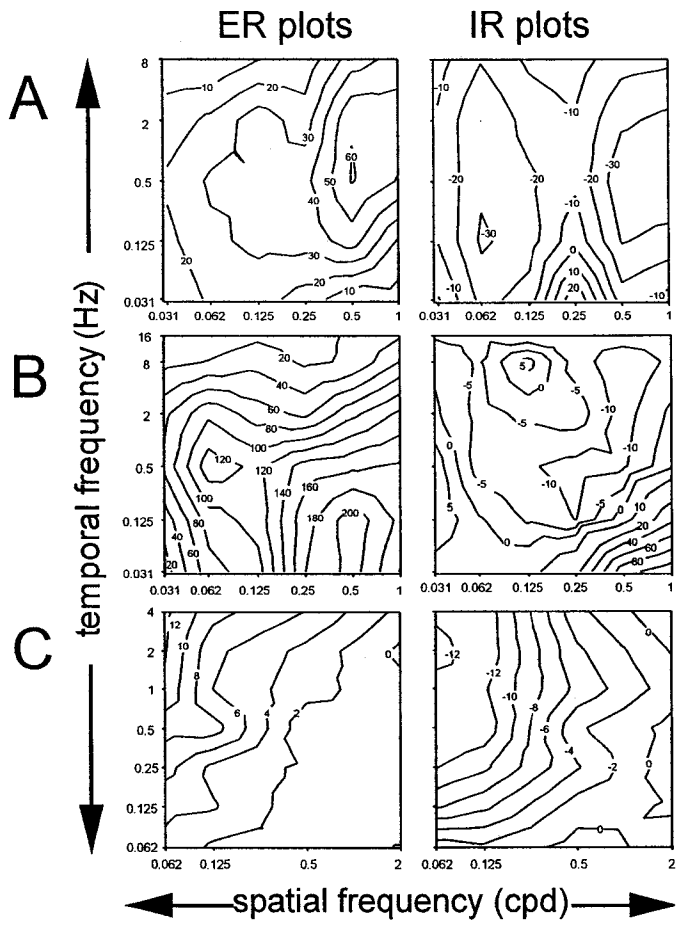

Figure 3.1

Spatio-temporal tuning of neurons in nucleus of the basal optic root (nBOR). **A-C** show contour plots of the responses of three nBOR neurons to gratings of varying Spatial Frequency (abscissa) and Temporal Frequency (ordinate) drifting in the preferred (ER plots) and anti-preferred (IR plots) directions. The scale on the iso-contour lines represents the firing rate (spikes/s) above (+) or below (-) the spontaneous rate. The spontaneous rates for the cells in A, B and C were 70, 21, and 17.5 spikes/s, respectively.

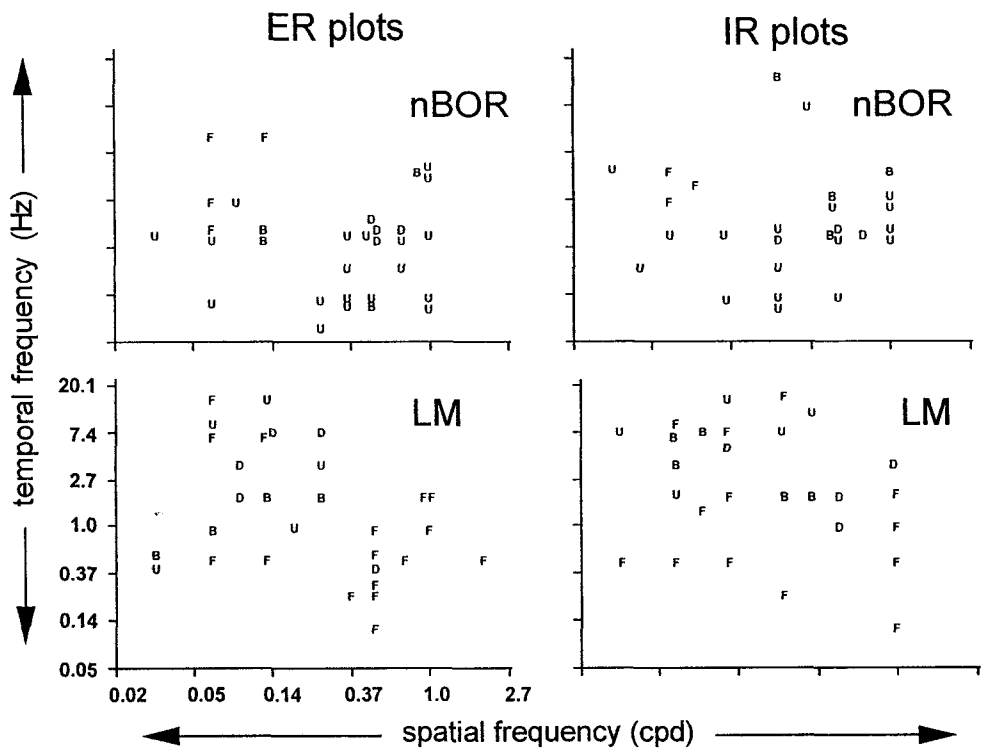

Figure 3.2

Locations of the peak excitatory and inhibitory responses of neurons in nucleus of the basal optic root (nBOR) to gratings of varying Spatial Frequency (abscissa) and Temporal Frequency (ordinate). In top-left and top-right, respectively, the locations of the peaks are shown for the ER plots and the IR plots of nBOR neurons. In bottom-left and bottom-right, respectively, the locations of the peaks are shown for the ER plots and the IR plots of neurons in the lentiformis mesencephali of pigeons (data from Wylie and Crowder, 2000). Included in this analysis are ER and IR plots that showed single peaks, as well as those that showed multiple peaks where there was a clear primary peak. (The locations of the primary peaks, but not the secondary peaks, are plotted). Locations of peak responses are indicated with a letter corresponding to the preferred direction of the cell (F = forward (temporal to nasal), B = backward, U = upward, D = downward

motion). Note that for the IR plots, (responses to motion in the anti-preferred direction), the preferred direction of the cell is indicated.

References

Burns S, Wallman J. Relation of single unit properties to the oculomotor function of the nucleus of the basal optic root (AOS) in chickens. *Exp Brain Res* 42: 171-180, 1981.

Fu YX, Gao HF, Guo MW, Wang SR. Receptive field properties of visual neurons in the avian nucleus lentiformis mesencephali. *Exp Brain Res* 118: 279-285, 1998a.

Fu YX, Xiao Q, Gao HF, Wang SR. Stimulus features eliciting visual responses from neurons in the nucleus lentiformis mesencephali in pigeons. *Vis Neurosci* 15: 1079-1087 1998b.

Gioanni H. Stabilizing gaze reflexes in the pigeon *(Columba livia)*. I. Horizontal and vertical optokinetic eye (OKN) and head (OCR) reflexes. *Exp Brain Res* 69 567-582, 1988.

Gioanni H, Rey J, Villalobos J, Bouyer JJ, Gioanni Y. Optokinetic nystagmus in the pigeon (*Columba livia)*. I. Study in monocular and binocular vision. *Exp. Brain Res* 44: 362-370, 1981.

Gioanni H, Rey J, Villalobos J, Dalbera A. Single unit activity in the nucleus of the basal optic root (nBOR) during optokinetic, vestibular and visuo-vestibular stimulations in the alert pigeon (*Columba livia*). *Exp Brain Res* 57: 49-60, 1984.

Gioanni H, Rey J, Villalobos J, Richard D, Dalbera A. Optokinetic nystagmus in the pigeon (*Columba livia*). II. Role of the pretectal nucleus of the accessory optic system. *Exp Brain Res* 50: 237-247, 1983a.

Gioanni H, Villalobos J, Rey J, Dalbera A. Optokinetic nystagmus in the pigeon (*Columba livia*). III. Role of the nucleus ectomammilaris (nEM): interactions in the accessory optic system. *Exp Brain Res* 50: 248-258, 1983b.

Grasse KL, Cyander MS. The accessory optic system in frontal-eyed animals. In: *Vision and Visual Dysfunction. The Neuronal Basis of Visual Function*, edited by Leventhal A. New York, NY: McMillan, 1990, p. 111-139.

Ibbotson MR, Mark RF, Maddess TL. Spatiotemporal response properties of direction-selective neurons in the nucleus of the optic tract and the dorsal terminal nucleus of the wallaby, *Macropus eugenii*. *J Neurophysiol* 72: 2927-2943, 1994.

Karten HJ, Hodos W. *A stereotaxic Atlas of the Brain of the Pigeon* (*Columba livia*). Baltimore: Johns Hopkins Press, 1967.

Morgan B, Frost BJ. Visual response properties of neurons in the nucleus of the basal optic root of pigeons. *Exp Brain Res* 42: 184-188, 1981.

Simpson JI. The accessory optic system. *A Rev Neurosci* 7: 13-41, 1984.

Simpson JI, Giolli RA, Blanks RHI. The pretectal nuclear complex and the accessory optic system. In *Neuroanatomy of the Oculomotor System* edited by Buttner-Ennever JA. Amsterdam: Elsevier, 1988, p.335-364.

Winterson BJ, Brauth SE. Direction-selective single units in the nucleus lentiformis mesencephali of the pigeon (Columba livia). *Exp Brain Res* 60: 215-226, 1985.

Wolf-Oberhollenzer F, Kirschfeld K. Motion sensitivity in the nucleus of the basal optic root of the pigeon. *J Neurophysiol* 71: 1559-1573, 1994.

Wylie DR, Crowder NA. Spatiotemporal properties of fast and slow neurons in the pretectal nucleus lentiformis mesencephali in pigeons. *J Neurophysiol* 84: 2529-2540, 2000.

Wylie DR, Frost BJ. Visual response properties of neurons in the nucleus of the basal optic root of the pigeon: A quantitative analysis. *Exp Brain Res* 82: 327-336, 1990.

Chapter 4

Temporal Frequency and Velocity-Like Tuning in the Pigeon Accessory Optic System

A version of this chapter has been accepted for publication. Crowder NA, Dawson MR, Wylie DRW. Journal of Neurophysiology. In Press.

Introduction

The pretectum and the accessory optic system (AOS) have been implicated in the processing of the visual consequences of self-motion, known as optic flow (Gibson, 1954), and the generation of the optokinetic response (OKR) to facilitate retinal image stabilization (for reviews see Grasse and Cynader, 1990; Simpson, 1984; Simpson et al., 1988). The AOS and pretectum are highly conserved in vertebrates. The mammalian pretectal nucleus of the optic tract (NOT) is homologous to the nucleus lentiformis mesencephali (LM) in birds, whereas the avian nucleus of the basal optic root (nBOR) of the AOS is homologous to the medial and lateral terminal nuclei (MTN, LTN) of the mammalian AOS (Fite, 1985; McKenna and Wallman, 1985a; Simpson, 1984; Simpson et al., 1988; Weber, 1985). In numerous species, it has been shown that pretectal and AOS neurons have large receptive fields in the contralateral eye, and exhibit direction-selectivity to moving large-field stimuli (NOT: Collewijn, 1975a,b; Hoffmann and Schoppmann, 1981; Mustari and Fuchs, 1990; Volchan et al., 1989; LM: Fan et al., 1995; Fite et al., 1989; Katte and Hoffmann, 1980; McKenna and Wallman, 1985b; Winterson and Brauth, 1985; Wylie and Frost, 1996; MTN/LTN: Cooper and Magnin, 1986; Grasse and Cynader, 1982; Grasse et al., 1984; Natal and Britto, 1987; Soodak and Simpson, 1988; nBOR: Burns and Wallman 1981; Gioanni et al. 1984; Morgan and Frost 1981; Rosenberg and Ariel, 1990; Wylie and Frost 1990a). The AOS and pretectum provide input to olivo-vestibulocerebellar pathways that respond best to patterns of optic flow resulting from self-translation and self-rotation (Graf et al., 1988; Simpson et al., 1981; Wylie and Frost, 1993, 1999; Wylie et al., 1993, 1998).

Using large-field drifting sine wave gratings of varying spatial frequency (SF) and temporal frequency (TF), a few studies have shown that AOS and pretectal neurons are tuned in the spatio-temporal domain. Ibbotson et al. (1994) recorded from the NOT of wallabies and found that there were two groups of neurons: those that preferred high SFs and low TFs vs. those that preferred low SFs and high TFs. As velocity = TF/SF, these two groups were referred to as "slow" and "fast" neurons, respectively. Strikingly similar observations were found in the pigeon LM and nBOR (Crowder and Wylie, 2001; Wylie and Crowder, 2000). Wolf-Oberhollenzer and Kirschfeld (1994) also recorded the responses of pigeon nBOR neurons to sine wave gratings, but they used a restricted range of SFs (<0.185 cpd), which did not include the SFs that maximally stimulate slow neurons (0.25-2Hz in pigeon nBOR and LM, and wallaby NOT; Crowder and Wylie, 2001; Ibbotson et al., 1994; Wylie and Crowder, 2000;). Both Ibbotson et al. (1994) and Wolf-Oberhollenzer and Kirschfeld (1994) emphasized that neurons were tuned to TF rather than stimulus velocity, consistent with the "correlation" model of motion detection (Barlow and Levick, 1965; Reichardt, 1957, 1961; van Santen and Sperling, 1985) as opposed to the "gradient" models, which predict velocity tuning over a broad range of SFs and TFs (e.g. Buchner, 1984; Marr and Ullmann, 1981; Srinivasan, 1990).

In the present study we recorded the responses of neurons in the pigeon nBOR to drifting sine wave gratings, but used a broader range of SFs than those used by Wolf-Oberhollenzer and Kirschfeld (1994). We found that, whereas the fast cells were tuned to TF, the responses of the slow cells were more closely related to velocity than to TF. Although is has been assumed that the correlation model of motion detection (Barlow and Levick, 1965; Reichardt, 1957, 1961; van Santen and Sperling, 1985) is not well suited

for the measurement of image velocity, some versions of the correlation model produce responses which are dependent on image speed (eg. Zanker et al., 1999). The data are discussed with regard to these recent elaborations of the correlation model of motion detection.

Methods

Surgery and Extracellular recording

The methods employed conformed to the Guidelines established by the Canadian Council on Animal Care and were approved by the Biosciences Animal Welfare and Policy Committee at the University of Alberta. Details for anaesthesia, extracellular recording, stimulus presentation and data analysis have been described by Wylie and Crowder (2000; Appendix 1). Briefly, pigeons were anaesthetized with a ketamine (65 mg/kg) - xylazine (8 mg/kg) mixture (i.m.) and supplemental doses were administered as necessary. Based on the pigeon stereotaxic atlas (Karten and Hodos, 1967), sufficient bone and dura were removed to access the nBOR with vertical penetrations. Recordings were made with tungsten microelectrodes (2-5MΩ impedance) or glass micropipettes filled with 2M NaCl (tip diameters 4-5 microns; impedance 2-5MΩ). The extracellular signal was amplified, filtered, displayed on an oscilloscope and fed to a window discriminator. TTL pulses representing single spikes were fed to a 1401*plus* (Cambridge Electronic Designs (CED)) and peri-stimulus time histograms were constructed with *Spike2* software (CED).

Stimulus Presentation

After neurons in the nBOR were isolated, the direction preference and the approximate locations of the receptive field boundaries were qualitatively determined by moving a large ($90^{o} \times 90^{o}$) hand-held stimulus in various areas of the visual field. Directional tuning and spatio-temporal tuning were determined quantitatively with sine-wave gratings that were generated by a VSG*Three* graphics computer (Cambridge Research Designs, Cambridge UK), and back-projected onto a tangent screen that was located 50cm from the bird ($90^{o} \times 75^{o}$). Direction tuning was tested using gratings of an effective SF and TF at 15^{o} or 22.5^{o} increments, while spatio-temporal tuning was tested using gratings of varying SF (0.03-2 cycles per degree (cpd)) and TF (0.03-16 cycles per second (Hz)) moving in the preferred and anti-preferred directions. Each sweep consisted of 4 sec of motion in one direction, a 3 sec pause, 4 sec of motion in the opposite direction, followed by a 3 sec pause. Firing rates were averaged over 3-5 sweeps. Contour plots of the mean firing rate in the spatio-temporal domain were made using *Sigma Plot*.

Histology

In some cases, when tungsten microelectrodes were used, electrolytic lesions were placed at the recording site (30μA for 8-10 seconds, electrode positive). At the end of each experiment, animals were given a lethal dose of sodium pentobarbitol (100 mg/kg i.p.) and immediately perfused with saline followed by 4% para-formaldehyde. Brains were extracted, post-fixed for 2-12 hours (4% para-formaldehyde with 20% sucrose) and then left in 30% sucrose for at least 24 hours. Frozen sections (45 μm thick in the

coronal plane) through the nBOR were collected. Sections were mounted onto gelatine-coated slides, and counterstained with neutral red. Light microscopy was used to localize electrode tracts and lesion sites.

Results

Extensive quantitative data, including directional and spatio-temporal tuning to sine wave gratings of varying SF and TF, was obtained from 53 nBOR neurons in 26 animals. Most neurons, although broadly tuned, were excited in response to motion in a particular direction ("preferred" direction) and inhibited below the spontaneous rate (SR) in response to motion in the (approximately) opposite direction (anti-preferred direction). Each neuron's direction preference was assigned by calculating the maximum of the best cosine fit to the tuning curve. As shown in figure 4.1, there was an obvious clustering into four groups. Five (9%), 9 (17%), 15 (28%) and 24 (45%) neurons preferred forward (temporal to nasal), backward (nasal to temporal), downward, and upward motion, respectively. These data are in agreement with previous studies of the pigeon nBOR. Wylie and Frost (1990a) found that upward, downward and backward cells are equally abundant, but forward cells were rare (see also, Gioanni et al., 1984; Rosenberg and Ariel, 1990). It has been noted that a small subpopulation of nBOR neurons have binocular receptive fields and respond best to particular patterns of optic flow resulting from either self-rotation or self-translation (Wylie and Frost, 1990b, 1999; Wylie et al., 1998). No such neurons were recorded in the present study.

Spatio-temporal Properties of nBOR neurons

Figure 4.2 shows the responses of an nBOR neuron to gratings drifting in the preferred (up) and anti-preferred (down) directions. PSTHs to 36 combinations of SF (abscissa) and TF (ordinate) are shown. Each PSTH is for a single sweep, where each sweep consisted of 4 sec motion in the preferred direction (upward motion, solid line), followed by a 3 sec pause, followed by 4 sec of motion in the anti-preferred direction (downward motion, broken line). Note that this cell showed strong excitation to motion in the preferred direction and strong inhibition to motion in the anti-preferred direction. The neuron responded to several of the gratings, but the degree of the excitation and inhibition was variable. Note that for 1cpd/0.03Hz the neuron showed excitation rather than inhibition to motion in the anti-preferred direction. The asterisk (*) and pound (#) symbols respectively indicate the peak excitatory and inhibitory responses in the spatio-temporal domain (0.25cpd/0.125Hz) based on the average firing rate over the 4 sec epoch. This average encompassed the steady-state and transient responses during the epoch. An onset transient, variable in size, was present in response to motion in the preferred direction for most gratings. Onset transients to motion in the anti-preferred direction were less common, as were offset transients to motion in the both directions. In this report we do not further address these transients and other temporal factors (such as oscillations in the responses apparent in some PSTHs in Fig. 4.2). (Wolf-Oberhollenzer and Kirschfeld (1994), Ibbotson et al. (1994), Price and Ibbotson (2002) provided extensive descriptions of temporal factors).

To graphically illustrate tuning in the spatio-temporal domain, contour plots were constructed for both the preferred and anti-preferred directions (see Fig. 4.3). Because large-field motion in the preferred direction elicits excitation and motion in the anti-

preferred direction elicits inhibition, we refer to these as excitatory response plots (ER plots) and inhibitory response plots (IR plots), respectively. TF and SF were plotted on the ordinate and abscissa, respectively, and firing rate (relative to the SR) was plotted on the z-axis. The diagonal lines overlaying the contour plots indicate particular velocities (TF/SF). In these plots, the black represents the SR, red represents excitation, and green represents inhibition. Progressively brighter and less saturated reds/greens represent greater magnitudes of excitation/inhibition, such that the peaks are shown as off-white. The neurons shown in figure 4.3A and B clearly had two peaks in their ER plots. For the neuron in figure 4.3A there was a primary peak at 1cpd/0.5Hz (60 spikes/s) and a smaller secondary peak at 0.125cpd/16Hz (20 spikes/s). For the neuron in figure 4.3B there was a primary peak at 0.063cpd/16Hz (45 spikes/s) and a smaller secondary peak at 0.5cpd/0.125Hz (35 spikes/s). The neuron shown in figure 4.3C had a single peak in its ER (200 spikes/s above SR) to high SF gratings (0.5-1cpd) drifting at mid-low TFs (0.5-2Hz). Of the 53 ER plots, 25 showed a single peak (e.g. Fig. 4.3C) and 28 showed multiple peaks (e.g. Fig. 4.3A,B). The IR plot in figure 4.3B showed a similar profile to the ER plot for that neuron, but this was not the case for the neuron shown in figure 4.3C. The neuron in figure 4.3C was maximally excited (200 spikes/s) by high SFs drifting at mid-TFs in the preferred direction, but maximally inhibited (-12 spikes/s) by mid SFs (0.25pd) drifting at high TFs (16Hz) in the anti-preferred direction. For 16 neurons the ER and IR plots showed a similar tuning profile (as in Fig. 4.3B, see also Fig. 4.2). However, for 33 neurons, the tuning in the spatio-temporal domain was quite different for the ER and IR plots (as in Fig. 4.3C).

Quantitative Analysis of the ER Plots

Stimulus velocity (in degrees per second; °/s) is calculated as TF/SF. Thus, from the contour plots it is straightforward to see if a cell is tuned to TF or velocity. A contour plot showing perfect velocity tuning would have an elongated peak, such that the slope is equal to 1. TF-tuning is exemplified by contour plots that are symmetrical about a horizontal line through the peak indicating a preference for the same TF over a range of SFs.

From Figure 4.3 it is clear that not all the neurons were tuned to TF. To quantify the orientation of the peaks in the ER plots, each peak was fit to a two-dimensional Gaussian function, using a slightly modified version of the method of Perrone and Thiele (2001):

$$G(u, \omega) = (\exp(-(u')^2/\sigma_x^2)) \times (-(\omega')^2/\sigma_y^2)) + P$$

where

$$u' = (u - x)\cos\theta + (\omega - y)\sin\theta$$

$$\omega' = -(u - x)\sin\theta + (\omega - y)\cos\theta$$

u is ln (SF), ω is ln (TF), θ is the angle of the Gaussian, (x,y) is the location of the peak of the Gaussian, σ_x and σ_y are the spread of the Gaussian in the u' and ω' dimensions, respectively, and P is a constant. The values σ_x, σ_y, x, y, θ and P were optimized to minimize the sum of the mean error between the real and G values using the solver function in *Microsoft Excel*.

Following Perrone and Thiele (2001), each ER peak was fitted to two different types of Gaussian functions: non-oriented and oriented. In the non-oriented function θ was constrained to zero, while θ was free to take on any value in the oriented Gaussian

function. The square of the Pearson product moment correlation coefficient (r^2) was calculated for each Gaussian to measure the overall fit to the data. Averaged across the entire data set, which consisted of 52 fitted peaks, the r^2 values of the oriented and non-oriented fits were 0.84 ± 0.09 and 0.77 ± 0.11, respectively (mean + standard deviation). These were significantly different (single sample Student t-test $p < 0.0001$). (There were 13 neurons that were not fit with Gaussians either because the two peaks in the ER plot appeared inseparable, or there were more than two peaks in the contour plot).

In Figure 4.3 oriented Gaussian fits to the ER plots of the 3 neurons are shown. For perfect velocity tuning θ would equal 45° (i.e. a slope of 1), but for TF-tuning θ would equal 0° or 90°. For the neurons in figure 4.3A and B, the peaks in the fast and slow region were fit separately, and the gray borders indicate the range of SFs and TFs used for each fit. For the neuron in figure 4.3A, the θ values for the fast and slow peaks were 85° and 42°, respectively. For the neuron in figure 4.3B, the θ values for the fast and slow peaks were 87° and 37°, respectively. For the neuron in figure 4.3C, which had a single slow peak, $\theta = 57^\circ$.

Figure 4.4 shows the location (x,y; circles) and orientation (θ; solid line) of each oriented Gaussian fit. For those ER plots with two peaks, the location of the primary and secondary peaks were plotted as filled and empty dots, respectively. Following previous studies of the pretectum and AOS (Crowder and Wylie, 2001; Ibbotson et al., 1994; Wylie and Crowder, 2000;), we use 4°/s as the border between "Fast" and "Slow" neurons, although the distinction in the data is not as apparent as in those previous studies. For fast cells the peak excitation occurred in response low-mid SFs (0.03-0.13cpd) and mid-high TFs (0.5-16Hz). For slow cells the peak excitation occurred in

response to mid-high SFs (0.3-2 cpd) and low-mid TFs (0.06-2Hz). Shown in Table 1, which considers data from only the primary peaks, the average SF and TF of the fast ERs were 0.078 cpd and 2.84 Hz, respectively. The average SF and TF of the slow neurons were 0.53 cpd and 0.30 Hz, respectively. (All values were first transformed to the natural log, the average was calculated, and then the inverse transformation was performed). As indicated by the orientation of lines in Figure 4.4, for most peaks in the fast zone θ approximated 0° or 90° (suggesting TF-tuning), whereas θ approached 45° for most peaks in the slow zone (suggesting velocity-tuning).

Figure 4.5 shows the responses of two cells as a function of velocity (left column) and TF (right column). Responses to low SFs (0.03 – 0.125 cpd) and high SFs (0.25 – 1 cpd) are separated into top and bottom panels, respectively. The neuron in figure 4.5A showed velocity tuning to high SFs with a peak response at 1°/s (bottom-left panel). At low SFs, this neuron was more closely tuned to TF (top-right panel; peak at 0.125 Hz) than velocity. Figure 4.5B also shows a neuron that was more closely tuned for velocity (peak at 0.1 – 1 $^{\circ}$/s) at high SFs, but TF-tuned at lower SFs, with a sharp peak at 16Hz.

Direction Tuning in Fast and Slow Zones

Figure 4.6 shows three down cells (A,C,D) and one back cell (B) from which direction tuning curves were collected using slow gratings (solid line, 0.5cpd/0.5Hz) and fast gratings (dashed line, 0.063/4Hz). Firing rate relative to the SR (gray circle) is plotted as a function of the direction of motion in polar coordinates (i.e. the SR has been set to zero; outside the gray circle= excitation, inside = inhibition). The neurons in figure 4.6A,C and D preferred the slow gratings, showing a much greater depth of modulation.

The neuron in figure 4.6B responded to slow and fast gratings equally. Solid and dashed arrows represent the neuron's preferred direction for slow and fast gratings, respectively, as calculated from the best-fit cosines to the tuning curves. The neurons in figure 4.6A and C showed very little variation in preferred direction in response to slow and fast gratings. The neurons in figure 4.6B and D had differences of about 20° in their preferred directions in response to slow and fast gratings, but these were the largest changes we observed. No cells showed large enough differences in direction preference to be classified as one direction-type in response to slow gratings and another direction-type in response to fast gratings.

Discussion

In the present study we examined the responses of neurons in the pigeon AOS to large-field drifting sine wave gratings. nBOR neurons clustered into two groups based on the location of peak response in the spatio-temporal domain: fast cells which preferred low SFs and high TFs, and slow cells that preferred high SFs and low TFs, although many neurons showed peaks in both the fast and slow regions. Most of the fast peaks were tuned to a specific TF (see Figs. 4.3A,B, 4.4, 4.5) whereas most of the slow peaks showed apparent velocity tuning, insofar as the 2-dimensional Gaussians fit to the slow peaks were oriented at about 45°(see Figs. 4.2 - 4.5). Strictly speaking, the slow neurons cannot be called velocity-tuned because the response is SF dependent. For example, the ER plot shown in Figure 4.3C shows a peak oriented at approximately 45°, suggestive of velocity tuning. However, the response to 1cpd/2Hz (2°/s) was about 200 spikes/s, whereas the response to 0.25cpd/0.5Hz (2 °/s) was 150 spikes/s. A velocity-tuned neuron

would respond equally well to a preferred velocity, irrespective of the SF, and the peak in the ER plot would appear as an elongated ridge (Zanker et al., 1999). Thus, we use the term "velocity-like" tuning, or "apparent velocity tuning".

Comparison with Previous Studies of the Pretectum of Birds and Mammals

Ibbotson et al. (1994) were the first to demonstrate that neurons in the pretectum (wallaby NOT) were tuned in the spatio-temporal domain to either low SF/high TFs (fast cells) or high SFs/low TFs (slow cells). Subsequently, Wylie and Crowder (2000) showed that neurons in the pretectum (nucleus LM) of pigeons contained such fast and slow neurons. Following Ibbotson and Price (2001), a direct comparison of the pigeon and wallaby pretectal data is offered in Table 1, along with data from the pigeon nBOR from the present study. The mean velocity of the slow and fast NOT neurons was 0.8 and 50°/s, respectively, remarkably similar to what we found for the pigeon LM (1.08 and 52°/s, respectively). Such similarities may arise from convergent evolution in response to similar visual environments, or point toward a highly conserved visual system of ancient origin (Ibbotson and Price, 2001). Table 1 shows that the TF, SF and velocity preferences of the fast and slow nBOR neurons are similar to their counterparts in the LM. Note that the percentage of fast cells in the nBOR is much less than that in the LM (also see Crowder and Wylie, 2001).

In our previous study of the spatio-temporal tuning in the pigeon LM (Wylie and Crowder, 2000), we reported that velocity tuning was rare. In fact, of 35 ER plots only 1 appeared as velocity-tuned, whereas 14 were TF-tuned. The results of the present study prompted us to re-examine the LM data, with emphasis on the slow cells. The data set

from Wylie and Crowder (2000) consisted of 12 slow cells, but we have subsequently recorded from an additional 8 slow LM neurons (e.g. from Crowder et al., in press). Two-dimensional Gaussian functions were fit to the peaks in the LM ER plots, and the locations (x,y) and orientations (θ) of each oriented Gaussian fit is shown in figure 4.4, alongside the same data from the nBOR cells. Of the 20 slow peaks, 12 had slopes that approached 45^{o} (i.e. within 20^{o}). Thus, it appears that slow neurons in nBOR and LM show apparent velocity tuning.

Implications for Models of Motion Detection

Initially proposed by Reichardt (1961), the correlation model of motion detection has been very successful in describing motion processing in animal vision (for reviews see Borst and Egelhaaf, 1989; Buchner, 1984; Clifford and Ibbotson, 2003; Srinivasen et al., 1999). The classic correlation detector consists of two subunits, or "half-detectors", each selective for motion in opposite directions. When the outputs of these two half-detectors are subtracted from each other a highly directional motion detector is created (see also Appendix 2, Fig. A2.1). Recent elaborations of the basic correlation-type detector have involved the addition of spatial and temporal pre-filters (e.g. Dawson and DiLollo, 1990; Ibbotson and Clifford, 2001; Price and Ibbotson, 2002). The energy model is a variant of this basic scheme, and generates similar response properties to elaborated correlation-type detectors (Adelson and Bergen, 1985; Zanker et al., 1999).

One of the most prominent features of the correlation model of motion detection is its dependence on the spatial structure and contrast of the visual stimulus (Buchner, 1984; Reichardt 1961;). Furthermore, correlation motion detectors are tuned to a

particular TF rather than a particular velocity (for reviews see, Buchner, 1984; Egelhaaf et al., 1989; Ibbotson et al., 1994; Srinivasen et al., 1999; Wolf-Oberhollenzer and Kirschfeld 1994). This TF-tuning has been used as an identifying characteristic of the correlation scheme for many years (e.g. Wolf-Oberhollenzer and Kirschfeld 1994). Behavioral and physiological studies of insects over the last 40 years have emphasized that the motion detectors underlying the optokinetic "turning response" are of the correlation type (Srinivasen et al., 1999). The amplitude of the turning response is dependent on TF rather than the velocity of the stimulus, and the responses of the optic flow sensitive neurons in the visual neuropile exhibit properties consistent with the correlation model, including tuning for TF rather than velocity (e.g. Borst and Egelhaaf, 1989; Buchner, 1984; Eckert, 1980; Egelhaaf et al., 1989, 1990; Hausen, 1984; O'Carroll et al., 1996; Reichardt, 1969). Moreover, there is behavioral and physiological evidence from cats, monkeys and humans indicating that detectors of the correlation type are involved in motion analysis in mammals (Borst and Egelhaaf, 1989; Miles and Kawano, 1987; Tolhurst and Movshon, 1975; see also Nakayama, 1985;).

Evidence in favor of the correlation scheme has also been reported for the optokinetic system. Neurons in the wallaby NOT were sensitive to contrast and most were tuned to TF (Ibbotson et al., 1994; Ibbotson and Price, 2001). Turke et al. (1996) recorded optokinetic head movements in unrestrained pigeons in response to horizontally drifting gratings of varying SF, contrast, and stimulus velocity. They noted a strong dependence on contrast and TF rather than velocity. In a study of responses of neurons in the pigeon nBOR, Wolf-Oberhollenzer and Kirschfeld (1994) reported that most neurons were TF-tuned, but only one neuron tested showed velocity tuning. This is in stark

contrast to our findings. However, neither Wolf-Oberhollenzer and Kirschfeld (1994) nor Turke et al. (1996) used the higher SFs that would maximally excite the slow nBOR cells discussed in the present study. Indeed, the classic correlation motion detection model cannot account for the velocity-like tuning of slow nBOR neurons.

Recently, Zanker et al. (1999) explicitly showed that altering the subtraction step, or "balance", of the two half-detectors critically affects the tuning of the detector. The classic correlation scheme described above is a fully balanced detector, where the inputs from the two anti-symmetric half detectors are equally weighted. Recall that this fully balance detector is TF-tuned. Conversely, Zanker et al. (1999) showed that a fully unbalanced detector, which is essentially a lone half-detector, is velocity-tuned. Finally, a partially balanced detector had responses between these two extremes, with velocity tuning that was weakly dependent on SF (Zanker et al., 1999). It is possible that the velocity-like tuning in the slow zone of nBOR neurons represents the output of a partially balanced correlation-type motion detector. We illustrate this in Figure 4.7, which shows the ER plots of simulations generated by a model of an elaborated Reichardt detector. The details of the model can be found in Appendix 2. We used a model from Dawson and DiLollo (1990), but with delay filters given by (Clifford et al., 1998) and temporal pre-filters described by Ibboston and Clifford (2001) and Price and Ibboston (2002). Moreover, following Zanker et al. (1999) we manipulated the balance by varying the gain (α) of the subtraction step where the response = $(S_1) - (\alpha \times S_2)$. When $\alpha = 1$ the detector is fully balanced, and when $\alpha = 0$ the detector is fully unbalanced (i.e. a half-detector) (Zanker et al., 1999). In Figure 4.7A we have modeled the ER plot of a slow cell with a peak response to 1cpd/0.5Hz. When $\alpha = 1$ (left) the ER plot shows TF-tuning, but when

$\alpha = 0.5$ (right) velocity-like tuning is evident. When a 2-dimensional Gaussian is fit to this peak $\theta = 56^{o}$, but clearly the response is dependent upon SF. Thus, we suggest that the slow nBOR neurons might represent the output of partially balanced correlation detectors, perhaps approaching half-detectors. Other electrophysiological evidence from the fly's visual system (Egelhaaf et al., 1989) and the wallaby pretectum (Ibbotson et al. 1994; Ibboston and Clifford, 2001; Price and Ibbotson, 2002) also suggests that the underlying motion detectors are not perfectly balanced.

In the present study we found that the fast nBOR neurons exhibit TF tuning. Although one could conclude that this implies that the underlying motion detectors are fully balanced, with Figure 4.7B we show that this is not necessarily the case. On the left, we modeled a fully balanced detector tuned to1cpd/8Hz, with rather restrictive temporal pre-filters. Note the TF-tuning. On the right we show the response of the model with the same parameters except $\alpha = 0$. The peak, which has been pushed to the lower range of SFs, appears TF-tuned. Clearly the shape of the peak in the spatio-temporal domain is dependent upon both the pre-filter settings and the balance of the detector. Dror et al. (2001) demonstrate that other processes such as response compression and adaptation are also critical when considering velocity estimations by Reichardt detectors.

Another model of motion detection that may be applied to the current results is the Weighted Intersection Mechanism (WIM) model developed by Perrone and Thiele (2002). The WIM model of velocity sensitivity was developed to show how MT neurons in the primate extra-striate cortex could build velocity-tuned spatio-temporal peaks by summing the spatio-temporal inputs from a sustained V1 neuron and a transient V1 neuron. In this model, the spatio-temporal tuning of the sustained V1 neuron must differ

slightly from the tuning of the transient V1 neurons, this difference produces a diagonal peak in the spatio-temporal domain enabling narrow velocity tuning (Perrone and Thiele, 2002). Although this model appears to be tailor-made for the geniculo-striate pathway, it demonstrates that the spatio-temporal tuning from multiple inputs can be combined to shape the spatio-temporal tuning of an afferent neuron. This shaping has already been shown experimentally in the AOS and pretectum. The spatio-temporal tuning of LM neurons is drastically altered when input from the nBOR is inactivated by tetrodotoxin (Crowder et al., in press). Similar results are expected for nBOR neurons if the LM were inactivated. Antidromic stimulation studies in the turtle AOS indicate that the receptive fields of AOS neurons result from the pooling of multiple directionally selective retinal inputs (Kogo et al., 1998). The spatio-temporal tuning of these retinal inputs could be combined to form velocity-like tuning.

Function of fast and slow neurons

Ibbotson et al. (1994) provide an extensive discussion of the potential role of the slow and fast NOT neurons in the generation and maintenance of optokinetic nystagmus (OKN). Immediately after the onset of an optokinetic stimulus, there is a 50-100msec latent period before ocular following begins (e.g. Collewijn, 1972). During this period, the retinal slip velocity (RSV) is high, and Ibbotson et al. (1994) suggest that the fast NOT neurons are responsible for initiating ocular following (the "direct" phase of OKN; Cohen et al., 1977; Miles et al., 1986; Gellman et al., 1990). Moreover, they suggest that the fast neurons are involved in the charging of the velocity storage mechanism ("indirect" phase of OKN) when stimulus speeds are high. Ibbotson et al. (1994) noted

that rapidly moving visual images become blurred, which is consistent with the fact that the fast NOT neurons respond best to low SFs. The slow NOT neurons would become active when the RSV is low, and they would continue to charge the velocity storage mechanism at these slow velocities. Pigeons lack the direct phase of OKN, but they do possess a velocity storage mechanism (Gioanni, 1988; Nalbach, 1992). This precludes the fast LM and nBOR neurons in pigeons from a role in the direct component of OKN, as proposed for the fast NOT neurons. However, it is reasonable to imagine that the fast and slow nBOR and LM neurons are involved in charging the velocity storage mechanism as proposed for the fast and slow NOT neurons. Those neurons with peaks in both the fast and slow regions would be active when RSV is high or low.

Srinivasan et al. (1999) offer another function for the fast and slow cells (see also Heeger, 1987; Simoncelli and Heeger, 1998). They refer to single motion detector with a peak in the spatio-temporal domain as a "correlator". The spatio-temporal tuning of a single correlator would look similar to a contour plot of a pretectal or AOS neuron with a sharp peak in the spatio-temporal domain. The response of a single correlator is ambiguous because all points that lie on a given response contour in the spatio-temporal domain represent combinations of SFs and TFs that elicit the same response. If contrast is allowed to vary, another degree of uncertainty is added. Because the response of the motion detector will increase with contrast (until saturation is reached), all points on a given response contour will be confounded with points on a weaker response contour if the contrast representing the weaker contour is appropriately increased. The above ambiguity can be removed if more than one correlator is incorporated into the movement detecting process, with each correlator having different spatio-temporal frequency

optimum. The velocity of a stimulus would be coded by the relative activity of the correlators. Manipulating the contrast of the stimulus would affect all correlators equally, but the stimulus velocity would still determine the ratio of the activity between the correlators. In this scheme, velocity of a stimulus can be estimated unambiguously and independently of spatial structure or contrast based on the population response (Srinivasan et al., 1999). Srinivasen et al. (1999) noted that visual systems of insects have two classes of direction-selective neurons differing with respect to preferred TF (Horridge and Marcelja, 1992) and the optokinetic system in crabs has three such classes of neurons (Nalbach, 1990).

When this model is applied to the AOS and pretectum, the fast and slow cells take on the roles of two classes of correlators. Theoretically, the RSV could be reliably be encoded by the pattern of activity in nBOR neurons, and the velocity storage mechanism would be provided with a velocity signal that is unambiguous and independent of spatial structure or contrast of the visual stimulus. Furthermore, this velocity information could be utilized for other behaviours such as flight speed and "odometry" which require an unambiguous velocity signal (Srinivasen et al., 1999).

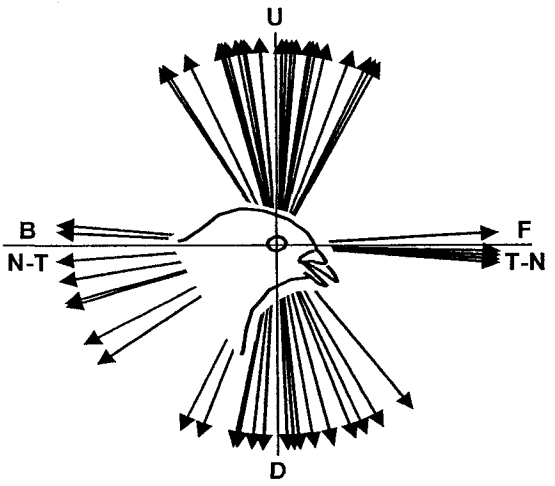

Figure 4.1

Directional tuning of neurons in the nucleus of the basal optic root. The orientation of each arrow represents the preferred direction for each neuron, as calculated from the peak of the best-fit cosine to the direction-tuning curve. U, B (N-T), D, and F(T-N) represent up, back (nasal to temporal), down, and forward (temporal to nasal) motion.

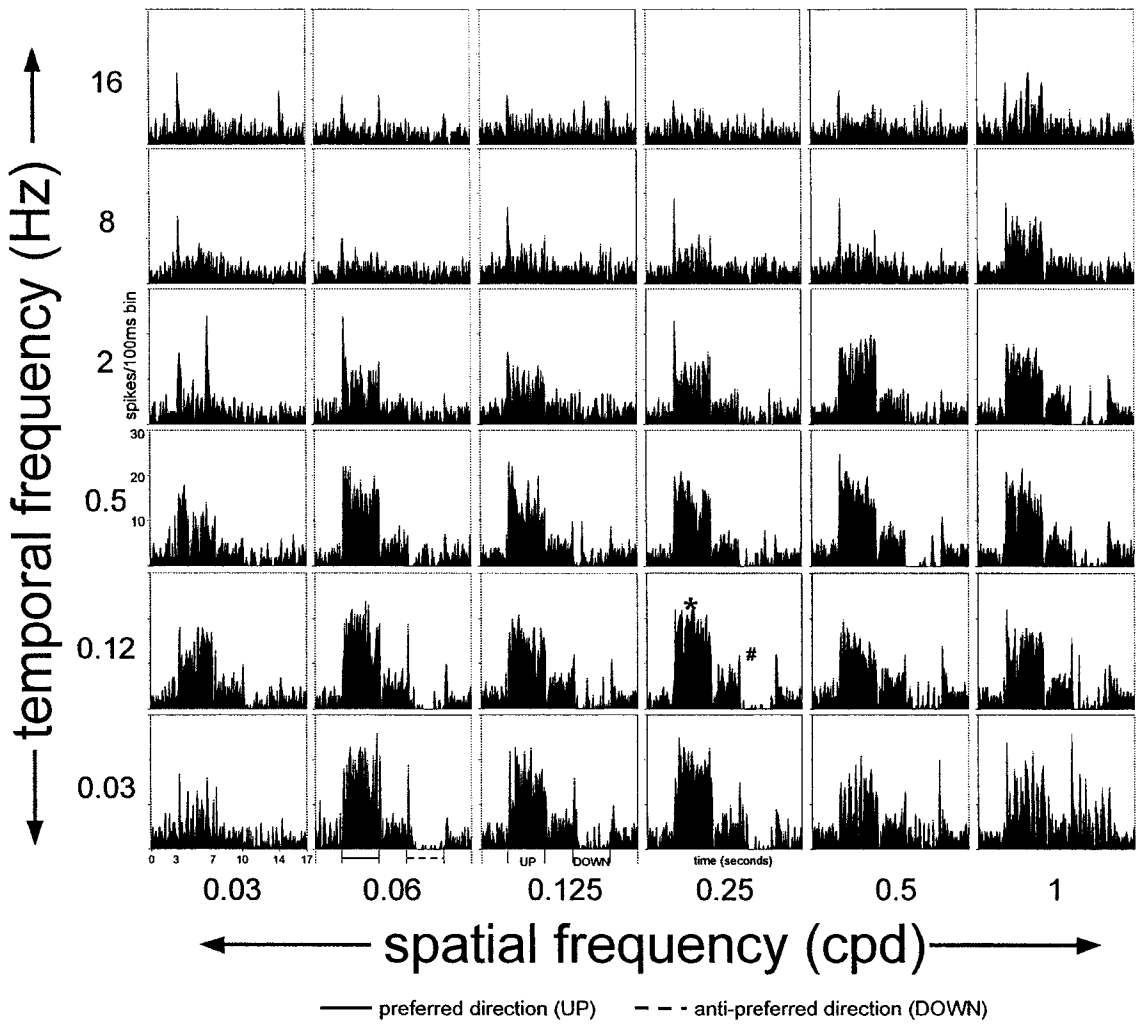

Figure 4.2

Responses of a neuron in the nucleus of the basal optic root (nBOR) to drifting gratings of varying spatial and temporal frequency (SF, TF). Peri-stimulus time histograms (PSTHs) show the responses of the neuron to 36 combinations of SF (abscissa) and TF (ordinate). Single sweeps are shown, where each sweep consisted of 4 sec motion in the preferred direction (upward motion, solid line), then a 3 sec pause, followed by 4 sec of motion in the anti-preferred direction (downward motion, broken line). The asterisk (*) and pound (#) indicate the peak excitatory and inhibitory responses in the spatio-temporal domain based on the average firing rate over the 4 sec epoch, respectively.

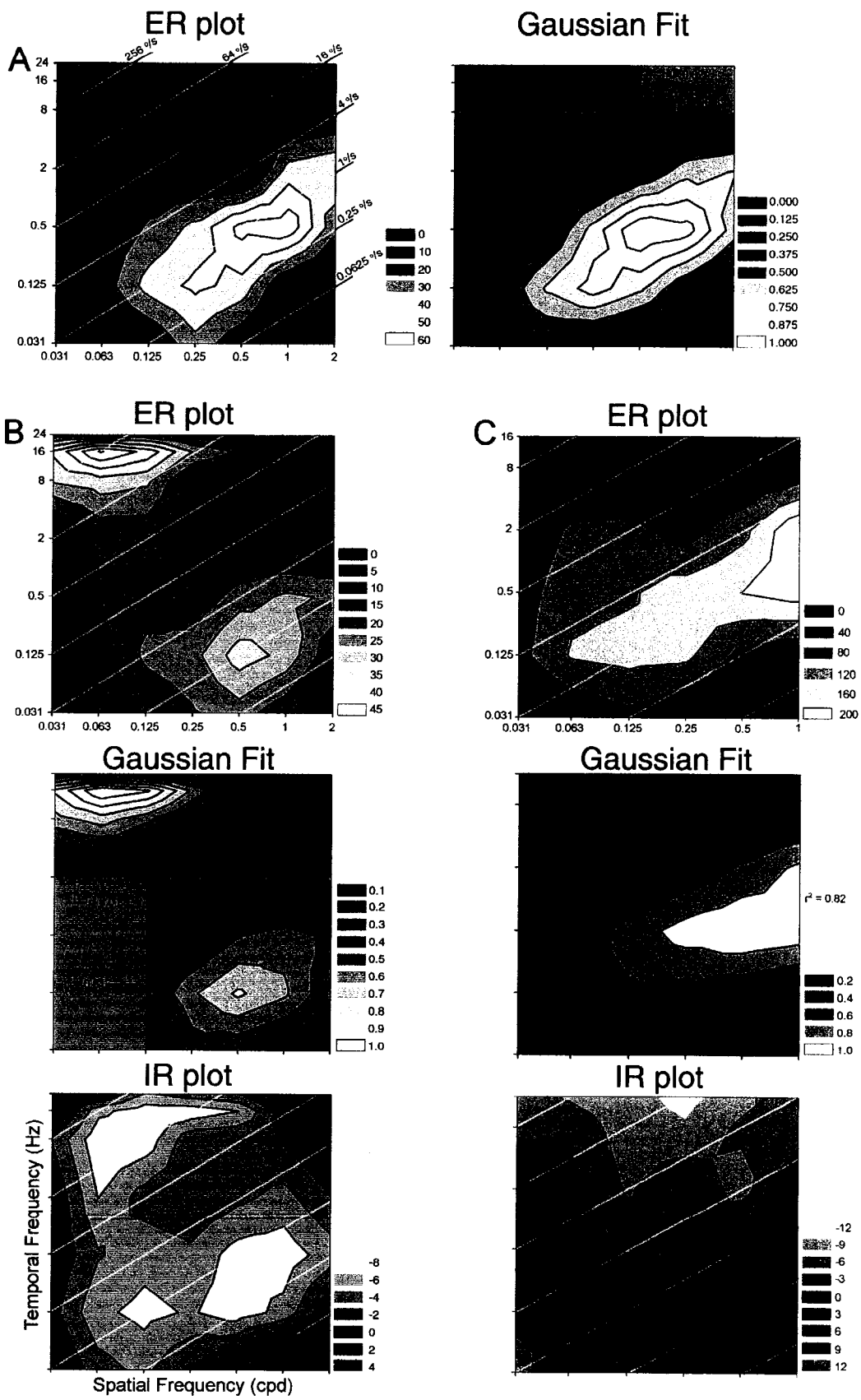

Figure 4.3

Spatio-temporal tuning of neurons in the nucleus of the basal optic root (nBOR). Contour plots of the responses of nBOR neurons to gratings of varying spatial frequency (abscissa) and temporal frequency (ordinate) are shown. **A** shows the response to gratings drifting in the preferred direction (ER plots) and the Gaussian fit of the ER plot (see results) for a slow neuron. **B** and **C** show the responses to gratings drifting in the preferred and anti-preferred (ER and IR plots) directions as well as the Gaussian fits of the ER plots for two other neurons. For the ER and IR plots, the scale on the iso-contour lines represents the firing rate (spikes/sec) above (+) or below (-) the spontaneous rate, and the diagonal lines overlaying the contour plots indicate particular velocities (TF/SF). Note that the ordinate and abscissa are not symmetrical, and the diagonal lines represent a slope of 1 (i.e. 45°). For the Gaussian fits, the scale has been normalized. The gray lines encompass the range of SF and TF used to create each Gaussian fit. The correlation coefficient for each of the Gaussian fits is also indicated. For the ER and IR plots, as well as the Gaussian fits, black fill represents the SR, red represents excitation, and green represents inhibition.

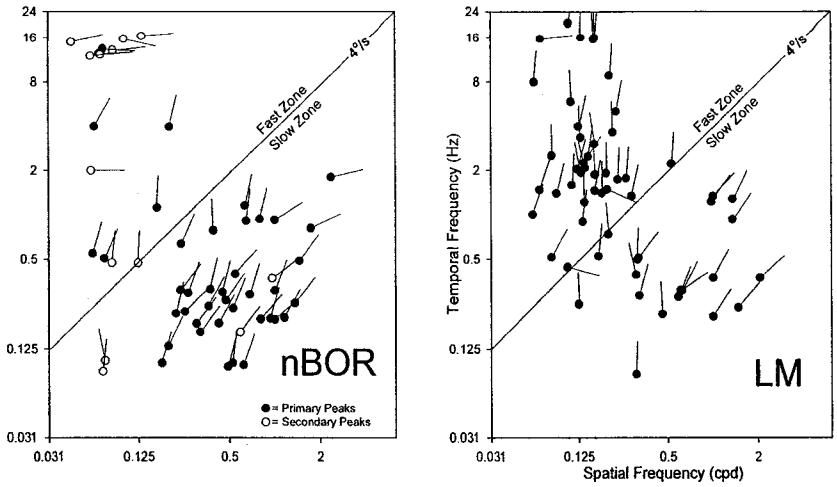

Figure 4.4

Spatio-temporal preferences of neurons in the nucleus of the basal optic root (nBOR, left) and pretectal nucleus lentiformis mesencephali (LM, right). Each circle respresents the location (x,y) of the peak of the best fit two dimesional Gaussian to the peaks in excitatory response (ER) plots. For ER plots that had multiple peaks, primary and secondary peaks are shown as filled and empty circles, respectively. The diagonal line indicates 4°/s, the boundary between the fast and slow zones in the spatio-temporal domain (Ibbotson and Price, 2001). The tail on each dot represents the orientation (θ) of the best fit Gaussian. Note that orientations of 45° indicate velocity-like tuning, and 0° or 90° indicate temporal frequency tuning. See results section for a detailed description of the Gaussian fitting procedure.

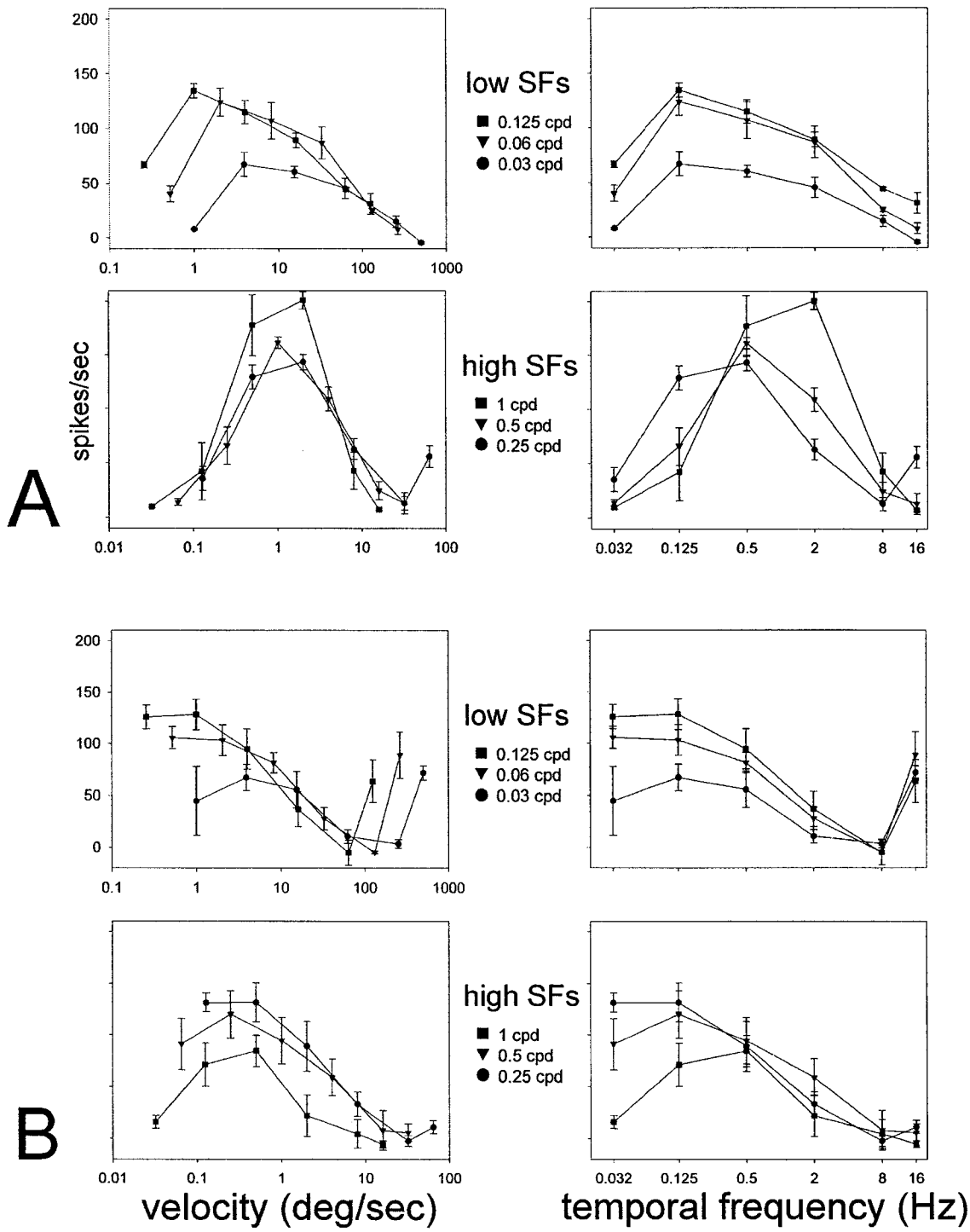

Figure 4.5

Velocity and temporal frequency tuning of neurons in the nucleus of the basal optic root (nBOR). The responses of two cells (**A** and **B**) are shown as a function of velocity

(abscissa, left column) and TF (abscissa, right column). Responses to low SFs (0.03 – 0.125 cpd) and high SFs (0.25 – 1 cpd) are separated into top and bottom panels, respectively. Firing rate (in spikes/sec) is shown on the ordinate for all graphs. Error bars indicate mean ± standard deviation.

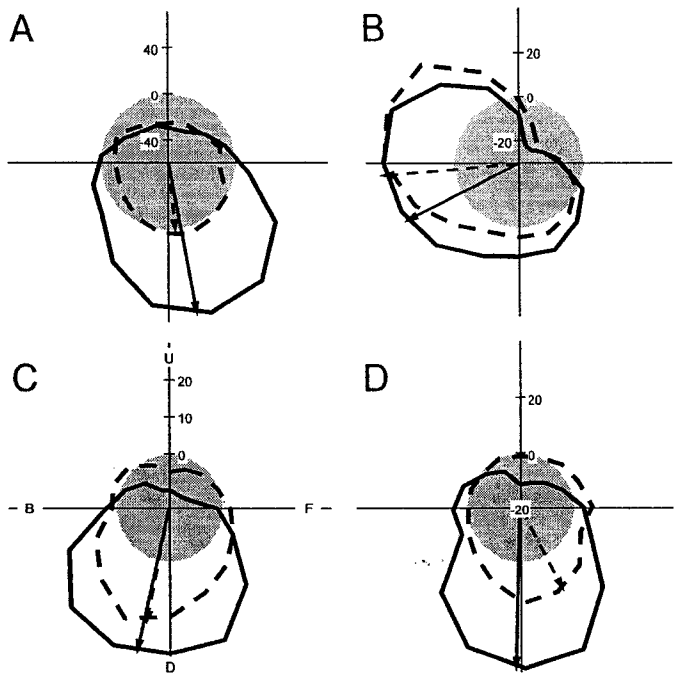

Figure 4.6

Directional tuning of neurons in the nucleus of the basal optic root (nBOR) to slow and fast stimuli. Polar plots illustrating the directional tuning of neurons in the nBOR in response to slow gratings (solid lines; SF= 0.5cpd, TF= 0.5Hz) and fast gratings (dashed lines; SF= 0.063cpd, TF= 4Hz). Firing rate (spikes/sec) relative to the spontaneous rate (SR; gray circle) is plotted as a function of the direction of motion in polar coordinates (i.e. the SR has been set to zero; outside the gray circle = excitation, inside = inhibition). Solid and dashed arrows represent the neuron's preferred direction for slow and fast stimuli, respectively, as calculated from the best fit cosines to the tuning curves. U, B, D, and F represent up, back (nasal to temporal), down, and forward (temporal to nasal) motion, respectively.

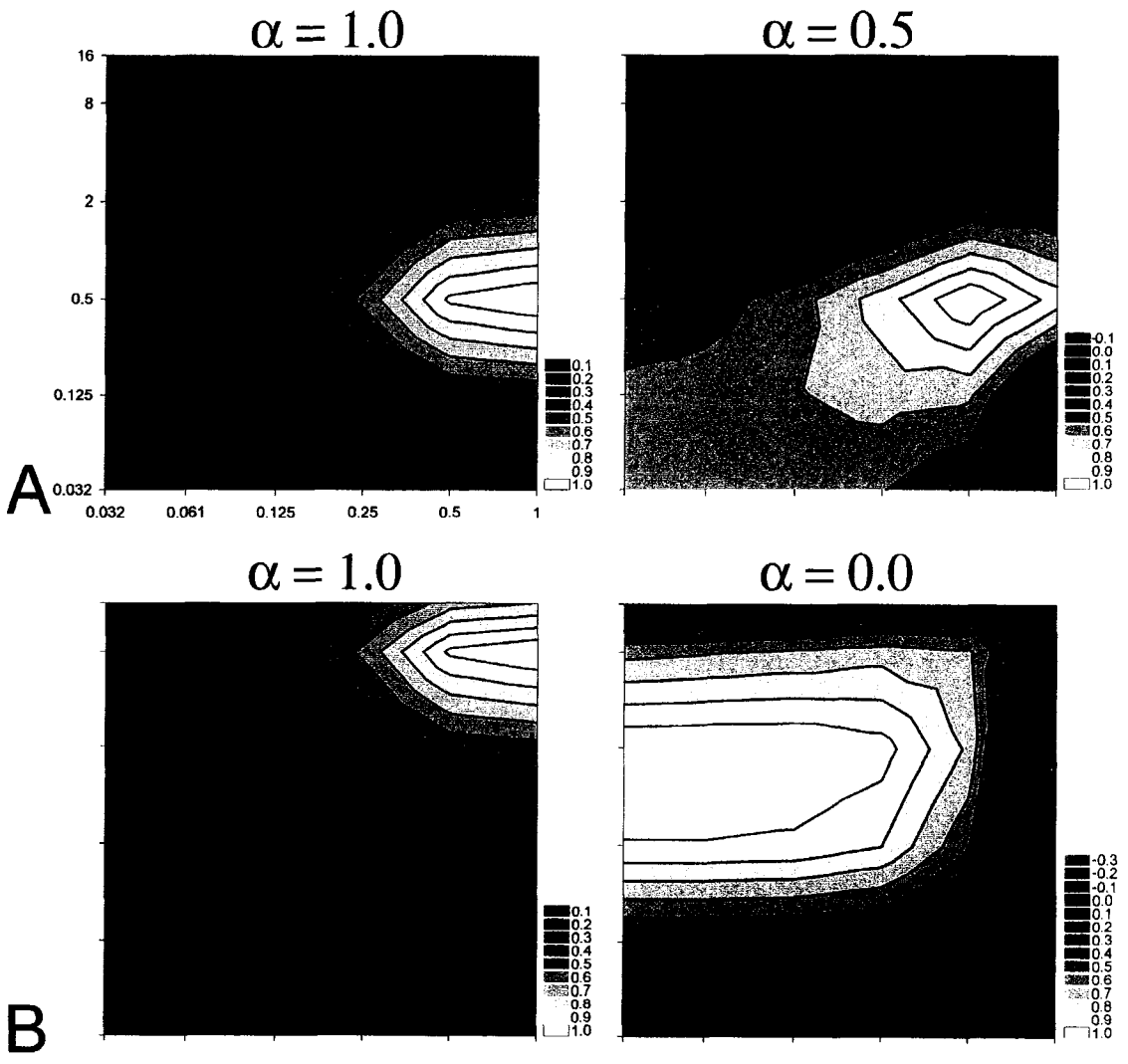

Figure 4.7

Spatio-temporal contour plots generated by an elaborated Reichardt detector model. Thirty-six combinations of spatial frequencies (abscissa) and temporal frequencies (ordinate) were entered into the model shown in Appendix 2 to build each contour plot. **A** shows a simulation for a slow cell, where the values for the temporal pre-filter were τ_1 = 20ms, τ_2 = 10000ms, β = 1, the time constant of the delay filter was τ = 0.4s, and the α level was equal to 1 (left; i.e. balanced) or 0.5 (right; partially balanced). **B** shows a simulation for a fast cell, where the values for the temporal pre-filter were τ_1 = 10ms, τ_2 =

1000ms, $\beta = 1$, the time constant of the delay filter was $\tau = 0.015$s, and the α level was equal to 1 (left; i.e. balanced) or 0.0 (right; i.e. fully unbalanced). See figure 4.3 for details regarding contour plot presentation.

	"Fast" Cells				"Slow" Cells			
	n (% total)	SF (cpd)	TF (Hz)	velocity (°/s)	n (% total)	SF (cpd)	TF (Hz)	velocity (°/s)
Pigeon nBOR	13 (25%)	0.078	2.84	36.2# [70.8*]	40 (75%)	0.53	0.30	0.57# [0.75*]
Pigeon LM	23 (66%)	0.10	2.49	25.8# [52.3*]	12 (34%)	0.67	0.55	0.82# [1.08*]
Wallaby NOT	31 (43%)			[50*]	41 (57%)			[0.8*]

#meanTF/meanSF. *arithmetic mean.

Table 4.1

Preferred spatial frequencies (SFs), temporal frequencies (TFs), and velocities of fast and slow neurons. Average SFs, TFs, and velocities of the primary peaks are shown for the fast and slow neurons in the pigeon nucleus of the basal optic root (nBOR; present study) and lentiformis mesencephali (LM; from Wylie and Crowder, 2000). The average velocities of fast and slow neurons found in the wallaby nucleus of the optic tract (NOT) are also shown (from Ibbotson and Price, 2001). See discussion for details.

References

Adelson EH, Bergen JR. Spatiotemporal energy models for the perception of motion. *Journal of the Optical Society of America A-Optics & Image Science* 2: 284-99, 1985.

Barlow HB, Levick WR. The mechanism of directionally selective units in rabbit's retina. *J Physiol* 178: 477-504, 1965.

Borst A, Egelhaaf M. Principles of visual motion detection. *Trends in Neurosci* 12: 297-306, 1989.

Buchner E. Behavioral analysis of spatial vision in insects. In: *Photoreception and Vision in Invertebrates*, edited by Ali MA. New York: Plenum Press, 1984, p. 561-621.

Burns S, Wallman J. (1981) Relation of single unit properties to the occulomotor function of the nucleus of the basal optic root (AOS) in chickens. *Exp Brain Res* 42: 171-180, 1981.

Clifford CWG, Ibbotson, MR. Fundamental mechanisms of visual motion detection: models, cells, and functions. *Progress in Neurobiology* 68: 409-437, 2003.

Clifford CWG, Freedman JN, Vaina LM. First- and second-order motion perception in Gabor micropattern stimuli: psychophysics and computational modelling. *Brain Res Cogn Brain Res* 26: 263-271, 1998.

Cohen B, Matsuo V, and Raphan T. Quantitative analysis of the velocity characteristics of optokinetic nystagmus and optokinetic after-nystagmus. *J Physiol London* 270: 321-344, 1977.

Collewijn H. Latency and gain of the rabbit's optokinetic reactions to small movements. *Brain Res* 36: 59-70. 1972

Collewijn H. Direction-selective units in the rabbit's nucleus of the optic tract. *Brain Res* 100: 489-508, 1975a.

Collewijn H. Oculomotor areas in the rabbit's midbrain and pretectum. *J Neurobiol* 6: 3-22, 1975b.

Cooper HM, Magnin M. A common mammalian plan of accessory optic system organization revealed in all primates. *Nature* 324: 457-459, 1986.

Crowder NA, Wylie DR. Fast and slow neurons in the nucleus of the basal optic root in pigeons. *Neurosci Letters* 304: 133-136, 2001.

Crowder NA, Lehmann H, Parent MB, Wylie DR. The Accessory Optic System Contributes to the Spatio-Temporal Tuning of Motion-Sensitive Pretectal Neurons. *J Neurophysiol*, in press.

Dawson M, Di Lollo V. Effects of adapting luminance and stimulus contrast on the temporal and spatial limits of short-range motion. *Vision Res* 30: 415-429, 1990.

Dror RO, O'Carroll DC, Laughlin SB. Accuracy of velocity estimation by Reichardt correlators. *J Opt Soc Am A Opt Image Sci Vis.* 18: 241-252, 2001.

Eckert H. Functional properties of the H1-neurone in the third optic ganglion of the blow fly, *Phaenicia. J Comp Physiol* 135: 29-39, 1980.

Egelhaaf M, Borst A, Reichardt W. Computational structure of a biological motion-detection system as revealed by local detector analysis in the fly's nervous system. *Journal of the Optical Society of America A-Optics & Image Science* 6: 1070-1087, 1989.

Egelhaaf M, Borst A, Pilz B. The role of GABA in detecting visual motion. *Brain Res* 509: 156-60, 1990

Fan TX, Weber AE, Pickard GE, Faber KM, Ariel M. Visual responses and connectivity in the turtle pretectum. *J Neurophysiol* 73: 2507-2521, 1995.

Fite KV, Kwei-Levy C, Bengston L. Neurophysiological investigation of the pretectal nucleus lentiformis mesencephali in *Rana pipiens*. *Brain Behav Evol* 34: 164-170, 1989.

Fite KV. Pretectal and accessory-optic visual nuclei of fish, amphibia and reptiles: theme and variations. *Brain Behav Evol* 26: 71-90, 1985.

Gellman RS, Carl JR, Miles FA. Short latency ocular-following responses in man. *Vis Neurosci* 5: 107-122, 1990.

Gibson JJ. The visual perception of object motion and subjective movement. *Psychol Rev* 61: 304-314, 1954.

Gioanni H, Rey J, Villalobos J, Dalbera A. Single unit activity in the nucleus of the basal optic root (nBOR) during optokinetic, vestibular and visuo-vestibular stimulations in the alert pigeon (*Columba livia*). *Exp Brain Res* 57: 49-60, 1984.

Gioanni H. Stabilizing gaze reflexes in the pigeon (*Columba livia*). I. Horizontal and vertical optokinetic eye (OKN) and head (OCR) reflexes. *Exp Brain Res* 69: 567-582, 1988.

Graf W, Simpson JI, Leonard CS. Spatial organization of visual messages of the rabbit's cerebellar flocculus. II. Complex and simple spike responses of Purkinje cells. *J Neurophysiol* 60: 2091-2121, 1988.

Grasse KL, Cynader MS. Electrophysiology of medial terminal nucleus of accessory optic system in the cat. *J Neurophysiol* 48: 490-504, 1982.

Grasse KL, Cyander MS, Douglas RM. Alterations in response properties in the lateral and dorsal terminal nuclei of the ca accessory optic system following visual cortex lesions. *Exp Brain Res* 55: 69-80, 1984.

Grasse KL, Cyander MS. The accessory optic system in frontal-eyed animals. In: *Vision and Visual Dysfunction. The Neuronal Basis of Visual Function,* edited by Leventhal A. New York: McMillan, 1990, p. 111-139.

Hausen K. The lobula complex of the fly: Structure, function and significance in visual behavior. In: *Photoreception and Vision in Invertebrates*, edited by Ali MA. New York: Plenum Press, 1984, p. 523-560.

Heeger DJ. Model for the extraction of image flow. *Journal of the Optical Society of America A-Optics & Image Science* 4: 1455-1471, 1987.

Hoffmann KP, Schoppmann A. A quantitative analysis of the direction-specific response of neurons in the cat's nucleus of the optic tract. *Exp Brain Res* 42: 146-157, 1981.

Horridge GA, Marcelja L. On the existence of 'fast' and 'slow' directionally sensitive motion detector neurons in insects. *Proceedings of the Royal Society of London - Series B: Biological Sciences* 248: 47-54, 1992.

Ibbotson MR, Clifford CW. Interactions between ON and OFF signals in directional motion detectors feeding the not of the wallaby. *J Neurophysiol* 86: 997-1005, 2001.

Ibbotson MR, Price NS. Spatiotemporal tuning of directional neurons in mammalian and avian pretectum: a comparison of physiological properties. *J Neurophysiol* 86: 2621-2624, 2001.

Ibbotson MR, Mark RF, Maddess TL. Spatiotemporal response properties of direction-selective neurons in the nucleus of the optic tract and the dorsal terminal nucleus of the wallaby, *Macropus eugenii*. *J Neurophysiol* 72: 2927-2943, 1994.

Karten HJ, Hodos W. *A stereotaxic Atlas of the Brain of the Pigeon (Columba livia)*. Baltimore: Johns Hopkins Press, 1967.

Katte O, Hoffmann KP. Direction specific neurons in the pretectum of the frog (*Rana esculenta*). *J Comp Physiol* 140: 53-57, 1980.

Kogo N, Rubio DM, Ariel M. Direction Tuning of Individual Retinal Inputs to the Turtle Accessory Optic System. *J Neurosci* 18: 2673-2684, 1998.

Marr D, Ullman S. Directional selectivity and its use in early visual processing. *Proceedings of the Royal Society of London - Series B: Biological Sciences*. 211: 151-180, 1981.

McKenna OC, Wallman J. Accessory optic system and pretectum of birds: comparisons with those of other vertebrates. *Brain Behav Evol* 26: 91-116, 1985a.

McKenna OC, Wallman J. Functional postnatal changes in avian brain regions responsive to retinal slip: a 2-deoxy-D-glucose study. *J Neurosci* 5: 330-342, 1985b.

Miles FA, Kawano K. Visual Stabilization of the eyes. *Trends Neurosci* 10: 153-158, 1987.

Miles FA, Kawano K, Optican LM. Short-latency ocular following responses of monkey. I. Dependence on temporospatial properties of visual input. *J Neurophysiol* 56:1321-1354, 1986.

Morgan B, Frost BJ. Visual response properties of neurons in the nucleus of the basal optic root of pigeons. *Exp Brain Res* 42: 184-188, 1981.

Mustari MJ, Fuchs AF. Discharge patterns of neurons in the pretectal nucleus of the optic tract (NOT) in the behaving primate. *J Neurophysiol* 64: 77-90, 1990.

Nakayama K. Biological image motion processing: a review. *Vis Res* 25: 625-660, 1985.

Nalbach HO. Three temporal frequency channels constitute the dynamics of the optokinetic system of the crab, *Carcinus maenas* (L.) *Biol Cybern* 61: 59-70, 1990.

Nalbach HO. Translational head movements of pigeons in response to a rotating pattern: characteristics and tool to analyze mechanisms underlying detection of rotational and translational optical flow. *Exp Brain Res* 92: 27-38, 1992.

Natal CL, Britto LRG. The pretectal nucleus of the optic tract modulates the direction selectivity of the accessory optic neurons in rats. *Brain Res* 419: 320-323, 1987.

O'Carrol DC, Bidwell NJ, Laughlin SB, Warrant EJ. Insect motion detectors matched to visual ecology. *Nature* 382: 63-66, 1996.

Perrone JA, Thiele A. A model of speed tuning in MT neurons. *Vision Res* 42: 1035-1051, 2002.

Perrone JA, Thiele A. Speed skills: measuring the visual speed analyzing properties of primate MT neurons. *Nat Neurosci* 4:526-532, 2001.

Price NS, Ibbotson MR. Direction-selective neurons in the optokinetic system with long-lasting after-responses. J Neurophysiol 88: 2224-2231, 2002.

Reichardt W. Autokorrelationsauswertung als Funktionsprinzip des Zentralnervensystems. *Z Naturforsch* 12: 448-457, 1957.

Reichardt W. Autocorrelation, a principle for the evaluation of sensory information by the central nervous system. In: *Sensory Communication,* edited by Rosenblith WA. New York: Wiley, 1961, p. 303-317.

Reichardt W. Movemnet perception in insects. In: *Processing of optical data by organisms and machines*, edited by Reichardt W. New York: Academic, 1969, p. 465-493.

Rosenberg AF, Ariel M. Visual-response properties of neurons in turtle basal optic nucleus in vitro. *J Neurophysiol* 63: 1033-1045, 1990.

Simoncelli EP, Heeger DJ. A model of neuronal responses in visual area MT. *Vis Res* 38: 743-761, 1998.

Simpson JI, Graf W, Leonard C. The coordinate system of visual climbing fibres to the flocculus. In: *Progress in oculomotor research*, edited by Fuchs AF Becker W. Amsterdam/New York/Oxford: Elsevier/North Holland, 1981.

Simpson JI, Leonard CS, Soodak RE. The accessory optic system: II. Spatial organization of direction selectivity. *J Neurophysiol* 60: 2055-2072, 1988.

Simpson JI. The accessory optic system. *A Rev Neurosci* 7: 13-41, 1984.

Soodak RE, Simpson JI. The accessory optic system of rabbit. I. Basic visual response properties. *J Neurophysiol* 60: 2055-2072, 1988.

Srinivasan MV. Generalized gradient schemes for the measurement of two-dimensional image motion. *Biol Cybern* 63: 421-431, 1990.

Srinivasan MV, Poteser M, Kral K. Motion detection in insect orientation and navigation. *Vis Res* 39: 2749-2766, 1999.

Tolhurst DJ, Movshon JA. Spatial and temporal contrast sensitivity of striate cortical neurones. *Nature* 257: 674-675, 1975.

Turke W, Nalbach HO, Kirschfeld K. Visually elicited head rotation in pigeons (Columba livia). *Vis Res* 36: 3329-3337, 1996.

van Santen JP, Sperling G. Elaborated Reichardt detectors. *Journal of the Optical Society of America A-Optics & Image Science* 2: 300-321, 1985.

Volchan E, Rocha-Miranda CE, Picanco-Diniz CW, Zinsmeisser B, Bernardes RF, Franca JG. Visual response properties of pretectal units in the nucleus of the optic tract of the opossum. *Exp Brain Res* 78: 380-386, 1989.

Weber JT. Pretectal complex and accessory optic system in alert monkeys. *Brain Behav Evol* 26: 117-140, 1985.

Winterson BJ, Brauth SE. Direction-selective single units in the nucleus lentiformis mesencephali of the pigeon (*Columba livia*). *Exp Brain Res* 60: 215-226, 1985.

Wolf-Oberhollenzer F, Kirschfeld K. Motion sensitivity in the nucleus of the basal optic root of the pigeon. *J Neurophysiol* 71: 1559-1573, 1994.

Wylie DR, Crowder NA. Spatiotemporal properties of fast and slow neurons in the pretectal nucleus lentiformis mesencephali in pigeons. *J Neurophysiol* 84: 2529-2540, 2000.

Wylie DR, Frost BJ. Visual response properties of neurons in the nucleus of the basal optic root of the pigeon: A quantitative analysis. *Exp Brain Res* 82: 327-336, 1990a.

Wylie DR, Frost BJ. Binocular neurons in the nucleus of the basal optic root (nBOR) of the pigeon are selective for either translational or rotational visual flow. *Vis Neurosci* 5: 489-495, 1990b.

Wylie DR, Frost BJ. Responses of pigeon vestibulocerebellar neurons to optokinetic stimulation. II. The 3-dimensional reference frame of rotation neurons in the flocculus. *J Neurophysiol* 70: 2647-259, 1993.

Wylie DRW, Frost BJ. The pigeon optokinetic system: Visual input in extraocular muscle coordinates. *Vis Neurosci* 13: 945-953, 1996.

Wylie DR, Frost BJ. Responses of neurons in the nucleus of the basal optic root to translational and rotational flowfields. *J Neurophysiol* 81: 267-276, 1999.

Wylie DR, Kripalani T, Frost BJ. Responses of pigeon vestibulocerebellar neurons to optokinetic stimulation. I. Functional organization of neurons discriminating between translational and rotational visual flow. *J Neurophysiol* 70: 2632-2646, 1993.

Wylie DR, Bischof WF, Frost BJ. Common reference frame for neural coding of translational and rotational optic flow. *Nature* 392: 278-282, 1998.

Zanker JM, Srinivasan MV, Egelhaaf M. Speed tuning in elementary motion detectors of the correlation type. *Biol Cybern* 80: 109-16, 1999.

Chapter 5

The Accessory Optic System Contributes to the Spatio-Temporal Tuning of Motion-Sensitive Pretectal Neurons

A version of this chapter has been accepted for publication. Crowder NA, Lehmann H, Parent MB, Wylie DRW. 2003. Journal of Neurophysiology. 90: 1140-1151.

Introduction

Self-motion induces patterns of optic flow across the retina (Gibson, 1954). The pretectum and accessory optic system (AOS) work together to analyze optic flow, and generate the optokinetic response (OKR) to facilitate retinal image stabilization (Grasse and Cynader, 1990; Simpson, 1984; Simpson et al., 1988;). Retinal image stabilization ensures optimal visual acuity (Carpenter, 1977; Westheimer and McKee, 1973) and velocity discrimination (Nakayama, 1981).

The AOS and pretectum are highly conserved in vertebrates. The mammalian pretectal nucleus of the optic tract (NOT) is homologous to the nucleus lentiformis mesencephali (LM) in birds, whereas the avian nucleus of the basal optic root (nBOR) of the AOS is homologous to the medial and lateral terminal nuclei (MTN, LTN) of the mammalian AOS (Fite, 1985; McKenna and Wallman, 1985a; Simpson, 1984; Simpson et al., 1988; Weber, 1985;). AOS and pretectal neurons have extremely large receptive fields and exhibit direction-selectivity to large-field visual stimuli moving in the contralateral visual field. Most LM and NOT neurons prefer temporal-to-nasal (T-N) motion (NOT: Collewijn, 1975a,b; Distler and Hoffmann, 1993; Hoffman and Schoppmann, 1975, 1981; Hoffmann et al., 1988; Hoffmann and Distler, 1989; Ibbotson et al., 1994; Ilg and Hoffmann, 1996; Mustari and Fuchs, 1990; Volchan et al., 1989; Yakushin et al., 2000; LM: Fan et al., 1995; Fite et al., 1989; Katte and Hoffmann, 1980; McKenna and Wallman, 1985b; Winterson and Brauth, 1985; Wylie and Frost, 1996; Wylie and Crowder, 2000). MTN and LTN neurons prefer upward or downward motion (Cooper and Magnin, 1986; Grasse and Cynader, 1982, 1984; Natal and Britto, 1987; Soodak and Simpson, 1988). nBOR neurons prefer upward, downward or nasal-to-

temporal (N-T) motion (Burns and Wallman 1981; Gioanni et al. 1984; Morgan and Frost 1981; Rosenberg and Ariel, 1990; Wylie and Frost 1990).

In response to drifting sine wave gratings, pretectal and AOS neurons exhibit tuning in the spatio-temporal domain. In the NOT of wallabies, Ibbotson et al. (1994) distinguished two groups of neurons: those that preferred high spatial frequencies (SFs) and low temporal frequencies (TFs) vs. those that preferred low SFs and high TFs. As velocity = TF/SF, these two groups were referred to as "slow" and "fast" neurons, respectively. Strikingly similar observations were found in the LM (Wylie and Crowder, 2000) and nBOR of pigeons (Crowder and Wylie, 2001).

There is a massive projection from the AOS to the pretectum (mammals: Baleydier et al., 1990; Blanks et al., 1982, 1995; Giolli et al., 1984, 1985a,b, 1992; Kato et al., 1995; Mustari et al., 1994; birds: Azevedo et al., 1983; Brecha et al., 1980; Wylie et al., 1997), however the physiological significance of this projection has not been studied extensively (Baldo and Britto, 1990; Gu et al., 2001; Hamassaki et al., 1988; Nogueira and Britto, 1991; Schmidt et al., 1994, 1998; van der Togt and Schmidt, 1994). In the present study we investigated the contributions of the nBOR-LM projection to the direction and spatio-temporal tuning of LM neurons by recording their responses before and after the nBOR was inactivated by injection of tetrodotoxin (TTX).

Methods

Surgery and Extracellular recording

The methods employed conformed to the Guidelines established by the Canadian Council on Animal Care and were approved by the Biosciences Animal Welfare and

Policy Committee at the University of Alberta. Details for anaesthesia, extracellular recording, stimulus presentation and data analysis have been described by Wylie and Crowder (2000; Appendix 1). Briefly, pigeons were anaesthetized with a ketamine (65 mg/kg) - xylazine (8 mg/kg) mixture (i.m.) and supplemental doses were administered as necessary. Based on the pigeon stereotaxic atlas (Karten and Hodos, 1967), sufficient bone and dura were removed to expose the brain and allow access the nBOR and LM with vertical penetrations. Recordings were made with tungsten microelectrodes (2-5MΩ impedance). The extracellular signal was amplified, filtered, displayed on an oscilloscope and fed to a window discriminator. TTL pulses representing single spikes were fed to a 1401*plus* (Cambridge Electronic Designs (CED)) and peri-stimulus time histograms were constructed with *Spike2* software (CED).

Stimulus Presentation

After units in either the nBOR or LM were isolated, the direction preference and the approximate locations of the receptive field boundaries and hot-spot were qualitatively determined by moving a large (90° X 90°) hand-held stimulus in various areas of the visual field. Directional tuning and spatio-temporal tuning were determined quantitatively with sine-wave gratings that were generated by a VSG*Three* graphics computer (Cambridge Research Designs, Cambridge UK), and back-projected onto a tangent screen that was located 50cm from the bird (90 X 75°). Direction tuning was tested using gratings of an effective SF and TF at 15° or 22.5° increments, while spatio-temporal tuning was tested using gratings of varying SF (0.03-2 cycles per degree (cpd)) and TF (0.03-16 cycles per second (Hz)) moving in the preferred and anti-preferred

directions. Each sweep consisted of 4 sec of motion in one direction, a 3 sec pause, 4 sec of motion in the opposite direction, followed by a 3 sec pause. Firing rates were averaged over 3-5 sweeps. Contour plots of the mean firing rate in the spatio-temporal domain were made using *Sigma Plot*.

General Procedure

The general procedure was as follows: 1.) Locate the nBOR based on stereotaxic coordinates and extracellular recording, noting the dorsal extent of the nBOR. 2.) Replace the recording electrode with an injection canula (30 gauge) filled with TTX (Sigma-Aldrich, St. Louis) in phosphate buffered saline (pH=7.4). The canula was positioned such that the tip was 100μm above the location of the dorsal-most responsive cell from the recording track. 3.) Lower a recording microelectrode into the pretectum, and characterize the direction and spatio-temporal tuning of an LM unit (see *Stimulus Presentation* above). 4.) Inject TTX into the nBOR. The time-course and maximum diameter of sodium-channel blockade following an injection of TTX in solution depends on the volume and concentration of TTX used, and has been shown to approximate the process of diffusion from an instantaneous point source (Zhuravin and Bures, 1991). In some experiments we used a rather large volume of TTX, 1-1.5μL, but at a weak concentration of 2ng/μL. In other experiments we used a more conservative volume of 0.3-0.5μL but at a concentration of 10ng/μL, which is typically used to produce a pharmacological inactivation (Baldi et al., 1998; Bielavska and Roldan, 1996; Gallo and Candido, 1995; Rashidy-Pour et al., 1996a,b; Roldan and Bures, 1994; Zhuravin and Bures, 1991). (Note that approximately the same absolute amount (2-4ng) of TTX was

used for both types of injections). 5.) After 15 minutes, the response properties of the LM unit were tested again. In some cases, an electrolytic lesion was placed at the recording site by passing a current of 30μA for 8-10 seconds (electrode positive).

Histology

At the end of the recording session, the animals were given an overdose of sodium pentobarbitol (100mg/kg) and immediately perfused with saline (0.9%) followed by paraformaldehyde (4% in 0.1M phosphate buffer (PB), 4°C). Brains were extracted, post-fixed for 2-12 hours (4% paraformaldehyde, 20% sucrose in 0.1M PB), and cryoprotected in sucrose overnight (20% in 0.1M PB). Frozen sections (45μm thick in the coronal plane) through the LM and nBOR were collected. Sections were mounted onto gelatin chrome aluminum coated slides and lightly counter-stained with neutral red or cresyl violet. The tissue was then examined using light microscopy to confirm the locations of electrode tracks and electrolytic lesions in the LM, and the canula tracks in the nBOR.

Results

We examined the directional and spatio-temporal properties of 18 LM units, before and after the nBOR was inactivated with TTX. Twelve animals were injected with 1-1.5μl of low concentration TTX (2ng/μl), and 6 with 0.3-0.5μl of high concentration TTX (10ng/μl) (see Table 5.1). The histology showed tissue damage caused by the canula tracks terminated above the dorsal border of nBOR or had penetrated a small distance into the nucleus (Fig. 5.1A), and electrode tracks were visible

in the pretectum. In 8 cases, electrolytic marking lesions were made at the recording sites (Fig. 5.1B). All 8 lesions were found in LM: four each were found in the medial and lateral subnuclei (LMm, LMl, Gamlin and Cohen, 1988b).

After isolating an LM unit, it took approximately one hour to collect the pre-TTX data. Upon subsequent injection of TTX into the nBOR, recording was maintained for up to five hours. As the effects of TTX begin to decay after as little as 2 hours (Zhuravin and Bures, 1991), we only considered the first 2 hours after the TTX injection in our analyses. The activity of a given neuron before and after the TTX injection is referred to as "pre-TTX" and "post-TTX", respectively.

"Normal" Properties of LM Units

All 18 LM units were direction selective (Fig. 5.3). A unit's direction preference was assigned by calculating the maximum of the best cosine fit to the tuning curve. Eleven, 4, 1 and 1 LM units preferred forward (i.e. temporal to nasal), downward, backward and upward motion, respectively (Fig. 5.2A, Table 5.1). The remaining unit was a bi-directional neuron, which showed excitation to both forward and backward motion (see Fig. 5.3D). The predominance of neurons preferring forward motion is consistent with previous studies of the pigeon LM (Gu et al., 2001; Winterson and Brauth, 1985; Wylie and Frost, 1996; Wylie and Crowder, 2000;).

All 18 units were tuned in the spatio-temporal domain. Contour plots were constructed where TF was on the ordinate, SF was on the abscissa, and firing rate (relative to the SR) was plotted on the z-axis. As motion in the preferred and anti-preferred directions generally result in excitation and inhibition of the neuronal firing respectively, we refer to

excitatory and inhibitory response plots (ER plots, IR plots) (e.g. Figs. 5.4 and 5.5). Some units showed a single maximum in the contour plot (e.g. Fig. 5.4A) but two peaks was more common (e.g. Fig. 5.4B, 5.5A-D). Based on the method of Perrone and Thiele (2001) the locations of the peaks in the contour plots were assigned quantitatively by fitting each peak to a two-dimensional Gaussian function: $G'(u, \omega) = (\exp(-(u')^2/\sigma_x^2)) \bullet (-(\omega')^2/\sigma_y^2)) + P$, where $u' = (u - x)\cos\theta + (\omega - y)\sin\theta$ and $\omega' = -(u - x)\sin\theta + (\omega - y)\cos\theta$. Where, u is the Ln SF of the test grating, ω is the Ln TF of the test grating, θ is the angle of the Gaussian, (x,y) is the location of the peak of the Gaussian (in u and ω coordinates), σ_x and σ_y are the spread of the Gaussian in the u' and ω' dimensions, respectively. The G values were normalized, and added to a constant (P). The values σ_x, σ_y, x, y, and P were optimized to minimize the sum of the mean error between the real and G values using the solver function in Microsoft Excel. In Figure 5.2B the locations of the primary peaks from the ER plots are shown. Consistent with previous studies of the pretectum (Ibbotson et al., 1994; Wylie and Crowder, 2000), the peaks cluster into two quadrants: units responding best to gratings of low SF/high TF (11 cells), or high SF/low TF (7 cells). Following Ibbotson et al. (1994) we refer to these as "fast" and "slow" cells, respectively.

Changes in Spontaneous Rate of LM Units following nBOR Inactivation

Table 5.1 shows the percentage change in the spontaneous rates (SR) of LM units following nBOR inactivation (for decreases, % change = [{post-TTX – pre-TTX] / pre-TTX}*100; for increases = [{post-TTX – pre-TTX] / post-TTX}*100). For 11 cases there was a significant decrease in SR (15-56%) whereas 2 cases showed a significant

increase (7 and 39%) (t-tests, $p<.0028$; Bonferroni correction for multiple comparisons), and 5 cases showed no significant change. The average change in SR across all 18 cases was −16.2%.

Effects of nBOR inactivation on the Direction Tuning of LM Units

Figure 5.3 shows the direction tuning curves for 6 LM units, pre-TTX (solid line) and post-TTX (broken line). Only one unit (Fig. 5.3F) showed a substantial change in direction preference (116°). For the other units, the direction change did not exceed 12° (mean = 5°) (see Table 5.1).

From Figure 5.3 it is apparent that the breadth of tuning changed for some LM units. Typically, the half-power ([maximal excitation – SR] / 2) is used to quantify the breadth of excitation. The half-power bandwidth was determined by measuring the angle from the origin to the two points where the tuning curve intersected the half-power value. (This type of analysis was not appropriate for the bi-directional unit). For example, the breadth of tuning increased for the unit in Fig. 5.3E (43°), and decreased for the unit in Fig. 5.3A (-16°). Four units showed an increase in the half-power bandwidth of at least 15° (post-TTX – pre-TTX) whereas 2 units showed a decrease of at least 15° (see Table 5.1)

The magnitude of modulation, both excitation and inhibition, was altered for some units (e.g. Fig. 5.3B). The percent change in the magnitude of excitation and inhibition was calculated from the tuning curves for each unit. Across all 18 cases, there was an average decrease in the magnitude of excitation post-TTX of -17.3%, which was significantly different from zero (single sample t-test, $p<.02$). With respect to the

magnitude of inhibition, a more dramatic and consistent pattern was observed. Averaged across 16 cases (i.e. excluding the units in Fig. 5.3D and F), the magnitude of inhibition decreased by –36.1%, which was significantly different from zero (single sample t-test, $p<.002$).

Spatio-temporal Changes Following nBOR Inactivation

The spatio-temporal properties were examined pre-TTX for all 18 units, and for all but one unit post-TTX (case#15). The bi-directional cell did not have an IR plot. Thus, we obtained pre- and post-TTX ER plots for 17 cells and pre- and post-TTX IR plots for 16 cells. The inactivation of the nBOR affected the spatio-temporal profiles of all LM units tested.

In figure 5.4 data from case#3 are shown. Pre-TTX and post-TTX ER and IR plots are shown in A and B, respectively. In these plots the SR is represented by the black fill, and excitation and inhibition are represented by red and green, respectively. The stronger the degree of excitation/inhibition, the progressively brighter and less saturated the red/green fill. Thus the peak excitation and inhibition appear off-white. In addition, "difference" plots are shown. These were calculated by subtracting the pre-TTX plot from the post-TTX plot. On the difference plots, black fill indicates no change pre- to post-TTX, blue represents negative values or a lower firing rate post-TTX, and yellow represents positive values or a greater firing rate post-TTX. For the cell shown in Fig. 5.4, with respect to the ER plots (Fig. 5.4A), pre-TTX there was a single excitatory peak at 1cpd / 1Hz. Post-TTX, although unchanged in magnitude, the peak was shifted lower on the TF scale. The difference ER plot had a negative peak in the fast region,

reflecting the fact that the unit was less responsive to fast stimuli. Note also the positive peak in the difference ER plot at high SFs and low TFs, indicating that the cell showed an increased excitation to these gratings and corroborating the fact that the peak shifted to lower TFs. With respect to motion in the anti-preferred direction (IR plots, Fig. 5.4B), pre-TTX this unit had a major inhibitory peak at 1cpd / 0.5Hz, and very small secondary peak (-5 spikes/s) at 0.03cpd / 2 Hz. Post-TTX, the secondary peak remained, but the peak in the slow region was virtually eliminated. In fact, post-TTX the cell was excited in response to high SF stimuli at the lowest TF drifting in the anti-preferred direction (+25 spikes/s). The difference IR plot had a positive peak in the slow region, reflecting the loss of the inhibitory response and the appearance of the excitatory response to high SF / low TF gratings post-TTX.

In Figure 5.4C, peri-stimulus time histograms (PSTHs) to three different SF/TF combinations are shown. Three sweeps pre-TTX and 3 sweeps post-TTX are shown, and the approximate time at which the PSTHs were collected relative to the TTX injection is provided. These data indicate the reliability of the effects we observed. To 0.6cpd/2Hz gratings (top), the excitation to motion in the preferred direction was clearly reduced post-TTX. To 0.5cpd/0.13Hz gratings (middle) there was an increased response to motion in the preferred direction post-TTX, and the inhibition to motion in the anti-preferred direction seen pre-TTX was absent. In fact, post-TTX this unit was excited in response to this grating drifting in the anti-preferred direction. To 0.5cpd/0.5Hz gratings (bottom) the excitation to motion in the preferred direction was unchanged post-TTX, but the strong inhibition to motion in the anti-preferred direction was absent.

The directional tuning curves for this case, shown in Fig. 5.3A, were established with 0.5cpd/0.5Hz gratings. Consistent with the data in Fig. 5.4, there was no change in the magnitude of excitation to motion in the preferred direction post-TTX, but the inhibition to motion in the anti-preferred direction was abolished. Clearly, the change in the depth of modulation pre- to post-TTX observed in the direction tuning curves was dependent on the SF/TF combination used. For case#3, if we had used 0.06cpd/2Hz gratings we would have observed a decrease in the magnitude of excitation. Likewise, if we had used 0.5cpd/0.13Hz gratings we would have observed an increase in the magnitude of excitation.

Changes in the ER plots Following nBOR Inactivation

Figures 5.5A,B show the effects of nBOR inactivation on the ER plots of two other LM units. The unit in Fig. 5.5A (case#10) showed two excitatory peaks in the pre-TTX ER plot (primary, 1cpd / 2Hz; secondary, 0.06cpd / 16Hz). Post-TTX the peak in the fast region was absent, but the peak in the slow region was unaffected. The difference ER plot showed a negative peak in the fast region, and a smaller positive peak to the lowest TFs. The unit in Fig. 5.5B (case#8) had two excitatory peaks in the fast region pre-TTX (primary, 0.125cpd / 0.5Hz; secondary, 0.125cpd / 16Hz). Post-TTX the primary peak is present, although at less than half the size, and the peak at 16Hz disappeared. In addition, a second peak appeared in the slow region (0.5cpd / 0.5Hz).

All three examples (Figs. 5.4A, 5.5A,B) are quite similar in that the difference ER plots had negative peaks in the fast region, indicating that LM units showed less excitation to low SF/high TF stimuli moving in the preferred direction post-TTX. This

was the most common and dramatic effect that we observed in the ER plots. In column eight of Table 5.1 the presence of peaks in the difference ER plots for all 17 units tested is noted. Negative fast peaks (-fast) and positive slow peaks (+slow) are shown in bold and italics, respectively. In addition, the magnitude of the peak is indicated as the percent change for that SF/TF combination (for -ve peaks, % change = [post-TTX – pre-TTX] / pre-TTX; for +ve peaks = [post-TTX – pre-TTX] / post-TTX *100). Of the 17 units tested, 14 had a negative peak in the fast region of the difference ER plots. For these 14 cells, there were four cases in which an excitatory peak in the fast region of the pre-TTX ER plot was virtually eliminated post-TTX (as in Fig. 5.5A). The average magnitude of these 14 peaks was –67%. For 7 cells there was a positive peak in the slow region of the difference ER plots (e.g. Fig. 5.4A) and the average magnitude was +61%.

In Figure 5.6A, the ER plots are averaged across all 17 cells. The responses for each cell were first normalized, using a common scale for the pre-TTX and post-TTX plots. Despite the averaging, two excitatory peaks were apparent pre-TTX, reflecting the spatio-temporal preferences of the fast and slow cells. Post-TTX both peaks were reduced in size, particularly the fast peak, and at the higher TFs. For the difference ER plot, based on the pooled variance of the associated with all points in the plot, values above 0.16 (and below –0.16) are statistically significant ($p<.05$)[♣]. The difference ER plot had a negative peak in the fast region which was largest in magnitude (-0.39) at 0.13cpd / 8Hz ($p<.002$, single-sample t-test). The positive peak (0.13) in the region of the lowest TFs and highest SFs was not significantly different from zero.

[♣] the critical difference (CD) was calculated as follows: $CD = t_{crit} * (\text{pooled variance} / n)^{1/2}$

Changes in the IR plots Following nBOR Inactivation

Figures 5.5C,D show pre-TTX and post-TTX IR plots for two other LM units. The unit in Fig. 5.5C showed a large inhibitory peak in the slow region pre-TTX (1cpd / 2Hz), with a secondary peak in the fast region. Post-TTX the primary peak was eliminated leaving a peak in the fast region (0.06cpd / 2Hz). The cell in Fig. 5.5D also had two inhibitory peaks pre-TTX (primary, 0.06cpd / 8Hz; secondary, 0.5cpd / 2Hz). Post-TTX, both peaks were reduced in magnitude.

For the 16 cells tested, the most common effect of the TTX injection on the IR plots was a decrease in the amount of inhibition in the slow and/or fast regions post-TTX. This was manifested as positive peaks in the slow and/or fast regions in the difference IR plots. The effect on the slow region was more consistent and more dramatic. In 3 cases an inhibitory peak in the slow region was eliminated post-TTX (as in Fig. 5.4B). Of the 16 difference IR plots, 10 (63%) had positive peaks in the slow region (as in Figs. 5.4B, 5.5C) with an average magnitude of –78%. Seven difference IR plots had positive peaks in the fast region with an average magnitude of –60%.

The averaged normalized IR plots are shown in Figure 5.6B. Note that post-TTX there is a reduction in the magnitude of inhibition to gratings throughout much of the spatio-temporal domain, although it is particularly dramatic to the high SF/low TF gratings. For the difference IR plot, values above 0.17 (and below –0.17) are statistically significant ($p<.05$). The difference plot had a large positive peak (0.5) in the slow region at 0.5cpd / 0.5Hz ($p<.0004$, single-sample t-test).

Discussion

In the present study we sought to determine the function of the projection from the AOS to the pretectum (Azevedo et al., 1983; Baleydier et al., 1990; Blanks et al., 1982, 1995; Brecha et al., 1980; Giolli et al., 1984, 1985a, 1992; Kato et al., 1995; Mustari et al., 1994; Schmidt et al., 1998; Wylie et al., 1997) by observing the directional and spatio-temporal tuning of LM units before and after inactivation of the nBOR with TTX. We found that, while the effects on the directional tuning were minor, the spatio-temporal properties of all LM units changed after nBOR inactivation.

Changes in the Directional Tuning of LM Neurons following nBOR Inactivation

In the present study we found that the direction preference of LM units was rarely altered post-TTX. In some cases the breadth of the tuning was altered, as was the depth of modulation. Gu et al. (2001) examined the directional tuning of LM neurons before and after the nBOR was temporarily inactivated by lidocaine. However they used moving bars as stimuli, which are not as appropriate as large-field stimuli (Frost, 1985). Nonetheless, with respect to the directional tuning of LM neurons, the results of the present study are in agreement with Gu et al. (2001). They found that the inactivation of the nBOR altered the breadth and depth of tuning, but not the direction preferences of LM neurons. Gu et al. (2001) used extremely small volumes of lidocaine and it is unlikely that there was any spread outside the nBOR. Given that we had similar observations with respect to directional tuning of LM neurons, we are confident that our observations are not due to the possibility that the TTX spread beyond the nBOR.

Changes in Spatio-Temporal Preferences of LM neurons following nBOR Inactivation

This study is the first to demonstrate that the spatio-temporal properties of LM neurons are affected by the activity of other nuclei in the optokinetic system. That pretectal neurons are tuned in the spatio-temporal domain was first shown in the wallaby NOT (Ibbotson et al., 1994; Ibbotson and Price, 2001). Two groups of neurons were found: "fast" neurons preferred low SF/high TF gratings, whereas "slow" neurons preferred high SF/low TF gratings. Subsequently we found such fast and slow neurons in the pigeon LM and the nBOR (Crowder and Wylie, 2001; Wylie and Crowder, 2000). In the present study we found that nBOR inactivation changed the spatio-temporal tuning of LM units. With respect to stimuli drifting in the preferred direction, after nBOR inactivation, most LM units showed less excitation to low SF/high TF (i.e. fast) gratings and some units showed more excitation to high SF/low TF (i.e. slow) gratings. With respect to stimuli drifting in the anti-preferred direction, after nBOR inactivation, most LM units showed less inhibition to slow and/or fast stimuli.

Implications for AOS-Pretectal Connectivity

Data from the present study offer several insights to the nature of the connection from the nBOR to LM. First, because LM neurons are directional after nBOR inactivation, it is apparent that other inputs contribute to the direction-selectivity of LM neurons. This is not surprising, given that the LM receives a direct retinal input (Gamlin and Cohen, 1988a). Using intracellular recording, Kogo et al. (1998) demonstrated that retinal inputs into the turtle AOS are direction selective. This is likely the case for the avian AOS and pretectum as well. The pretectum also receives input from the telencephalon in many species (Hoffmann et al. 1991; Hollander et al. 1979; Ilg and

Hoffmann 1993; Lui et al. 1994; Mustari et al. 1994; Schoppmann 1981; Shintani et al. 1999) including pigeons (Miceli et al., 1979), and the lateral cerebellar nucleus in pigeons (Arends and Zeigler, 1991). Clearly, the visual response properties of LM neurons arise from the interaction of many inputs. Second, since most LM neurons showed very little change in their preferred directions following nBOR inactivation, it appears that the LM receives inputs from nBOR neurons with a similar preferred axis. Thus, nBOR neurons preferring horizontal motion (forward and back cells) project to LM neurons preferring horizontal motion, and nBOR neurons preferring vertical motion (up and down cells) project to LM neurons preferring vertical motion. Finally, it appears that information from nBOR to LM is specific in the spatio-temporal domain for stimuli drifting in the preferred and anti-preferred directions.

The most parsimonious explanation for our results would be that the LM receives excitatory input from fast nBOR cells of the same direction preference and/or inhibitory input from slow nBOR cells of the opposite direction preference. In figure 5.7 we consider the input to the most common type of LM neurons, those that are excited by forward motion and inhibited by backward motion (i.e. a FORWARD LM neuron). On the top and bottom of Figure 5.7 we show directional and spatio-temporal tuning for two nBOR neurons (from Crowder and Wylie, 2001). The ER plots, direction tuning curve, and IR plots are shown for a nBOR neuron that preferred backward (N-T) motion (top) and a nBOR neuron that preferred forward (T-N) motion (bottom). The BACK neuron was maximally excited by slow gratings (high SFs, mid TFs), and maximally inhibited by fast gratings (mid SFs, high TFs) drifting forward. The FORWARD neuron was maximally excited by fast gratings (low SFs, mid-high TFs), and maximally inhibited by

slow gratings (high SFs, low TFs) drifting backward. To account for our observations of the effects of nBOR inactivation on the responses of LM neurons, we propose that a FORWARD LM cell receives inhibitory input from the slow BACK cell, and/or excitatory input from the fast FORWARD cell. Although our study does not address which of these two scenarios is more likely, for a few reasons we favor the inhibitory projection. First, BACK cells are much more common than FORWARD cells in the nBOR (Gioanni et al., 1984; Rosenberg and Ariel, 1990; Wylie and Frost, 1990). Second, slow cells are more common than fast cells in the nBOR (Crowder and Wylie, 2001). Finally, previous studies involving electrical stimulation of the AOS have shown that the projection to the pretectum is largely inhibitory. This has been shown both in rats (van der Togt and Schmidt, 1994) and pigeons (Baldo and Britto, 1990).

It is important to note that the proposed model is descriptive and does not address the reciprocal connection between the nBOR and LM (Brecha et al., 1980; Gamlin and Cohen, 1988b). Thus, in addition to preventing retina-to-nBOR information from reaching the LM, nBOR inactivation may also interfere with bi-directional dynamic interactions between the two nuclei.

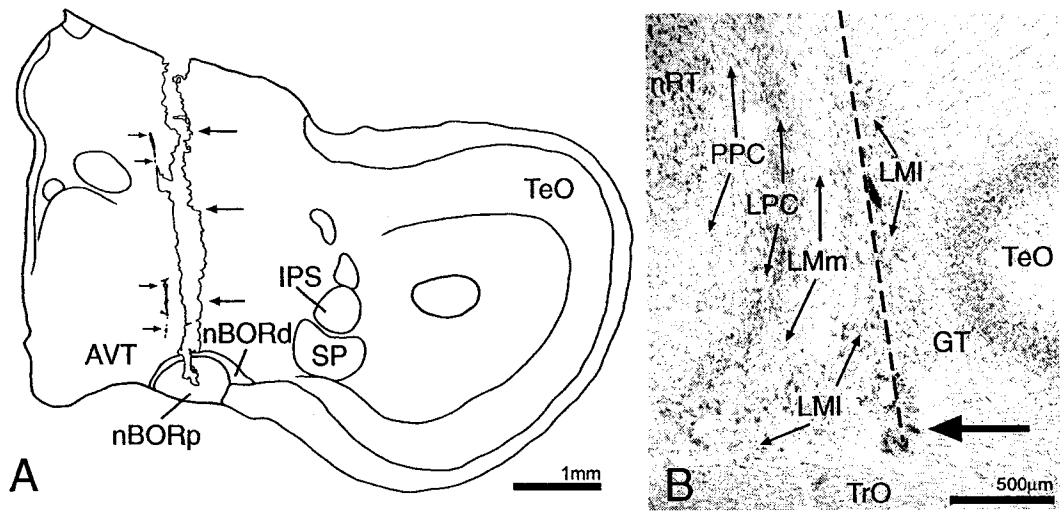

Figure 5.1

Histology. **A** shows a camera lucida tracing of a coronal section through the mesencephalon highlighting locations of an electrode track (small arrows) and a canula track (large arrows) into the nucleus of the basal optic root (nBOR). The nBOR is divided into nBOR proper (nBORp) and nBOR pars dorsalis (nBORd). **B** shows a photomicrograph of a coronal section through the pretectum indicating the location of electrode track (dashed line) and marking lesion (large arrow) in the nucleus lentiformis mesencephali (LM). The nomenclature of Gamlin and Cohen (1988b) is used. The LM consists of medial and lateral subnuclei (LMm, LMl). LMm is bordered medially by the nucleus laminaris precommisuralis (LPC). The nucleus principalis precommisuralis (PPC) resides between the LPC and the nucleus rotundus (nRt). AVT, area ventralis of Tsai; GT, tectal grey; IPS, nucleus interstitio-pretecto-subpretectalis; SP, nucleus subpretectalis; TeO, optic tectum; TrO, tractus opticus. Scale bars; 1mm in **A**, 500µm in **B**.

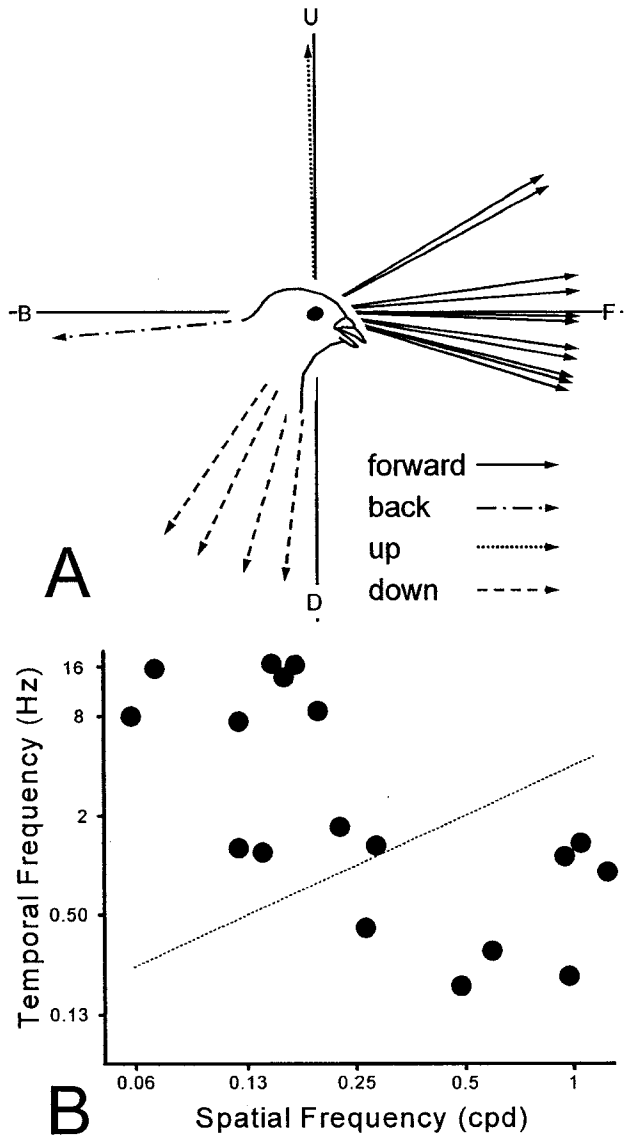

Figure 5.2

Directional and spatio-temporal tuning of lentiformis mesencephali units. In **A**, each arrow represents the preferred direction for each unit, as calculated from the peak of the best fit cosine to the direction tuning curve. U, B, D, and F = up, back (nasal to temporal), down, and forward (temporal to nasal) motion. In **B**, the filled circles represent the locations of the primary peaks from the excitatory response (ER) contour plots. The dashed diagonal line represents a stimulus velocity of 4°/s, which Ibbotson and

Price (2001) used to distinguish the "fast" and "slow" groups in both the wallaby NOT and the pigeon LM.

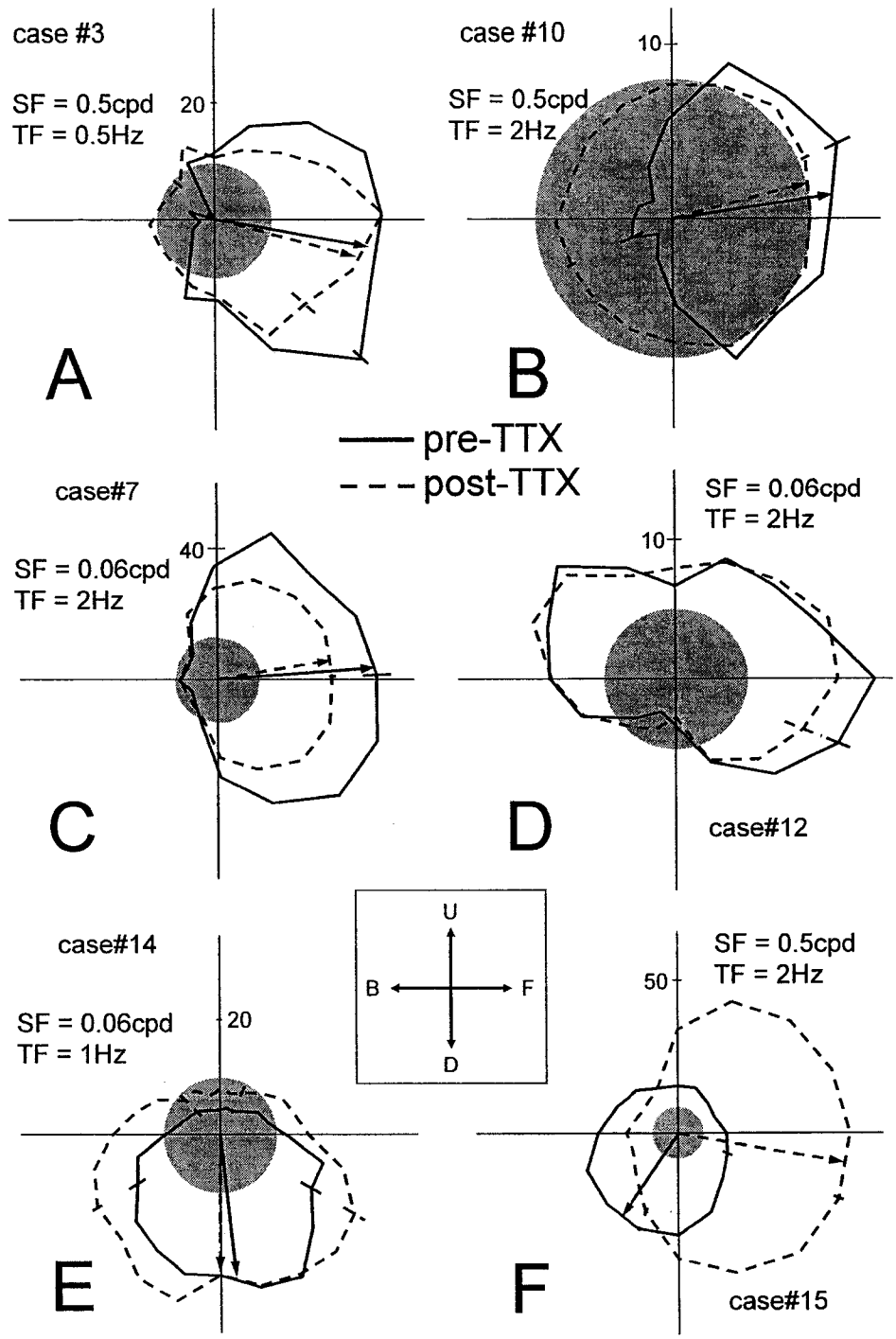

Figure 5.3

Directional tuning of lentiformis mesencephali units pre-TTX and post-TTX. Polar plots illustrating the directional tuning of units in the lentiformis mesencephali (LM) before and after the nucleus of the basal optic root (nBOR) was injected with tetrodotoxin (TTX)

(pre-TTX, solid line; post-TTX, dashed line). Firing rate (spikes/s) relative to the spontaneous rate (SR; gray circle) is plotted as a function of the direction of motion in polar coordinates (i.e. the SR has been set to zero; outside the gray circle = excitation, inside = inhibition). Solid and dashed arrows represent the unit's preferred direction pre-TTX and post-TTX, respectively, as calculated from the best fit cosines to the tuning curves. (A cosine could not be fit to the tuning curves for the bi-directional unit (Fig. 5.3D)). The spatial and temporal frequency (SF, TF) of the gratings used for the directional tuning are illustrated for each case. U, B, D, and F represent up, back (nasal to temporal), down, and forward (temporal to nasal) motion.

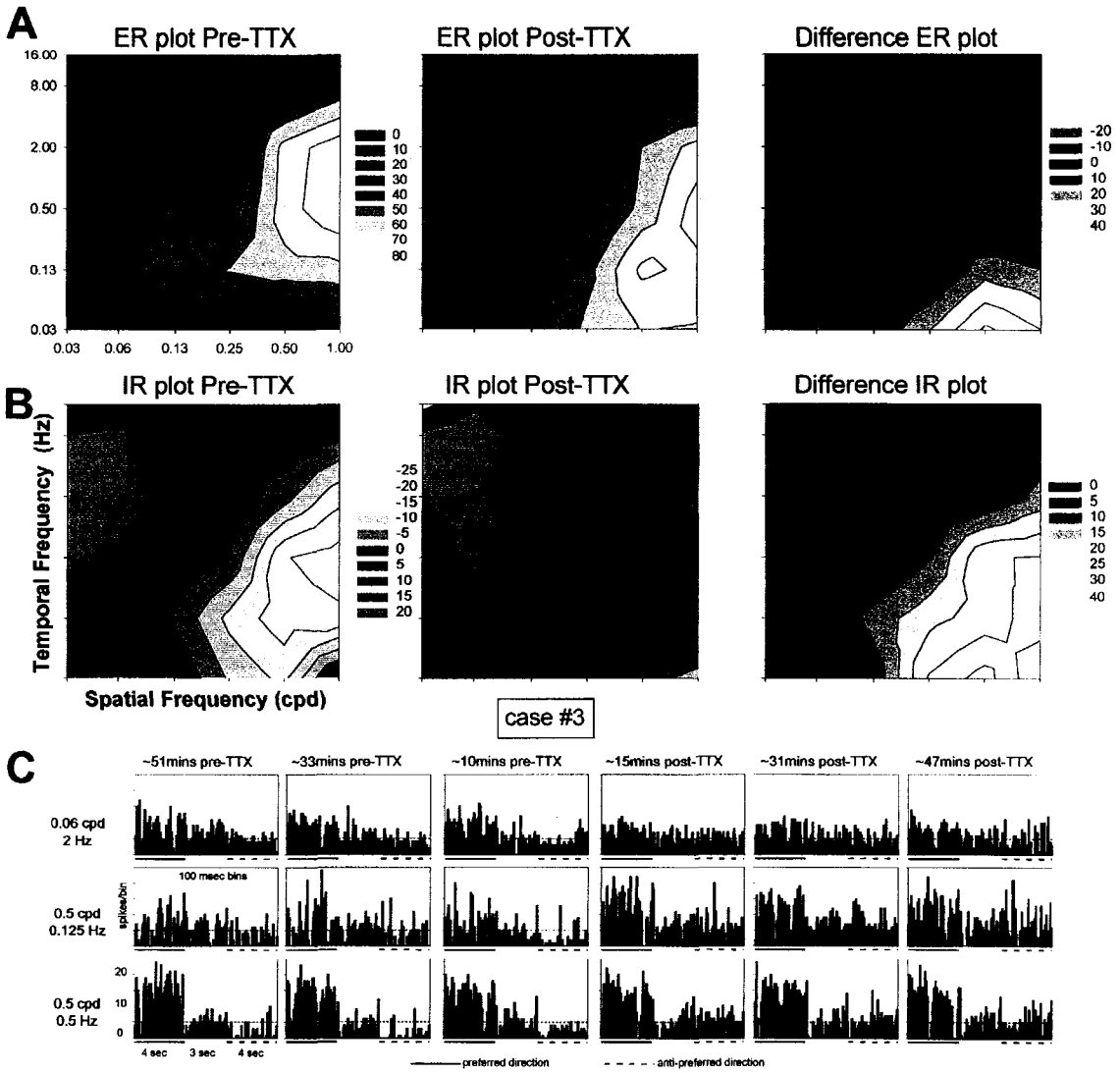

Figure 5.4

Effects of inactivation of the nucleus of the basal optic root on the spatio-temporal tuning of a lentiformis mesencephali unit. Data from case#3 is shown. In **A** and **B** respectively, contour plots of the responses to gratings of varying temporal and spatial frequency (SF, TF) drifting in the preferred direction (ER plots) and anti-preferred direction (IR plots) are shown. SF and TF are plotted on the abscissa and ordinate, respectively. Pre-TTX, post-TTX, and difference (Post-TTX – Pre-TTX) plots are shown in the left, middle, and right columns, respectively. Pre-TTX and post-TTX contour plots use a common scale to represent the firing rate (spikes/s) above (+; reds) or below (-; greens) the spontaneous

rate (black). These scales are shown between the pre-TTX and post-TTX columns. The scale for the difference plot is shown on the far right. Black represents a value of zero; i.e. no change in the response pre- to post-TTX, blues represent negative values, i.e. a lower firing rate post-TTX, and yellow represent positive values, i.e. a higher firing rate post-TTX. Progressively brighter and less saturated colors indicate progressively larger magnitudes in the contour plots. **C** shows a series of peri-stimulus time histograms (PSTHs) of individual sweeps of the responses to three different SF/TF combinations. Three sweeps pre-TTX and three sweeps post-TTX are shown, and the approximate time relative to the TTX injection is shown. Each sweep consisted of 4s motion in the preferred direction, followed by a 3s pause, followed by 4s motion in the anti-preferred direction. The dotted lines in the PSTHs represent the spontaneous rate.

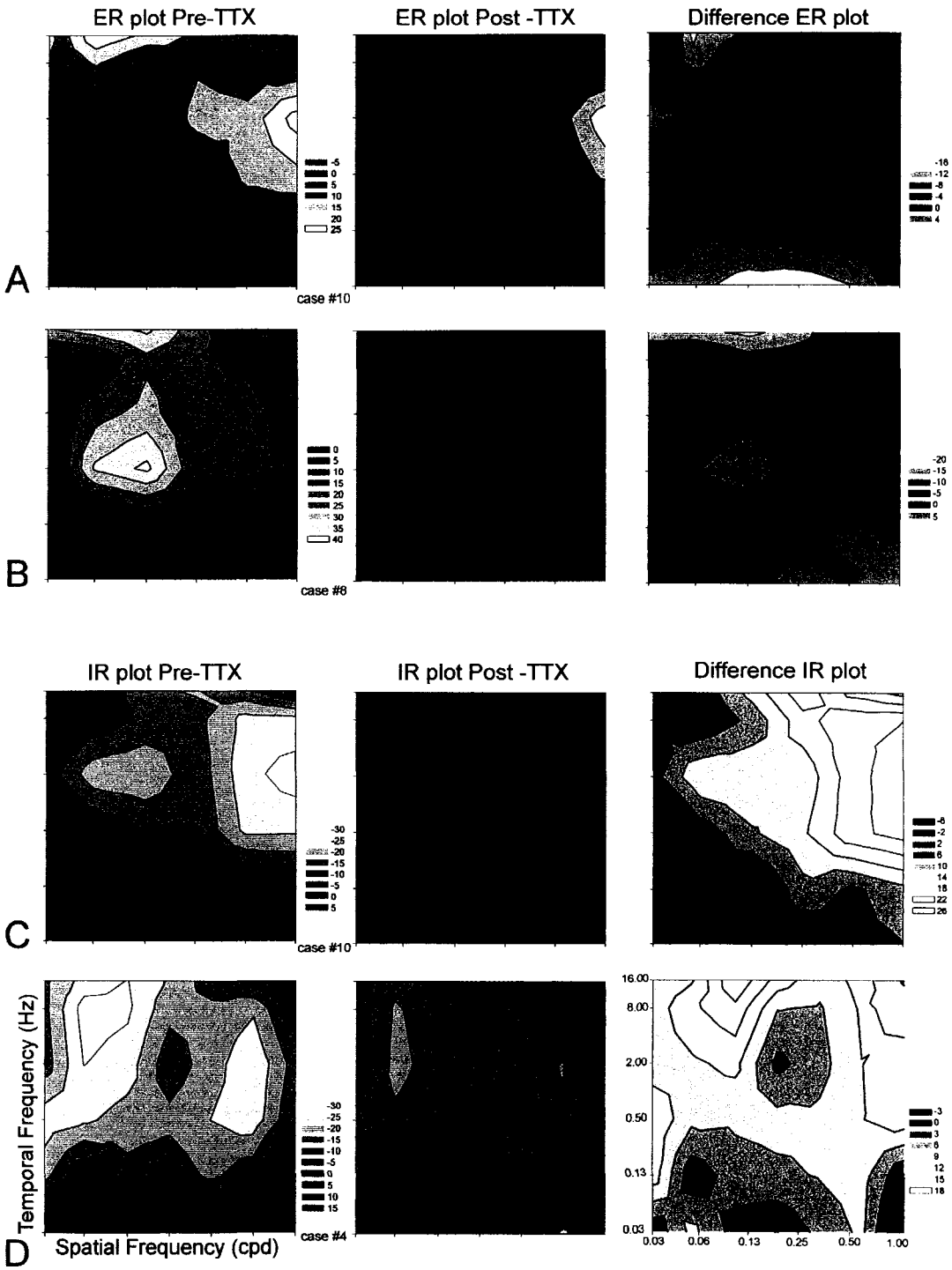

Figure 5.5

Effects of inactivation of the nucleus of the basal optic root on the spatio-temporal tuning of lentiformis mesencephali units. Spatio-temporal tuning of lentiformis mesencephali units to gratings drifting in the preferred (ER plots, **A**,**B**) and anti-preferred directions (IR plots, **C**,**D**) before and after the nucleus of the basal optic root (nBOR) was injected with tetrodotoxin (TTX) (pre-TTX, post-TTX). Note that **A** and **C** are from the same case. See caption to Figure 5.4 for additional details.

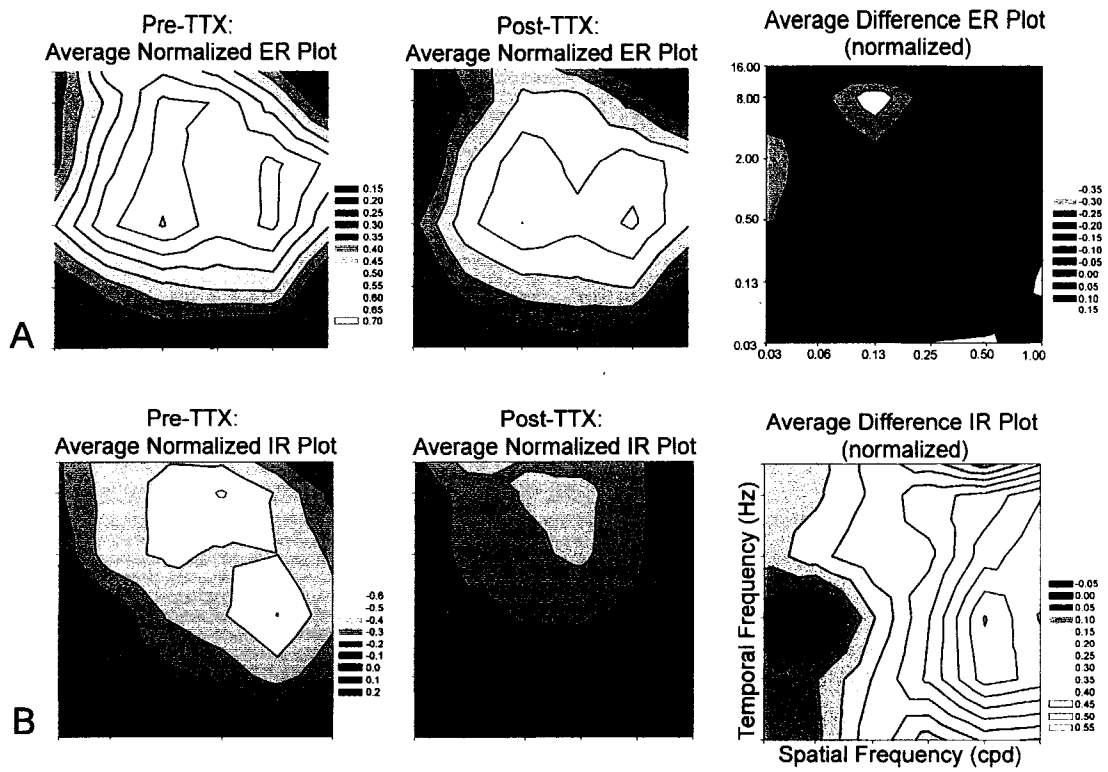

Figure 5.6

Effects of the inactivation of the nucleus of the basal optic root on the spatio-temporal tuning of lentiformis mesencephali units to gratings drifting in the preferred (ER plots, **A**) and anti-preferred directions (IR plots, **B**). Normalized data averaged across all cases are shown. See caption to Figure 5.4 and Results for additional details.

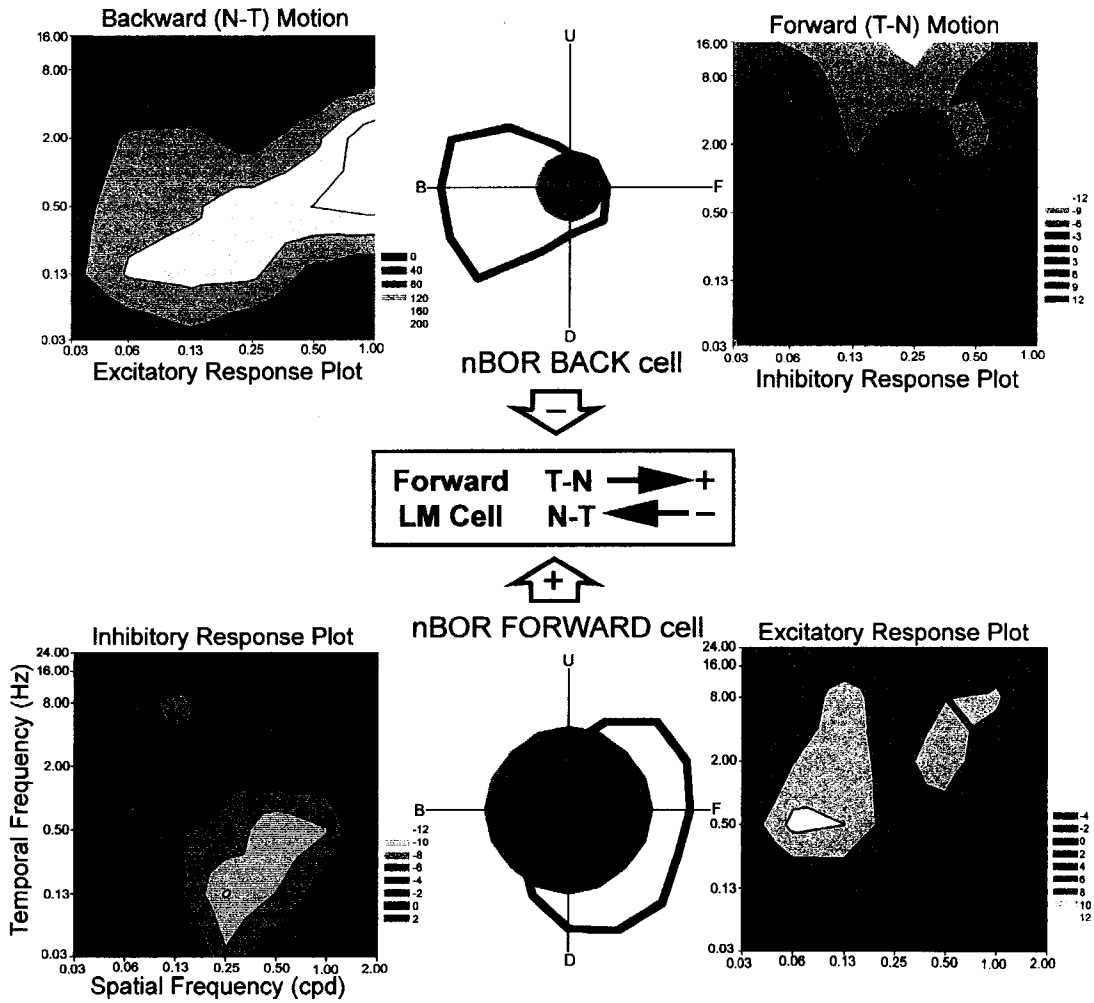

Figure 5.7

A descriptive model of the projection from the nucleus of the basal optic root to a neuron in the lentiformis mesecephali. Data from two neurons in the nucleus of the basal optic root (nBOR) show possible inputs to a lentiformis mesecephali (LM) neuron that is excited by forward motion and inhibited by backward motion. The proposed connectivity could account for the observed changes in spatio-temporal tuning after blockade of the nBOR. The directional tuning of the two neurons is shown in addition to the spatio-temporal tuning to gratings drifting in the preferred direction (Excitatory

Response plots) and anti-preferred direction (Inhibitory Response plots). U, B, D, and F represent up, back (nasal to temporal), down, and forward (temporal to nasal) motion. See caption to Figure 5.4 for additional details and the discussion for a comprehensive description.

column #	2	3	4	5	6	7	8		9	
case#	injection size (μL)	conc. TTX (ng/μL)	SR change (%)	preferred direction	direction change (°)	breadth of tuning change (°)	peaks in difference ER plot (%)		peaks in difference IR plot (%)	
1	1	2	-42.4*	F	12	+11	**-fast** *+slow*	**-75** *+40*	**+slow** *+fast*	**-100** *-100*
2	1	2	+2.4	F	11	-10	**-fast**	**-54**	**+slow** *+fast*	**-53** *-54*
3	1	2	+2.4	F	4	-16	**-fast** *+slow*	**-65** *+41*	**+slow**	**-100**
4	1.25	2	-20.5*	F	6	+10	**-fast**	**-74**	*+fast*	*-59*
5	1.25	2	-14.5*	F	7	-80	**-fast** -slow	**-81** -45	**+slow** *+fast*	**-48** *-48*
6	1.5	2	-3.4	F	6	+23	**-fast**	**-25**	*+fast*	*-72*
7	2	2	-55.5*	F	5	+5	**-fast** *+slow*	**-59** *+71*	**+slow**	**-63**
8	1.5	2	+38.8*	F	2	+4	**-fast**	**-68**	**+slow**	**-100**
9	1	2	-9.3	F	2	+2	+fast	+37	**+slow** *+fast*	**-100** *-27*
10	0.3	10	-32.1*	F	7	-3	**-fast** -slow	**-85** -74	**+slow**	**-73**
11	0.5	10	+6.8*	F	3	+11	+fast *+slow*	+32 *+31*	no change	
12	1.5	2	-40.7*	bi-dir	---	---	**-fast** *+slow*	**-100** *+64*	---	
13	1.25	2	-39.5*	B	2	-10	**-fast**	**-68**	no change	
14	1	2	-6.7	D	6	+43	**-fast**	**-48**	**+slow**	**-100**
15	0.3	10	+11.2	D	116*	+25	---		---	
16	0.3	10	-37.7*	D	1	-4	**-fast** *+slow*	**-91** *+76*	*+fast*	*-64*
17	0.4	10	-16.9*	D	2	+10	**-fast**	**-42**	no change	
18	0.3	10	-33.9*	U	4	+17	+fast *+slow*	+28 *+94*	**+slow**	**-48**

Table 5.1

The effect of inactivation of the nucleus of the basal optic root on the direction and spatio-temporal tuning of units in the lentiformis mesencephali. Details from each of the 18 cases are summarized. For spontaneous rate (SR) and breadth of tuning change, negative numbers indicate a reduction post-TTX and * indicates statistical significance. F,B,U and D = forward (temporal to nasal), backward (nasal to temporal), upward and downward motion, respectively. bi-dir = bi-directional neuron. In columns eight and nine, respectively, the peaks in the difference excitatory and inhibitory response (ER, IR) plots are given. "-fast", for example, indicates that there was a negative in the difference plot. The magnitudes of the peaks are also tabulated. See Results for additional details.

References

Arends JJ, Zeigler HP. Organization of the cerebellum in the pigeon (*Columba livia*): II. Projections of the cerebellar nuclei. *J Comp Neurol* 306:245-272, 1991.

Azevedo TA, Cukiert A, Britto LR. A pretectal projection upon the accessory optic nucleus in the pigeon: an anatomical and electrophysiological study. *Neurosci Letters* 43: 13-8, 1983.

Baldi E, Ambrogi Lorenzini C, Sacchetti B, Tassoni G, Bucherelli C. Entorhinal cortex and fimbria-fornix role in rat's passive avoidance response memorization. *Brain Res* 799: 270-277, 1998.

Baldo MV, Britto LR. Accessory optic-pretectal interactions in the pigeon. *Brazilian J Med Biol Res* 23: 1037-1040, 1990.

Baleydier C, Magnin M, Cooper HM. Macaque accessory optic system: II. Connections with the pretectum. *J Comp Neurol* 302: 405-416, 1990.

Bielavska E, Roldan G. Ipsilateral connections between the gustatory cortex, amygdala and parabrachial nucleus are necessary for acquisition and retrieval of conditioned taste aversion in rats. *Behav Brain Res* 81: 25-31, 1996.

Blanks RH, Giolli RA, Pham SV. Projections of the medial terminal nucleus of the accessory optic system upon pretectal nuclei in the pigmented rat. *Exp Brain Res* 48: 228-237, 1982.

Blanks RH, Clarke RJ, Lui F, Giolli RA, Van Pham S, Torigoe Y. Projections of the Lateral terminal accessory optic nucleus of the common marmoset (*Callithrix jacchus*). *J Comp Neurol* 354: 511-532, 1995.

Brecha N, Karten HJ, Hunt SP. Projections of the nucleus of basal optic root in the pigeon: An autoradiographic and horseradish peroxidase study. *J Comp Neurol* 189: 615-670, 1980.

Burns S, Wallman J. Relation of single unit properties to the occulomotor function of the nucleus of the basal optic root (AOS) in chickens. *Exp Brain Res* 42: 171-180, 1981.

Carpenter RHS. *Movement of the Eyes*. London: PION Ltd, 1977.

Collewijn H. Direction-selective units in the rabbit's nucleus of the optic tract. *Brain Res* 100: 489-508, 1975a.

Collewijn H. Oculomotor areas in the rabbit's midbrain and pretectum. *J Neurobiol* 6: 3-22, 1975b.

Cooper HM, Magnin M. A common mammalian plan of accessory optic system organization revealed in all primates. *Nature* 324: 457-459, 1986.

Crowder NA, Wylie DR. Fast and slow neurons in the nucleus of the basal optic root in pigeons. *Neurosci Letters* 304: 133-6, 2001.

Crowder NA, Dawson MR, Wylie DR. Temporal Frequency and Velocity-Like Tuning in the Pigeon Accessory Optic System. *J Neurophysiol* in press.

Distler C, Hoffmann KP. Visual receptive field properties in kitten pretectal nucleus of the optic tract and dorsal terminal nucleus of the accessory optic tract. *J Neurophysiol* 70: 814-827, 1993.

Fan TX, Weber AE, Pickard GE, Faber KM, Ariel M. Visual responses and connectivity in the turtle pretectum. *J Neurophysiol* 73: 2507-2521, 1995.

Fite KV. Pretectal and accessory-optic visual nuclei of fish, amphibia and reptiles: themes and variations. *Brain Behav Evol* 26: 71-90, 1985.

Fite KV, Kwei-Levy C, Bengston L. Neurophysiological investigation of the pretectal nucleus lentiformis mesencephali in Rana pipiens. *Brain Behav Evol* 34: 164-170, 1989.

Frost BJ. Neural mechanisms for detecting object motion and figure-ground boundaries contrasted with self-motion detecting systems. In *Brain Mechanisms of Spatial Vision* edited by Ingle D, Jeannerod M, Lee D. Dordrecht: Martinus Nijhoft, 1985, p. 415-449.

Gallo M, Candido A. Reversible inactivation of dorsal hippocampus by tetrodotoxin impairs blocking of taste aversion selectively during the acquisition but not the retrieval in rats. *Neurosci Letters* 186: 1-4, 1995.

Gamlin PDR, Cohen DH. Retinal projections to the pretectum in the pigeon (*Columba livia*). *J Comp Neurol* 269:1-17, 1988a.

Gamlin PDR, Cohen DH. Projections of the retinorecipient pretectal nuclei in the pigeon (*Columba livia*). *J Comp Neurol* 269: 18-46, 1988b.

Gibson JJ. The visual perception of object motion and subjective movement. *Psychol Rev* 61: 304-314, 1954.

Gioanni H, Rey J, Villalobos J, Dalbera A. Single unit activity in the nucleus of the basal optic root (nBOR) during optokinetic, vestibular and visuo-vestibular stimulations in the alert pigeon (*Columba livia*). *Exp Brain Res* 57: 49-60, 1984.

Giolli RA, Blanks RH, Torigoe Y. Pretectal and brain stem projections of the medial terminal nucleus of the accessory optic system of the rabbit and rat as studied by

anterograde and retrograde neuronal tracing methods. *J Comp Neurol* 227: 228-251, 1984.

Giolli RA, Blanks RH, Torigoe Y, Williams DD. Projections of medial terminal accessory optic nucleus, ventral tegmental nuclei, and substantia nigra of rabbit and rat as studied by retrograde axonal transport of horseradish peroxidase. *J Comp Neurol* 232: 99-116, 1985a.

Giolli RA, Peterson GM, Ribak CE, McDonald HM, Blanks RH, Fallon JH. GABAergic neurons comprise a major cell type in rodent visual relay nuclei: an immunocytochemical study of pretectal and accessory optic nuclei. *Exp Brain Res* 61: 194-203, 1985b.

Giolli RA, Torigoe Y, Clarke RJ, Blanks RH, Fallon JH. GABAergic and non-GABAergic projections of accessory optic nuclei, including the visual tegmental relay zone, to the nucleus of the optic tract and dorsal terminal accessory optic nucleus in rat. *J Comp Neurol* 319: 349-358, 1992.

Grasse KL, Cynader MS. Electrophysiology of medial terminal nucleus of accessory optic system in the cat. *J Neurophysiol* 48: 490-504, 1982.

Grasse KL, Cyander MS, Douglas RM. Alterations in response properties in the lateral and dorsal terminal nuclei of the cat accessory optic system following visual cortex lesions. *Exp Brain Res* 55: 69-80, 1984.

Grasse KL, Cyander MS. The accessory optic system in frontal-eyed animals. In: *Vision and Visual Dysfunction. The Neuronal Basis of Visual Function*, edited by Leventhal A. New York, NY: McMillan, 1990, p. 111-139.

Gu Y, Wang Y, Wang SR. Directional modulation of visual responses of pretectal neurons by accessory optic neurons in pigeons. *Neurosci* 104: 153-159, 2001.

Hamassaki DE, Gasparotto OC, Nogueira MI, Britto LRG. Telencephalic and pretectal modulation of the directional selectivity of accessory optic neurons in the pigeon. *Brazilian j Med Biol Res* 21: 649-652, 1988.

Hoffmann KP, Schoppmann A. Retinal input to direction selective cells in the nucleus tractus opticus of the cat. *Brain Res* 99: 359-366, 1975.

Hoffmann KP Schoppmann A. A quantitative analysis of the direction-specific response of neurons in the cat's nucleus of the optic tract. *Exp Brain Res* 42: 146-157, 1981.

Hoffmann KP, Distler C. Quantitative analysis of visual receptive fields of neurons in nucleus of the optic tract and dorsal terminal nucleus of the accessory optic tract in macaque monkey. *J Neurophysiol* 62: 416-428, 1989.

Hoffmann KP, Distler C, Erickson RG, Mader W. Physiological and anatomical identification of the nucleus of the optic tract and dorsal terminal nucleus of the accessory optic tract in monkeys. *Exp Brain Res* 69: 635-644, 1988.

Hoffmann KP, Distler C, Erickson RG. Functional projections from striate cortex and superior temporal sulcus to the nucleus of the optic tract (NOT) and dorsal terminal nucleus of the accessory optic tract (DTN) of macaque monkeys. *J Comp Neurol* 313: 707-724, 1991.

Hollander H, Tietze J, Distel H. An autoradiographic study of the subcortical projections of the rabbit striate cortex in the adult and during postnatal development. *J Comp Neurol* 184: 783-794, 1979.

Ibbotson MR, Mark RF, Maddess TL. Spatiotemporal response properties of direction-selective neurons in the nucleus of the optic tract and the dorsal terminal nucleus of the wallaby, *Macropus eugenii*. *J Neurophysiol* 72: 2927-2943, 1994.

Ibbotson MR, Price NS. Spatiotemporal tuning of directional neurons in mammalian and avian pretectum: a comparison of physiological properties. *J Neurophysiol* 86: 2621-2624, 2001.

Ilg UJ, Hoffmann KP. Functional grouping of the cortico-pretectal projection. *J Neurophysiol* 70: 867-869, 1993.

Ilg UJ, Hoffmann KP. Responses of neurons of the nucleus of the optic tract and the dorsal terminal nucleus of the accessory optic tract in the awake monkey. *Eur J Neurosci* 8: 92-105, 1996.

Karten HJ, Hodos W. *A stereotaxic Atlas of the Brain of the Pigeon* (*Columba livia*). Baltimore: Johns Hopkins Press, 1967.

Kato I, Watanabe S, Sato S, Norita M. Pretectofugal fibers from the nucleus of the optic tract in monkeys. *Brain Res* 705: 109-117, 1995.

Katte O, Hoffman KP. Direction specific neurons in the pretectum of the frog (Rana esculenta). *J Comp Physiol* 140: 53-57, 1980.

Kogo N, McGartland Rubio D, Ariel M. Direction tuning of individual retinal inputs to the turtle accessory optic system. J Neurosci 18: 2673-2684.

Lui F, Giolli RA, Blanks RH, Tom EM. Pattern of striate cortical projections to the pretectal complex in the guinea pig. *J Comp Neurol* 344: 598-609, 1994.

McKenna OC, Wallman J. Accessory optic system and pretectum of birds: comparisons with those of other vertebrates. *Brain, Behavior & Evolution* 26:91-116, 1985a.

McKenna OC, Wallman J. Functional postnatal changes in avian brain regions responsive to retinal slip: a 2-deoxy-D-glucose study. *J Neurosci* 5: 330-342, 1985b.

Miceli D, Gioanni H, Reperant J, Peyrichoux J. The avian visual wulst: I. An anatomical study of afferent and efferent pathways. II. An electrophysiological study of the functional properties of single neurons. In: *Neural Mechanisms of Behavior of the Pigeon*, edited by Granda, AM, Maxwell JH. New York, NY: Plenum Press, 1979, p. 223-354.

Morgan B, Frost BJ. Visual response properties of neurons in the nucleus of the basal optic root of pigeons. *Exp Brain Res* 42: 184-188, 1981.

Mustari MJ, Fuchs AF. Discharge patterns of neurons in the pretectal nucleus of the optic tract (NOT) in the behaving primate. *J Neurophysiol* 64: 77-90, 1990.

Mustari MJ, Fuchs AF, Kaneko CR, Robinson FR. Anatomical connections of the primate pretectal nucleus of the optic tract. *J Comp Neurol* 349: 111-128, 1994.

Nakayama K. Differential motion hyperacuity under conditions of common image motion. *Vision Res* 21:1475-1482, 1981.

Natal CL, Britto LRG. The pretectal nucleus of the optic tract modulates the direction selectivity of the accessory optic neurons in rats. *Brain Res* 419: 320-323, 1987.

Nogueira MI, Britto LRG. Extraretinal modulation of accessory optic units in the pigeon. *Brazilian J Med Biol Res* 24: 623-631, 1991.

Perrone JA, Thiele A. Speed skills: measuring the visual speed analyzing properties of primate MT neurons. *Nature Neurosci* 4: 526-531, 2001.

Rashidy-Pour A, Motamedi F, Semnanian S, Zarrindast MR, Fatollahi Y, Behzadi G. Effects of reversible inactivation of the medial septal area on long-term potentiation and recurrent inhibition of hippocampal population spikes in rats. *Brain Res* 734: 43-48, 1996a.

Rashidy-Pour A, Motamedi F, Motahed-Larijani Z. Effects of reversible inactivations of the medial septal area on reference and working memory versions of the Morris water maze. *Brain Res* 709:131-40, 1996b.

Roldan G, Bures J. Tetrodotoxin blockade of amygdala overlapping with poisoning impairs acquisition of conditioned taste aversion in rats. *Behav Brain Res* 65: 213-219, 1994.

Rosenberg AF, Ariel M. Visual-response properties of neurons in turtle basal optic nucleus in vitro. *J Neurophysiol* 63: 1033-1045, 1990.

Schmidt M, Lewald J, van der Togt C, Hoffmann KP. The contribution of GABA-mediated inhibition to response properties of neurons in the nucleus of the optic tract in the rat. *Eur J Neurosci* 6: 1656-1661, 1994.

Schmidt M, van der Togt C, Wahle P, Hoffmann KP. Characterization of a directional selective inhibitory input from the medial terminal nucleus to the pretectal nuclear complex in the rat. *Eur J Neurosci* 10: 1533-1543, 1998.

Schoppmann A. Projections from areas 17 and 18 of the visual cortex to the nucleus of the optic tract. *Brain Res* 223: 1-17, 1981.

Shintani T, Hoshino K, Meguro R, Kaiya T, Norita M. A light and electron microscopic analysis of the convergent retinal and visual cortical projections to

the nucleus of the optic tract (NOT) in the pigmented rat. *Neurobiology* 7: 445-460, 1999.

Simpson JI. The accessory optic system. *A Rev Neurosci* 7: 13-41, 1984.

Simpson JI, Leonard CS, Soodak RE. The accessory optic system: II. Spatial organization of direction selectivity. *J Neurophysiol* 60: 2055-2072, 1988.

Soodak RE, Simpson JI. The accessory optic system of rabbit. I. Basic visual response properties. *J Neurophysiol* 60: 2037-2054, 1988.

van der Togt C, Schmidt M. Inhibition of neuronal activity in the nucleus of the optic tract due to electrical stimulation of the medial terminal nucleus in the rat. *Eur J Neurosci* 6: 558-64, 1994.

Volchan E, Rocha-Miranda CE, Picanco-Diniz CW, Zinsmeisser B, Bernardes RF, Franca JG. Visual response properties of pretectal units in the nucleus of the optic tract of the opossum. *Exp Brain Res* 78: 380-386, 1989.

Weber JT. Pretectal complex and accessory optic system in alert monkeys. *Brain Behav Evol* 26: 117-140, 1985.

Westheimer G, McKee SP. Failure of Donders' law during smooth pursuit eye movements. *Vision Res.* 13: 2145-253, 1973.

Winterson BJ, Brauth SE. Direction-selective single units in the nucleus lentiformis mesencephali of the pigeon (Columba livia). *Exp Brain Res* 60: 215-226, 1985.

Wylie DR, Frost BJ. Visual response properties of neurons in the nucleus of the basal optic root of the pigeon: A quantitative analysis. *Exp Brain Res* 82: 327-336, 1990.

Wylie DRW, Frost BJ. The pigeon optokinetic system: Visual input in extraocular muscle coordinates. *Vis Neurosci* 13: 945-953, 1996.

Wylie DR, Linkenhoker B, Lau KL. Projections of the nucleus of the basal optic root in pigeons (*Columba livia*) revealed with biotinylated dextran amine. *J Comp Neurol* 384: 517-536, 1997.

Wylie DR, Crowder NA. Spatiotemporal properties of fast and slow neurons in the pretectal nucleus lentiformis mesencephali in pigeons. *J Neurophysiol* 84: 2529-2540, 2000.

Yakushin SB, Gizzi M, Reisine H, Raphan T, Buttner-Ennever J, Cohen B. Functions of the nucleus of the optic tract (NOT). II. Control of ocular pursuit. *Exp Brain Res* 131: 433-447, 2000.

Zhuravin MA, Bures J. Extent of the tetrodotoxin induced blockade examined by papillary paralysis elicited by intracerebral injection of the drug. *Exp Brain Res* 83: 687-690, 1991.

Chapter 6

Telencephalic Input to the Pretectum of Pigeons: an Electrophysiological and Pharmacological Inactivation Study

A version of this chapter has been submitted. Crowder NA, Dickson CT, Wylie DRW.

Journal of Neurophysiology.

Introduction

The pretectum and accessory optic system (AOS) are involved in the generation of the optokinetic response (OKR), and the processing of optic flow that results from self-motion (Gibson, 1954; Simpson, 1984; Simpson et al., 1988; Grasse and Cynader, 1990). The OKR facilitates retinal image stabilization, which is important for optimal visual acuity (Westheimer and McKee, 1973; Carpenter, 1977) and velocity discrimination (Nakayama, 1981).

The AOS and pretectum are highly conserved in vertebrates. The medial and lateral terminal nuclei (MTN, LTN) of the mammalian AOS are homologous to the avian nucleus of the basal optic root (nBOR), and the pretectal nucleus of the optic tract (NOT) in mammals is homologous to the nucleus lentiformis mesencephali (LM) in birds (Simpson, 1984; McKenna and Wallman, 1985a; Fite, 1985; Weber, 1985; Simpson et al., 1988). AOS and pretectal neurons have large receptive fields in the contralateral visual field, and exhibit direction-selectivity to drifting large-field visual stimuli. Most neurons in the LM and NOT prefer temporal-to-nasal (T-N) motion (NOT: Collewijn, 1975a,b; Hoffman and Schoppmann, 1975, 1981; Hoffmann et al., 1988; Hoffmann and Distler, 1989; Volchan et al., 1989; Mustari and Fuchs, 1990; Distler and Hoffmann, 1993; Ibbotson et al., 1994; Ilg and Hoffmann, 1996; Yakushin et al., 2000, LM: Katte and Hoffmann, 1980; McKenna and Wallman, 1985b; Winterson and Brauth, 1985; Fite et al., 1989; Fan et al., 1995; Wylie and Frost, 1996; Wylie and Crowder, 2000). In mammals, AOS neurons prefer upward or downward motion (e.g. Simpson et al., 1979; Soodak and Simpson, 1988; Grasse and Cynader, 1982, 1984), whereas nBOR neurons prefer upward, downward or nasal-to-temporal motion (Burns and Wallman, 1981;

Morgan and Frost, 1981; Gioanni et al., 1984; Wylie and Frost, 1990; Rosenberg and Ariel, 1990). When drifting sine wave gratings are used as visual stimuli, neurons in the pretectum and AOS exhibit tuning in the spatio-temporal domain, preferring either high spatial frequencies (SFs) and low temporal frequencies (TFs), or low SFs and high TFs. As velocity = TF/SF, these two groups were referred to as "slow" and "fast" neurons, respectively (Ibbotson et al., 1994; Wylie and Crowder, 2000; Crowder and Wylie, 2001; Ibbotson and Price, 2001; Crowder et al., in press a,b).

Both the AOS and pretectum receive massive retinal input (Mammals: Hayhow et al., 1960; Garey and Powell, 1968; Giolli and Guthrie, 1969; Scalia and Arango, 1979; Birds: Karten et al. 1977; Reiner et al. 1979; Fite et al. 1981; Gamlin and Cohen 1988a). However, the AOS and pretectum also receive numerous extra-retinal inputs that could influence the visual response properties of neurons within these nuclei. For example, there is a heavy reciprocal connection between the AOS and pretectum (Rats: Terasawa et al., 1979; Blanks et al., 1982, Rabbits: Holstege and Collewijn, 1982; Giolli et al., 1984, Cats: Itoh, 1977; Berson and Graybiel, 1980; Weber and Harting, 1980; Pigeons: Clarke 1977; Brecha et al. 1980; Gamlin and Cohen 1988b; Wylie et al. 1997). Furthermore, the AOS and pretectum receive input from the telencephalon, although this input is quite variable between species. In cats and monkeys, the cortical input to NOT is quite heavy (Schoppmann, 1981; Hoffmann et al., 1991; Ilg and Hoffmann, 1993; Mustari et al., 1994), but is absent in other frontal-eyed species such as the opossum (Pereira et al., 2000). Moreover, the NOT receives cortical input in rabbits (Hollander et al., 1979), guinea pigs (Lui et al., 1994), and rats (Shintani et al., 1999), but not in hamsters (Lent, 1982) or tree shrews (Huerta et al., 1985). In pigeons, both the nBOR and

LM receive afferents from the Wulst (Rio et al., 1983; Miceli et al., 1979), which is thought to be the avian homolog of primary visual cortex (Karten and Shimizu, 1989; Medina and Reiner, 2000).

In the present study we investigated the effects of electrical stimulation and reversible pharmacological inactivation of the Wulst on the activity of LM neurons. There were a number of issues we wished to address. Is the Wulst projection excitatory or inhibitory? Do both fast and slow LM cells receive input from the Wulst? Is the connection correlated with direction preference? Finally with the Wulst inactivation, we sought to determine if the afferents from the Wulst contribute to the directional and spatio-temporal tuning of LM neurons.

Methods

Surgery and Extracellular recording

The methods employed conformed to the Guidelines established by the Canadian Council on Animal Care and were approved by the Biological Sciences Animal Welfare and Policy Committee at the University of Alberta. Details for anaesthesia, extracellular recording, stimulus presentation and data analysis have been described by Wylie and Crowder (2000). Briefly, pigeons were anaesthetized with a ketamine (65 mg/kg) - xylazine (8 mg/kg) mixture (i.m.), and supplemental doses were administered as necessary. Based on the pigeon stereotaxic atlas (Karten and Hodos, 1967), sufficient bone and dura were removed to expose the brain and allow access the LM, nBOR, and Wulst with vertical penetrations. Recordings were made with glass micropipettes filled with 2M NaCl and Pontamine sky blue (tip diameters 4-5 microns). The extracellular

signal was amplified, filtered, displayed on an oscilloscope and fed to a window discriminator. TTL pulses representing single spikes were fed to a 1401*plus* (Cambridge Electronic Designs (CED)) and peri-stimulus time histograms were constructed with *Spike2* software (CED).

Visual Stimulus Presentation

After neurons in the LM were isolated, the direction preference and the approximate locations of the receptive field boundaries and hot-spot were qualitatively determined by moving a large (90^{o} X 90^{o}) hand-held stimulus in various areas of the visual field. Directional and spatio-temporal tuning were determined quantitatively with sine-wave gratings that were generated by a VSG*Three* graphics computer (Cambridge Research Designs, Cambridge UK), and back-projected onto a tangent screen that was located 50cm from the bird (90^{o} X 75^{o}). Direction tuning was tested using gratings of an effective SF and TF at 22.5^{o} increments. Direction preference was quantitatively assigned by calculating the peak of the best-fit cosine to the tuning curve. Spatio-temporal tuning was tested using gratings of varying SF (0.03-2 cycles per degree (cpd)) and TF (0.03-16 cycles per second (Hz)) moving in the preferred and anti-preferred directions. Each sweep consisted of 4 sec of motion in one direction, a 3 sec pause, 4 sec of motion in the opposite direction, followed by a 3 sec pause. Firing rates were averaged over 3-5 sweeps.

Orthodromic Stimulation

Neurons in the LM received orthodromic electrical stimulation with single shocks (0.5 ms, 25-400 μA, 0.3 Hz) that were delivered through a Teflon coated stainless-steel bipolar stimulating electrode positioned in the Wulst (12.5mm anterior and 1.5mm lateral from interaural zero, 1.5mm ventral to the surface of the telencephalon). The tips of the bipolar electrode were staggered by 0.5mm. The constant current pulses were produced by a S48 stimulator (Grass-Telefactor, West Warwick, RI) connected to a PSIU6 stimulus isolation unit (Grass-Telefactor).

Wulst Inactivation General Procedure

The procedure to measure the effects of Wulst inactivation was as follows: 1.) Based on stereotaxic coordinates, bone and dura overlaying the Wulst were removed, and the bipolar stimulating electrode and injecting pipette (~25 μm tip diameter, filled with 4% lidocaine (Sigma-Aldrich, St. Louis) in phosphate buffered saline (pH=7.4)), were positioned in the Wulst. The stimulating electrode was angled at 45° in the coronal plane and penetrated 1.5 mm into the surface of the telencephalon. The pipette was positioned vertically such that the tip was located as close as possible to the two poles of the stimulating electrode. 2.) Pre-lidocaine Measures: A recording microelectrode was lowered into the pretectum, and the direction and spatio-temporal tuning of an LM neuron was characterized (see *Visual Stimulus Presentation* above), as was the response to electrical stimulation of the Wulst (see *Orthodromic Stimulation* above). 3.) Lidocaine was injected into the Wulst (2-4 μl) using a picospritzer (General Valve Corporation). Because the wash-out time of lidocaine is approximately 20 minutes (Sandkühler et al., 1987), supplemental injections of lidocaine were administered every 10 minutes in order

to prolong the inactivation of the Wulst. 4.) Post-lidocaine Measures: Five minutes after the initial injection of lidocaine, the response properties of the LM neuron, and the effects of Wulst electrical stimulation, were tested again. 5.) Recovery Measures: Following the last application of the pharmacological blockade, lidocaine was allowed to wash-out for 40-60 minutes, and the response properties of the LM neuron and the effects of electrical stimulation, were tested a final time.

nBOR Inactivation General Procedure

The procedure to measure the effects of nBOR inactivation was as follows: 1). The nBOR was located based on stereotaxic coordinates (Karten and Hodos, 1967), and the dorsal border of the nBOR was determined with extracellular recording. 2.) The recording electrode was replaced with an injecting pipette filled with lidocaine (see *Wulst Inactivation General Procedure* above). The pipette was positioned such that the tip was at the approximate depth of the dorsal-most responsive nBOR cell from the recording track. 3.) A bipolar stimulating electrode was positioned in the Wulst (see *Wulst Inactivation General Procedure* above). 4.) A recording microelectrode was lowered into the pretectum, and the direction and spatio-temporal tuning of an LM neuron was characterized (see *Visual Stimulus Presentation* above), as was the response to electrical stimulation of the Wulst (see *Orthodromic Stimulation* above). 5.) Lidocaine was injected into the nBOR (for details see *Wulst Inactivation General Procedure* above). 6.) Five minutes after the initial injection of lidocaine, the response properties of the LM neuron, and the effects of Wulst electrical stimulation, were tested again. 7.) Following the last application of the pharmacological blockade, lidocaine was allowed to wash-out for 40-

60 minutes, and the response properties of the LM neuron and the effects of electrical stimulation, were tested a final time.

Histology

In some cases, a dye spot was left at the final recording site by iontophoretically injecting the Pontamine sky blue and NaCl from the recording electrode (+3μA, 3sec on / 3sec off, for 20 minutes). At the end of the recording session, the animals were given an overdose of sodium pentobarbitol (100mg/kg) and immediately perfused with saline (0.9%) followed by paraformaldehyde (4% in 0.1M phosphate buffer (PB), 4°C). Brains were extracted, post-fixed for 2-12 hours (4% paraformaldehyde, 20% sucrose in 0.1M PB), and cryoprotected in sucrose overnight (20% in 0.1M PB). Frozen sections (45μm thick in the coronal plane) through the LM, nBOR, and Wulst were collected. Sections were mounted onto gelatin chrome aluminum coated slides and lightly counter-stained with neutral red. The tissue was then examined using light microscopy to confirm the locations of electrode tracks and dye spots in the LM, and the stimulating electrode tracks in the Wulst.

Results

We recorded from a total of 69 LM neurons. The directional and spatio-temporal properties of 45 LM neurons were quantitatively analyzed, while the directional preferences of 9 additional neurons were obtained from the hand-held stimulus alone. Fifty-nine LM neurons were tested with orthodromic stimulation from the Wulst. Furthermore, the directional tuning and spatio-temporal response properties of 20 LM

neurons were tested before, during, and after the Wulst was inactivated with lidocaine. Histological analysis revealed that the stimulating electrode was in the desired position in the Wulst (Rio et al., 1983). Dye spots and electrode tracks were seen in the lateral and medial subnuclei of LM (LMl and LMm, respectively; Gamlin and Cohen, 1988b).

Normal Properties of LM Neurons

All 45 LM neurons that were quantitatively examined for directional tuning exhibited direction selectivity. A unit was assigned a direction preference by calculating the maximum of the best cosine fit to the tuning curve. Twenty, 4, 5 and 16 LM neurons preferred forward (i.e. temporal to nasal), downward, backward and upward motion, respectively. Of the nine LM neurons tested with the hand-held stimulus, 2, 4, 2, and 1, preferred forward, downward, backward and upward motion. The predominance of neurons preferring forward motion is consistent with previous studies of the pigeon LM (Winterson and Brauth, 1985; Wylie and Frost, 1996; Wylie and Crowder, 2000; Crowder et al., in press a).

The spatio-temporal response properties of the 45 neurons were also quantitatively examined. Using *SigmaPlot*, contour plots were constructed where TF was on the ordinate, SF was on the abscissa, and mean firing rate relative to the spontaneous firing rate (SR) was plotted on the z-axis. As motion in the preferred and anti-preferred directions generally result in excitation and inhibition of the neuronal firing, respectively, we refer to excitatory and inhibitory response plots (ER plots, IR plots) (e.g. Figs. 6.5 and 7). The location of the peak in the contour plots were assigned quantitatively by fitting the primary peak in each contour plot to a two-dimensional Gaussian function (Perrone

and Thiele, 2001; Crowder et al., in press a,b). Consistent with previous studies of the pretectum (Ibbotson et al., 1994; Wylie and Crowder, 2000; Crowder et al., in press a), the peaks cluster into two quadrants: cells responding best to gratings of low SF/high TF (29 cells), or high SF/low TF (16 cells). Following Ibbotson et al. (1994), we refer to these as "fast" and "slow" cells, respectively.

Orthodromic Wulst Stimulation

All 59 LM neurons that were tested with orthodromic stimulation of the Wulst showed a modulation in firing. The average stimulation threshold to elicit modulation was 65μA (s.d. = 38μA). Two distinct effects were observed following Wulst stimulation. One group of cells showed a short-latency excitation followed by longer-latency inhibition. The second group of cells showed only the longer-latency inhibition. We refer to these groups as W+ cells and W- cells, respectively. Figure 6.1 shows data from a W+ cell, including the average spike waveform (a), the effects of subthreshold (b; 25μA) and suprathreshold stimulation (c and d; 200μA). Suprathreshold stimulation of the Wulst elicited a burst of 3-5 spikes at an average first-spike latency of 20ms (s.d. = 1.6ms). As expected with orthodromic stimulation, the average first spike latency decreased as the current intensity increased (in this case from 21 ± 2.3ms at 50μA to 20 ± 1.6ms at 200μA). As shown in Figure 6.1d, the excitatory burst was followed by a period of inhibition (at about 40-90ms). At higher intensities, the effects of the stimulation were often manifested as oscillations between excitation and inhibition lasting up to a one second (d). The consistency of the stimulation effect is shown in the raster plot and peri-stimulus time histogram (PSTH) (d).

Figure 6.2 shows raster plots and PSTHs illustrating the effects of stimulation of the Wulst for a W+ (Fig. 6.2a) and W- cell (Fig. 6.2b). We used 5ms bins for the PSTHs because inter-spike-interval analysis revealed that most LM neurons have an inter-spike interval of above 5ms (average = 7.2ms, s.d. = 3.7ms). Figure 6.2a shows PSTHs of the response of a W+ neuron to varying stimulation intensities (50μA, 100μA, 200μA). When the Wulst was stimulated with 200μA pulses, there was a short latency excitation (beginning at approximately 10ms) followed by inhibition at a latency of approximately 50ms and a smaller excitatory period at a latency of approximately 110ms. At 100μA, the short latency excitation was less marked, as was the rebound inhibition. Stimulation at 50μA failed to elicit any stimulation effect. The neuron in Figure 6.2b only showed inhibition following Wulst stimulation (i.e. a W- neuron), but showed a similar progression of stimulation effects with varying stimulation intensities. At 200μA this neuron showed inhibition at a latency of approximately 25ms, followed by excitation at a latency of approximately 150ms. This pattern was less pronounced at 100μA, and absent at 50μA.

Stimulation effects were quantitatively analyzed by converting every 5ms bin in the PSTH of an LM neuron into z-scores. Trials using subthreshold or no stimulation were used to calculate the average spontaneous rate of the neuron, and were compared to the results for suprathreshold stimulation intensity of 200μA. Deviations from the spontaneous rate were not considered significant unless they exceeded a z-score of 2. The stimulation latencies for W+ and W- neurons were 13.5 ± 5ms and 28.3 ± 8ms, respectively (mean ± standard deviation). These latencies were significantly different (single sample Student t-test $p < 0.0000001$). The rebound inhibition exhibited by W+

neurons occurred significantly later (35 ± 7ms; single sample Student t-test $p < 0.004$), than the initial inhibitory effect of W- neurons. It is likely that the inhibition shown by W+ and W- neurons occurs at a similar latency, but the true latency of W+ inhibition is masked by the excitatory burst that precedes it. Of the 59 LM neurons tested, 34 (58%) were W+ cells, and 25 (42%) were W- cells.

Directional tuning, as determined by best fit to cosines, for 27 W+ and 18 W- neurons is shown in Figure 6.3a,b. The orientation of each line represents the direction preference of individual W+ (Fig. 6.3a) and W- (Fig. 6.3b) neurons. From this figure it is clear that there were no differences between W+ and W- cells with respect to their direction preferences. Figure 6.3c plots the locations of the primary ER peaks from the spatio-temporal contour plots of 27 W+ (empty circles) and 17 W- neurons (filled circles). Of the W+ cells, 18 were fast cells, and 9 were slow cells. Of the W- neurons, 11 were fast cells, and 6 were slow cells. From Figure 6.3c it is clear that there were no differences between W+ and W- cells with respect to their spatio-temporal tuning, although the cells with the fastest peaks were all W+ cells.

Effects of Wulst Inactivation

The directional tuning and spatio-temporal response properties of 20 LM neurons were tested before, during, and after the Wulst was inactivated with lidocaine. Of these 20 neurons, 13 were also tested with orthodromic stimulation from the Wulst before, during, and after the Wulst was inactivated with lidocaine. Wulst inactivation completely eliminated all electrical stimulation effects. Figure 6.4 shows a W+ neuron before the Wulst was injected with lidocaine (Fig. 6.4a), a few minutes after the lidocaine injection

(Fig. 6.4b), and after the lidocaine effect had washed out (Fig. 6.4c). This explicit reversible inactivation effect was evident for all 13 LM neurons that were tested with Wulst electrical stimulation.

i) Changes in Spontaneous Rate of LM Neurons following Wulst Inactivation

Changes in the SR of LM neurons following Wulst inactivation were calculated as percent difference (for decreases, % change = {[post-lidocaine – pre-lidocaine] / pre-lidocaine}*100; for increases = {[post- lidocaine – pre- lidocaine] / post- lidocaine }*100). In 5 cases there was a significant decrease in SR (21-66%), whereas 2 cases showed a significant increase (23 and 35%) (t-tests, $p < 0.0025$; Bonferroni correction for multiple comparisons), and 13 cases showed no significant change. The average change in SR across all 20 cases was –7.9%.

ii) Effects of Wulst Inactivation on the Direction Tuning of LM Neurons

None of the LM neurons showed a showed a significant change in direction preference following Wulst inactivation. Two neurons showed changes of 14^{o} and 16^{o}, while the direction change for other neurons did not exceed 6^{o} (mean = 2.5^{o}). The magnitude of modulation, both excitation and inhibition, remained unchanged for all neurons. Figure 6.5a shows the direction tuning of an LM neuron before (black) and after (red) Wulst inactivation.

iii) Spatio-temporal Changes Following Wulst Inactivation

The spatio-temporal properties of all 20 LM neurons were examined before and during Wulst inactivation, and for 16 neurons following lidocaine wash-out. Inactivation of the Wulst did not significantly affect the spatio-temporal profiles of any LM neurons tested. Figure 6.5b shows the ER and IR plots of a single LM neuron before (Fig. 6.5b;

left) and during (Fig. 6.5b; right) Wulst inactivation. In these plots the black fill represents the SR, and excitation and inhibition are represented by red and green, respectively. The stronger the degree of excitation/inhibition, the progressively brighter and less saturated the red/green fill. Thus the peak excitation and inhibition appear off-white. For the cell shown in Figure 6.5b, both the ER plot pre-lidocaine (Fig. 6.5b; top left) and ER plot post-lidocaine (Fig. 6.5b; top right) had a main peak at 1cpd/0.5Hz (+50 spikes/s), and a smaller peak at 0.06cpd/16Hz (30 spikes/s). Similarly, the IR plot pre-lidocaine (Fig. 6.5b; bottom left) and post-lidocaine (Fig. 6.5b; bottom right) looked very similar, with a single inhibitory peak at 1cpd/0.5Hz (-16 spikes/s).

Effects of nBOR Inactivation on the Response Properties of LM Neurons

There is a reciprocal connection between the LM and nBOR (Brecha et al., 1980; Azevedo et al., 1983; Wylie et al., 1997). Since the Wulst also projects to the nBOR (Rio et al., 1983), we hypothesized that the longer latency modulation of LM cells that resulted from Wulst stimulation might arise from the nBOR cells that are also activated by Wulst stimulation. In order to test this possibility, the effect of Wulst electrical stimulation on 4 LM neurons was measured before, during, and after the nBOR was inactivated with lidocaine. The direction and spatio-temporal response properties of these LM neurons were also measured during nBOR inactivation, serving to replicate the data presented by Crowder et al. (in press a), and confirm inactivation of the nBOR.

Figure 6.6 shows PSTHs from a W- neuron before the nBOR was injected with lidocaine (Fig. 6.6a), a few minutes after the lidocaine injection (Fig. 6.6b), and after the lidocaine has washed out (Fig. 6.6c). Before nBOR inactivation, and following the

lidocaine wash-out period, the W- neuron showed long latency inhibition starting at 20ms. When the nBOR was inactivated, this inhibition was strongly diminished. This decrease in long latency inhibition was evident in 2 W+ cells and 1 W- cell. The remaining neuron was a W- cell that showed a lengthening in the duration of its long latency inhibition (20 - 130ms pre-lidocaine, and 20 - 180ms during lidocaine). The short latency excitation shown by W+ cells was not affected by nBOR inactivation (not shown).

Figure 6.7a shows the effect of nBOR inactivation on the ER plot of an LM neuron. Pre-lidocaine, the ER plot showed two excitatory peaks (primary, 0.25cpd / 0.5Hz; secondary, 0.25cpd / 8Hz). Both peaks diminished in size during nBOR inactivation, but returned following lidocaine wash-out. Generally, ER plots showed less excitation to low SF/high TF stimuli (3 of 4 cells), and more excitation to high SF/low TF stimuli (all cells) moving in the preferred direction following nBOR inactivation. Figure 6.7b shows the effect of nBOR inactivation on the IR plot of another LM neuron. Pre-lidocaine, the IR plot showed one main inhibitory peak (1cpd / 0.5Hz), which completely disappeared during nBOR inactivation, and returned following lidocaine wash-out. The majority of IR plots (3 of 4 cells) showed less inhibition to high SF/low TF stimuli moving in the anti-preferred direction. Figure 6.7c shows the effect of nBOR inactivation on the direction tuning of a LM neuron that preferred forward motion. Note that preferred direction for this neuron is not directly opposite the anti-preferred direction. During nBOR inactivation this neuron showed no changes in its preferred direction, but there is more excitation to motion in the preferred direction, and less inhibition to motion in the anti-preferred direction. One other neuron showed this same pattern, while the depth of

tuning for the remaining 2 neurons was not affected. None of the neurons showed changes in their preferred direction following nBOR inactivation.

Discussion

In the present study we investigated the function of the projection from the Wulst to the pretectum (Gottlieb and McKenna, 1986; Miceli et al., 1979). We electrically stimulated the Wulst, and found that LM neurons were either excited (W+ cells) or inhibited (W- cells). However, when the Wulst was temporarily inactivated by lidocaine neither the directional nor spatio-temporal response properties of LM neurons were affected.

W+ and W- cells in the LM

This study is the first to demonstrate the effects of Wulst stimulation on the activity of pretectal neurons. Just over half of the LM neurons tested showed short latency (13.5ms) excitation to Wulst stimulation, while the remainder showed longer latency (28.3ms) inhibition to Wulst stimulation. We refer to these LM neurons as W+ cells and W- cells, respectively. Wulst stimulation effects did not appear to correlate with directional or spatio-temporal tuning. The bimodal distribution of latencies for W+ and W- neurons suggests a direct and indirect route from the Wulst to the LM. The short latency excitatory stimulation effects seen in LM W+ neurons likely arise from the monosynaptic inputs they receive from the Wulst (Gottlieb and McKenna, 1986; Miceli et al., 1979; Rio et al., 1983). Longer latency inhibitory effects could be due to polysynaptic feed forward or even feed back circuits within the LM itself or due to feed

forward inhibitory projections from other pretectal nuclei also receiving Wulst input (see below).

W+ and W- cells in the nBOR

Nogueira and Britto (1991) examined the effects of Wulst stimulation on the firing rate of nBOR neurons. Their findings were strikingly similar to those of the present study: nBOR neurons showed either a short latency excitation (26%; average latency = 13 ms) or a longer latency inhibition (38%; average latency = 35ms). Clearly the nBOR has counterparts to the W+ (average latency = 13.5 ms) and W- (average latency = 28.3 ms) LM cells described in the present study. This argues for a similar function of the telencephalic projection to the pretectum and AOS.

Longer Latency Modulation of LM neurons from Wulst Stimulation: Wulst, LM, nBOR Interactions

The initial longer latency inhibition of the W- cells in response to Wulst stimulation, as well as the longer lasting inhibitory/excitatory oscillations seen in both W+ and W- neurons, could arise from inhibitory interneurons in the pretectum, and/or from Wulst stimulation following an indirect route through the nBOR (Clarke 1977; Brecha et al. 1980; Gamlin and Cohen 1988b; Wylie et al. 1997). When we inactivated nBOR, the long-latency modulation in response to Wulst stimulation was clearly affected. For three of four cases, there was a reduction in long-latency inhibition, and in one case there was an increase. It has been suggested that the projection from the nBOR to LM is predominantly inhibitory (Baldo and Britto, 1990; van der Togt and Schmidt,

1994), but also excitatory (Baldo and Britto, 1990; Crowder et al., in press a). Oscillations seen in some LM neurons following electrical stimulation are likely due to the delicate balance in reciprocating activity between the nBOR and LM. Nogueira and Britto (1991), who examined the effects of Wulst stimulation on the activity of nBOR neurons (see above), came to an identical conclusion. They suggest that short latency stimulation effects arise from direct Wulst input to the nBOR, while the longer latency effects result from stimulation of the LM, which projects to the nBOR.

Function of the Wulst Projection to the LM

Neurons in the LM show clear directional tuning (Katte and Hoffmann, 1980; McKenna and Wallman, 1985b; Winterson and Brauth, 1985; Fite et al., 1989; Fan et al., 1995; Wylie and Frost, 1996; Wylie and Crowder, 2000), and are also tuned in the spatio-temporal domain (Wylie and Crowder, 2000; Ibbotson and Price, 2001). Furthermore, it has been shown that input from the nBOR affects the spatio-temporal tuning (but not direction preference) of LM neurons (Crowder et al., in press a). In addition to the nBOR, the Wulst represents another prominent source of extra-retinal input to the LM. In this study, the Wulst was temporally inactivated with lidocaine to determine the function of the projection from Wulst to LM. Although Wulst inactivation altered the spontaneous rate of some LM neurons, it had no effect on the directional or spatio-temporal tuning of LM neurons. Despite the fact that we have negative findings in this regard, we have a very clear positive control: in every experiment (and as shown in Figure 6.4), lidocaine injection did inactivate the input from the Wulst to the LM.

In a pair of studies investigating the function of the projection from the Wulst to the nBOR, Britto and colleagues (Hamassaki et al., 1988; Britto et al., 1990) argued that the Wulst contributes to the directional tuning of nBOR neurons. They compared the distribution of preferred directions in normal pigeons vs. those that had the Wulst removed by aspiration. They observed that the proportion of neurons preferring upward motion was reduced and the proportion of neurons preferring temporal-to-nasal motion was increased in the group with Wulst lesions. Given the results of the present study, these previous findings are difficult to reconcile. One could conclude that the Wulst contributes to directional tuning of nBOR neurons, but not LM neurons. However, this explanation is unsatisfactory because the electrical stimulation of the Wulst results in similar modulation of nBOR and LM units (Nogueira and Britto, 1991, present study). We suggest that there is an inherent problem with the between groups design used by Hamassaki et al. (1988) and Britto et al. (1990) insofar as the differences observed could represent a sampling bias. In fact, their control groups suggest that perhaps this is the case. From figure 2 of Britto et al. (1990), most of the nBOR neurons in the control group preferred upward or downward motion, but neurons preferring nasal-to-temporal motion were absent. However, three different labs have found that nBOR in normal pigeons contains equal proportions of neurons preferring upward, downward, and nasal-to-temporal motion (Gioanni et al., 1984; Wylie and Frost, 1990; Zhang et al., 1999; see also Rosenberg and Ariel, 1990). It is likely that this issue will not be resolved until the reversible inactivation methods employed in the present studied are applied to the nBOR. Indeed, Nogueira and Britto (1991) themselves stated that reversible inactivation studies are needed to precisely evaluate the effect of visual Wulst on nBOR neurons (p.629).

If the Wulst does not contribute to the directional or spatio-temporal tuning of LM neurons, what is the function of this projection? The Wulst is considered to be a homologue of mammalian primary visual cortex based on embryological, histochemical and physiological characteristics (Karten et al., 1973; Karten and Shimizu, 1989; Medina and Reiner, 2000). Like V1, neurons in the visual Wulst have small receptive fields and are thought to be involved in form vision. Many respond to small moving stimuli, and there is evidence of orientation tuning, binocularity, and columnar organization (Revzin, 1969, Miceli et al., 1979; Pettigrew and Konishi, 1976; Wilson, 1980; Liu and Pettigrew, 2003). Given the involvement of the Wulst in form vision, it is possible that the projection to the pretectum and AOS is to adjust the gain of a subset of optic flow sensitive neurons when the animal is attending to small object-like stimuli.

It is also possible that the Wulst neurons that project to the LM are somatosensory or somatosensory/visual neurons. Deng and Wang (1992; 1993) demonstrated that there is significant overlap between areas of the Wulst that process visual and somatosensory information, with some neurons even responding to both visual and somatosensory stimuli (also see Medina and Reiner, 2000). Somatosensory information such as air passing through the pigeon's feathers could be used in addition to optic flow information to analyze self-motion. In support of this idea, neurons classified as bimodal (visual and somatosensory) as well as trimodal (visual, somatosensory, and vestibular) have been found in the ventral intraparietal area (VIP) of macaque monkeys, which along with the middle superior temporal area (MST) is responsible for the cortical processing of optic flow in primates (Bremmer et al., 2000).

Function of the Telencephalic Input to the Pretecum and AOS in Mammals

The presence of a telencephalic projection upon the AOS and pretectum appears to be highly variable among both lateral-eyed and frontal-eyed species. For example, the pretectum receives cortical afferents in frontal-eyed species such as cats and monkeys (Schoppmann, 1981; Hoffmann et al., 1991; Ilg and Hoffmann, 1993; Mustari et al., 1994), but not opossums (Pereira et al., 2000). In lateral-eyed animals, the NOT receives cortical input in rats (Shintani et al., 1999), guinea pigs (Lui et al., 1994) and rabbits (Hollander et al., 1979), but not in hamsters (Lent, 1982) or tree shrews (Huerta et al., 1985). Electrophysiological, behavioral, and developmental studies in cats have suggested that the cortical projection to the AOS and pretectum alters the gain asymmetries of vertical and horizontal optokinetic nystagmus as an adaptation to frontal eye placement (Grasse and Cynader, 1986, 1987, 1988, 1990). Since the pigeon is a lateral eyed animal, and the telencephalic inputs to the LM do not affect the directional tuning of these neurons, this projection likely serves a different purpose than in the cat.

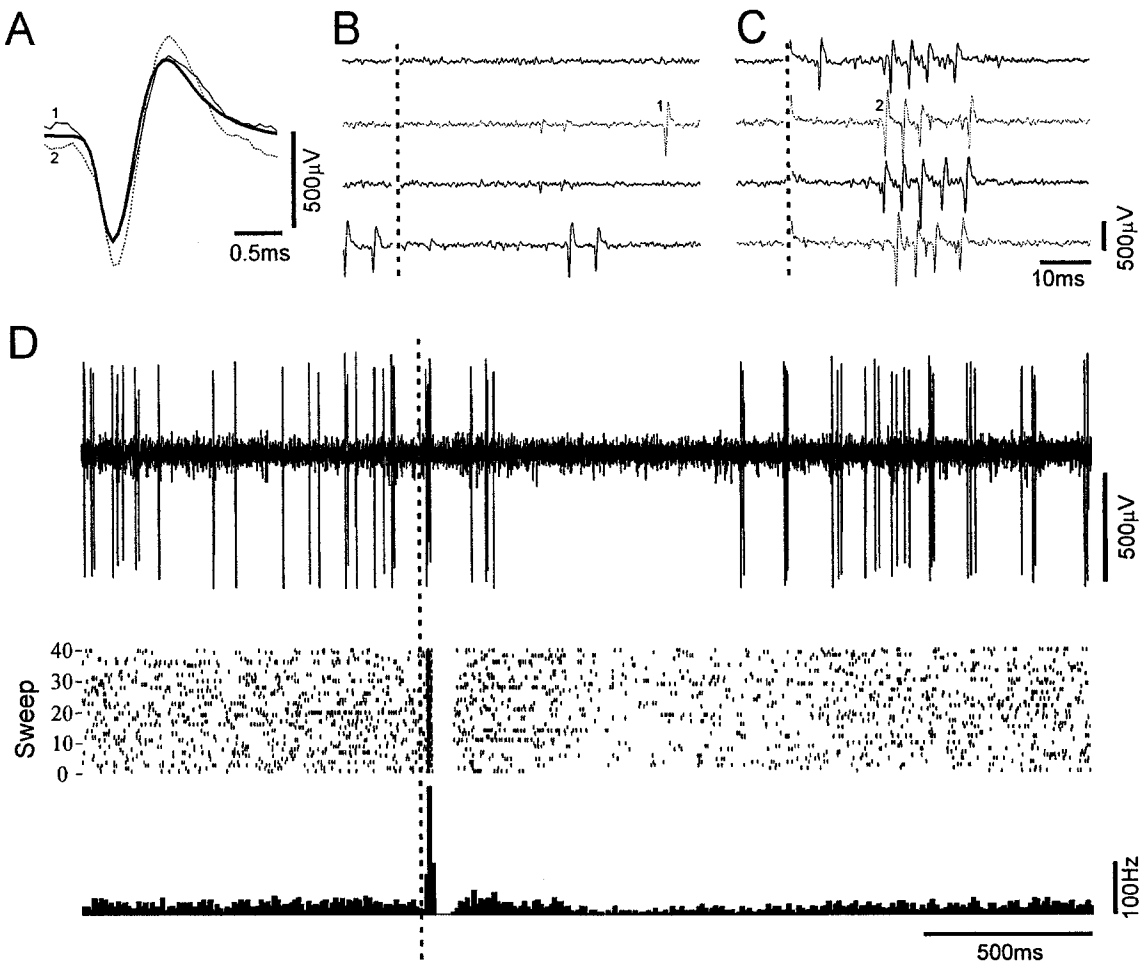

Figure 6.1

Raw traces, raster plot, and peri-stimulus time histograms (PSTHs) illustrating the effect of electrical stimulation of the Wulst on a W+ neuron in the lentiformis mesencephali (LM). **A** shows the average waveform of the LM unit (thick line). Superimposed are two raw traces denoted by Arabic numerals and representing individual spikes as shown in (**B**) and (**C**). The effects of subthreshold (25µA), and suprathreshold (200µA) electrical stimulation are shown in raw form for four separate raw sweeps in (**B**) and (**C**), respectively. The dotted vertical lines indicate the time of stimulation (stimulus artifact cropped). **D** shows the shows the stimulation effect on a longer time-scale. The raw trace

(top panel) shows a single stimulation trial from the raster sweep and PSTH (middle and bottom panels, respectively). A prominent excitation/inhibition sequence can be observed in this neuron.

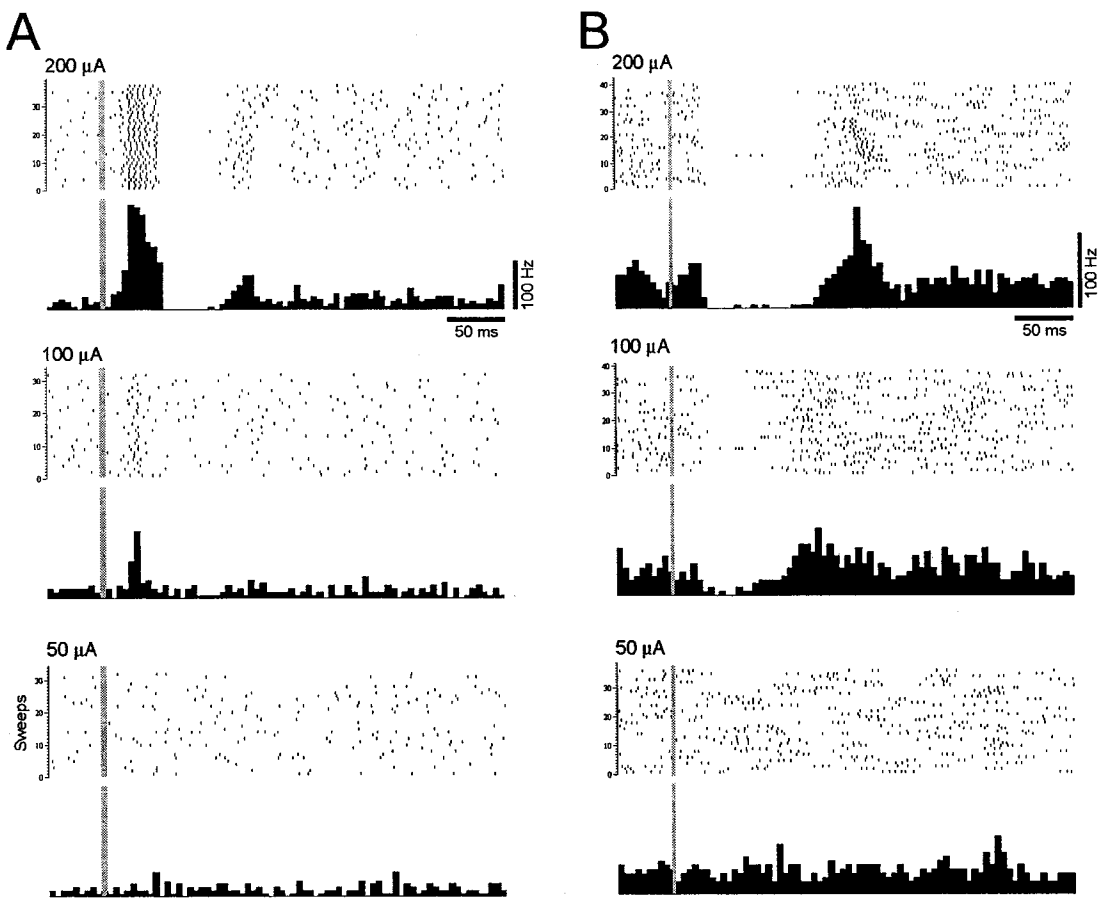

Figure 6.2

Raster plots and peri-stimulus time histograms illustrating the effects of electrical stimulation of the Wulst on neurons in the lentiformis mesencephali (LM). **A** and **B** show the effects of 50, 100, and 200µA Wulst stimulation on a W+ and W- neuron, respectively. The gray bars indicate the time of the stimulation artifact.

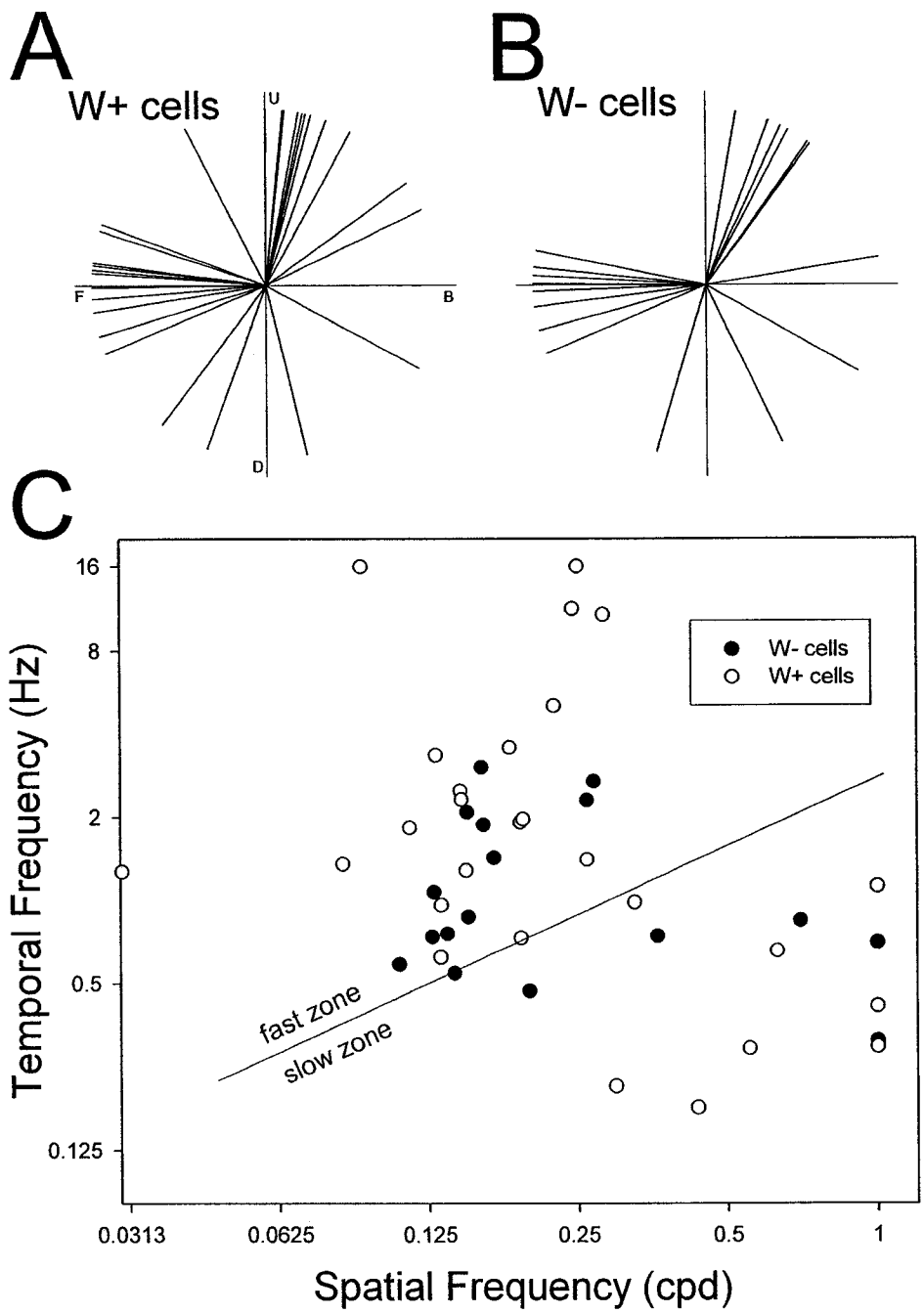

Figure 6.3

Directional and spatio-temporal tuning of lentiformis mesencephali neurons. Preferred directions for W+ and W- neurons, as calculated from the peak of the best fit cosine to the direction tuning curve are shown in **A** and **B**, respectively. U, B, D, and F = up, back

(nasal to temporal), down, and forward (temporal to nasal) motion. In **C**, the locations of the primary peaks from the excitatory response (ER) contour plots for W- and W+ neurons are shown as filled and empty dots, respectively. The diagonal line represents a stimulus velocity of 4°/s, which Ibbotson and Price (2001) used to distinguish the "fast" and "slow" groups in both the wallaby NOT and the pigeon LM.

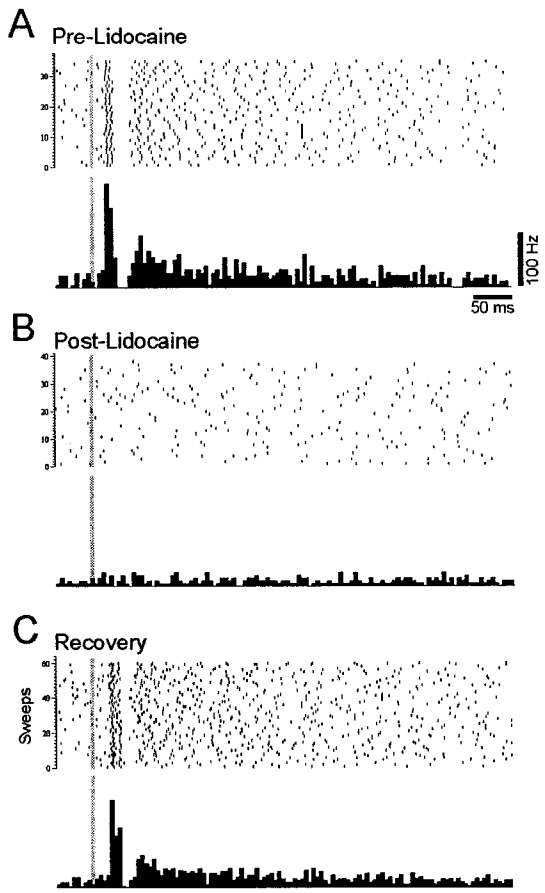

Figure 6.4

Effects of Wulst inactivation on stimulation effects. Raster plots and peri-stimulus time histograms illustrating the effects of Wulst electrical stimulation on a W+ neuron before the Wulst was injected with lidocaine (**A**), a few minutes after the lidocaine injection (**B**), and after the lidocaine has washed out (**C**). The gray bars indicate the time of the stimulation artifact.

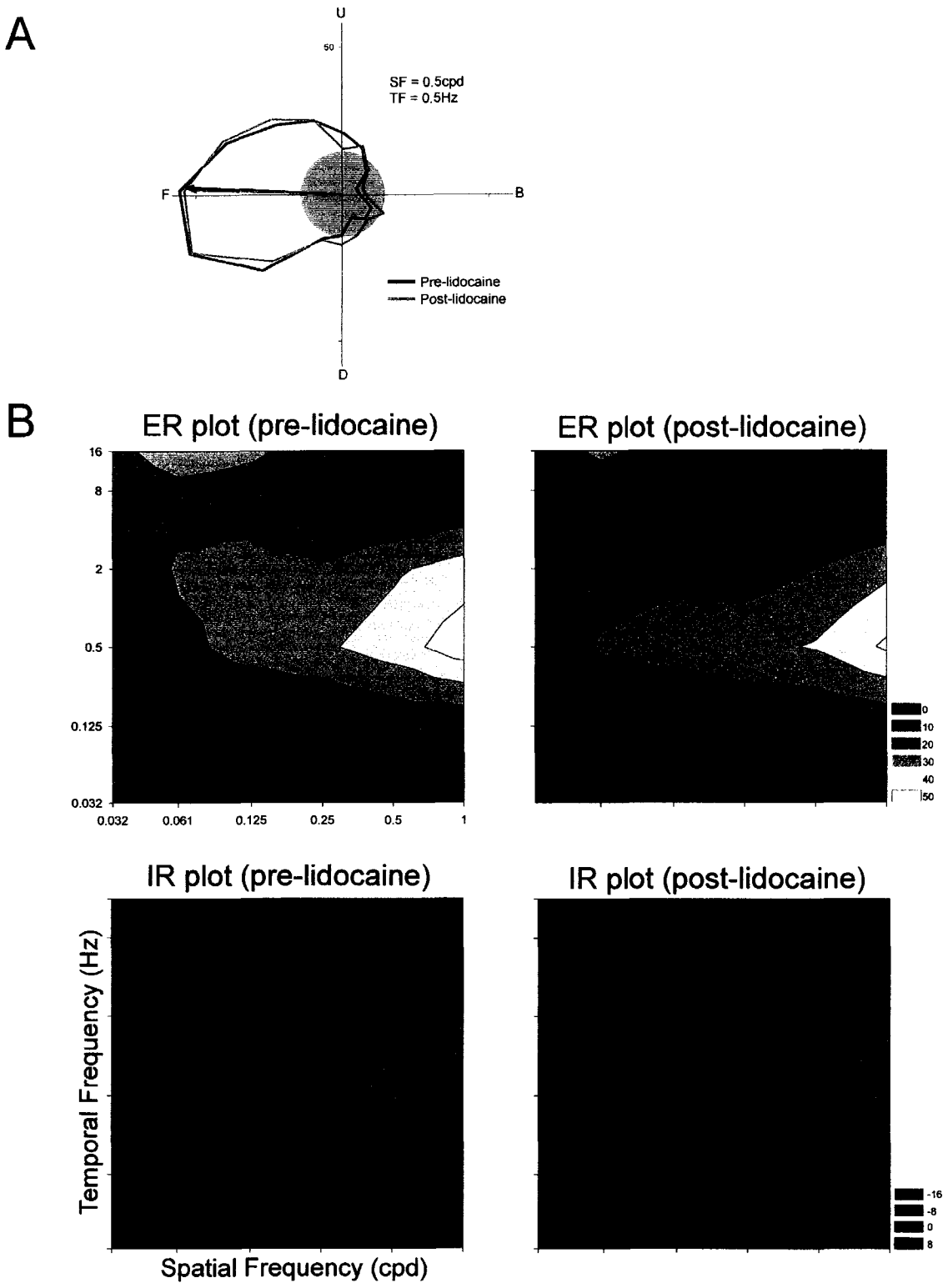

Figure 6.5

Effects of visual Wulst inactivation on the directional and spatio-temporal tuning of a lentiformis mesencephali (LM) neuron. **A** shows a polar plot illustrating the directional tuning of an LM neuron before (black lines) and after (red lines) the Wulst was injected lidocaine. Firing rate (spikes/s) relative to the spontaneous rate (SR; gray circle) is plotted as a function of the direction of motion in polar coordinates (i.e. the SR has been set to zero; outside the gray circle = excitation, inside = inhibition). Black and red arrows represent the neuron's preferred direction pre-lidocaine and post-lidocaine, respectively. U, B, D, and F represent up, back (nasal to temporal), down, and forward (temporal to nasal) motion. The temporal and spatial frequency (SF, TF) used to collect the directional tuning is indicated. In **B**, contour plots of the responses to gratings of varying SF and TF drifting in the preferred direction (ER plots) and anti-preferred direction (IR plots) are shown. SF and TF are plotted on the abscissa and ordinate, respectively. Pre-lidocaine plots are shown on the left, and post-lidocaine plots are shown on the right. Pre-lidocaine and post-lidocaine contour plots use a common scale to represent the firing rate (spikes/s) above (+; reds) or below (-; greens) the spontaneous rate (black).

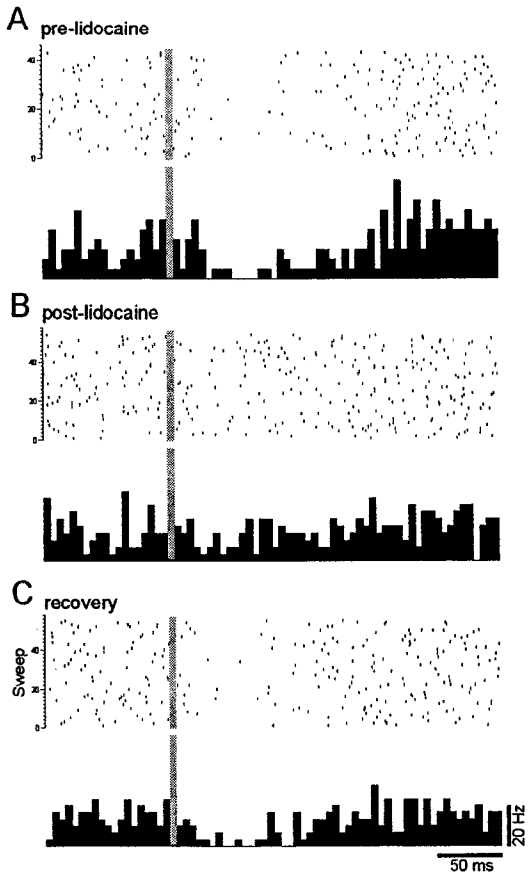

Figure 6.6

Effects of inactivation of the nucleus of the basal optic root (nBOR) on Wulst stimulation effects. Raster plots and peri-stimulus time histograms illustrating the effects of Wulst electrical stimulation on a W- neuron before the nBOR was injected with lidocaine (**A**), a few minutes after the nBOR injection (**B**), and after the lidocaine has washed out (**C**). The gray bars indicate the time of the stimulation artifact.

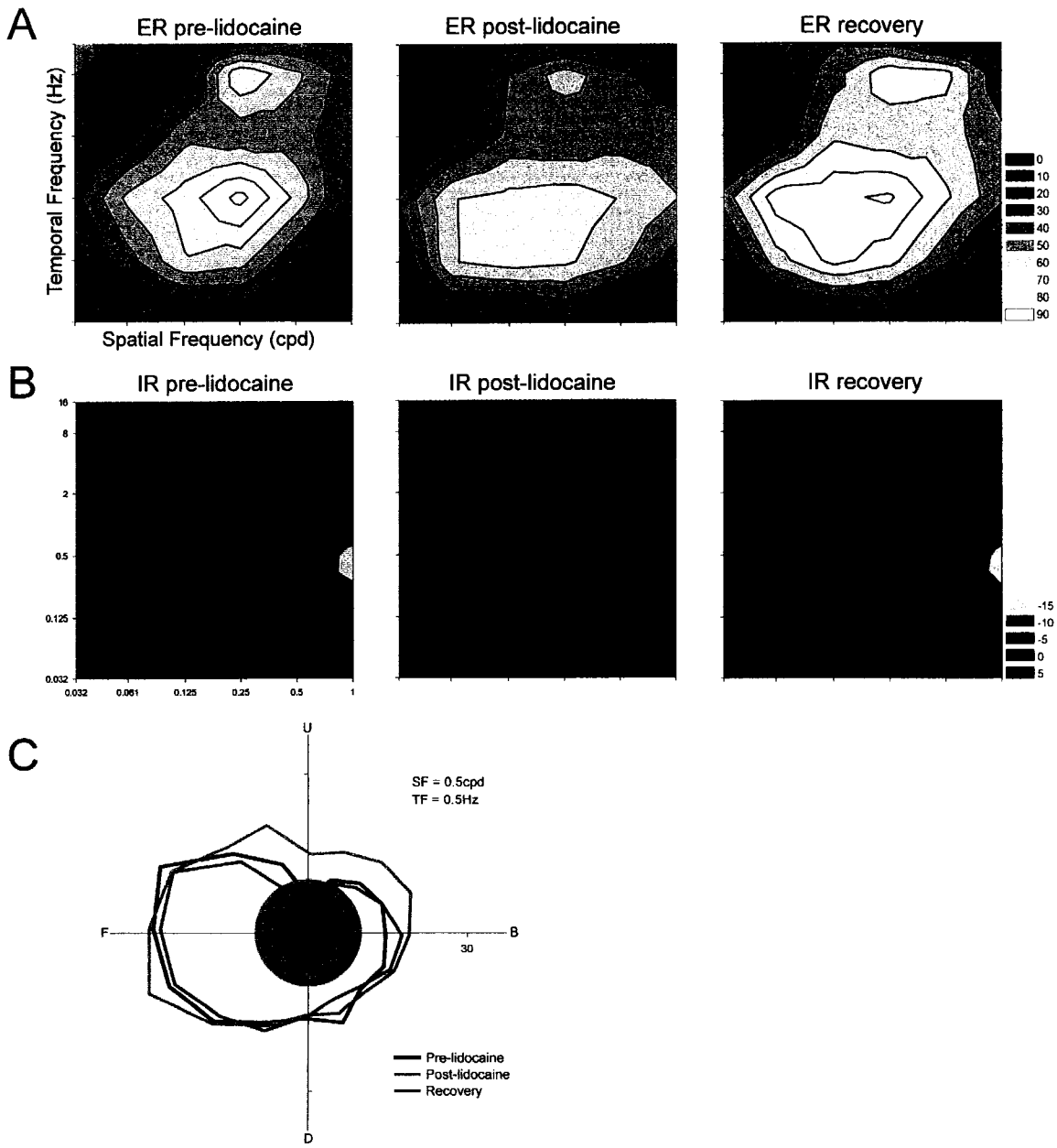

Figure 6.7

Effects of inactivation of the nucleus of the basal optic root (nBOR) on the directional and spatio-temporal tuning of neurons in the lentiformis mesencephali (LM). Spatio-temporal tuning of LM neurons to gratings drifting in the preferred (ER plot, **A**) and anti-

preferred directions (IR plot, **B**) before, during, and after the nBOR was inactivated with lidocaine (pre-lidociane, post-lidocaine, recovery). **C** shows a polar plot indicating the direction tuning of an LM neuron before (black), during (red) and after (green) nBOR inactivation. See caption to Figure 6.5 for additional details.

References

Azevedo TA, Cukiert A, Britto LRG. A pretectal projection upon the accessory optic nucleus in the pigeon: an anatomical and electrophysiological study. *Neurosci Lett* 43: 13-18, 1983.

Baldo MV, Britto LR. Accessory optic-pretectal interactions in the pigeon. *Brazilian J Med Biol Res* 23: 1037-1040, 1990.

Berson DM, Graybiel AM. Some cortical and subcortical fiber projections to the accessory optic nuclei in the cat. *Neuroscience* 5: 2203-2217, 1980.

Blanks RH, Giolli RA, Pham SV. Projections of the medial terminal nucleus of the accessory optic system upon pretectal nuclei in the pigmented rat. *Exp Brain Res* 48: 228-237, 1982.

Brecha N, Karten HJ, Hunt SP. Projections of the nucleus of basal optic root in the pigeon: An autoradiographic and horseradish peroxidase study. *J Comp Neurol* 189: 615-670, 1980.

Bremmer F, Duhamel JR, Hamed SB, Graf, W. Stages of self-motion processing in primate posterior parietal cotex. *International Review of Neurobiology* 44: 173-198, 2000.

Britto LR, Gasparotto OC, Hamassaki DE. Visual telencephalon modulates directional selectivity of accessory optic neurons in pigeons. *Vis Neurosci* 4: 3-10, 1990.

Burns S, Wallman J. Relation of single unit properties to the occulomotor function of the nucleus of the basal optic root (AOS) in chickens. *Exp Brain Res* 42: 171-180, 1981.

Carpenter RHS. *Movement of the Eyes*. London: PION Ltd, 1977.

Clark PGH. Some visual and other connections to the cerebellum of the pigeon. *J Physiol* 243: 267-285, 1977.

Collewijn H. Direction-selective units in the rabbit's nucleus of the optic tract. *Brain Res* 100: 489-508, 1975a.

Collewijn H. Oculomotor areas in the rabbit's midbrain and pretectum. *J Neurobiol* 6: 3-22, 1975b.

Crowder NA, Wylie DR. Fast and slow neurons in the nucleus of the basal optic root in pigeons. *Neurosci Letters* 304: 133-136, 2001.

Crowder NA, Lehmann H, Parent MB, Wylie DR. The Accessory Optic System Contributes to the Spatio-Temporal Tuning of Motion-Sensitive Pretectal Neurons. *J Neurophysiol*, In Press a.

Crowder NA, Dawson MRW, Wylie DRW. Temporal Frequency and Velocity-like tuning in the Pigeon Accessory Optic System. *J Neurophysiol*, In Press b.

Deng C, Wang B. Overlap of somatic and visual response areas in the Wulst of pigeon. *Brain Res* 582: 320-322, 1992.

Deng C, Wang B. Convergence of somatic and visual afferent impulses in the Wulst of pigeon. *Exp Brain Res* 96: 287-290, 1993.

Distler C, Hoffmann KP. Visual receptive field properties in kitten pretectal nucleus of the optic tract and dorsal terminal nucleus of the accessory optic tract. *J Neurophysiol* 70: 814-827, 1993.

Fan TX, Weber AE, Pickard GE, Faber KM, Ariel M. Visual responses and connectivity in the turtle pretectum. *J Neurophysiol* 73: 2507-2521, 1995.

Fite KV, Brecha N, Karten HJ, Hunt SP. Displaced ganglion cells and the accessory optic system of pigeon. *J Comp Neurol* 195: 279-88, 1981.

Fite KV, Kwei-Levy C, Bengston L. Neurophysiological investigation of the pretectal nucleus lentiformis mesencephali in Rana pipiens. *Brain Behav Evol* 34: 164-170, 1989.

Fite KV. Pretectal and accessory-optic visual nuclei of fish, amphibia and reptiles: themes and variations. *Brain Behav Evol* 26: 71-90, 1985.

Gamlin PDR, Cohen DH. Retinal projections to the pretectum in the pigeon (*Columba livia*). *J Comp Neurol* 269:1-17, 1988a.

Gamlin PDR, Cohen DH. Projections of the retinorecipient pretectal nuclei in the pigeon (*Columba livia*). *J Comp Neurol* 269: 18-46, 1988b.

Garey LJ, Powell TP. The projection of the retina in the cat. *J Anat* 102: 189-222, 1968.

Gibson JJ. The visual perception of object motion and subjective movement. *Psychol Rev* 61: 304-314, 1954.

Gioanni H, Rey J, Villalobos J, Dalbera A. Single unit activity in the nucleus of the basal optic root (nBOR) during optokinetic, vestibular and visuo-vestibular stimulations in the alert pigeon (*Columba livia*). *Exp Brain Res* 57: 49-60, 1984.

Giolli RA, Guthrie MD. The primary optic projections in the rabbit. An experimental degeneration study. *J Comp Neurol* 136:99-126, 1969..

Giolli RA, Blanks RH, Torigoe Y. Pretectal and brain stem projections of the medial terminal nucleus of the accessory optic system of the rabbit and rat as studied by anterograde and retrograde neuronal tracing methods. *J Comp Neurol* 227: 228-251, 1984.

Gottlieb MD, McKenna OC. Light and electron microscopic study of an avian pretectal nucleus, the lentiform nucleus of the mesencephalon, magnocellular division. *J Comp Neurol* 248: 133-145, 1986.

Grasse KL, Cynader MS. Electrophysiology of medial terminal nucleus of accessory optic system in the cat. *J Neurophysiol* 48: 490-504, 1982.

Grasse KL, Cyander MS, Douglas RM. Alterations in response properties in the lateral and dorsal terminal nuclei of the cat accessory optic system following visual cortex lesions. *Exp Brain Res* 55: 69-80, 1984.

Grasse KL, Cynader MS. Response properties of single units in the accessory optic system of the dark-reared cat. *Brain Res* 392: 199-210, 1986.

Grasse KL, Cynader MS. The accessory optic system of the monocularly deprived cat. *Brain Res* 428: 229-241, 1987.

Grasse KL, Cynader MS. The effect of visual cortex lesions on vertical optokinetic nystagmus in the cat. *Brain Res* 455: 385-389, 1988.

Grasse KL, Cyander MS. The accessory optic system in frontal-eyed animals. In: *Vision and Visual Dysfunction. The Neuronal Basis of Visual Function*, edited by Leventhal A. New York: McMillan, 1990, p. 111-139.

Hamassaki DE, Gasparotto OC, Nogueira MI, Britto LRG. Telencephalic and pretectal modulation of the directional selectivity of accessory optic neurons in the pigeon. *Brazilian j Med Biol Res 21*: 649-652, 1988.

Hayhow WR, Webb C, Jervie A. The accessory optic fiber system in the rat. *J Comp Neurol* 115: 187-215, 1960.

Hoffmann KP, Schoppmann A. Retinal input to direction selective cells in the nucleus tractus opticus of the cat. *Brain Res* 99: 359-366, 1975.

Hoffmann KP, Schoppmann A. A quantitative analysis of the direction-specific response of neurons in the cat's nucleus of the optic tract. *Exp Brain Res* 42: 146-157, 1981.

Hoffmann KP, Distler C. Quantitative analysis of visual receptive fields of neurons in nucleus of the optic tract and dorsal terminal nucleus of the accessory optic tract in macaque monkey. *J Neurophysiol* 62: 416-428, 1989.

Hoffmann KP, Distler C, Erickson RG, Mader W. Physiological and anatomical identification of the nucleus of the optic tract and dorsal terminal nucleus of the accessory optic tract in monkeys. *Exp Brain Res* 69: 635-644, 1988.

Hoffmann KP, Distler C, Erickson RG. Functional projections from striate cortex and superior temporal sulcus to the nucleus of the optic tract (NOT) and dorsal terminal nucleus of the accessory optic tract (DTN) of macaque monkeys. *J Comp Neurol* 313: 707-724, 1991.

Hollander H, Tietze J, Distel H. An autoradiographic study of the subcortical projections of the rabbit striate cortex in the adult and during postnatal development. *J Comp Neurol* 184: 783-794, 1979.

Holstege G, Collewijn H. The efferent connections of the nucleus of the optic tract and the superior colliculus in the rabbit. *J Comp Neurol* 209: 139-175, 1982.

Huerta MF, Weber JT, Rothstein LR, Harting JK. Subcortical connections of area 17 in the tree shrew: an autoradiographic analysis. *Brain Res* 340: 163-170, 1985.

Ibbotson MR, Price NS. Spatiotemporal tuning of directional neurons in mammalian and avian pretectum: a comparison of physiological properties. *J Neurophysiol* 86: 2621-2624, 2001.

Ibbotson MR, Mark RF, Maddess TL. Spatiotemporal response properties of direction-selective neurons in the nucleus of the optic tract and the dorsal terminal nucleus of the wallaby, Macropus eugenii. *J Neurophysiol* 72: 2927-2943, 1994.

Ilg UJ, Hoffmann KP. Functional grouping of the cortico-pretectal projection. *J Neurophysiol* 70: 867-869, 1993.

Ilg UJ, Hoffmann KP. Responses of neurons of the nucleus of the optic tract and the dorsal terminal nucleus of the accessory optic tract in the awake monkey. *Eur J Neurosci* 8: 92-105, 1996.

Itoh K. Efferent projections of the pretectum in the cat. *Exp Brain Res* 30: 89-105, 1977.

Karten HJ, Hodos W. *A stereotaxic Atlas of the Brain of the Pigeon (Columba livia)*. Baltimore: Johns Hopkins Press, 1967.

Karten HJ, Shimizu T. The origins of the neocortex: connections and lamination as distinct events in evolution. *J Cognitive Neurosci* 1: 291-301, 1989.

Karten HJ, Fite KV, Brecha N. Specific projection of displaced retinal ganglion cells upon the accessory optic system in the pigeon (*Columba livia*). *Proc Natl Acad Sci* 74: 1752-1756, 1977.

Karten HJ, Hodos W, Nauta WJ, Revzin AM. Neural connections of the "visual wulst" of the avian telencephalon. Experimental studies in the piegon (*Columba livia*) and owl (*Speotyto cunicularia*). *J Comp Neurol* 150: 253-78, 1973.

Katte O, Hoffmann KP. Direction specific neurons in the pretectum of the frog (*Rana esculenta*). *J Comp Physiol* 140: 53-57, 1980.

Lent R. The organization of subcortical projections of the hamster's visual cortex. *J Comp Neurol* 206: 227-242, 1982.

Liu GB, Pettigrew JD. Orientation mosaic in barn owl's visual Wulst revealed by optical imaging: comparison with cat and monkey striate and extra-striate areas. *Brain Res* 961: 153-8, 2003.

Lui F, Giolli RA, Blanks RH, Tom EM. Pattern of striate cortical projections to the pretectal complex in the guinea pig. *J Comp Neurol* 344: 598-609, 1994.

McKenna OC, Wallman J. Accessory optic system and pretectum of birds: comparisons with those of other vertebrates. *Brain, Behavior & Evolution* 26:91-116, 1985a.

McKenna OC, Wallman J. Functional postnatal changes in avian brain regions responsive to retinal slip: a 2-deoxy-D-glucose study. *J Neurosci* 5:330-342, 1985b.

Medina L, Reiner A. Do birds possess homologues of mammalian primary visual, somatosensory and motor cortices? *Trends Neurosci* 23: 1-12, 2000.

Miceli D, Gioanni H, Reperant J, Peyrichoux J. The avian visual wulst: I. An anatomical study of afferent and efferent pathways. II. An electrophysiological study of the functional properties of single neurons. In: *Neural Mechanisms of Behavior of the Pigeon*, edited by Granda, AM, Maxwell JH. New York, NY: Plenum Press, 1979, p. 223-354.

Morgan B, Frost BJ. Visual response properties of neurons in the nucleus of the basal optic root of pigeons. *Exp Brain Res* 42: 184-188, 1981.

Mustari MJ, Fuchs AF. Discharge patterns of neurons in the pretectal nucleus of the optic tract (NOT) in the behaving primate. *J Neurophysiol* 64: 77-90, 1990.

Mustari MJ, Fuchs AF, Kaneko CR, Robinson FR. Anatomical connections of the primate pretectal nucleus of the optic tract. *J Comp Neurol* 349: 111-128, 1994.

Nakayama K. Differential motion hyperacuity under conditions of common image motion. *Vision Res* 21:1475-1482, 1981.

Nogueira MI, Britto LRG. Extraretinal modulation of accessory optic units in the pigeon. *Brazilian J Med Biol Res* 24: 623-631, 1991.

Pereira A, Volchan E, Vargas CD, Penetra L, Rocha-Miranda CE. Cortical and subcortical influences on the nucleus of the optic tract of the opossum. *Neurosci* 95: 953-963, 2000.

Perrone JA, Thiele A. Speed skills: measuring the visual speed analyzing properties of primate MT neurons. *Nature Neurosci* 4: 526-531, 2001.

Pettigrew JD, Konishi M. Neurons selective for orientation and binocular disparity in the visual Wulst of the barn owl (*Tyto alba*). *Science* 193: 675-678, 1976.

Reiner A, Brecha N, Karten HJ. A specific projection of retinal displaced ganglion cells to the nucleus of the basal optic root in the chicken. *Neurosci* 4: 1679-88, 1979.

Revzin AM. A specific visual projection area in the hyperstriatum of the pigeon (*Columba livia*). *Brain Res* 15: 246-469, 1969.

Rio JP, Villalobos J, Miceli D, Reperant J. Efferent projections of the visual wulst upon the nucleus of the basal optic root in the pigeon. *Brain Res* 271: 145-151, 1983.

Rosenberg AF, Ariel M. Visual-response properties of neurons in turtle basal optic nucleus in vitro. *J Neurophysiol* 63: 1033-1045, 1990.

Sandkuhler J, Maisch B, Zimmermann M. The use of local anaesthetic microinjections to identify central pathways: a quantitative evaluation of the time course and extent of the neuronal block. *Exp Brain Res* 68: 168-178, 1987.

Scalia F, Arango V. Topographic organization of the projections of the retina to the pretectal region in the rat. *J Comp Neurol* 186: 271-92, 1979.

Schoppmann A. Projections from areas 17 and 18 of the visual cortex to the nucleus of the optic tract. *Brain Res* 223: 1-17, 1981.

Shintani T, Hoshino K, Meguro R, Kaiya T, Norita M. A light and electron microscopic analysis of the convergent retinal and visual cortical projections to the nucleus of the optic tract (NOT) in the pigmented rat. *Neurobiology* 7: 445-460, 1999.

Simpson JI, Soodak RE, Hess R. The accessory optic system and its relation to the vestibulocerebellum. *Prog Brain Res* 50: 715-724, 1979.

Simpson JI, Leonard CS, Soodak RE. The accessory optic system: II. Spatial organization of direction selectivity. *J Neurophysiol* 60: 2055-2072, 1988.

Simpson JI. The accessory optic system. *A Rev Neurosci* 7: 13-41, 1984.

Soodak RE, Simpson JI. The accessory optic system of rabbit. I. Basic visual response properties. *J Neurophysiol* 60: 2055-2072, 1988.

Terasawa K, Otani K, Yamada J. Descending pathways of the nucleus of the optic tract in the rat. *Brain Res.* 1979 Sep 21;173(3):405-17.

van der Togt C, Schmidt M. Inhibition of neuronal activity in the nucleus of the optic tract due to electrical stimulation of the medial terminal nucleus in the rat. *Eur J Neurosci* 6: 558-64, 1994.

Volchan E, Rocha-Miranda CE, Picanco-Diniz CW, Zinsmeisser B, Bernardes RF, Franca JG. Visual response properties of pretectal units in the nucleus of the optic tract of the opossum. *Exp Brain Res* 78: 380-386, 1989.

Weber JT, Harting JK. The efferent projections of the pretectal complex: an autoradiographic and horseradish peroxidase analysis. *Brain Res.* 1980 Jul 21;194(1):1-28.

Weber JT. Pretectal complex and accessory optic system in alert monkeys. *Brain Behav Evol* 26: 117-140, 1985.

Westheimer G, McKee SP. Failure of Donders' law during smooth pursuit eye movements. *Vision Res.* 13: 2145-253, 1973.

Wilson P. The organization of the visual hyperstriatum in the domestic chick. II. Receptive field properties of single units. *Brain Res* 188: 333-345, 1980.

Winterson BJ, Brauth SE. Direction-selective single units in the nucleus lentiformis mesencephali of the pigeon (*Columba livia*). *Exp Brain Res* 60: 215-226, 1985.

Wylie DR, Crowder NA. Spatiotemporal properties of fast and slow neurons in the pretectal nucleus lentiformis mesencephali in pigeons. *J Neurophysiol* 84: 2529-2540, 2000.

Wylie DR, Frost BJ. Visual response properties of neurons in the nucleus of the basal optic root of the pigeon: A quantitative analysis. *Exp Brain Res* 82: 327-336, 1990.

Wylie DRW, Frost BJ. The pigeon optokinetic system: Visual input in extraocular muscle coordinates. *Vis Neurosci* 13: 945-953, 1996.

Wylie DR, Linkenhoker B, Lau KL. Projections of the nucleus of the basal optic root in pigeons (Columba livia) revealed with biotinylated dextran amine. *J Comp Neurol* 384: 517-536, 1997.

Yakushin SB, Gizzi M, Reisine H, Raphan T, Buttner-Ennever J, Cohen B. Functions of the nucleus of the optic tract (NOT). II. Control of ocular pursuit. *Exp Brain Res* 131: 433-447, 2000.

Zhang T, Fu Y-X, Wang SR. Receptive field characteristics of neurons in the nucleus of the basal optic root in pigeons. **Neurosci** 91: 33-40, 1999.

Chapter 7

Conclusion

The movement of an organism through an environment containing visual stimuli results in visual flow-fields, or optic flow, across the retina (Gibson, 1954). Distinct and informative patterns of optic flow arise from different types of self-motion, and this information can be used to determine the position, orientation and movement of the body (Gibson, 1966). The accessory optic system and pretectum are retinal recipient nuclei that are believed to be involved in the processing of optic flow because: 1) OKN is severely impaired following lesions to the AOS or pretectum; 2) neurons in the AOS and pretectum respond best to large-field visual motion; and 3) there is anatomical and physiological evidence that the AOS and pretectum, as well as structures they send efferents to (e.g. the vestibulocerebellum), are associated with the vestibular system and extraocular muscles, which are also involved in the processing of self-motion. Thoroughly characterizing the visual response properties of neurons in the AOS and pretectum provides insight into the neuronal mechanisms that the AOS and pretectum utilize to process optic flow.

Summary of Chapters

This dissertation consisted of five studies that investigated the visual response properties of neurons in the pigeon's AOS and pretectum. Each study used large-field sine wave gratings as visual stimuli to measure the directional and spatio-temporal tuning of neurons in the nBOR or LM.

In Chapter 2, neurons in the nBOR and LM were presented with large-field "plaids" composed of two non-parallel sine-wave gratings. Previous studies of visual motion pathways in the geniculostriate pathway have used plaid stimuli to investigate the

visual system's ability to detect the global direction of pattern motion (pattern-selectivity), as opposed to the direction of motion of the components within the plaids (component-selectivity) (e.g. Movshon et al. 1985). Most LM and nBOR neurons were classified as pattern-selective, and very few were classified as component-selective. The prevalence of pattern-selective responses indicates that most of the input to the optokinetic system is orientation-insensitive. However, the component-selective responses indicate that some orientation-sensitive information is entering the pigeon optokinetic system. This was the first study to examine single unit responses of neurons in the AOS and pretectum to plaid stimuli.

In Chapter 3, the spatio-temporal response properties of neurons in the nBOR were measured using large-field drifting sine wave gratings with a broad spectrum of SFs and TFs. Neurons in the nBOR were classified as "Fast" cells that preferred low SFs and high TFs, or "Slow" cells that preferred high SFs and low TFs. Very similar spatio-temporal tuning has been found in the pretectum of the pigeon and wallaby (Ibbotson et al., 1994; Wylie and Crowder, 2000). A comparison of fast and slow neurons in the nBOR and LM revealed an interaction between directional and spatio-temporal tuning. Up, down and back cells prefer slow stimuli in the nBOR, forward cells prefer slow stimuli in the LM, and fast cells include all direction types in both nuclei. Fast and slow neurons were first classified in the pretectum of wallabies (Ibbotson et al., 1994) and pigeons (Wylie and Crowder, 2000); however, Chapter 3 demonstrates that this functional division into fast vs. slow extends beyond the pretectum to include all optokinetic nuclei. Based on the similarity of spatio-temporal tuning in the nBOR and LM, we predict that fast and slow cells could be found in the mammalian AOS as well.

The spatio-temporal tuning of nBOR neurons was investigated further in Chapter 4. It was shown that fast nBOR neurons were tuned for TF, while the tuning of slow nBOR neurons was more closely related to velocity (TF/SF) than to TF. However, slow cells' peak responses were not independent of SF, thus they have "velocity-like tuning". Slow LM neurons also showed velocity-like tuning when data from Wylie and Crowder (2000; appendix 1) was re-analyzed. Computer modeling revealed that both the TF-tuning and velocity-like tuning may be explained by modified versions of correlation model of motion detection (Appendix 2). This model provides insight into the neural mechanisms of motion detection utilized by the AOS and pretectum.

In Chapter 5, the directional and spatio-temporal tuning of LM neurons was recorded before and after the ipsilateral nBOR was inactivated with tetrodotoxin to determine the function of the projection from the nBOR to LM. Following nBOR inactivation, the spatio-temporal tuning of LM neurons was dramatically altered, but their direction preferences remained unchanged. This study was the first to demonstrate the functional importance of the projection from the nBOR to the LM. A model was proposed to describe the information being sent from the nBOR to LM. This model has major implications regarding how the spatio-temporal tuning of neurons in the LM is constructed. Furthermore, this study highlights the importance of considering the spatio-temporal tuning of motion-sensitive neurons. The alteration in the spatio-temporal tuning of LM neurons resulting from nBOR inactivation would have been overlooked if the spatio-temporal tuning of LM neurons was not examined.

In Chapter 6, the effect of electrical stimulation of the Wulst on the activity of LM neurons was investigated. As well, the directional and spatio-temporal tuning of LM

neurons was recorded before and after the ipsilateral Wulst was inactivated with lidocaine to determine the function of the projection from the Wulst to LM. When the Wulst was electrically stimulated, about half of the LM neurons tested showed short latency (13.5ms) excitation (W+ cells), while the remainder showed longer latency (28.3ms) inhibition (W- cells). However, when the Wulst was temporarily inactivated with lidocaine neither the directional nor spatio-temporal response properties of LM neurons were affected.

Conclusions

Neurons in the AOS and pretectum show remarkably similar visual response properties. Neurons in the nBOR and LM respond best to large-field motion in the contralateral eye, although they are complimentary to each other in terms of direction preference. Moreover, both the nBOR and LM have a similar proportion of pattern-selective and component-selective neurons, and both contain fast and slow cells. These findings provide strong evidence that the neural mechanisms for the detection of visual motion are similar in the nBOR and LM. The spatio-temporal tuning of neurons in the nBOR and LM suggests that partially-balanced elaborated Reichardt detectors provide the main visual motion signal that is used by the AOS and pretectum. There is a large body of evidence suggesting that Reichardt detectors also provide the motion signal in invertebrate visual systems (e.g. Reichardt, 1969, Eckert, 1980; Hausen, 1984; Buchner, 1984; Borst and Egelhaaf, 1989; Egelhaaf et al., 1989, 1990; O'Carroll et al., 1996). It appears that Reichardt-like configurations may be a fundamental mechanism of motion detection in vertebrates and invertebrates.

As discussed in Chapter 4, both the balance between half-detectors and spatio-temporal pre-filtering can affect the shape of a Reichardt detectors' spatio-temporal tuning. Thus, slow cells that show velocity-like tuning likely represent partially-balanced Reichardt detectors, but TF-tuned fast cells could represent the output of fully-balanced Reichardt detectors or the output of partially-balanced Reichardt detectors that have been subjected to restrictive spatio-temporal pre-filtering. The location of the peak response in the spatio-temporal domain (i.e. fast vs. slow neurons) is also likely due to spatio-temporal pre-filtering. Neurons in the nBOR and LM that have peaks in both the fast and slow regions may represent the combination of outputs from multiple Reichardt detectors with different pre-filter values. This combining of outputs may represent a multi-detector version of the "subtraction stage" in the Reichardt model of motion detection discussed in Chapter 4 and Appendix 2. The outputs that are combined in this subtraction stage could arise from partially balanced, or fully unbalanced, Reichardt detectors of retinal or extra-retinal origin.

Retinal ganglion cell recordings in the rabbit (Oyster and Barlow, 1967; Oyster et al., 1972), and antidromic stimulation studies in the turtle AOS (Kogo et al., 1998), indicate that the retinal input to the AOS and pretectum is directionally selective. Furthermore, it is clear from Chapter 5 that extra-retinal inputs also affect the activity of neurons in the LM. It is likely that neurons in the nBOR are also modulated by extra-retinal inputs (see Future Directions below). Thus, the reciprocal connection between the nBOR and LM may serve to further shape the directional and spatio-temporal tuning of AOS and pretectal neurons before they send information to the IO and VbC.

The AOS and pretectum have homologous structures among all vertebrates (Fite, 1985; McKenna and Wallman, 1985a; Weber, 1985). This high degree of evolutionary conservation suggests that many of the findings of this dissertation could be expanded beyond avians. One exception to this evolutionary conservation is the cortical input to the AOS and pretectum, which appears to be highly variable in both frontal and lateral eyed animals (see Chapters 2 and 6). Electrophysiological, behavioral, and developmental studies in cats have suggested that the cortical projection to the AOS and pretectum alters the directional tuning of neurons that are involved in vertical and horizontal optokinetic nystagmus as an adaptation to frontal eye placement (Grasse and Cynader, 1986, 1987, 1988, 1990). The projection from the telencephalon to the AOS and pretectum likely serves a different function in the pigeon because it is a lateral eyed animal and inactivating the Wulst does not affect the directional tuning of LM neurons (see Chapter 6). The precise role of the Wulst input to the LM and nBOR remains a to be discovered by future research (see Chapter 6 and Future Directions below).

Future Directions

In Chapter 4 it was shown that the spatio-temporal tuning of neurons in the pigeon nBOR and LM was quite similar to that of wallaby NOT neurons. If the spatio-temporal tuning of AOS and pretectal neurons was tested in a wider variety of species, further interspecies comparisons could be made. Most notably, the influence of eye-position, binocularity, and cortical afferentation of the AOS and pretectum could be determined.

In Chapters 5 and 6 the influences of extra-retinal inputs into the LM were examined. However, it is clear from the reciprocal connection between the nBOR and LM (Brecha et al., 1980; Gamlin and Cohen, 1988b) that the AOS and pretectum work together in a complimentary fashion. Thus, it would be beneficial to examine the influences of extra-retinal inputs to the nBOR. Pharmacological inactivation studies, similar to the ones in Chapters 5 and 6, could be used to determine the effects of LM or Wulst inactivation on the directional and spatio-temporal tuning of nBOR neurons. These studies would further elucidate the role of the reciprocal connection between the nBOR and LM in the processing of optic flow information.

Determining the response properties of Wulst neurons that project to the nBOR or LM would clarify the role of the Wulst in the processing of optic flow. Antidromic stimulation from electrodes placed in the nBOR or LM could be used to determine which Wulst neurons send efferents to the AOS or pretectum. Once identified, the response properties of these Wulst neurons could be measured quantitatively using stimuli from any sensory modality.

Neurons in the IO and VbC have large panoramic receptive fields that respond best to specific types of optic flow resulting from self-translation and self-rotation. Furthermore, it has been shown that visually responsive neurons in the VbC and IOmc are topographically organized in terms of optic flow preference (Wylie et al., 1993; Wylie et al., 1998, 1999; Wylie and Frost, 1999; Crowder et al., 2000). While the directional tuning of these neurons has been explored extensively, their spatio-temporal tuning remains unknown. Extracellular recording studies in the IO or VbC using sine wave grating stimuli, similar to the ones used in Chapters 3-6, could provide insight into

how information from the fast and slow cells in the AOS and pretectum are integrated in the IO and VbC. Possible questions that could be addressed are: 1) do fast and slow cells project to anatomically distinct regions in the IO or VbC? 2) do fast and slow cells send differential projections through mossy and climbing fibres to the VbC? and 3) how do the binocular receptive fields of neurons in the IO and VbC combine inputs from fast and slow cells? Additionally, pharmacological inactivation techniques, similar to the ones used in Chapters 5 and 6, could be used to determine the specific role of nBOR or LM in binocular integration. For example, the binocularity, ocular dominance, direction preference, and spatio-temporal tuning of neurons in the VbC could be measured before and after the inactivation of the nBOR or LM.

References

Borst A, Egelhaaf M. Principles of visual motion detection. *Trends in Neurosci* 12: 297-306, 1989.

Brecha N, Karten HJ, Hunt SP. Projections of the nucleus of basal optic root in the pigeon: An autoradiographic and horseradish peroxidase study. *J Comp Neurol* 189: 615-670, 1980.

Buchner E. Behavioral analysis of spatial vision in insects. In: *Photoreception and Vision in Invertebrates*, edited by Ali MA. New York: Plenum Press, 1984, p. 561-621.

Crowder NA, Winship IR, Wylie DR. Topographic organization of inferior olive cells projecting to translational zones in the vestibulocerebellum of pigeons. *J Comp Neurol* 419: 87-95, 2000.

Eckert H. Functional properties of the H1-neurone in the third optic ganglion of the blow fly, Phaenicia. *J Comp Physiol* 135: 29-39, 1980.

Egelhaaf M, Borst A, Reichardt W. Computational structure of a biological motion-detection system as revealed by local detector analysis in the fly's nervous system. *Journal of the Optical Society of America A-Optics & Image Science* 6: 1070-1087, 1989.

Egelhaaf M, Borst A, Pilz B. The role of GABA in detecting visual motion. *Brain Res* 509: 156-60, 1990

Fite KV. Pretectal and accessory-optic visual nuclei of fish, amphibia and reptiles: themes and variations. *Brain Behav Evol* 26: 71-90, 1985.

Gamlin PDR, Cohen DH. Projections of the retinorecipient pretectal nuclei in the pigeon (*Columba livia*). *J Comp Neurol* 269: 18-46, 1988b.

Gibson JJ. The visual perception of object motion and subjective movement. *Psychol Rev* 61: 304-314, 1954.

Gibson JJ. The problem of temporal order in stimulation and perception. *J Psychol* 62: 141-149, 1966.

Grasse KL, Cynader MS. Response properties of single units in the accessory optic system of the dark-reared cat. *Brain Res* 392: 199-210, 1986.

Grasse KL, Cynader MS. The accessory optic system of the monocularly deprived cat. *Brain Res* 428: 229-241, 1987.

Grasse KL, Cynader MS. The effect of visual cortex lesions on vertical optokinetic nystagmus in the cat. *Brain Res* 455: 385-389, 1988.

Grasse KL, Cyander MS. The accessory optic system in frontal-eyed animals. In: *Vision and Visual Dysfunction. The Neuronal Basis of Visual Function*, edited by Leventhal A. New York: McMillan, 1990, p. 111-139.

Hausen K. The lobula complex of the fly: Structure, function and significance in visual behavior. In: *Photoreception and Vision in Invertebrates*, edited by Ali MA. New York: Plenum Press, 1984, p. 523-560.

Ibbotson MR, Mark RF, Maddess TL. Spatiotemporal response properties of direction-selective neurons in the nucleus of the optic tract and the dorsal terminal nucleus of the wallaby, Macropus eugenii. *J Neurophysiol* 72: 2927-2943, 1994.

Kogo N, Rubio DM, Ariel M. Direction Tuning of Individual Retinal Inputs to the Turtle Accessory Optic System. *J Neurosci* 18: 2673-2684, 1998.

McKenna OC, Wallman J. Accessory optic system and pretectum of birds: comparisons with those of other vertebrates. *Brain Behav Evol* 26: 91-116, 1985a.

Movshon JA, Adelson EH, Gizzi MS, Newsome WT. The analysis of visual moving patterns. In *Study group on pattern recognition mechanisms* edited by Chagas C, Gattass R, Gross C. Vatican City: Pontificia Academia Scientiarum, 1985, p. 117-151.

O'Carrol DC, Bidwell NJ, Laughlin SB, Warrant EJ. Insect motion detectors matched to visual ecology. *Nature* 382: 63-66, 1996.

Oyster CW, Barlow HB. Direction-selective units in rabbit retina: distribution of preferred directions. *Science* 155: 841-842, 1967.

Oyster CW, Takahashi E, Collewijn H. Direction-selective retinal ganglion cells and control of optokinetic nystagmus in the rabbit. *Vision Res* 12: 183-193, 1972.

Reichardt W. Movemnet perception in insects. In: *Processing of optical data by organisms and machines*, edited by Reichardt W. New York: Academic, 1969, p. 465-493.

Weber JT. Pretectal complex and accessory optic system in alert monkeys. *Brain Behav Evol* 26: 117-140, 1985.

Wylie DR, Crowder NA. Spatiotemporal properties of fast and slow neurons in the pretectal nucleus lentiformis mesencephali in pigeons. *J Neurophysiol* 84: 2529-2540, 2000.

Wylie DR, Frost BJ. Responses of neurons in the nucleus of the basal optic root to translational and rotational flowfields. *J Neurophysiol* 81: 267-276, 1999.

Wylie DR, Kripalani T, Frost BJ. Responses of pigeon vestibulocerebellar neurons to optokinetic stimulation. I. Functional organization of neurons discriminating between translational and rotational visual flow. *J Neurophysiol* 70: 2632-2646, 1993.

Wylie DR, Bischof WF, Frost BJ. Common reference frame for neural coding of translational and rotational optic flow. *Nature* 392: 278-282, 1998.

Wylie DR, Winship IR, Glover RG. Projections from the medial column of the inferior olive to different classes of rotation-sensitive Purkinje cells in the flocculus of pigeons. *Neurosci Lett* 268: 97-100, 1999b.

Appendix 1

Spatio-temporal Properties of Fast and Slow Neurons in the Pretectal Nucleus Lentiformis Mesencephali in Pigeons

A version of this appendix has been published. Wylie DRW, Crowder NA. 2000. Journal of Neurophysiology. 84: 327-336.

Introduction

The pretectal nucleus lentiformis mesencephali (LM) is a retinal-recipient structure that is implicated in the processing of visual information resulting from self-motion ("optic flow" or "flowfields" (Gibson, 1954)). The LM and nuclei in the accessory optic system (AOS) are principally involved in the generation of visual optomotor responses including optokinetic nystagmus (OKN) and the opto-collic reflex (OCR) to facilitate retinal image stabilization (birds: Fite et al., 1979; Gioanni et al., 1983a,b; for reviews see Grasse and Cynader, 1990; Simpson, 1984; Simpson et al., 1988). The LM is homologous to the nucleus of the optic tract (NOT) in mammals (Simpson et al., 1988). In numerous species, it has been shown that neurons in the LM and NOT exhibit direction-selectivity in response to moving largefield stimuli that are rich in visual texture (i.e. random dot patterns or checkerboards). Although broadly tuned, most neurons are maximally excited in response to motion in the "preferred" direction and strongly inhibited in response to motion in the (approximately) opposite ("anti-preferred") direction (mammals: Collewijn, 1975a,b; Hoffmann and Distler, 1989; Hoffman and Schoppmann, 1975, 1981; Hoffmann et al., 1988; Ibbotson et al., 1994; Mustari and Fuchs, 1990; Volchan et al., 1989; birds: Fu et al., 1998a,b; Winterson and Brauth, 1985; Wylie and Frost, 1996; amphibians: Fan et al., 1995; Fite et al., 1989; Katte and Hoffmann, 1980; Li et al., 1996; Manteuffel, 1984).

Almost all of the above listed studies noted velocity tuning of LM and NOT in response to largefield stimuli consisting of random dot patterns, square-wave gratings and/or checkerboards. However, Ibbotson et al. (1994), in a study of the wallaby NOT, used drifting sine wave gratings of varying spatial and temporal frequency (SF, TF) and

suggested that cells were tuned to TF rather than velocity. They described two types of cells. "Slow" cells responded best to low TFs (<1 Hz) and high SFs (0.5-1 cycles/deg (cpd)). "Fast" cells were most responsive to high TFs (>10Hz) and lower SFs (0.1-0.5 cpd) but had a secondary peak at low TFs and high SFs. In the present study we recorded from neurons in the LM of pigeons in response to drifting sine wave gratings moving in the preferred and anti-preferred directions. This study permits a comparison of the spatio-temporal properties of pretectal neurons in differing species. Moreover, Wolf-Oberhollenzer and Kirschfeld (1994) have recorded the responses of neurons in the nucleus of the basal optic root (nBOR) of the AOS in pigeons to drifting sine wave gratings. Thus, the present study also affords a comparison of the spatio-temporal properties of AOS and pretectal neurons in the same species. We have several previously unreported features to note.

Methods

The methods reported herein conformed to the guidelines established by the Canadian Council on Animal Care and were approved by the Biosciences Animal Care and Policy Committee at the University of Alberta. Silver King and Homing Pigeons (obtained from a local supplier) were anaesthetized with a ketamine (65 mg/kg) - xylazine (8 mg/kg) mixture (i.m.). Depth of anaesthesia was monitored periodically with a toe pinch, and supplemental doses were administered as necessary. The animals were placed in a stereotaxic device with pigeon ear bars and beak adapter so that the orientation of the skull conformed to the atlas of Karten and Hodos (1967). Based on the stereotaxic coordinates of Karten and Hodos (1967), sufficient bone and dura were

removed to expose the brain and allow access the LM with a vertical penetration. Recordings were made with either tungsten microelectrodes (Frederick Haer Inc.) or glass micropipettes filled with 2M NaCl and having tip diameters of 4-5μm. The extracellular signal was amplified, filtered, displayed on an oscilloscope and fed to a window discriminator. The window discriminator produced TTL pulses, each representing a single spike time, which were fed to a CED 1401*plus* (Cambridge Electronic Designs). The stimuli (see below) were synchronized with the collection of the TTL pulses and peri-stimulus time histograms (PSTHs) were constructed with *Spike2 for Windows* software (Cambridge Electronic Designs).

Cells in LM are easily identifiable based on their direction-selective responses to largefield visual stimuli (e.g. Winterson and Brauth, 1985; Wylie and Frost, 1996; Fu et al., 1998a,b). Direction-selectivity was initially assessed by moving a large (about 90 X 90°) handheld stimulus, (consisting of black bars, dots and squiggles on a white background), in various directions in the contralateral visual field. Once a responsive cell was isolated, a directional tuning curve was obtained using high contrast sine wave gratings of an effective SF and TF. The directional tuning curves were done with either 15° or 22.5° increments. Each sweep consisted of 4 sec of motion in one direction, a 3 sec pause, 4 sec of motion in the opposite direction, followed by a 3 sec pause. The directions were presented randomly, and firing rates were averaged over 3-5 sweeps. Subsequent to establishing the direction preference, the spatio-temporal properties were determined by presenting high contrast gratings in the preferred and anti-preferred directions. For the majority of cells, we presented several different SFs (in the range of 0.015 - 2 cpd) at several different TFs (in the range of 0.15 – 16 Hz). For most cells, the

standard stimulus protocol consisted of 6 SFs (0.031, 0.063, 0.125, 0.25, 0.5 and 1 cpd) presented at 6 TFs (0.031, 0.125, 0.5, 2, 8 and 16 Hz). Each sweep consisted of 4-5 sec motion in the preferred direction, a 3-5 sec pause, 4-5 sec of motion in the anti-preferred direction, followed by a 3-5 sec pause. The different stimuli were presented randomly, and firing rates were averaged from at least 3 sweeps. Contour plots of the mean firing rate in the spatio-temporal domain were made using *Sigma Plot*. The peak firing rate in the contour plot was used to assign the preferred SF/TF combination for each neuron. There are limitations to this procedure for assigning a neuron's spatio-temporal preference. In particular, with the lower TFs used (0.031 and 0.125 Hz) much less than one cycle of motion occurs in the 4-5 second epoch. Because of this, for some cells we presented the low TF stimuli for longer durations such that at least 2 cycles occurred. (see below, Figure A1.6).

The drifting gratings were produced using a visual stimulus generator (VSG *Three*, Cambridge Research Services) and displayed in one of two ways. In some cases the stimuli were displayed on a SONY multiscan 17se II monitor that was placed 35cm from the bird. This stimulus, which was circular, measured approximately 40^{o} in diameter. In other instances the stimuli were backprojected by an *InFocus* LP750 data projector onto a tangent screen placed 50 cm from the bird. The circular stimulus measured approximately 75^{o} in diameter. The receptive fields of LM neurons are quite large, often as large as the entire contralateral hemifield. The borders of a receptive field are rather difficult to define, but a hot-spot is present near the center (Fu et al., 1998a,b). The monitor or screen was always centered at the hot-spot of the receptive field. The

location of the receptive field was qualitatively noted as either frontal, lateral (i.e. at the inter-aural axis) or midway between these two positions.

Histology

In some cases, when the tungsten microelectrodes were used, electrolytic lesions were made with a stimulator (*Grass Medical Instruments S-48*) and constant current unit (*Grass;* 30 ③amps, 10 sec, electrode positive). At the end of the experiment, all animals were given a lethal dose of sodium pentobarbitol (100 mg/kg i.p.) and immediately perfused with saline followed by 4% para-formaldehyde. The brains were extracted, post-fixed for several hours (4% para-formaldehyde with 20% sucrose) and then left in 30% sucrose for at least 24 hours. Using a microtome, frozen sections (45 ③m thick in the coronal plane) through the pretectum were collected. The sections were mounted onto gelatin coated slides, dried, counterstained with neutral red, and coverslipped with Permount. Light microscopy was used to localize electrode tracts and the lesion sites.

Results

Direction-Selectivity

We examined the responses of 35 pretectal cells to largefield drifting sine wave gratings of various SFs and TFs. Polar plots showing direction tuning curves of representative LM neurons are shown in Figure A1.1. Most neurons, although broadly tuned, were excited in response to motion in a particular direction ("preferred" direction) and inhibited below the spontaneous rate in response to motion in the (approximately) opposite direction (anti-preferred direction). Of the 35 cells, 30 behaved in this manner

(see Figure A1.1A-E). Of the other 5 cells, 3 showed the excitation to motion in the preferred direction but were either unaffected by stimuli moving in the anti-preferred direction or showed a small amount of excitation to motion in the anti-preferred direction (i.e. there was no inhibitory portion of the tuning curve; Figure A1.1F; Figure A1.6). Shown in Figure A1.1H, one neuron showed strong excitation in response to motion in all directions. Fu et al. (1998a,b) have dubbed these as "omni-directional" neurons. However, this neuron was not found amongst the direction-selective cells (see discussion). The other neuron, shown in Figure A1.1G, had a bi-directional tuning curve (Fu et al., 1998a,b). This neuron was excited by gratings moving in both the forward (temporal to nasal) and backward directions, although there was a slight preference for forward motion. Two tuning curves are shown for this neuron, in response to stimuli of either high SF (0.5 cpd) or low SF (0.0625 cpd) drifting at 2 Hz. For this cell, gratings of higher TF moving in the anti-preferred direction did result in inhibition of the firing rate below the spontaneous level (see below and discussion).

A neuron's direction preference was assigned by calculating the maximum of the best cosine fit to the tuning curve. In Figure A1.2 the direction preferences of the 33 direction-selective LM neurons (i.e. excluding the omni-directional and the bi-directional neurons) are plotted as unit vectors in polar coordinates. Note that there is an obvious clustering into four groups. Seventeen (53%), 5 (15%), 5 (15%) and 6 (18%) neurons preferred forward, backward, downward and upward motion, respectively.

Spatio-temporal Properties

We obtained contour plots of the spatio-temporal tuning in response to sine wave gratings moving in both the preferred and anti-preferred directions. Because, for most neurons, largefield motion in the preferred direction elicits excitation and motion in the anti-preferred direction elicits inhibition, we refer to these as excitatory response plots (ER plots) and inhibitory response plots (IR plots), respectively. Thirty-one of the 35 LM neurons showed both the excitatory and inhibitory responses (Figure A1.1A-E), whereas 2 showed only the ER (Figure A1.1F), and there was no IR for the omni-directional neuron. Thus, we obtained 35 ER plots and 31 IR plots of spatio-temporal tuning.

Figures A1.3 and A1.4 show ER and IR plots of representative LM neurons. (Figure A1.3 shows neurons that had fast ERs whereas Figure A1.4 shows neurons that had slow ERs (see below)). For the majority of contour plots, there was a single peak in the spatio-temporal domain. In some cases the peaks were quite sharp. For example, the ER plot for the LM cell in Figure A1.3B shows a single peak at low SFs and high TFs. Relatively sharp singular peaks are also apparent in the ER plots shown in Figs. A1.4A,C and A1.3A, and the IR plots in Figs. A1.3A-C. In other cases, contour plots exhibited a broad peak, as in the ER plots in Figure A1.3C and A1.4B and the IR plots in Figs. A1.3D and A1.4A,B.

In some contour plots there were clearly multiple peaks. For example, the ER plot in Figure A1.3D contains two clear peaks. The primary peak was at 0.062cpd /16 Hz (45 spikes/sec above the spontaneous rate (SR)), but there was a secondary peak at 0.5cpd/1Hz (40 spikes/sec above SR). Similarly, the ER plot of the LM neuron shown in Figure A1.4D also contains two peaks (the peak at 2cpd/0.5 Hz was the larger). In Figure

A1.4C, there are two peaks in the IR, but one was much larger. The primary peak was at 1cpd/0.5Hz (25 spikes/sec below SR), and the smaller secondary peak was at low SFs and high TFs (5 spikes/sec below SR). The neuron in Figure A1.4D also showed two peaks in the IR plot. Of the 35 ER plots, 11 showed multiple (2 or 3) peaks. Of the 31 IR plots, 6 showed multiple peaks.

The ER of the bi-directional neuron shown in Figure A1.1G had 2 peaks: one at 0.5cpd/2Hz, and the other at 0.625cpd/2Hz. Although this was not routinely done, directional tuning curves were assessed with both low SF and high SF gratings. Note that the directional tuning is similar for both SFs.

Bi-directional IR plots

In some IR plots, it was apparent that there were zones of inhibition and excitation. An example of this is shown in Fig A1.3D. This cell showed a broad inhibitory peak for the lower SFs. However, gratings of high SFs and mid-high TFs, but still moving in the anti-preferred direction, caused excitation. This is particularly salient in the bottom PSTH shown on the right in Figure A1.3D. (The symbols accompanying the PSTHs correspond to the symbols indicating locations on the contour plot). In the top two PSTHs, one can see that the cell was silenced during the period of time that the grating was drifting in the anti-preferred direction (backward). However, a grating of 0.5cpd/2Hz drifting in the anti-preferred direction caused a small excitatory response. That is, this cell was excited in response to gratings of high SF and mid-high TF drifting in both the forward and backward directions. Another example of this bi-directional response to stimuli moving in the anti-preferred direction can be seen in Figure A1.3C,

but in this case the excitatory region of in the IR plot was at low SFs (see also Figure A1.4B). In total, the IR plots of 10 LM neurons showed this property. (The neuron with the bi-directional tuning curve (Figure A1.1G) was one of these 10). There was a tendency for this excitation peak in the IR to occur for stimuli of high SFs and low TFs, or low SFs and high TFs. Similarly, two of the ER plots of LM neurons showed a weak inhibitory zone.

Independence of Excitation and Inhibition

For a given cell, we expected that the ER and IR plots would be identical. Although this was the case for some cells, this was not the norm. For example, for the LM neuron shown in Figure A1.3B, the peak in the ER plot was at low SFs and high TFs, whereas the peak in the IR plot was at high SFs and mid-TFs. Likewise, in Figs. A1.4A,B, the cells were maximally excited by high SF/mid-TF gratings drifting in the preferred direction, but were maximally inhibited by low SF/high TF gratings drifting in the anti-preferred direction. In fact, for none of the 8 cells shown in Figures A1.3 and A1.4 did the ER plot show a similar response profile to the IR plot. Of the 31 LM neurons for which we obtained both ER and IR plots, 25 had markedly different spatio-temporal response profiles for the ER and IR.

Slow and Fast Responses

In Figure A1.5 the locations of the response maxima are shown for the ER and IR plots of LM neurons. For those contour plots in which there were multiple peaks, the location of the primary peak was plotted. ER and IR plots with multiple maxima of equal

size were excluded from this analysis, as was the IR of one LM neuron that had an extremely broad plateau. In Figure A1.5A, the peaks from the ER plots are shown. A cluster analysis using Ward's method with squared-Euclidean distance measures clearly revealed the two clusters shown in Figure A1.5A. A discriminate analysis revealed that the groups were completely non-overlapping. The first group, indicated by the filled circles, preferred low-mid SFs (0.031-0.25 cpd) and mid-high TFs (0.5-16 Hz). The second group, indicated by the open circles, preferred mid-high SFs (0.3-2 cpd) and low-mid TFs (0.125-2 Hz). We refer to these groups as fast and slow neurons, respectively (velocity = TF/SF). The average SF, TF and velocity of the fast neurons were, 0.097 cpd, 2.88 Hz and 29.2 deg/sec, respectively. The average SF, TF and velocity of the slow neurons were, 0.67 cpd, 0.55 Hz and 0.82 deg/sec, respectively. (All values were first transformed to the natural log, the average was calculated, and then the inverse transformation was performed).

Figure A1.5B show locations of the peaks from the IR plots. Unlike the ERs, the locations of the peak IRs do not exhibit any obvious clustering in the spatio-temporal domain. Although many of the peaks fell in the slow (high SF/low TF) and fast (low SF/high TF) regions, there were also several peaks in the high SF/high TF quadrant. (However, note that there is still an overall negative correlation between SF and TF).

On the right-hand side of Figure A1.5, the same data is plotted as that on the left, but the direction preference is also indicated. There are a couple things to note. First, with respect to the ER plots, all but one of the slow cells preferred forward motion. Some cells that preferred forward motion had fast ERs, as did most of the LM cells that

preferred up, down and backward motion. Second, for the IR plots, there was a tendency for those cells with IR peaks in the lower TF range to prefer forward motion.

Examples of fast and slow LM neurons are shown in Figures A1.3 and A1.4, respectively. We would like to emphasize two things about this classification. First, the designation of a neuron as "fast" or "slow" refers only to the ER. For example, the ER plot of LM cell in Figure A1.3B had a peak in the fast region, but the peak for the IR was in the slow region. The peak ER for the cell shown in Figure A1.4A was in the slow region, but the peak IR was in the fast region. Second, for neurons with multiple peaks in the ER, the designation of a neuron as "fast" or "slow" refers to the primary peak. The cell shown in Figure A1.3D had peak ERs in both the fast and slow regions, although the former was slightly larger. Likewise, the ER plot of the cell shown in Figure A1.4D showed maxima in both the fast and slow region, although the peak in the slow region was slightly larger. This was generally the case for the ER (and IR) plots with multiple peaks: there were maxima in both the slow and fast regions.

Transients and Temporal Effects

Figure A1.6 shows PSTHs of the responses of an LM neuron to gratings drifting in the preferred (up) and anti-preferred (down) directions. In Figure A1.6A, the responses of the neuron to 36 combinations of SF (abscissa) and TF (ordinate) are shown. Each PSTH is for a single sweep, where each sweep consisted of 4 sec motion in the preferred direction (upward motion, solid line), followed by a 3 sec pause, followed by 4 sec of motion in the anti-preferred direction (downward motion, broken line). Note that this cell showed strong excitation to motion in the preferred direction and a small amount

of excitation to motion in the anti-preferred direction. In Figure A1.6B, PSTHs show the responses for the same cell to drifting gratings of 0.125 Hz at 3 different SFs. Each sweep consisted of 16 sec of motion in the preferred, followed by a 3 sec pause, followed by 16 sec of motion in the anti-preferred direction. That is, there were two complete cycles of motion. This figure is shown to indicate some of the limitations with our procedure. Moreso than any other cell, this cell showed dramatic transient and temporal effects in the PSTHs. The response to motion in the preferred direction consisted of an onset transient, followed by a steady state response. In response to some gratings there was also an offset transient (e.g. 0.03cpd/0.12Hz), and onset and offset transients to motion in the anti-preferred direction (e.g. 0.25cpd//0.12Hz). The asterisk (*) indicates the peak excitatory response in the spatio-temporal domain (0.125cpd/16Hz) based on the average firing rate over the 4 sec epoch. This encompasses the steady-state and transient responses. Note however, that the largest onset transient occurred in response to 0.25cpd/2Hz. The data in Figure A1.6B indicate another possible shortcoming of our standard protocol. For the two lowest TFs used, less than one cycle of motion occurred during the 4 sec epoch. When a 16 sec epoch was used for stimuli drifting at 0.125 Hz (i.e. two complete cycles), other temporal effects were observed at some SFs. The PSTH in response to the lowest SF grating (0.03 cpd) clearly shows that the response to motion in both the preferred and anti-preferred directions was modulated at the TF of the stimulus. This TF modulation was not apparent in the response to the 0.125 cpd grating, which had a higher average firing rate. The response to the 0.5 cpd grating was modulated in the range of 0.5-0.6 Hz. Thus, the standard protocol that we used, which limited the motion to 4 or 5 sec epochs, would not necessarily capture all the temporal

effects and might misrepresent the firing rate. For this neuron, the average firing rate to a 0.03cpd/0.12Hz grating was 8.35 spikes/sec over the 4 sec epoch, but 14.96 spikes/sec over the 16 sec epoch. This translates to an 80% increase, but only a 6% increase relative to the maximal firing rate to the preferred SF/TF combination (0.125cpd/16Hz; 115 spikes/sec). The difference was not as marked for the other two stimulus conditions shown in Figure A1.6B. In response to a 0.125cpd/0.12Hz grating, the average firing rate was 55 spikes/sec over the 4 sec epoch and 45 spikes/sec over the 16 sec epoch. In response to a 0.5cpd/0.12Hz grating, the average firing rate was 21.35 spikes/sec over the 4 sec epoch and 19.86 spikes/sec over the 16 sec epoch. For 5 neurons (2 fast and 3 slow neurons) we tested the responses to the lower TF (0.12 and 0.03 Hz) gratings using the standard protocol and longer epochs that allowed 2 complete cycles of motion in each direction. Although the average firing rates over the two conditions were sometimes different, there were no changes with respect to the shapes of the contour plots or the location of the peaks in the contour plots.

Tuning for Temporal Frequency or Velocity?

From the contour plots it is easy to see if a cell is tuned to TF or velocity. Cells tuned to velocity have elliptical peaks and iso-contour lines that are oriented diagonally with a slope of 1. Cells tuned to TF have contour plots that are symmetrical about a horizontal line through the peak. For example, the ER plot of the LM cell in Figure A1.3A showed velocity tuning. The elliptical peak and iso-contour lines are oriented diagonally with a slope of about 1. In Figure A1.7A, the responses of this cell are shown as a function of velocity (left) and TF (right) for each SF tested. Responses to stimuli

drifting in the preferred and anti-preferred directions are represented by the filled and open symbols, respectively. To stimuli moving in the preferred direction, a peak response occurred at about 10 deg/sec for most SFs tested. On the right-hand side of Figure A1.7A, where the response is plotted as a function of TF, there is not a common peak for all the SFs tested. However, responses tuned to velocity were uncommon (2 ER plots, 1 IR plots). More cells seemed to be tuned to a particular TF. For example, the ER of the LM cell in Figure A1.7B showed a peak at 0.5-2 Hz for each SF tested. Similarly, the IR of the cell shown in Figure A1.7A was tuned to higher TFs and the IR for the cell in Figure A1.7C was tuned to 0.5-2 Hz. (The IR plot for this cell is shown in Fig A1.4D). The ERs of 14 LM neurons were reasonably well tuned to TF, as were the IRs of 12 cells.

Many responses, including most of those that showed multiple peaks in the contour plots, could not be described as tuned to either a particular velocity or TF. For example, the ER for the cell shown in Figure A1.7C was tuned to mid-TFs for stimuli of high and low SF, and low TFs for stimuli of mid-SFs. Likewise the IR in Figure A1.7B was tuned to neither TF nor velocity (see also the ER plots in Figs. A1.3D, A1.4C, and the IR plots in Figure A1.3B, A1.4A,C).

Histological Results

For eight neurons the recording sites were localized with electrolytic lesions. In Figure A1.8 the lesion sites are collapsed onto two coronal sections through the pretectum. We have used the nomenclature for the pigeon pretectum as established by Gamlin and Cohen (1988). All 8 lesions were found in the LM, either in the medial or lateral subnuclei (LMm, LMl; four lesions each). There was no obvious anatomical

separation of cells with respect to either direction preference or spatio-temporal properties (fast/slow), although the size of our sample is insufficient in this regard.

Discussion

In the present study we examined the responses of neurons in pigeon pretectum to largefield drifting sine wave gratings varying in spatial and temporal frequency. Although we did not leave marking lesions at all of the recording sites, all of the lesions were located in LM (see Figure A1.8). However, this does not preclude the possibility that some of the other visually responsive units were located in other areas of the pretectum (Winterson and Brauth, 1985).

As previously reported in numerous other studies in several species, pretectal neurons exhibit directional selectivity in response to such largefield stimuli (mammals: Collewijn, 1975a,b; Hoffmann and Distler, 1989; Hoffman and Schoppmann, 1975, 1981; Hoffmann et al., 1988; Ibbotson et al., 1994; Mustari and Fuchs, 1990; Volchan et al., 1989; birds: Fu et al., 1998a,b; Winterson and Brauth, 1985; Wylie and Frost, 1990, 1996; amphibians: Fan et al., 1995; Katte and Hoffmann, 1980; Fite et al., 1989; Li et al., 1996; Manteuffel, 1984). Unlike previous studies, we used drifting sine wave gratings as stimuli. We are aware of only two previous studies that used such stimuli: Wolf-Oberhollenzer and Kirschfeld (1994) in a study of neurons in pigeon nBOR, and Ibbotson et al. (1994) in a study of neurons in the wallaby NOT, the mammalian homolog of the LM. The bulk of the discussion will focus on comparing the results of the present study with those previous studies.

Independence of Excitation and Inhibition

One of the surprising findings of the present study was that spatio-temporal properties of the inhibitory and excitatory responses for a given cell were often quite different. This was that case for 25/31 LM neurons. This was not noted in the study of the NOT by Ibbotson et al. (1994), but they only showed contour plots for stimuli moving in the preferred direction. However, one figure (Figure 7, p. 2933) clearly shows a NOT cell for which there was a difference in the preferred TF to stimuli drifting in the preferred vs. anti-preferred directions. The independence of excitatory and inhibitory responses of AOS and pretectal neurons has been noted with respect to other properties. First, with respect to direction tuning, the preferred and anti-preferred directions of AOS neurons are often not 180° apart (e.g. Burns and Wallman, 1981; Rosenberg and Ariel, 1998; Soodak and Simpson, 1988; Wylie and Frost, 1990). Second, it has been noted that the excitatory and inhibitory receptive fields of an individual LM or nBOR neuron may differ with respect to their size and position (Fu et al., 1998a; Wylie and Frost, 1990; Zhang et al., 1999). Together, these findings suggest that the inhibitory and excitatory inputs to direction-selective LM neurons arise from different inputs. Perhaps the excitatory input is of retinal origin (Kogo et al., 1998) whereas the inhibitory inputs are extra-retinal (Brecha et al., 1980; Miceli et al., 1979).

Comparison with Previous Studies of the pigeon LM

Previous studies have examined the responses of pigeon LM neurons to largefield stimuli that contain multiple SF components (random dot patterns, checkerboards and/or square wave gratings (Fu et al., 1998a,b; Winterson and Brauth, 1985; Wylie and Frost,

1996). As with these previous studies, we found that most LM neurons prefer largefield stimuli moving forward in the contralateral visual field, whereas fewer prefer upward, downward or backward motion (Fu et al., 1998a,b; Winterson and Brauth, 1985; Wylie and Frost, 1996). With respect to fast and slow neurons, our findings are in strong agreement with Winterson and Brauth (1985). They described slow neurons that preferred stimuli moving at <1.0 deg/sec and fast neurons that preferred velocities in the range of 3.3 to 80 deg/sec. These data are confirmed by the present study: with respect to the ER plots, we describe slow neurons (0.25-2 deg/sec) and fast neurons (4 to 256 deg/sec). Further, we show that velocity is not the correct referent for the vast majority of cells: slow neurons preferred high SF/low TF gratings and fast neurons preferred low SF/high TF gratings. In their sample, Winterson and Brauth (1985) noted that most (8/9) of the slow neurons preferred forward motion, whereas the fast neurons preferred either forward, backward, upward or downward motion. This is essentially identical to what we found: 11/12 slow neurons were forward cells, whereas the fast cells included forward, backward, downward and upward cells. Stated another way, there were fast and slow forward cells in LM, in addition to fast cells that preferred upward, downward and backward motion.

The results of the present study are, for the most part, in agreement with the findings of Fu et al. (1998b). Using square wave gratings and other largefield moving stimuli, they described three types of neurons: (i) uni-directional cells (74%) responded to motion in a particular direction, were inhibited by motion in the opposite direction and preferred slow velocities (0.1 – 11 deg/sec); (ii) omni-directional neurons (9%) responded equally well to motion in all directional and preferred fast velocities (34-67 deg/sec); and

(iii) bi-directional neurons (17%) had bi-lobed tuning and were excited by motion in two, approximately opposite, directions. The results of the present study are different from these of Fu et al. (1998b) on several accounts. First, most (33/35) of the LM cells we recorded from would be classified as uni-directional, but these included fast and slow neurons. Fu et al. (1998b) did note within this group of unidirectional cells, the average preferred velocity of the forward cells was slower than that of the backward cells. Second, we did record from one omni-directional neuron that preferred low SFs and high TFs, but it was not found amongst the unidirectional cells. In subsequent experiments, when we encountered omni-directional neurons, we moved caudally to find the direction-selective cells. Although we have no supportive histology, we believe that the omni-directional cells may not reside in the LM, but are located elsewhere in the pretectum; (perhaps the nucleus laminaris precommissuralis (LPC), the nucleus principalis precommissuralis (PPC) or the tectal gray; Figure A1.8; see Gamlin and Cohen, 1988). In their study of the LM, Winterson and Brauth (1985) did not report these omni-directional cells. Third, we also only encountered one of the bi-directional cells described by Fu et al. (1998b). However, we must emphasize that the cell showed either excitation or inhibition to gratings moving in the anti-preferred direction, dependent on the SF and TF. The directional tuning curve shown in Figure A1.1G was not done with the appropriate SF and TF to elicit inhibition to stimuli moving in the anti-preferred direction. Thus, it is possible that the bi-directional cells found by Fu et al. (1998b) were actually unidirectional cells, but the stimuli used did not contain the appropriate SF/TF combination in the range of the inhibitory peak. Recall that, in the present study, the IR plots of 32% of the LM neurons had zones of excitation and inhibition in response to

stimuli moving in the anti-preferred direction. This is clearly illustrated by the cell in Figure A1.3D: gratings of high SF/mid-TF moving in the anti-preferred direction excite the cell, whereas gratings of low SF/high TF inhibit the cell. For this cell, if directional tuning was established with stimuli containing low SFs, this cell would be classified as unidirectional, but if tested with high SFs the cell could be classified as bi-directional.

Finally, Fu et al. (1998b) concluded that LM neurons are essentially "edge detectors" (see also Zhang et al. (1999)). That is, LM neurons require a sharp edge to elicit a maximal response. We find this hard to reconcile given that we recorded from many neurons that showed maximal responses to low SF sine wave gratings that are essentially bars with blurry edges. Moreover, in the initial open-loop stages of OKN and until the steady-state OKN is achieved, (i.e. when the OKN gain is very low), any edges will be blurred (Ibbostson et al., 1994). We have closely examined the methods Fu et al. (1998b) used to reach this conclusion, and offer an alternative explanation. They had an edge drift across a screen that subtended about 140 deg. Leading the edge, the stimulus was completely white, and trailing the edge the stimulus was completely black. They found that the neurons responded vigorously to a sharp edge, but the response was progressively reduced as the edge was progressively blurred by altering the spatial rate of luminance change at the border. However, note that such a stimulus is effectively an extremely low SF grating (about 0.004 cpd) with progressively more power at higher SFs as the edge becomes progressively sharper. As we interpret their results, the progressively sharper edges simply had progressively more power at higher SFs. That is, it is possible that the sharp edges had sufficient power in the range of SFs that the cell preferred, whereas the blurred edges did not.

Comparison with Previous Studies of nBOR

Like the LM, the nBOR is also involved in the analysis of optic flow and the generation of compensatory head and eye movements (Fite et al., 1979; Gioanni et al., 1983a). The major difference between the LM and nBOR is that most nBOR neurons prefer largefield stimuli moving either upward, downward or backward in the contralateral visual field, whereas few prefer forward motion (Burns and Wallman, 1981; Gioanni et al., 1984; Wylie and Frost, 1990; Zhang et al., 1999). Wolf-Oberhollenzer and Kirschfeld (1994) examined the responses of neurons in nBOR to drifting sine wave gratings, but they did not use as extensive a battery of stimuli as we used in the present study. They used TFs in the range of 0.1 to 10 Hz but only four levels of SF in the range of 0.024 to 0.185 cpd. This is the lower half of the SF range we used. They noted that most nBOR neurons could not be described as velocity detectors. In fact only 1 of 15 (7%) neurons tested responded to stimulus velocity, whereas 7 (47%) were described as selective for a given TF at all SFs tested. This is strikingly similar to what we found for LM neurons. Collapsing across the ERs and IRs, 5% showed velocity selectivity whereas about 40% showed similar TF response profiles for all SFs tested.

Because Wolf-Oberhollenzer and Kirschfeld (1994) did not use a more broad range of SFs, it is difficult to compare our results directly. Nonetheless, they described two groups of nBOR neurons. The first group showed a single peak TF at about 0.2 Hz although it is not stated if these neurons responded better to the higher SF used. In the present study, on average, the slow ERs of LM neurons preferred a TF of about 0.5 Hz. Wolf-Oberhollenzer and Kirschfeld (1994) did not report any neurons that had a single peak in the high TF region. The second group they described showed two peaks in the

TF domain: one at 0.2 Hz and the other in the range of 1-7 Hz. Similarly, we described neurons with multiple peaks, most with one each in the low SF/high TF region and the high SF/low TF region. Although, Wolf-Oberhollenzer and Kirschfeld (1994) assumed that these neurons receive inputs from two types of motion detectors that have low pass filters with differing time constants, we would add that the two types of detectors might also have different SF preferences.

Comparison with the spatio-temporal preferences of NOT neurons

Ibbotson et al. (1994) examined the spatio-temporal properties of neurons in the NOT of the wallaby using a broad range of SFs (0.063 to 2 cpd) and TFs (0.38 to 24.3 Hz). They found two groups of cells. "Slow" cells preferred high SFs (0.5-1.0 cpd) and low TFs (<1 Hz) whereas "fast" neurons preferred low SFs (0.1-0.5 cpd) and high TFs (>10Hz). These findings are similar to the findings of the present study, but there were some differences. First, the slow NOT neurons were inhibited by low SF/high TF gratings moving in the preferred direction. We saw such bi-directional responses, but in response to gratings moving in the anti-preferred direction. Second, all of the fast NOT neurons showed a secondary peak in the slow region. We did find neurons with peaks in both the fast and slow regions, but others with a single peak in the fast region. Third, the range of preferred SFs for the fast NOT neurons is higher than that of the fast ERs of LM neurons. Finally, both the slow and fast NOT neurons in the wallaby are faster than their counterparts in the pigeon LM. This difference might be related to the differences that are seen in the properties of the OKN (see below).

Function of Fast and Slow Neurons

Ibbotson et al. (1994) provide an excellent discussion of the potential role of the slow and fast NOT neurons in the generation and maintenance of OKN. Immediately after the onset of an optokinetic stimulus, there is a 50-100 msec latent period before ocular following begins (e.g. Collewijn, 1972). During this period, the retinal slip velocity (RSV) is high, and Ibbotson et al. (1994) suggest that the fast NOT neurons are responsible for initiating ocular following (the "direct" phase of OKN; Cohen et al., 1977). Moreover, they suggest that the fast neurons are involved in the charging of the velocity storage mechanism ("indirect" phase of OKN) when stimulus speeds are high. Ibbotson et al. (1994) note that rapidly moving visual images become blurred, which is consistent with the fact that the fast NOT neurons respond best to low SFs. The slow NOT neurons do not become active until the RSV is low, and they continue to charge the velocity storage mechanism at these slow velocities. Finally, Ibbotson et al. (1994) suggested that omni-directional neurons in NOT inhibit direction-selective neurons in the early stages of saccades.

Gioanni and colleagues (Gioanni et al., 1981; Gioanni, 1988) have provided a comprehensive description of the OKN and head-free OCR in pigeons. OKN in pigeons is different from that of frontal-eyed mammals in (at least) two respects. First, pigeons lack the direct phase of OKN, but they do possess a velocity storage mechanism (Gioanni, 1988). This precludes the fast LM ERs in pigeon from a role in the direct component of OKN, as proposed for the fast NOT neurons. However, it is reasonable to imagine that the fast and slow LM neurons are involved in charging the velocity storage mechanism as proposed for the fast and slow NOT neurons. The second difference

between the dynamics of the OKN in pigeons and frontal-eyed mammals is that, in pigeons, the gain of the OKN falls markedly as stimulus velocity increases beyond 20 deg/sec, (although the OCR gain remains high at 40 deg/sec) (Gioanni, 1988). In frontal-eyed mammals the gain of the OKN remains high beyond 60 deg/sec (e.g. Lisberger et al., 1981). In the present study, the average preferred velocity of the fast LM neurons was about 20 deg/sec: the point at which the OKN gain begins to decline in pigeons. The fast NOT neurons in the wallaby preferred higher TFs than the fast LM ERs, which is correlated with a higher OKN gain at faster velocities in frontal-eyed mammals.

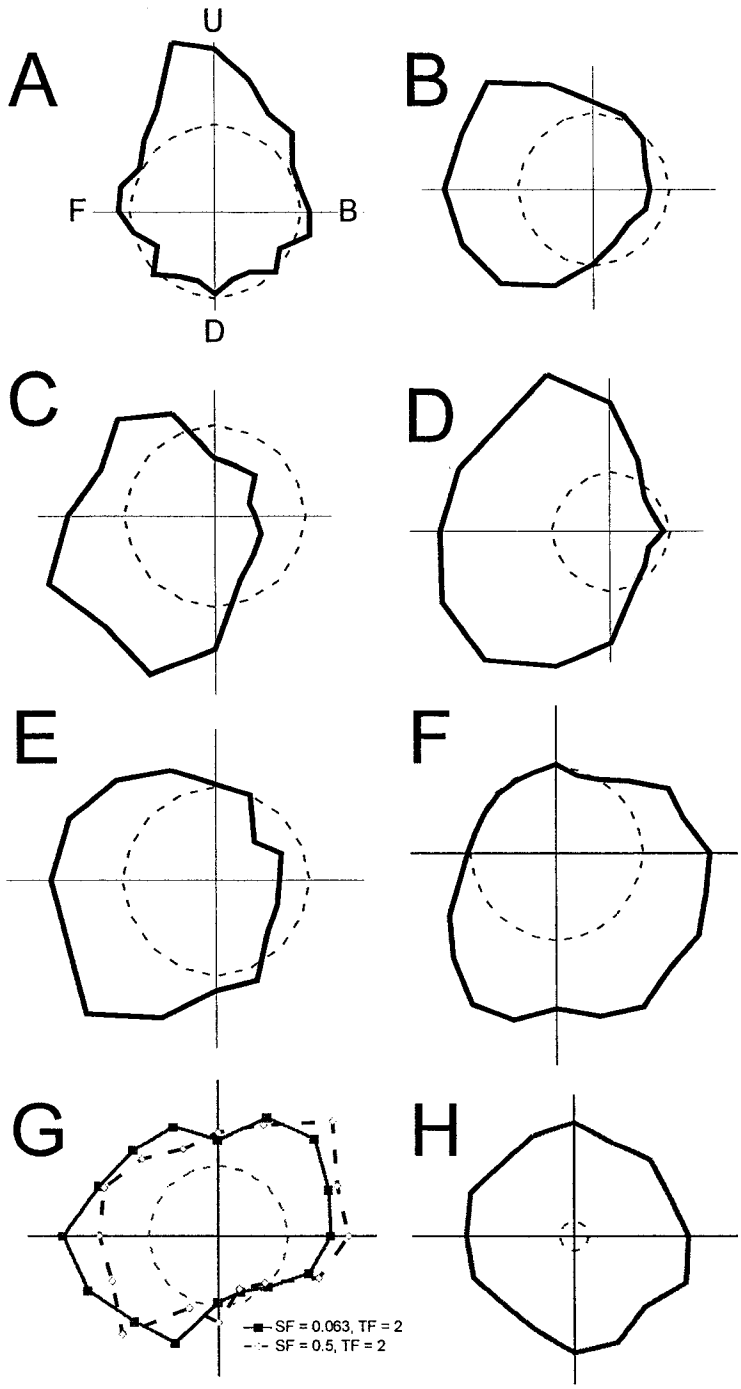

Figure A1.1

Directional tuning curves of neurons in the pretectal nucleus lentiformis mesencephali (LM). Firing rate (normalized) is plotted as a function of the direction of grating motion in polar coordinates. Two tuning curves are shown for different SFs for the neuron in G.

The broken circles represent the spontaneous firing rates. U, D, B, F, represent upward, downward, forward (temporal to nasal), and backward motion, respectively. See text for details.

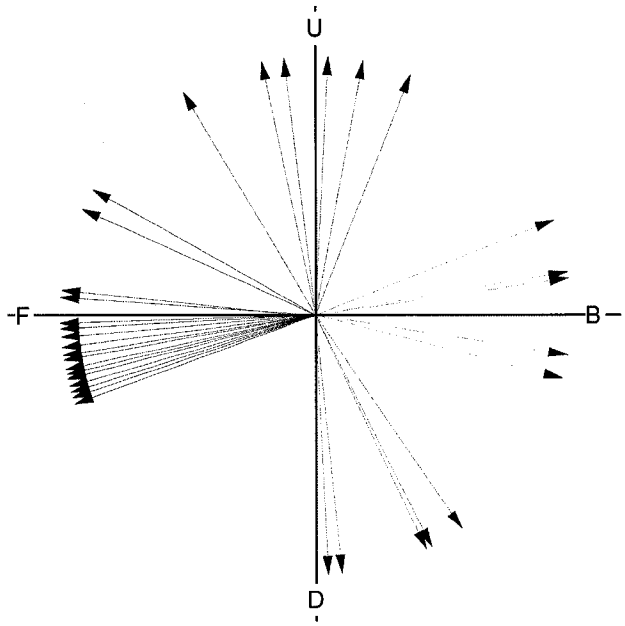

Figure A1.2

Direction preferences of neurons in the nucleus lentiformis mesencephali (LM). The arrows are unit vectors representing the preffered direction of LM neurons as calculated from the best fit cosines to the tuning curves. Note the tight clustering of the forward (temporal to nasal) selective neurons. U, D, F, B represent up, down, forward (temporal to nasal) and backward motion, respectively.

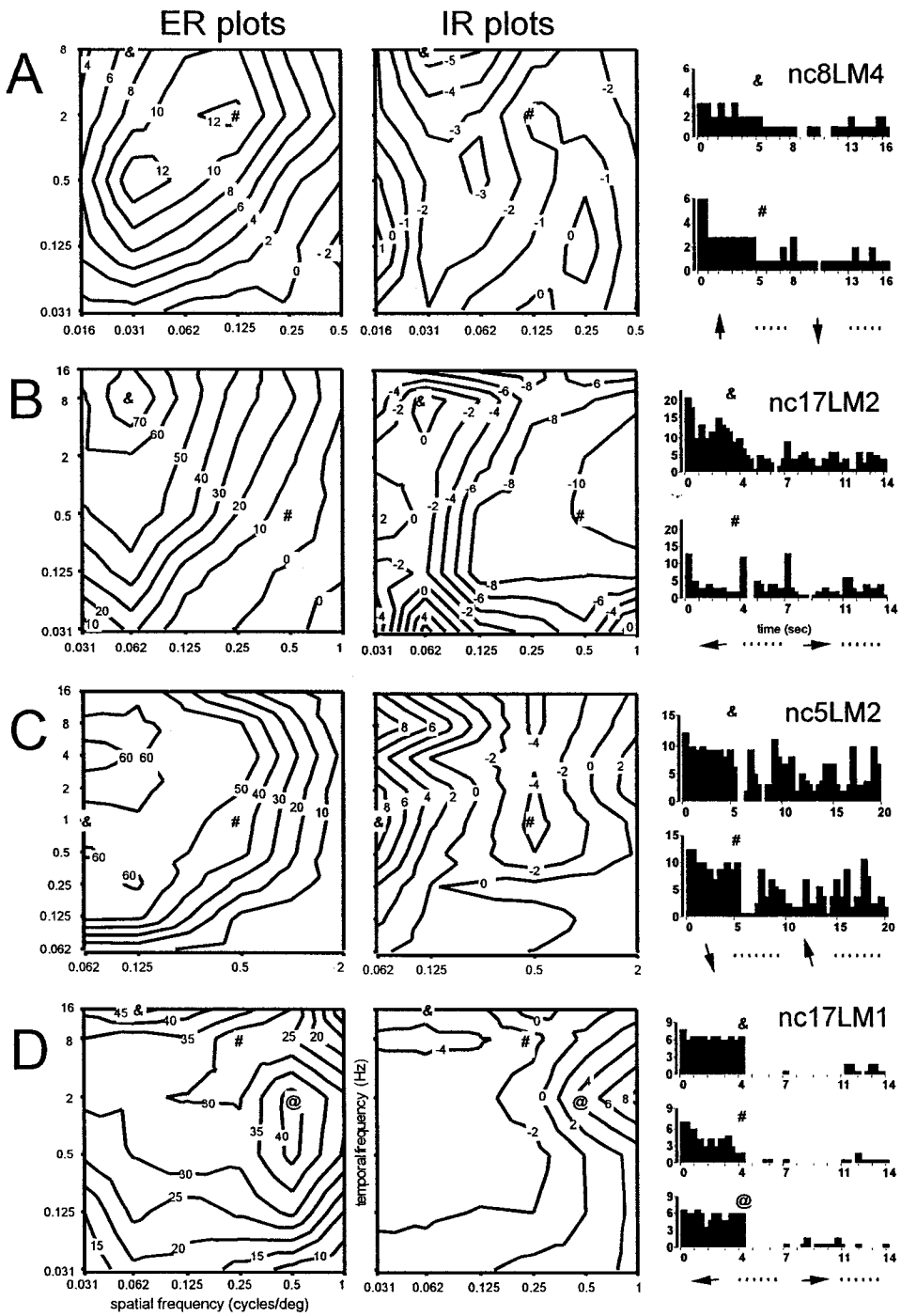

Figure A1.3

Spatio-temporal tuning of fast neurons in the pretectal nucleus lentiformis mesencephali (LM). Contour plots of the responses of four LM neurons to gratings of varying SF (abscissa) and TF (ordinate) drifting in the preferred (ER plots) and anti-preferred (IR

plots) directions are shown. The scale on the iso-contour lines represents the firing rate (spikes/sec) above (+) or below (-) the spontaneous rate. To the right of the contour plots, 2 or 3 peri-stimulus time histograms (PSTHs) show individual sweeps for a particular SF and TF. The particular SF and TF are indicated by the corresponding symbols (&, @, #) on the PSTH and the contour plot. For each sweep there was 4-5 sec of motion in the preferred direction (indicated by the orientation of the arrow; left = forward), followed by a 3-5 sec pause (i.e. a stationary grating; dashed line), followed by 4-5 sec of motion in the anti-preferred direction, followed by a 3-5 sec pause.

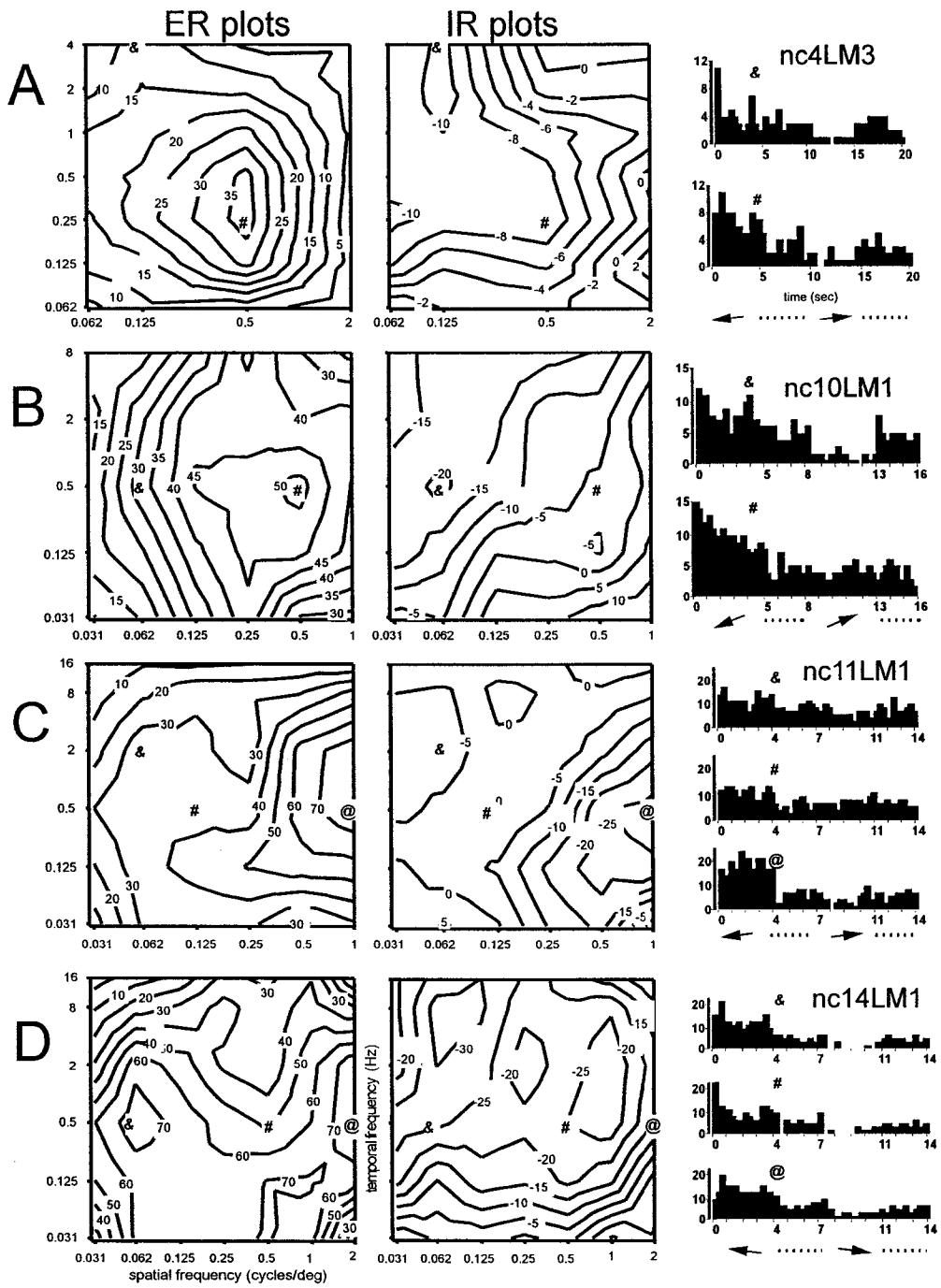

Figure A1.4

Spatio-temporal tuning of slow neurons in the pretectal nucleus lentiformis mesencephali (LM). See legend for Figure A1.3 for additional details.

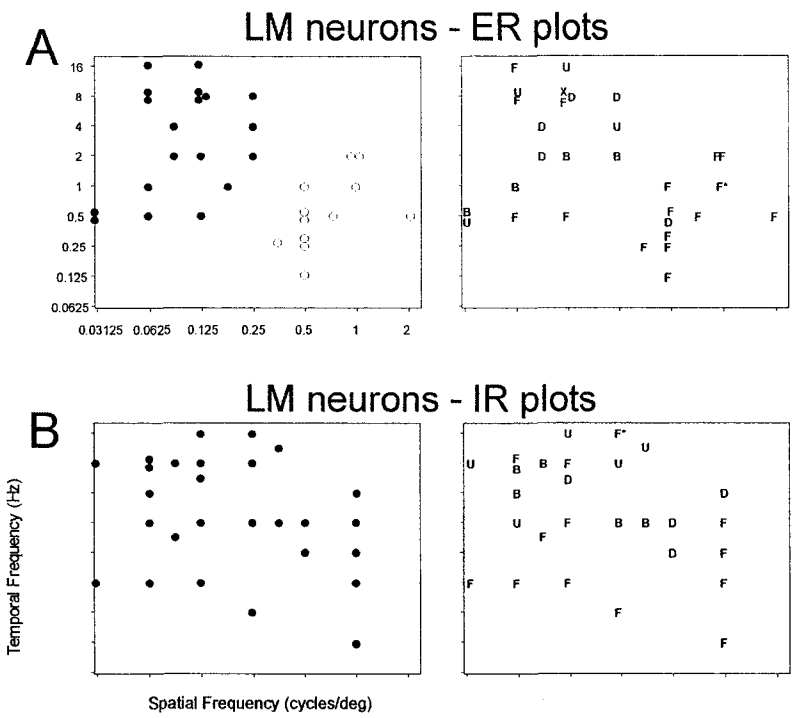

Figure A1.5

Locations of the peak excitatory and inhibitory responses in the spatio-temporal domain for neurons in lentiformis mesencephali (LM). In A and B, respectively, the locations of the peaks are shown for the ER plots and the IR plots. Included in this analysis are ER and IR plots that showed single peaks, as well as those that showed multiple peaks where there was a clear primary peak. (The locations of the primary peaks, but not the secondary peaks, are plotted). In A, the filled circles indicate the group of fast ERs, and the open circles represent the group of slow ERs. On the right, the same data is plotted, but the locations are indicated with a letter corresponding to the preferred direction of the cell (F = forward (temporal to nasal), B = backward, U = upward, D = downward motion). "X" represents the omni-directional cell (Figure A1.1H) and "F*" indicates the bi-directional cell (Figure A1.1G). Note that for the IR plots, (responses to motion in the anti-preferred direction), the preferred direction of the cell is indicated.

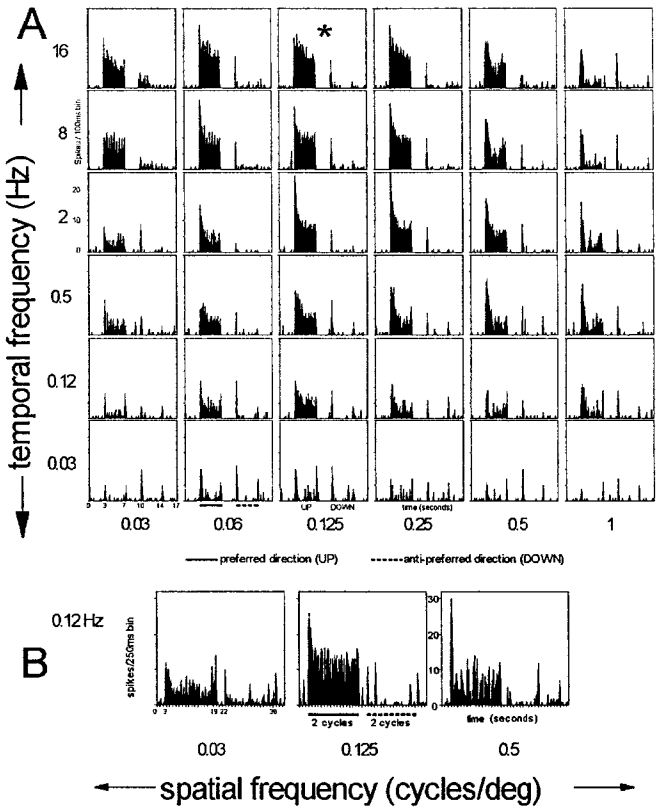

Figure A1.6

Responses of a neuron in lentiformis mesencephali (LM) to drifting gratings of varying spatial and temporal frequency (SF, TF). In A, Post-stimulus time histograms (PSTHs) show the responses of the neurons to 36 combinations of SF (abscissa) and TF (ordinate). Single sweeps are shown, where each sweep consisted of 4 sec motion in the preferred direction (upward motion, solid line), followed by a 3 sec pause, followed by 4 sec of motion in the anti-preferred direction (downward motion, broken line). Note that the grid is not scaled. The asterisk (*) indicates the peak excitatory response in the spatio-temporal domain based on the average firing rate over the 4 sec epoch. In B, PSTHs show the responses (for the same cell) to drifting gratings of 0.125 Hz at 3 different SFs. Each sweep consisted of 16 sec of motion in the preferred direction (i.e. 2 complete

cycles), followed by a 3 sec pause, followed by 16 sec of motion in the anti-preferred direction. See text for details.

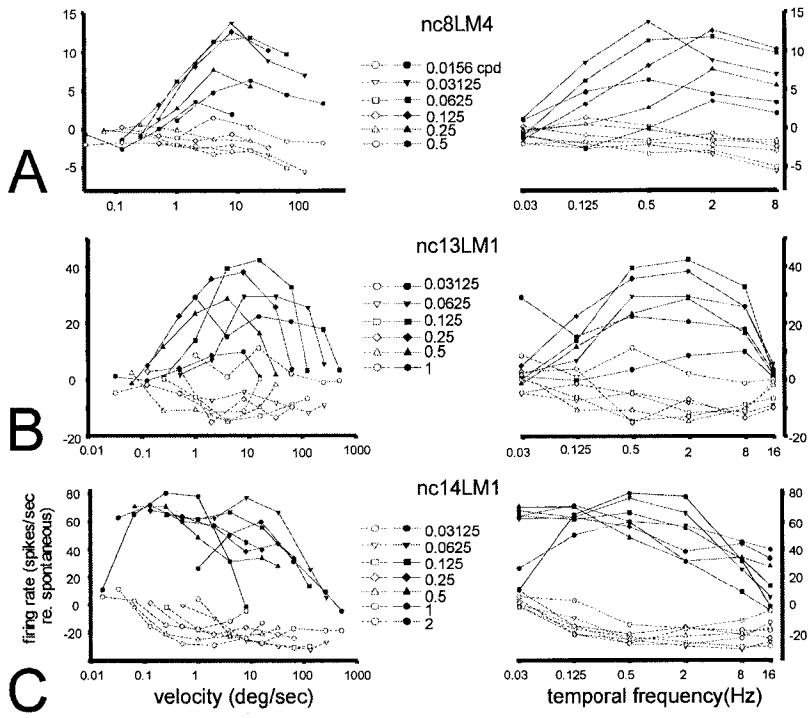

Figure A1.7

Velocity and temporal frequency tuning of neurons in the pretectal nucleus lentiformis mesencephali (LM). On the left, average firing rate (spikes/sec above (+) or below (-) the spontaneous rate (SR)) is plotted as a function of velocity (deg/sec) for each SF used. On the right, the same data are plotted, but as a function of TF (Hz). The filled and open symbols represent the responses to gratings moving in the preferred and anti-preferred directions, respectively. The neurons in A and C correspond to those in Figure A1.3A and A1.4D, respectively. See text for details.

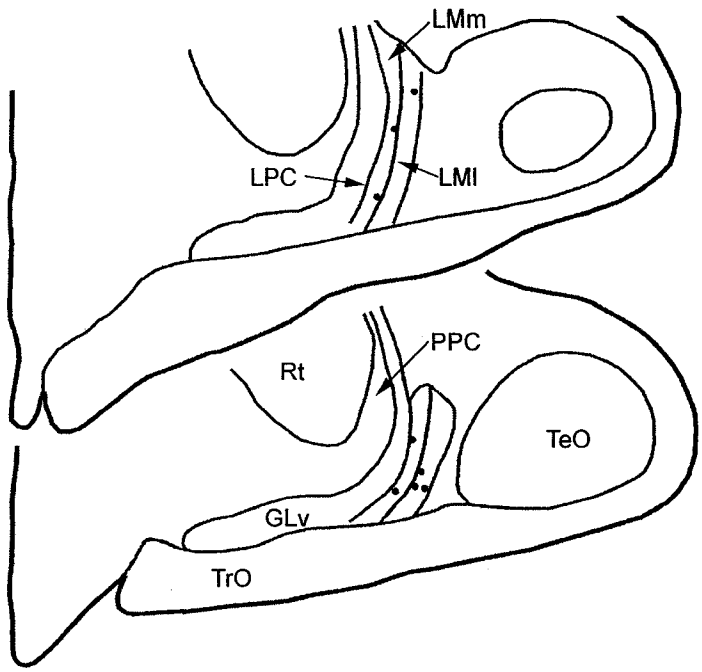

Figure A1.8

Location of directionally selective units in the pretectum. Two coronal sections through the pretectum are shown (top = caudal) indicating the locations (●) of eight recording sites marked by electrolytic lesions. The nomenclature of Gamlin and Cohen (1988) is used. The LM consists of medial and lateral subnuclei (LMm, LMl). LMm is bordered medially by the nucleus laminaris precommisuralis (LPC). The nucleus principalis precommisuralis (PPC) resides between the LPC and the nucleus rotundus (Rt). Note that all the marking lesions were located in the LM. GLv, nucleus geniculatus lateralis, pars ventralis; TeO, optic tectum; TrO, tractus opticus.

References

Brecha N, Karten HJ, Hunt SP. Projections of the nucleus of basal optic root in the pigeon: An autoradiographic and horseradish peroxidase study. *J Comp Neurol* 189: 615-670, 1980.

Burns S, Wallman J. Relation of single unit properties to the oculomotor function of the nucleus of the basal optic root (AOS) in chickens. *Exp Brain Res* 42: 171-180, 1981.

Cohen B, Matsuo V, Raphan T. Quantitative analysis of the velocity characteristics of optokinetic nystagmus and optokinetic after-nystagmus. *J Physiol London* 270: 321-344, 1977.

Collewijn H. Latency and gain of the rabbit's optokinetic reactions to small movements. *Brain Res* 36: 59-70. 1972.

Collewijn H. Direction-selective units in the rabbit's nucleus of the optic tract. *Brain Res* 100: 489-508, 1975a.

Collewijn H. Oculomotor areas in the rabbit's midbrain and pretectum. *J Neurobiol* 6: 3-22, 1975b.

Fan TX, Weber AE, Pickard GE, Faber KM, Ariel M. Visual responses and connectivity in the turtle pretectum. *J Neurophysiol* 73: 2507-2521, 1995.

Fite KV, Reiner T, Hunt S. Optokinetic nystagmus and the accessory optic system of pigeon and turtle. *Brain Behav Evol* 16: 192-202, 1979.

Fite KV, Kwei-Levy C, Bengston L. Neurophysiological investigation of the pretectal nucleus lentiformis mesencephali in *Rana pipiens*. *Brain Behav Evol* 34: 164-170, 1989.

Fu YX, Gao HF, Guo MW, Wang SR. Receptive field properties of visual neurons in the avian nucleus lentiformis mesencephali. *Exp Brain Res* 118: 279-285, 1998a.

Fu YX, Xiao Q, Gao HF, Wang SR. Stimulus features eliciting visual responses from neurons in the nucleus lentiformis mesencephali in pigeons. *Vis Neurosci* 15: 1079-1087, 1998b.

Gamlin PDR, Cohen DH. Projections of the retinorecipient pretectal nuclei in the pigeon (*Columba livia*). *J Comp Neurol* 269: 18-46, 1988.

Gibson JJ. The visual perception of objective motion and subjective movement. *Psychol Rev* 61: 304-314, 1954.

Gioanni H. Stabilizing gaze reflexes in the pigeon *(Columba livia)*. I. Horizontal and vertical optokinetic eye (OKN) and head (OCR) reflexes. *Exp Brain Res* 69: 567-582, 1988.

Gioanni H, Rey J, Villalobos J, Bouyer JJ, Gioanni Y. Optokinetic nystagmus in the pigeon (*Columba livia)*. I. Study in monocular and binocular vision. *Exp Brain Res* 44: 362-370, 1981.

Gioanni H, Rey J, Villalobos J, Dalbera A. Single unit activity in the nucleus of the basal optic root (nBOR) during optokinetic, vestibular and visuo-vestibular stimulations in the alert pigeon (*Columba livia*). *Exp Brain Res* 57: 49-60, 1984.

Gioanni H, Rey J, Villalobos J, Richard D, Dalbera A. Optokinetic nystagmus in the pigeon (*Columba livia*). II. Role of the pretectal nucleus of the accessory optic system. *Exp Brain Res* 50: 237-247, 1983a.

Gioanni H, Villalobos J, Rey J, Dalbera A. Optokinetic nystagmus in the pigeon (*Columba livia*). III. Role of the nucleus ectomammilaris (nEM): interactions in the accessory optic system. *Exp Brain Res* 50: 248-258, 1983b.

Grasse KL, Cynader MS. The accessory optic system in frontal-eyed animals. In: *Vision and Visual Dysfunction, Vol. IV, The Neuronal Basis of Visual Function.* Edited by A. Leventhal. New York: MacMillan, 1990, p. 111-139.

Hoffmann KP, Distler C. Quantitative analysis of visual receptive fields of neurons in nucleus of the optic tract and dorsal terminal nucleus of the accessory optic tract in macaque monkey. *J Neurophysiol* 62: 416-428, 1989.

Hoffmann KP, Distler C, Erickson RG, Mader W. Physiological and anatomical identification of the nucleus of the optic tract and dorsal terminal nucleus of the accessory optic tract in monkeys. *Exp Brain Res* 69: 635-644, 1988.

Hoffmann KP, Schoppmann A. A quantitative analysis of the direction-specific response of neurons in the cat's nucleus of the optic tract. *Exp Brain Res* 42: 146-157, 1981.

Hoffmann KP, Schoppmann A. Retinal input to direction selective cells in the nucleus tractus opticus of the cat. *Brain Res* 99: 359-366, 1975.

Ibbotson MR, Mark RF, Maddess TL. Spatiotemporal response properties of direction-selective neurons in the nucleus of the optic tract and the dorsal terminal nucleus of the wallaby, *Macropus eugenii*. *J Neurophysiol* 72: 2927-2943, 1994.

Karten HJ, Hodos W. *A Stereotaxic Atlas of the Brain of the Pigeon (Columba Livia).* Baltimore: Johns Hopkins Press, 1967.

Katte O, Hoffman KP. Direction specific neurons in the pretectum of the frog *(Rana esculenta). J Comp Physiol* 140: 53-57, 1980.

Kogo N, Rubio DM, Ariel M. Direciton-tuning of individual retinal inputs to the turtle accessory optic system. *J Neurosci* 18: 2673-2684, 1998.

Li Z, Fite KV, Montgomery NM, Wang SR. Single-unit response to whole-field visual stimulation in the pretectum of *Rana pipiens. Neurosci Letters.* 218: 193-197, 1996.

Lisberger SG, Miles FA, Optican LM, Eighmy BB. Optokinetic response in monkey: underlying mechanisms and their sensitivity to long-term adaptive changes in the vestibuloocular reflex. *J Neurophysiol* 45: 869-890, 1981.

Manteuffel G. Electrophysiology and anatomy of direction-specific pretectal units in Salamandra salamandra. *Exp Brain Res* 54: 415-425, 1984.

Miceli D, Gioanni H, Repérant J, Peyrichoux J. The avian visual wulst. I. An anatomical study of afferent and efferent pathways. In: *Neuronal Mechanisms of Behaviour in the Pigeon*, edited by A.M. Granda and J.H. Maxwell. New York and London: Plenum Press, 1979, p. 223-239.

Mustari MJ, Fuchs AF. Discharge patterns of neurons in the pretectal nucleus of the optic tract (NOT) in the behaving primate. *J Neurophysiol* 64: 77-90, 1990.

Rosenberg AF, Ariel M. Analysis of direction-tuning curves of neurons in the turtle's accessory optic system. *Exp Brain Res* 121: 361-370, 1998.

Simpson JI. The accessory optic system. *Annu Rev Neurosci* 7: 13-41, 1984.

Simpson JI, Giolli RA, Blanks RHI. The pretectal nuclear complex and the accessory optic system. In: *Neuroanatomy of the Oculomotor System,* edited by J.A. Buttner-Ennever. Amsterdam: Elsevier, 1988, p. 335-364.

Soodak RE, Simpson JI. The accessory optic system of rabbit. I. Basic visual response properties. *J Neurophysiol* 60: 2055-2072, 1988.

Volchan E, Rocha-Miranda CE, Picanco-Diniz CW, Zinsmeisser B, Bernardes RF, Franca JG. Visual response properties of pretectal units in the nucleus of the optic tract of the opossum. *Exp Brain Res* 78: 380-386, 1989.

Winterson BJ, Brauth SE. Direction-selective single units in the nucleus lentiformis mesencephali of the pigeon (*Columba livia*). *Exp Brain Res* 60: 215-226, 1985.

Wolf-Oberhollenzer F, Kirschfeld K. Motion sensitivity in the nucleus of the basal optic root of the pigeon. *J Neurophysiol* 71: 1559-1573, 1994.

Wylie DR, Frost BJ. Visual response properties of neurons in the nucleus of the basal optic root of the pigeon: A quantitative analysis. *Exp Brain Res* 82: 327-336, 1990.

Wylie DRW, Frost BJ. The pigeon optokinetic system: Visual input in extraocular muscle coordinates. *Vis Neurosci* 13: 945-953, 1996.

Zhang T, Fu Y-X, Wang SR. Receptive field characteristics of neurons in the nucleus of the basal optic root in pigeons. *Neurosci* 91: 33-40, 1999.

Appendix 2

A Model of an Elaborated Reichardt detector

A version of this appendix has been accepted for publication. Crowder NA, Dawson MR, Wylie DRW. Journal of Neurophysiology. In Press.

For the simulations shown in Figure 4.7 we examined the responses of an elaborated version of the Reichardt detector, depicted in Figure A2.1, to 36 SF/TF combinations. It was created by modifying a model originally proposed by Dawson and Di Lollo (1990) by incorporating alternative temporal filters proposed by Ibbotson and Clifford (2001) and Price and Ibbotson (2002). The stimuli for the model, designed to closely resemble the stimuli used during the neural recordings, consisted of a blank gray screen (at mean luminance) for 2 seconds, followed by a drifting sine wave grating for 2 seconds. The elementary motion detector (EMD) consists of two subunits (A, B) that we assume to be separated by 2^{o}. The model consists of 5 stages; (i) prefiltering (ii) delay filtering, (iii) multiplication, (iv) subtraction, and (v) phase averaging.

Stage I: Prefiltering. In the original Dawson and Di Lollo (1990) model, spatial and temporal band-pass prefiltering was performed to respresent photoreceptor responses. In that model, impulses were used as stimuli, a difference of Gaussians (DOG) was used to perform spatial filtering, and temporal filtering was accomplished via an impulse response function defined by Adelson and Bergen (1985). In the current study, we were interested in studying the model's responses to drifting sine gratings. For such stimuli, spatial DOG filtering produces a sinusoid of the same frequency and phase. Because of this, we did not employ spatial prefilters, although we assume that such prefiltering is carried out by the visual system. Ibbotson and Clifford (2001) also adopted this approach in their simulations.

In the current model, the raw signal s(t) that was presented to a subunit of the EMD at time t was defined as:

$$s(t) = \begin{cases} L, t \leq 2 \\ L + C \times Sin((f_s \times x) - (f_t \times t) - P), t > 2 \end{cases}$$

where L is mean luminance in arbitrary units, C is contrast in arbitrary units, f_s is spatial frequency in cycles/radian, f_t is temporal frequency in $2\pi \times$ cycles/second, x is the spatial location of the subunit's detector, P is a phase shift of the signal (radians), and t is time (seconds). In the simulation, the value of x for the left detector was 0, and the value of x for the right detector was π /90 radians (2°).

Temporal filtering was then performed by convolving the signal for each detector with a band pass filter of the type used by Price and Ibbotson (2002):

$$h(t) = \begin{cases} 0, t \leq 0 \\ \left(\frac{1}{\tau_1}\right)\exp\left(\frac{-t}{\tau_1}\right) - \left(\frac{\beta}{\tau_2}\right)\exp\left(\frac{-t}{\tau_2}\right), t > 0 \end{cases}$$

This filter is a difference between exponential functions, where τ_1 and τ_2 are the time constants of these respective functions in seconds, and β is the gain of the temporal filter, which has a value between 0 and 1.

Stage II: Delay filtering. In order to detect motion, delayed versions of the signals being detected by both receptors in the EMD were computed. In the original Dawson and Di Lollo (1990) model, this was accomplished by a pure phase shift. In the current

model, this was instead achieved by convolving the prefiltered signals from stage I with a first-order low-pass filter that was used by Clifford et al. (1998):

$$d(t) = \begin{cases} 0, t \leq 0 \\ \left(\frac{1}{\tau}\right)\exp\left(\frac{-t}{\tau}\right), t > 0 \end{cases}$$

where t is time (seconds), and τ is the time constant of the filter in seconds.

Stage III: Multiplication. In the multiplication step, the left-delayed signal was multiplied by the right-undelayed signal to produce the signal from the left half of the detector (S_1). The signal from the right half of the detector (S_2) was calculated in a similar fashion, by multiplying the right-delayed signal by the left-undelayed signal.

Stage IV: Subtraction. In the subtraction step, the signal from the right half of the EMD (S_2) was subtracted from that from the left half of the detector (S_1), but scaled by α which controls the "balance" of the detector (Zanker et al., 1999), such that

Output = $(S_1) - (\alpha \times S_2)$, where $0 \leq \alpha \leq 1$

When $\alpha = 1$, the detector is fully balanced, but with $\alpha < 1$, the detector is said to be partially balanced. With $\alpha = 0$, the fully unbalanced EMD is referred to as a "half-detector" (Zanker et al., 1999).

Stage V: Phase Averaging. The final step, phase-averaging, serves the purpose of spatial integration that is found in models that employ an array of EMDs (e.g. Zanker et al., 1999; Ibbotson and Clifford, 2001; Price and Ibbotson, 2002). Because the response of an EMD is sensitive to the phase of the grating (e.g. Buchner, 1984), and because we were using a rather short duration of motion for the slower TFs, we averaged the response of the detector to 4 different stimuli. The only difference between each of these stimuli in terms of phase, which was manipulated by varying the value of P in the equation for the drifting sinusoid that was provided earlier. The values of P for the four different stimuli were 0, $\pi/2$, π, and $3\pi/2$ radians (i.e. 0, 90, 180, and 270 degrees).

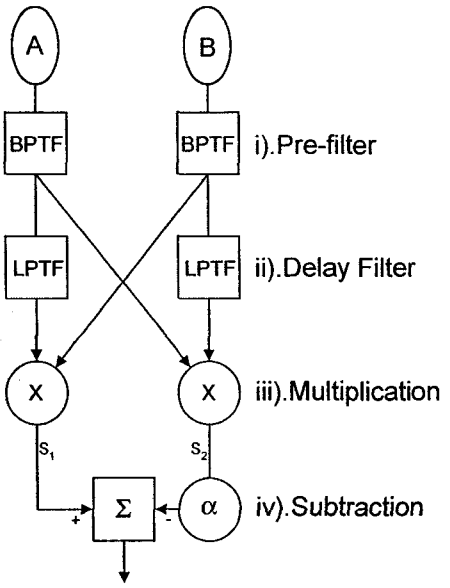

Figure A2.1

Schematic representation of the correlation model of motion detection with variable balance between half-detectors. See text in Appendix for details. BPTF = band pass temporal filter. LPTF = low pass temporal filter.

References

Adelson EH, Bergen JR. Spatiotemporal energy models for the perception of motion. *Journal of the Optical Society of America A-Optics & Image Science* 2: 284-99, 1985.

Buchner E. Behavioral analysis of spatial vision in insects. In: *Photoreception and Vision in Invertebrates*, edited by Ali MA. New York: Plenum Press, 1984, p. 561-621.

Clifford CWG, Freedman JN, Vaina LM. First- and second-order motion perception in Gabor micropattern stimuli: psychophysics and computational modelling. *Brain Res Cogn Brain Res* 26: 263-271, 1998.

Dawson M, Di Lollo V. Effects of adapting luminance and stimulus contrast on the temporal and spatial limits of short-range motion. *Vision Res* 30: 415-429, 1990.

Ibbotson MR, Clifford CW. Interactions between ON and OFF signals in directional motion detectors feeding the not of the wallaby. *J Neurophysiol* 86: 997-1005, 2001.

Price NS, Ibbotson MR. Direction-selective neurons in the optokinetic system with long-lasting after-responses. *J Neurophysiol* 88: 2224-2231, 2002.

Zanker JM, Srinivasan MV, Egelhaaf M. Speed tuning in elementary motion detectors of the correlation type. *Biol Cybern* 80: 109-16, 1999.